

Cemented Tibial Tray Fixation

Vom Promotionsausschuss der
Technischen Universität Hamburg-Harburg
zur Erlangung des akademischen Grades
Doktor-Ingenieurin (Dr.-Ing.)

genehmigte Dissertation

von
Katrin Nagel

aus
Hannover

2017

Erster Gutachter: Prof. Dr. habil. Michael M. Morlock

Zweiter Gutachter: Prof. Dr.-Ing. habil. Nicholas E. Bishop

Tag der mündlichen Prüfung: 29.08.2016

Researchers discover a previously unknown phenomenon, principally by demonstrating that an observation cannot be explained by any known phenomena, and then explore its various effects and learn how to maximise and control them.

from "The Knowledge"
by Lewis Dartnell

Acknowledgements

This thesis would have been impossible without the support of others.

First of all, I would like to thank my doctoral adviser Prof. Dr. habil. Michael M. Morlock for his encouragement and his pressure, both of these given at the right time. Thank you for leaving room to find my way.

My supervising tutor Prof. Dr.-Ing. habil. Nicholas E. Bishop taught me how to derive theories of all kinds, how to decompose them and how to finally re-construct them. His willingness to discuss things to the very end was pivotal for learning that things are never discussed to the very end.

Dr. Ulf J. Schlegel came to Hamburg several times from the other side of Germany to spend days working with me in a windowless lab. His scientific experience, medical input and skills have been irreplaceable and helped me through my less confident phases of the project. This research was financially supported by DePuy International. In particular, I would like to thank David Wolfson and Mark Heldreth. Their attentive comments on manuscripts and reports have been valuable input.

Prof. Dr. med. Klaus Püschel from the Legal Medicine Department of the University Medical Center Hamburg-Eppendorf and his staff have been a great support regarding handling of cadaveric specimens and CT-scanning.

I thank Dr. Gerd Huber for always being there for my whole time at the TUHH. Nobody could have been a better supervisor in making the first steps in the world of science. Julian Gührs tolerated 26°C room temperature without ventilation for those months in WS2014/15 and was still willing to review my thesis. Also, thanks for making me laugh at least once a day and creating a wonderful atmosphere for research and discussion.

Gabriele Mielke, Kay Sellenschloh and Matthias Vollmer have always been willing to share their experience and ideas with me. They were there when I needed their advice and support in organising whatever I required. Inga Schmidt and Gabriele Lange have been lovely friends and great help in all administrative issues. My colleagues Johanna Bätz, Graeme Campbell and Annika Krull spent thoughts and time on my project and also reviewed my thesis. Their honest comments improved the manuscript a lot.

Prof. Dr. Michael Amling and Dr.-Ing-Michael Hahn from the Department of Osteology and Biomechanics of the University Medical Center Hamburg-Eppendorf shared their experience on histology and micro analyses of bone and bone cement with me, which saved a lot of time and revealed interesting aspects.

All colleagues, project partners, researchers, and students I have been in contact with made my time in Hamburg an invaluable experience. Thanks to all of you for being there at the same time as I was.

Finally, this would not have been possible without the support of my family in Hannover, München and Hamburg. In particular, thanks to my mum and dad for standing beside me and my decisions although my way was not always the fast and direct one. Thanks to Michael Zielinski for the backing he provided. Thanks for being forbearing with me, when I was in the office seven days a week. Thanks for absorbing tears and frustration and thanks for giving me room to finish this thesis.

Kurzfassung

Die totale Kniearthroplastie ist ein erfolgreicher chirurgischer Eingriff, führte aber in 2013 in Deutschland zu etwa 25 000 Revisionseingriffen. Häufig ist die tibiale Komponente der Prothese betroffen. Die Vermeidung oder ein Hinauszögern des Revisionseingriffes ist im Hinblick auf das erhöhte Infektionsrisiko und den Knochenverlust bei der Implantatextraktion im Interesse des Patienten. Bis zu ein Drittel der Revisionen werden aufgrund einer aseptischen Lockerung der Prothesenkomponenten durchgeführt, die durch eine unzureichende Implantatfixation ausgelöst wird. Die Fixierung der Implantate wird vorwiegend mit Knochenzement durchgeführt, der einen Formschluss mit dem trabekulären Knochen bildet. Ein Indikator für die Festigkeit der Fixierung ist die Auszugsfestigkeit, für die eine Korrelation mit der Zementeindringtiefe in den Knochen gezeigt wurde. Im Hinblick auf die Formschlussverbindung spielt vermutlich die Architektur des trabekulären Knochens eine Rolle für die Fixationsfestigkeit. Die trabekuläre Struktur ist patienten- und ortsabhängig, deshalb sind fallspezifische Analysen notwendig.

Das Ziel dieser Studie war die Verbesserung des Formschlusses zwischen Zement und Knochen, was durch die Analyse der Zementmantel-Morphologie in humanen Tibiae erreicht wurde. Der Einfluss von Zementeindringtiefe, Zementierungstechnik, aber auch von Knochendichte und -porosität auf die Fixationsfestigkeit wurde mit Hilfe von Computer-Tomographie(CT)-Analyse, mechanischen Auszugsversuchen und statistischer Modellierung der Fixationsfestigkeit durch Regressionsanalysen ermittelt. Die untersuchten Zementierungstechniken waren Zementauftrag mittels Zementpistole oder manuell, Voll- oder Plateauzementierung, zweischichtiger Zementauftrag und Knochenreinigung mittels gepulster oder Spritzenspülung.

In dieser Arbeit wurde eine Prozedur entwickelt, die die 3D-Rekonstruktion des Zementmantels aus CT-Aufnahmen zementierter Implantate in humanen Tibiae ermöglicht. Die Auflösung klinischer CT-Bildgebung ist nicht ausreichend für die Darstellung der trabekulären Architektur. Daher wurde die trabekuläre Struktur anhand von Mikro-CT-Aufnahmen von Knochenproben charakterisiert, die aus dem trabekulären Knochen unter dem tibialen Plateau von nativen Tibiae gewonnen wurden. Die Ergebnisse wurden auf die Knochendichte, bestimmt aus klinischen CT-Aufnahmen, bezogen. Die Kontaktfläche zwischen Knochen und Zement im belasteten Formschluss wurde bestimmt und als entscheidend für die Fixationsfestigkeit identifiziert. Die Zementeindringtiefe spiegelt die Fläche wider, die zur Übertragung der aufgetragenen Last vom Zement auf den Knochen zur Verfügung steht. Ist die Zementeindringtiefe unter einem kritischen Wert so entstehen Spannungen und Verformung von Zement sowie porenbildenden Trabekeln, bis zur Überlastung der wenigen Trabekel, die sich im Formschluss befinden. Der Zement wird aus den Knochenporen gezogen. Ab einer kritischen Größe der Last-Übertragungsfläche sind Spannungen und Verformung so gering, dass die Last auf den unter dem Zementmantel liegenden Knochen übertragen werden kann. Die zur Verfügung stehende Last-Übertragungsfläche hängt von der Zementeindringtiefe und der Porosität des trabekulären Knochens ab.

Die Ergebnisse dieser Arbeit zeigen, dass von den untersuchten Zementierungstechniken nur Zementauftrag mittels Zementpistole die Morphologie des Zementmantels

verbessern konnte und das auch nur, wenn die Knochenoberfläche vorher gründlich gereinigt wurde. Nach einer solchen gründlichen Reinigung wurde die notwendige Zementeindringtiefe jedoch immer erreicht.

Das statistische Model zur Abschätzung der Fixationsfestigkeit kann genutzt werden, um die Zementeindringtiefe zu ermitteln, die notwendig ist um die entscheidende Last-Übertragungsfläche bereitzustellen. Dieses Ergebnis sollte in der präoperativen Planung eingesetzt werden, um Extremfälle zu identifizieren und die Zementierung anzupassen, aber auch in der postoperativen Risikoabschätzung in Bezug auf eine aseptische Lockerung.

Abstract

Although a successful surgical intervention, total knee arthroplasty resulted in about 25 000 revision procedures in 2013 (Germany). The majority of cases concern the tibial component of the prosthesis. Avoidance or at least postponement of revision surgery is desirable in order to decrease infection risk and bone loss related to implant extraction. In up to one third of the cases the reason for revision is aseptic loosening, which is caused by poor implant fixation. Fixation is typically performed using bone cement that forms an interlock with the trabecular bone. An indicator for the fixation strength is pull-out strength, which has been shown to correlate to penetration depth of the cement into the bone. Considering the interlock connection, the architecture of trabecular bone may play a role in fixation strength. The trabecular architecture is patient- and location-dependent, requiring patient-specific analysis.

The aim of this thesis was to improve interlock between cement and bone. This goal was achieved by investigation of cement layer morphology in cadaveric specimens. The influence of cement penetration depth, cementation technique, as well as of bone density and porosity on fixation strength was analysed using computed tomography (CT) image analysis, mechanical pull-out testing and statistical modelling of fixation strength by regression. Investigated cementation techniques were gun and manual application, full and plateau-only cementation, two-layered cementation and bone cleansing using pulsatile or syringe lavage. A procedure was developed that enabled 3D reconstruction of the cement layer from the CT images of cemented tibial implants within cadaveric specimens. Clinical CT imaging offers insufficient resolution for the accurate representation of trabecular architecture, limiting the analysis of the role of trabecular architecture in fixation strength. Micro-CT was used to characterise the trabecular architecture in samples obtained from below the tibial plateau of native tibias. The results were related to the bone density as determined in normal CT. The cement-bone contact area within the loaded interlock was determined and shown to be crucial for fixation strength. The cement penetration depth indicates the area available to transfer the applied load to the bulk bone of the tibial head. Cement penetration depth below a critical value leads to deformation of cement and pore-forming trabeculae close to the surface. The few existing interlocking trabeculae are overloaded and fail, so that the cement pulls out of the pores. Above the critical value, load acts on a larger contact area, stress and strain are lower and load can be transferred to the bone below the cement mantle. The available load-transfer area depends on the cement penetration depth and the porosity of the trabecular bone.

The results of this thesis show that from the investigated cementation techniques only cement application using a cement gun had an improving effect on the cement layer, but only, if the resection surface underwent pulsatile lavage cleansing preceding cement application. However, regardless of the cement application technique, the critical cement penetration depth was always exceeded after thorough cleansing.

The statistical model for estimating fixation strength allows patient-specific determination of the penetration depth that is necessary to obtain the critical load-transfer area. These findings should be applied in pre-operative planning to identify extreme cases and select cementation technique accordingly, as well as in postoperative risk assessment with regard to aseptic loosening.

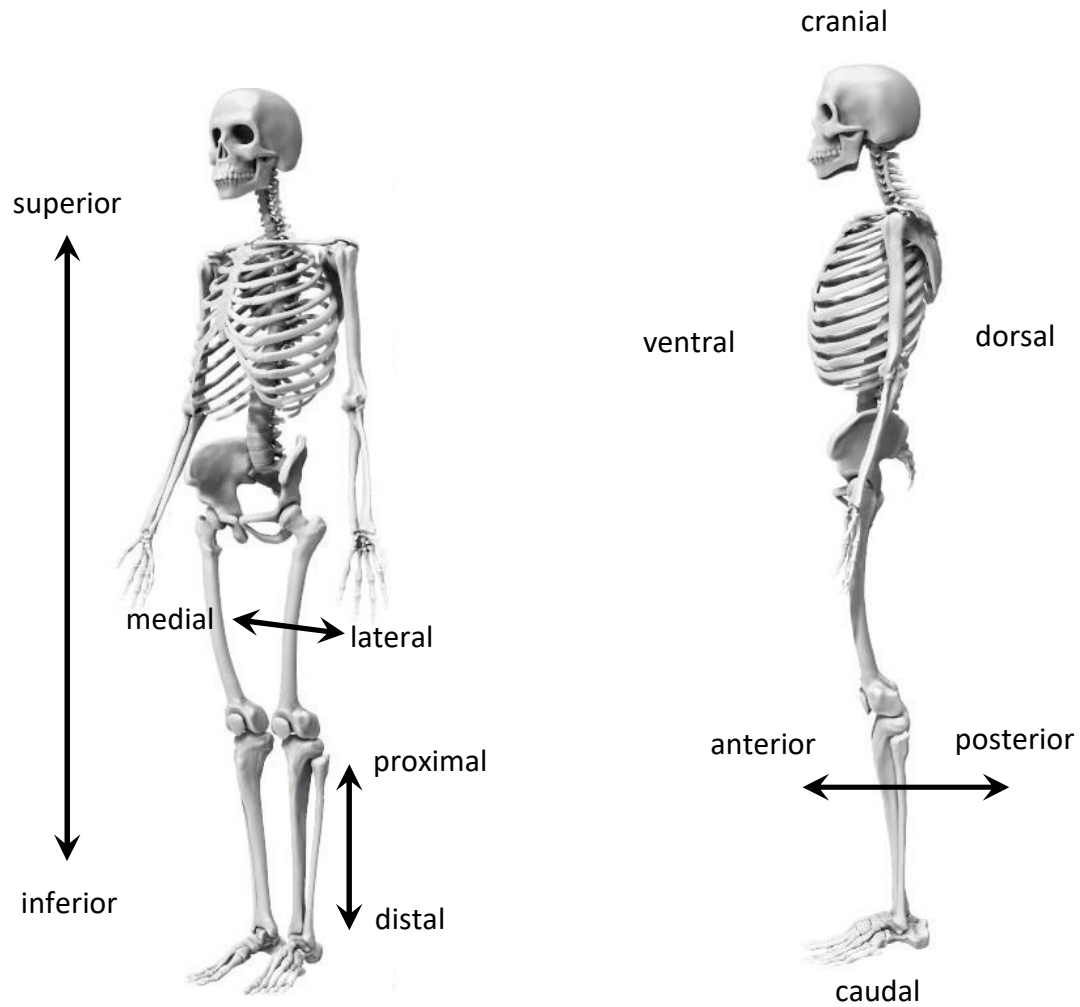
Table of Contents

Kurzfassung	III
Abstract	V
Table of Contents	VI
Anatomical Terms of Location	IX
Glossary	X
List of Symbols and Abbreviations	XII
1 Introduction	1
1.1 Motivation.....	1
1.2 Study Aim	4
1.3 Structure of the Thesis	5
2 Background	7
2.1 Architecture of Bones	7
2.2 Anatomy and Function of the Human Knee Joint	10
2.2.1 Anatomical and Mechanical Axis.....	14
2.2.2 Load on the Knee Joint	15
2.2.3 Indications for Total Knee Arthroplasty	16
2.3 Total Endoprotheses in Knee Joint Reconstruction	17
2.3.1 Evolution of Modern Implant Design	18
2.3.2 Fixation of the Tibial Tray in Total Knee Arthroplasty.....	22
2.3.3 Clinical Loosening of the Tibial Tray in Total Knee Arthroplasty	33
2.4 <i>In Vitro</i> Testing of Cement-Bone Interfaces.....	35
2.5 Conclusion.....	40
3 Impact of Cementation Techniques on Cement-Bone Interfaces in Total Knee Arthroplasty	42
3.1 Introduction	42
3.2 Material and Methods.....	43
3.2.1 Specimens	43
3.2.2 Bone Mineral Density	43
3.2.3 Tibial Tray Implant.....	44
3.2.4 Preparation and Implantation.....	46
3.2.5 Computed Tomography and Re-gluing of Implant.....	48

3.2.6	Pull-out Testing.....	49
3.2.7	Cement Layer Morphology Analysis.....	51
3.2.8	Statistical Analysis	57
3.3	Results.....	58
3.3.1	Failure Mode	58
3.3.2	Bone Mineral Density	59
3.3.3	Cementation and Penetration-Increasing Techniques.....	61
3.4	Discussion.....	64
3.4.1	Effect of Cementation and Preparation Techniques on Cement Penetration	64
3.4.2	Aspects in Cement Layer Analysis.....	66
3.4.3	Relevance of the Cement Penetration Depth Range Measured.....	67
3.4.4	Challenges of the Experimental Method.....	68
3.4.5	Limitations of the Study Design.....	69
3.4.6	Conclusion.....	70
4	Failure of Cement-Bone Interfaces in Total Knee Arthroplasty.....	72
4.1	Introduction	72
4.2	Material and Methods.....	74
4.2.1	Specimens and Implants.....	74
4.2.2	Computed Tomography and Evaluated Parameters	75
4.2.3	Statistics.....	78
4.3	Results.....	80
4.3.1	Classification Potential of Parameters	81
4.3.2	Contribution of Cement Layer Characteristics and Bone Density to Fixation Strength.....	84
4.3.3	Prediction Capacity of Combined Parameters	85
4.4	Discussion	87
4.4.1	Relation of Cement Layer Characteristics to Fixation Strength and Failure Mode.....	87
4.4.2	Relation between Bone Density, Cement Layer Morphology and Fixation Strength	90
4.4.3	Mechanism and Mathematical Modelling of Cement-Bone Interface Failure.....	92
4.4.4	Limitations of the Analysis	94
4.4.5	Conclusion.....	94

5	Role of Trabecular Architecture in Cement-Bone Interfaces in Total Knee Arthroplasty	97
5.1	Introduction	97
5.2	Methods	99
5.2.1	Preparation of Trabecular Bone Samples	99
5.2.2	Architectural Parameters of Tibial Trabecular Bone	100
5.2.3	Interlock Parameters of Tibial Trabecular Bone	103
5.2.4	Statistical Modelling of Bone Failure Based on the Trabecular Structure	108
5.2.5	Statistics	110
5.3	Results	111
5.3.1	Characterisation of Tibial Trabecular Bone	111
5.3.2	Modelling of Fixation Strength Based on Trabecular Parameters	114
5.4	Discussion	116
5.4.1	Architectural and Interlock Parameters of Tibial Trabecular Bone	116
5.4.2	Statistical Modelling of Strength Based on Trabecular Architecture and Interlock	119
5.4.3	Limitations of the Analysis	120
5.4.4	Conclusion	121
6	Conclusions	124
6.1	Characterisation of Cement-Bone Fixation	124
6.2	Relevance for Aseptic Loosening	127
6.3	Limitations	131
6.4	Future Work	133
7	Literature	135
	Appendices	153
	A Pilot Studies	153
	B Algorithm for Cement Layer Morphology Analysis	163
	C Supplementary Data	171
	D Curriculum Vitae	203

Anatomical Terms of Location



[Adapted from [alvesan.deviantart.com](https://www.deviantart.com/alvesan)²²⁶]

Glossary

anteroposterior	In direction from anterior to posterior
arthroplasty	artificial joint replacement procedure
aseptic loosening	loosening of an implant that is not related to infection
bone cement	a two-component polymer that is used to fix implants to bone
cortical bone	compact bone that forms the shell of bones
compartment	medial or lateral half of the knee joint; the femoro-tibial knee joint is anatomically separated into two independent halves
cross-validation	confirming a derived model by applying it to an independent data set
diaphysis	shaft of a long bone
epiphysis	ends of a long bone
extension-flexion	movement of a body part that changes the angle between body parts; during knee bending the knee joint performs an extension-flexion motion
finger packing	manual application and pressurisation of cement
full cementation	shaft and tray of a tibial tray are cemented (→ plateau-only cementation)
hybrid cementation	either the tibial or the femoral component is cemented and the respective other component is left cementless
<i>in situ</i>	Latin: “in place”; at the designated site, implies a more function-specific investigation than <i>in vitro</i>
<i>in vitro</i>	Latin: “within the glass”; refers to studies that are investigating effects in artificial surroundings or dead organisms
<i>in vivo</i>	Latin: “within the living”; refers to studies that are investigating effects in whole living objects
infection	pathophysiological process due to disease-causing agents, such as viruses and bacteria
inferosuperior	in direction from inferior to superior
intramedullary	the medullary cavity is the central cavity within the shaft of long bones, “intra” refers to devices that are placed within the medullary cavity
kernel filter	filtering in image processing based on a convolution matrix (kernel)
lavage	here: irrigation of the trabecular surface to remove bone debris from the bone preparation process; a more intense lavage intends to remove fat and marrow from the trabecular cavities
malpositioning	“wrong” positioning of a functional implant within the human body, so that the intended function is compromised or the surrounding body is harmed
metaphysis	transition zone between the end of a long bone and its shaft

pairwise study design	one side of a tibial pair undergoes treatment, while the other side serves as control
plateau-only cementation	cement is applied to the plateau of the resected tibia, the stem is left cementless
polymerisation	formation of chains from monomeric molecules in a chemical reaction; here: curing of bone cement
pull-out testing	test mode in which a device is removed from bone by displacement in its axial direction; applied in interface testing
Register	here: a - commonly national - collection of all arthroplasty procedures performed; it covers surgical parameters such as indication, revision indication, implant design, implant manufacturer, fixation method; reports are published yearly for quality assessment
resection	surgical removal of tissue, here: removal of the native joint surfaces
revision	surgical procedure in which an implant is removed and/or replaced due to reasons as infection, fixation loosening, bone fracture, pain, implant wear, implant failure and dislocation
trabecular bone	spongy bone structure within the ends of long bones
tribology	science of the interaction between surfaces, concerns friction, lubrication and wear
valgus	angulation of the distal part of a joint or bone away from the central axis of the body
varus	angulation of the distal part of a joint or bone towards the central axis of the body

List of Symbols and Abbreviations**Mathematical Symbols^a**

α	type-1 error level	-
A	area	mm ²
A _{bone}	cross-sectional area of bone in a cut plane normal to the applied load	mm ²
a _i	regression coefficients	
β	type-2-error level	-
$\frac{dBS}{dr}$	change of bone surface area BS with radius of a trabecular structure	$\frac{mm^2}{mm}$
E	Young's modulus	MPa
F	force	N
F _U	ultimate load	N
H	fabric tensor	-
i	index variable	-
MIL	mean intercept length	mm
n	sample size	-
p	probability value in statistical hypothesis testing	-
ρ	density	$\frac{kg}{m^3}$
r	Pearson's correlation coefficient	-
R ²	coefficient of determination	-
σ	stress	MPa
σ_U	ultimate strength	MPa
x	predictor in regression model	
y	dependent variable in regression model	

Parameters in the Analyses of This Thesis

<i>Ang_{RMS}</i>	angle between cement layer surface triangles and resection plateau	°
<i>A_{proj}</i>	projected area	mm ²
<i>A_{proj0}</i>	standardised projected area	-
<i>A_{projEx}</i>	extrapolated projected area	mm ²
<i>bearA</i>	bearing area of the tibial tray on the cement	mm ²
<i>BMD</i>	bone mineral density	$\frac{mg}{cm^3}$

^a Hyphen indicates dimensionless variables. If no dimension is listed at all, various dimensions may occur for the symbol.

<i>BV/TV</i>	bone volume fraction in a trabecular sample: bone volume/total volume	-
<i>CLASS</i>	classification variables	-
<i>CSA</i>	cross-sectional area	mm ²
<i>CSA₀</i>	specific cross-sectional area	-
<i>CumPen</i>	cumulated penetration depth	mm
<i>DevAng</i>	trabecular orientation in terms of deviation from vertical axis	°
<i>evalA</i>	evaluated area	mm ²
<i>Folding</i>	ratio between surface area and projected area of the lower cement layer	-
<i>IA</i>	interlock area projected to the resection plateau	mm ²
<i>IA₀</i>	specific interlock area	-
<i>KurtPen</i>	kurtosis of the penetration depth distribution	-
<i>MaxPen</i>	maximum penetration depth	mm
<i>mCSA₀</i>	mean of the specific cross-sectional area	-
<i>MeanPen</i>	mean penetration depth	mm
<i>MedPen</i>	median penetration depth	Mm
<i>ModePen</i>	mode penetration depth	mm
<i>PEN</i>	penetration depth	mm
<i>PEN₀</i>	relative penetration depth	-
<i>RIM</i>	index for peripheral region	
<i>S</i>	fixation strength	MPa
<i>SDPen</i>	standard deviation of the penetration depth distribution	mm
<i>sIA₀</i>	increase of the specific interlock area with PEN	$\frac{1}{\text{mm}}$
<i>SkewPen</i>	skewness of the penetration depth distribution	-
<i>SMI</i>	structure model index	-
<i>Tb.N</i>	number of trabeculae per mm structure	$\frac{1}{\text{mm}}$
<i>Tb.Sp</i>	trabecular spacing	mm
<i>Vol</i>	volume	mm ³
<i>Vol_{spec}</i>	specific volume	mm
<i>VolStem_{spec}</i>	specific cement volume of stem region	mm ³

Abbreviations

μCT	micro-computed tomography
ACL	anterior cruciate ligament
ANOVA	analysis of variance
BMC	bone mineral content
BMD	bone mineral density
BW	body weight
CoCr	cobalt chrome
CT	computed tomography
EDX	energy dispersive X-ray spectroscopy
F	female
FE	finite element method
H _A	alternative hypothesis
HA	hydroxyl apatite
HRCT	high resolution computed tomography
HU	Hounsfield units
M	male
m.	musculus
PCL	posterior cruciate ligament
PE	polyethylene
PMMA	polymethylmethacrylate
qCT	quantitative computed tomography
ROC	receiver operating characteristic
RSA	radio stereometric analysis
SD	standard deviation
SEM	scanning electron microscopy
THA	total hip arthroplasty
Ti	titanium
TKA	total knee arthroplasty
UKA	unicompartmental knee replacement
VOI	volume of interest

1

Introduction

1.1 Motivation

Osteoarthritis is a widespread chronic disease of the joint cartilage. Insufficient nutrition of the cartilage due to manifold reasons leads to degeneration of the tissue structure, climaxing in painful bone-on-bone articulation. After fully utilising all conservative and cartilage-preserving approaches, joint reconstruction in a surgical procedure using artificial materials — referred to as arthroplasty — remains the last solution to restore joint function and maintain the patient's life quality.

Due the role of arthroplasty as gold standard treatment for end-stage osteoarthritis, constant assessment of implant designs and surgical techniques is required for quality assurance. For this purpose, national Arthroplasty Registers have been introduced in many countries, containing each procedure executed, with detailed information about indication, implant and technique. Amongst others, commonly consulted Registers with long observation periods are the Swedish¹ and the British² Registers, as well as the Australian Register³.

Although all joints may be affected by arthritis, the majority of surgical arthroplasty procedures concern hip and knee joints, comprising 50 % and 48 %, respectively, of all procedures carried out in Britain in 2013². Total knee replacement (TKA) is the focus of this thesis.

TKA is a successful surgical procedure to restore the knee joint function. In a healthy joint, the condyles of the femur articulate with the tibial plateau and the posterior surface of the patella. A TKA consists of three to four components: a tibial tray replacing the cartilage on the tibial plateau, a femoral component replacing the surface of the femoral condyles and a polymeric inlay that is placed on the tibial plateau to articulate with the femoral component (**Figure 1-1**). If also affected by arthritis, the posterior side of the patella is also replaced.

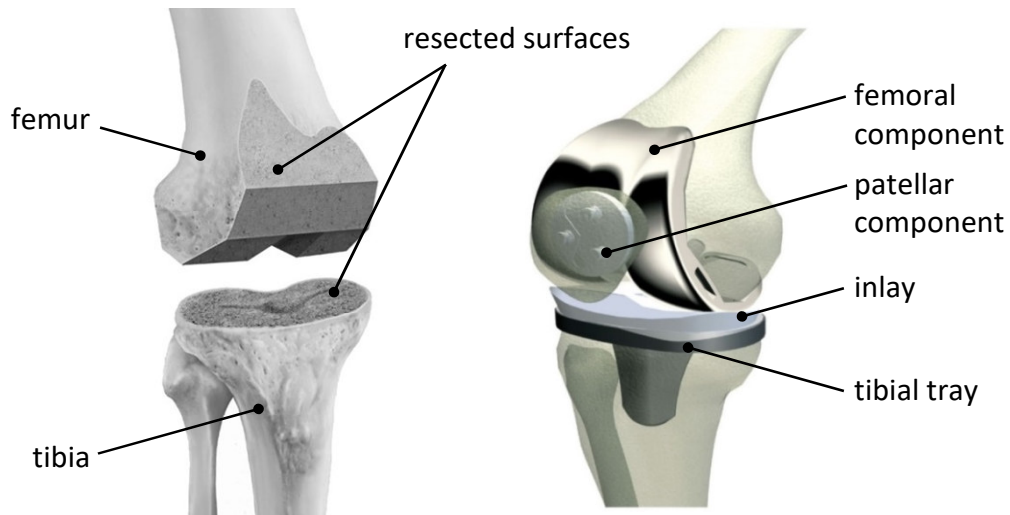


Figure 1-1: Human knee joint with total arthroplasty. Left: Femoral and tibial articulating surfaces have been resected, underlying trabecular bone is exposed [Adapted from phamy-medical.com⁴]. Right: Resected surfaces have been replaced by artificial bearing surfaces. [Adapted from bonesmart.org⁵]

Data from Sweden and Britain show a survival rate of TKA of about 96 % at 9 years^{1,2}, which appears to be comparable to that of total hip arthroplasty (THA, 95 % at 9 years²). Survival refers to a prosthesis that has not had to be revised and replaced in a subsequent surgical procedure. Reasons reach from infection to implant failure and will be discussed later. However, in THA the articulation occurs between the artificial femoral head and the acetabulum, where various materials such as metal, ceramic and polyethylene may be used on both sides. In the case of metal-on-metal articulation, the revision rate has recently increased up to 20 % at 9 years², which biases the overall Register statistics. The poor outcome of this specific bearing type makes the overall THA revision rate seem higher than if metal-on-metal articulations were excluded from the statistics. In general, TKA survival is inferior to that of THA.

In 2013, more than 143 000 primary TKA procedures were carried out in Germany. More than 25 000 patients operated before had to undergo revision surgery, which is accompanied by increased infection risk and inevitable loss of bone that may be strongly attached to the implant locally⁶. Revision of the tibial component is more likely than revision of the femoral: the Swedish Register reports more tibia-only revisions than femur-only in the same period¹. The main indications for revision reported by the Swedish Register were loosening and infection, each accounting for about one-quarter of cases¹. Loosening may be septic or aseptic, that is with or without the presence of infection, which is not accounted for in the Swedish Register and may complicate the interpretation of the reported numbers. While infection risk is an omnipresent challenge, persisting even after years of implant survival, initiation of aseptic loosening is a mechanical phenomenon. The British Register reports 32 % of revisions as being due to aseptic loosening and 22 % due to infection².

Aseptic loosening is related to the initial implant fixation, which may be based on an additional fixation material, referred to as bone cement (cemented fixation, **Figure 1-2, B**), or on bone ingrowth or ongrowth (uncemented fixation, **Figure 1-2, B**). For the tibial tray in TKA, survival rate of cemented fixation was shown to be higher than of

uncemented implantation^{2,3}. Cemented fixation is the standard procedure with a proportion of 86 % in 2012 in the British Register^{1,2,7}. In conclusion, aseptic loosening of tibial trays is currently addressed most effectively by optimising the cemented fixation. Cemented fixation takes advantage of the porosity of the trabecular bone, exposed when the diseased native bone surface is removed in an arthroplasty procedure (**Figure 1-1**, left). Bone cement is a two-component polymer that is mixed in the operating theatre and starts to cure immediately. It is applied to the trabecular bone surface in a doughy state and pressed into the porous trabecular structure during subsequent implant insertion. Bone cement processability is limited to a few minutes after component mixing, successively forming an interlock connection with the bone.

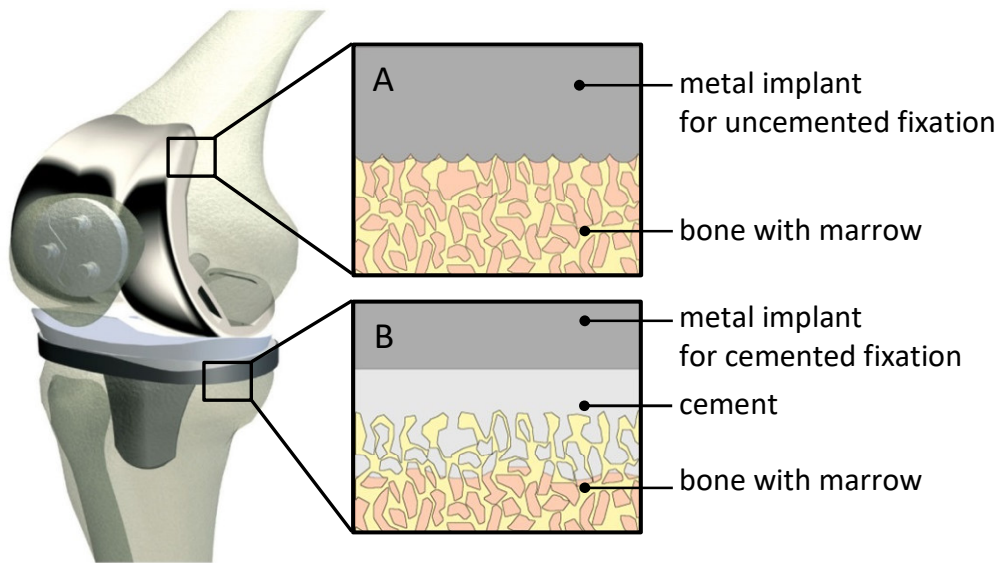


Figure 1-2: Fixation options of arthroplasty implants. A: Uncemented fixation based on bone in- or ongrowth. The implant surface is rough. B: Cemented fixation based on a polymer compound that is applied to the porous bone surface in a doughy state, pressed into the bone and forming an interlock with the bone after curing. The implant surface is smooth.

In hip arthroplasty, it was found that the cementation technique had a considerable influence on the implant stability and associated resistance to loosening, which led to the development of a standard cementation technique⁸. This standard covers thorough irrigation of the trabecular bone surfaces by a pulsatile fluid jet, vacuum mixing of the cement, insertion of a restrictor device to prevent cement leakage into the medullary cavity distally to the implant, and retrograde cement application to the stem cavity using a cement gun⁸. THA survival rate was improved from more than 30 % loosening to 3 % within ten years when the described techniques were established⁹⁻¹¹. In TKA, cement-bone interface between tibial component and bone has been shown to improve in terms of cement penetration depth into the bone and strength of the interface, when pulsatile irrigation was applied before cement application¹². However, a variety of different techniques regarding bone irrigation, cement application and cement pressurisation was developed in the past and is still controversially discussed¹³⁻¹⁸. A standard cementation

technique can be expected to improve survival rate in TKA as in THA, but is yet to be established.

Loosening of arthroplasties is accompanied by a layer of connective tissue that develops between bone and implanted material and is either due to wear particles (of bone cement or implanted devices, Type I tissue layer), infection (Type II), both (Type III) or micromotion within the cement-bone interlock (Type IV)^{19,20}. Micromotion is increased in primarily insufficient fixation and is suspected of preventing the healing of microfractures occurring naturally in the trabecular bone¹⁹.

In a cadaver study, increased micromotion between cement and bone on the trabecular level has been found for lower penetration depth of the cement into the bone²¹. Trabecular bone is a living tissue that constantly models and re-models based on mechanical stimulus. Stress-shielded and therefore unloaded bone structures are resorbed²⁰. The cement-interdigitated trabecular bone is shielded from load and resorbed progressively with time *in vivo*. Thereby, the effective interdigitation depth between cement and bone is reduced. It has been shown that the residual effective interdigitation depth is larger, when the initial penetration depth is larger^{22,23}.

As well as application of pulsatile lavage, higher porosity in bone with low bone mineral density (BMD) will result in deeper cement penetration, which was found to increase fixation strength^{24–27}. However, decreased fixation strength was found to be related to low-density bone²⁸. In other studies, the tensile strength of the interface was found to be independent of BMD^{12,29}. From these contrary findings, an interaction between BMD and cement penetration may be assumed. Identification of the interaction is necessary to improve cementing technique and help to assess patient-specific failure risk of arthroplasties.

The postulated interaction between BMD and penetration depth is related to the interlock mechanics of the fixation. In cemented fixation, acrylic bone cement interdigitates with trabecular bone. The architecture of the latter dictates the interlock geometry; however, it is unclear what aspect of the geometry is crucial for fixation capacity and how an interaction may evolve from it.

The trabecular structure is a network of rod- and plate-like elements^{30,31}. Orientation and proportion of rods and plates as well as their geometry dictate the mechanical properties of trabecular bone and also the mechanical capacity of the cement-bone interface^{28,30}. The trabecular architecture between anatomical sites differs widely³². Values for the geometry of trabeculae and bone volume fraction in the proximal tibia have been published, but measures of the anisotropy at this anatomical location have not as yet been determined^{33,34}. They are essential to characterise the fixation between trabecular bone and cement.

Macroscopic morphology of the cement layer as well as BMD influence fixation stability. It is unclear what aspect of the interlock leads to greater stability. Clarification enables improvement of cementation techniques, but also patient-related risk assessment.

1.2 Study Aim

This thesis focuses on cemented fixation of the tibial tray in TKA. The aim of the study was to improve the interlock between cement and bone with regard to aseptic loosening and

was approached by addressing three specific research questions that are presented in the following paragraphs.

The first question concerns the clinical aspects of cementation:

Can the penetration of cement into the bone be increased by particular cementation techniques?

This question refers to cement application as well as to bone preparation techniques. Morphology of the cement layer is influenced by application pressure and volume of the applied dough, but also cleansing of the porous surface of the bone plateau prior to cement application. Establishing a standard procedure appears overdue in order to improve fixation.

The second question concerns an understanding of the fixation characteristics:

How do cement layer morphology and bone mineral density influence fixation strength?

Cement penetration depth into the bone is a parameter commonly used to describe cement layers in arthroplasty. It has been postulated that bone with low density (high porosity) results in increased penetration and also that it provides low fixation stability²⁸. This indicates a confounding relationship between the effects of penetration depth and BMD on implant fixation stability. A deeper understanding of this interaction should support the optimisation of cementation procedure to improve fixation stability.

The third question concerns cemented fixation at the micro-mechanical level:

How does the structure of the trabecular bone influence fixation mechanics?

The trabecular architecture is responsible for the interlock mechanics with cement and thereby determines fixation stability. The amount of engaged trabecular bone at specific penetration depths varies with bone porosity²⁵. Several parameters derived from the trabecular structure may be more decisive than others. Focusing on those enables improved risk assessment of cemented fixation.

1.3 Structure of the Thesis

In Chapter 2, the anatomy, morphology and biomechanics of trabecular bone, cemented fixation, implant loosening and the current state of *in vivo* test methods for cement-bone interfaces are described. Chapters 3, 4 and 5 separately address the three above-mentioned study questions and are built on one another. In Chapter 3, mechanical testing procedures are described. In Chapter 4, the failure mechanisms observed in mechanical testing are analysed. A statistical model for fixation strength is developed based on BMD and penetration depth. In Chapter 5, the trabecular architecture of tibial bone is analysed and corresponding aspects are implemented into the model.

In the Conclusions in Chapter 6, the results of the three research questions are summarised and related to the loosening mechanism in cemented fixations.

The Appendices comprise reports describing the pilot studies, validation studies and an overview of the algorithm for cement layer reconstruction (Appendix A and Appendix B), as well as chapter-specific raw and supplementary data and statistical information (Appendix C).

2

Background

Fixation of arthroplasty implants within the body generates an interface between bone and artificial material. The interface mechanics are clearly dependent on the mechanics of the implanted components, as well as on anatomical and physiological aspects. This chapter comprises basic knowledge and current state of the art.

2.1 Architecture of Bones

The human skeleton is composed of different types of bones that are shaped according to their function and position within the body: long bones, flat bones, short bones irregular bones and sesamoid bones (**Figure 2-1**, left). The outer shell of bones is composed of cortical bone tissue, a compact structure built up from hydroxyl apatite (HA) as mineral and collagen as organic proportion. The second bone tissue type is trabecular bone, which is a porous network of connected rod- and plate-like elements (trabeculae) based on the same substance as cortical bone^{30,31}. Trabecular bone is present in the interior of bones (**Figure 2-2**, left). The voids are filled with bone marrow. Exterior cortical bone and interior trabecular bone comprise a lightweight construction with compliance and stiffness optimised to absorb energy, whether applied by the own body or external impacts.

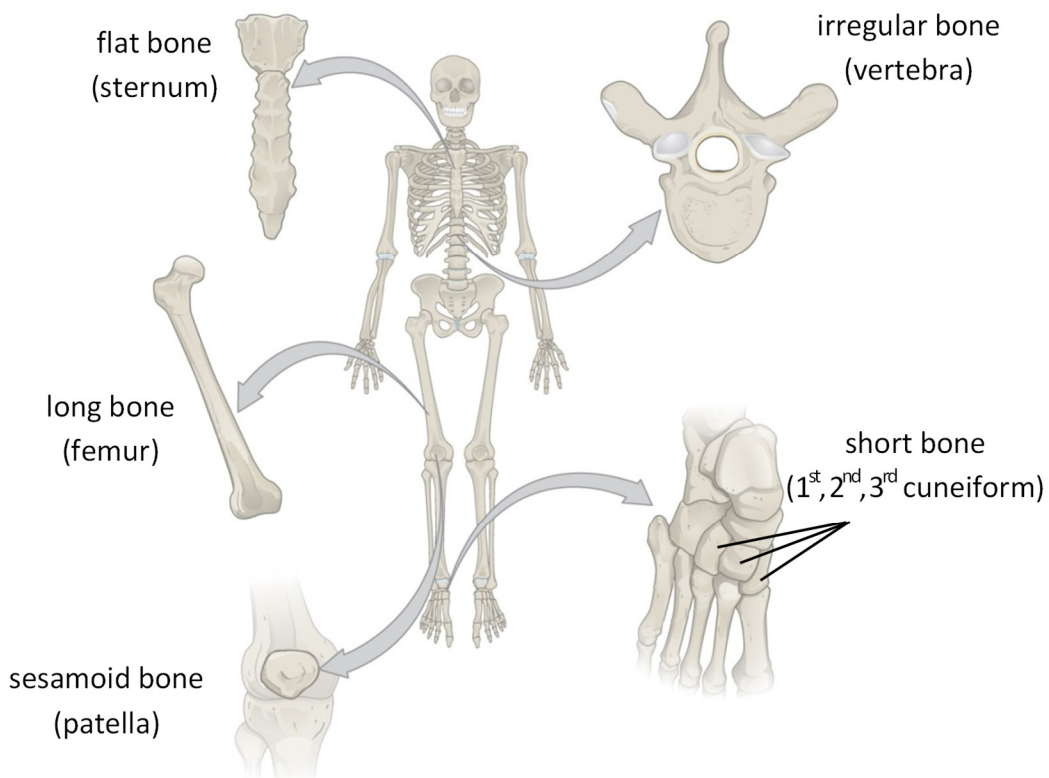


Figure 2-1: Geometry of different bone types and examples. [Adapted from cnx.org³⁵]

Compact bone consists of osteons, which are cylindrical units of about 10 μm to 500 μm , present in aligned orientation³¹ (**Figure 2-2**, right). Stiffness in alignment direction is

greater than in the transverse direction, so bone is an anisotropic material. In principle, the underlying bone substance of trabecular bone corresponds to that of compact bone. Trabecular diameter is about 50 μm to 300 μm and thereby in the range of osteons. The trabecular structure will be discussed in more detail in Section 2.3.2.2. The following section concentrates on the macroscopic structure and metabolism of bone and bone tissue. Long bones will be used as example, as they are the major elements of a knee joint (femur and tibia).^{36,37}

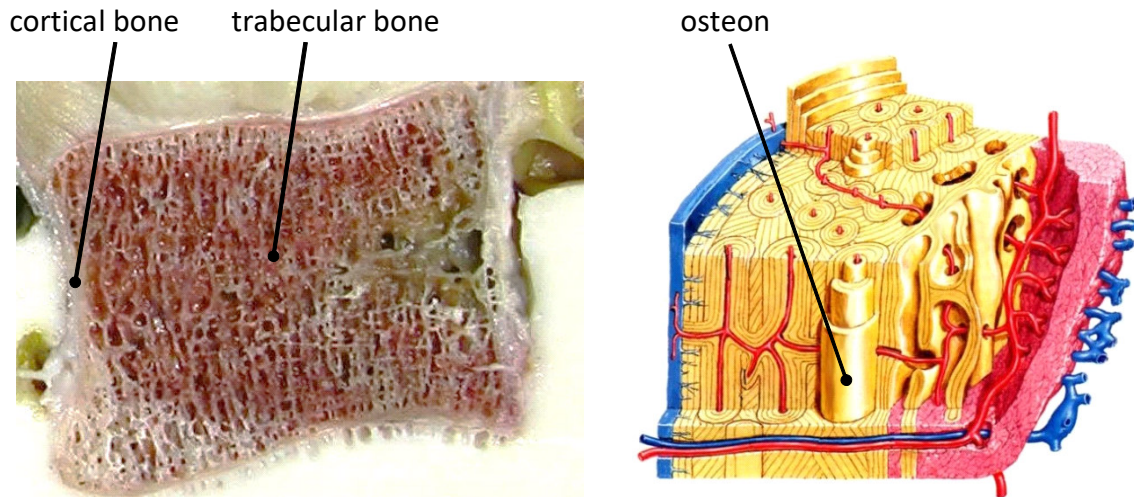


Figure 2-2: Bone composition. Left: Cross-sectional view of a vertebral body revealing cortical and trabecular bone distribution. Right: Cortical bone is composed of aligned osteons [adapted from Netter & Mühlbauer³⁸].

Long bones support the extremities of the human body. They are tube-shaped with thickened ends forming joints with the adjacent bones (**Figure 2-3**). The thickened ends are the epiphyses and the tube-like middle is the diaphysis. The transition zone between epiphysis and diaphysis is the metaphysis. Epiphysis and metaphysis are filled with trabecular bone. The diaphysis is formed by thick cortical bone, enclosing the medullary cavity, which contains marrow and fat that also fill the voids of trabecular bone.^{36,37}

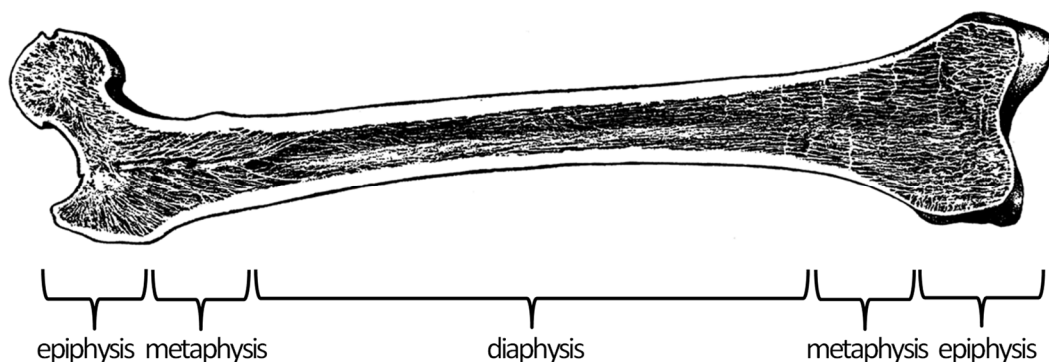


Figure 2-3: Structure of a long bone. The bone shell is built up from cortical bone; metaphysis and epiphysis are filled with trabecular bone. [Adapted from etc.usf.edu³⁹]

Bone is a living tissue that is constantly modelled and remodelled by bone cells: osteoclasts resorb mineralised bone; osteoblasts secrete a bone substance that

mineralises and forms new bone. Some osteoblasts become deactivated during the bone formation process and remain in the bone matrix as osteocytes. The process of bone resorption and formation is referred to as bone remodelling. Pathological bone resorption is referred to as osteolysis. This may be caused by corresponding diseases, infection-related immune processes, but also inappropriate mechanical stress on a long-term basis. Diseases may cause unbalanced activity of osteoclasts and osteoblasts. A common disease is osteoporosis, which is denoted by a loss of bone mass due to over-activation of osteoclasts^{37,40}. The structural elements become thinner and plate structures disappear: the bone becomes more porous. No difference in Young's Modulus was found between osteoporotic and healthy trabeculae, but ultimate tensile strain was reduced from 5.1 % in healthy to 2.4 % in osteoporotic bone⁴¹. The trabecular structure of osteoporotic bone is more fragile with an increased fracture risk⁴² (**Figure 2-4**). Further mechanical properties of trabecular bone are discussed in Section 2.3.2.2.

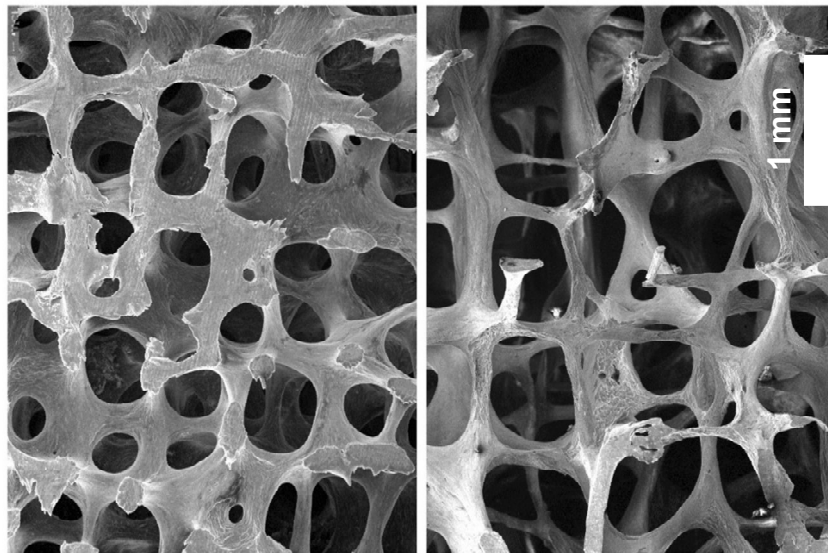


Figure 2-4: Trabecular bone structure. Left: Healthy bone with rod and plate elements. Right: Osteoporotic bone with fewer plates and thinner rods. The distance between structures is larger. [Adapted from ectsoc.org⁴³]

Bone remodelling is the basis for the functional adaptivity of bone that was formulated by Julius Wolff as early as in 1892 and referred to as Wolff's "Law of Bone Transformation"⁴⁴. Wolff observed that the internal structure of trabeculae is oriented towards external loading. According to Wolff's Law, the orientation of trabeculae within a bone is adapted to stresses due to the external load regime⁴⁴. The exact mechanism of this stress adaptation is subject to discussion, but it has been found that bone remodelling processes are triggered by mechanical stimuli, such as microcracks^{45,46}. Osteocytes are suspected of transmitting the stimulus⁴⁵. However, the cellular activity within bone tissue is clearly related to mechanical stress.

On the one hand, stress adaptation of bone leads to bone formation, where long-term loading is increased. On the other hand, long-term reduction of load corresponds to reduced mechanical stimulus, which causes bone resorption in the corresponding region. Especially with regard to joint implants, bone resorption is a crucial aspect. Joint implants

bear and transfer cyclic dynamic load that greatly exceeds the body weight. Established implant materials, such as cobalt-chrome (CoCr) and titanium (Ti), exhibit high fatigue strength but also a high stiffness, greater than that of bone ($E_{\text{CoCr}} \approx 225 \text{ GPa}$ $E_{\text{Ti}} \approx 114 \text{ GPa}$, $E_{\text{bone}} \approx 20 \text{ GPa}$). Loading on the implant will be transferred via the implant; the adjacent bone tissue is “stress-shielded” and resorbs due to the lack of mechanical stimulus. This has been shown by Miller *et al.*⁴⁷ who found empty cavities in the cement layer of implant fixations that have been attributed to resorbed trabecular bone. The loss of bone due to stress shielding leads to demineralisation of bone stock, which is a major problem with regard to long-term implants. The implant may be exchanged in a revision surgery, if its functionality is impaired or an infection occurs. Due to the foregoing bone resorption, less bone is available for stable implant fixation in revision, which is addressed by revision-specific implants with a larger anchorage area to cover the regions of remaining bone that provide stability. These initially unaffected regions are now under risk of bone resorption. Overall bone loss increases with each revision surgery, thereby progressively complicating the anchorage of the new implant. Reduction of stress shielding and optimised load transfer between implant and bone regarding mechanical stimulus is as crucial for the patient as postponing revision surgery.

2.2 Anatomy and Function of the Human Knee Joint

The knee joint (articulatio genus) transfers loads between femur, tibia and patella (**Figure 2-5**). Anatomically, the joint between the fibula and tibia is part of the knee joint but, since it does not influence the research questions, it will not be discussed further in this study. The knee joint comprises three articulating surfaces between three bones. The proximal tibia articulates with the distal femur (**Figure 2-5**, left). The tibial plateau is sub-divided into two compartments — lateral and medial — each in contact with the respective femoral condyle. The third joint is formed by the posterior surface of the patella and the patellar surface of the distal femur.

Both compartments of the tibial plateau are rather flat and covered by hyaline cartilage (**Figure 2-5**, left). The medial plateau is biconcave and lies somewhat lower than the lateral compartment. The latter is concave in the transverse plane and convex in the sagittal plane. The medial compartment is larger than the lateral. The bearing circumference of the sagittal profile of the distal femur is larger than the corresponding line on the tibial plateau. The femoral condyles have an evolvent-like shape in the sagittal plane. From posterior to anterior, the evolvent radius becomes smaller with overall larger radius at the lateral condyle (**Figure 2-5**, left). The bearing areas of tibia and femur are incongruent. Congruent contact is generated by the menisci, two half-circles of fibrocartilage on the tibial compartment (**Figure 2-5**, right). The ends of the menisci are attached to the tibial plateau close to the intercondylar area. The remaining meniscal structure lies movably on the tibial cartilage. The geometry of the bony structures of the knee basically corresponds to two cylinders moving on a plate, and relatively to it, however, the knee joint movement is actually not restricted by the bony geometry.

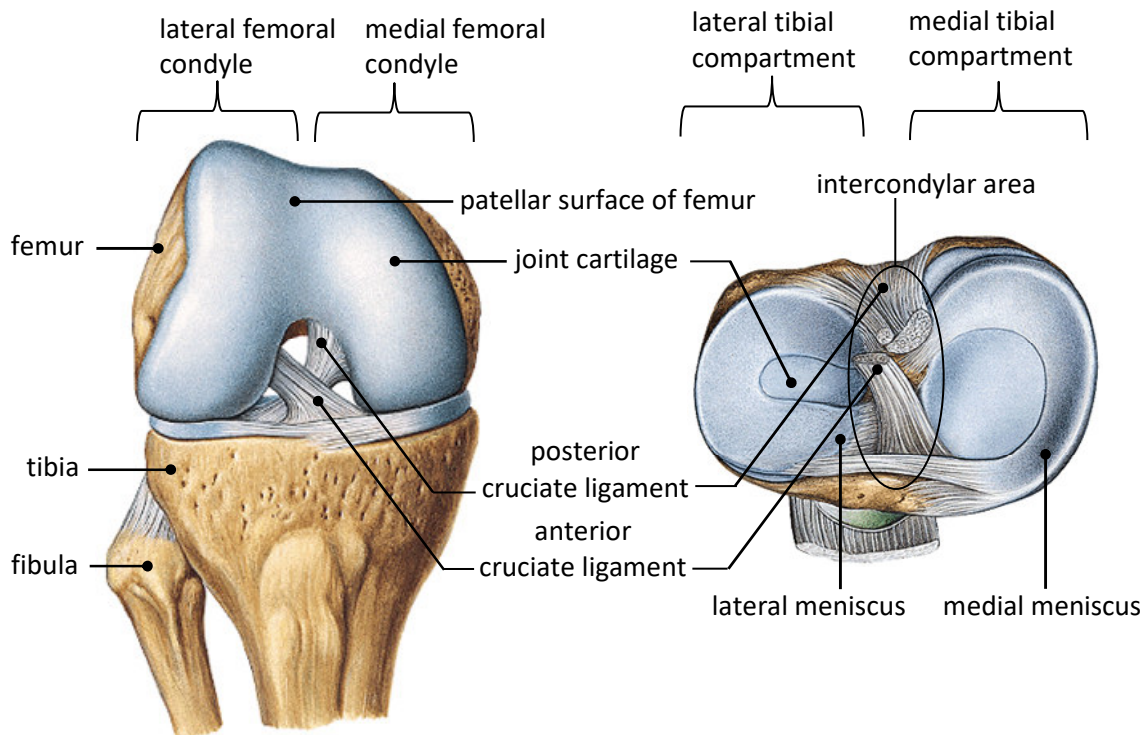


Figure 2-5: Anatomy of a right knee joint. Left: Anteroposterior view of the flexed knee joint, patella is not displayed. Right: Top view of the tibial plateau with cartilage, menisci and cruciate ligaments. [Adapted from Sobotta⁴⁸]

In extension, the patella is positioned ventrally and centrally to the femoral condyles in the patellar surface of the femur (facies patellaris femoris). It is cranially connected with the musculus (m.) quadriceps femoris and caudally with the patellar ligament to the tibia (**Figure 2-6**). Femur and tibia are connected by four ligaments: the medial and lateral collateral ligament (**Figure 2-6**) and the anterior and posterior cruciate ligaments (**Figure 2-5**, left). The anterior cruciate ligament (ACL) stretches from the medial anterior tibia to the lateral posterior femur. The posterior cruciate ligament (PCL) stretches from the lateral posterior tibia to the medial anterior femur. They are twisted with each other around the inferosuperior axis (**Figure 2-6**, left). The collateral ligaments are slightly twisted in the other direction. In extension, the collateral ligaments are in tension, while the cruciate ligaments are relaxed. In flexion, the collateral ligaments are relaxed and the cruciate ligaments are in tension. This indicates a rotation around the shaft axis from extension to flexion. Both movements — internal-external rotation and extension-flexion — are restricted by these four ligaments. The knee motion is guided by the soft tissue structures and not by the hard tissue geometry.⁴⁹

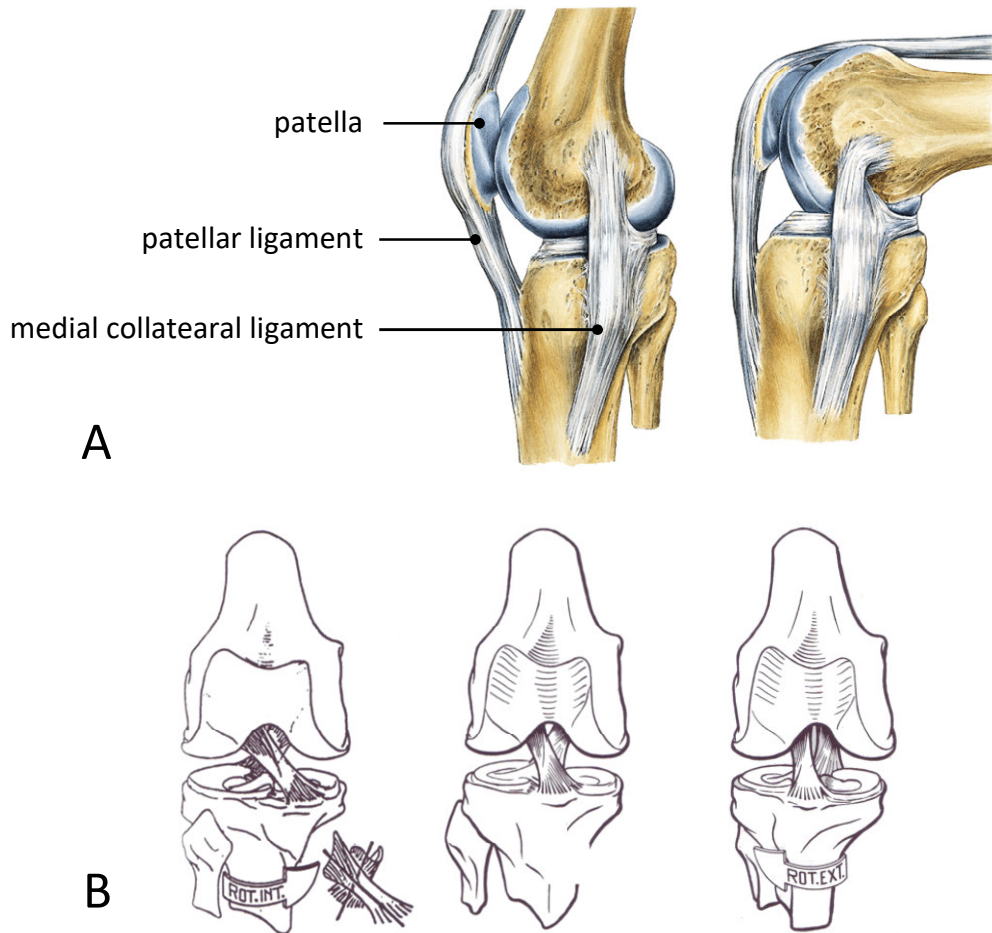


Figure 2-6: Kinematics of the knee joint. A) Medio-lateral view of a right knee in extension-flexion. Left: In extension, the patella is positioned ventrally to the distal femur, collateral ligaments are tensed. Right: In flexion, the patella is positioned superiorly to the femoral condyles, collateral ligaments are relaxed. [Adapted from Sobotta⁴⁸] B) Frontal view of a right knee in rotation, neutral position displayed in central image. Left: Internal rotation with further twisting of the cruciate ligaments. Right: External rotation with untwisting of ligaments. [Adapted from Kapandji⁴⁹]

The range of motion of the knee is 0° to 120° in flexion with an extended hip joint. With a flexed hip joint, up to 140° active flexion is possible. This phenomenon is due to the position of the three muscles of the pes anserinus group (m. sartorius, m. gracilis, m. semitendinosus) and the m. semimembranosus (**Figure 2-7, A**). They originate at the pelvis and insert medially at the proximal tibia. They are less tensed when the hip joint is flexed and thereby allow wider flexion of the knee joint. The range of active motion of the knee joint is not solely determined by the ligaments but also by the preload of the muscles due to hip flexion. However, passive flexion may approach 160° .⁴⁹

The antagonist of the flexing pes anserinus group is the quadriceps femoris, four muscles (M. rectus femoris, M. vastus medialis, M. vastus intermedius, M. vastus lateralis) that originate at the proximal femur and the pelvis and share a tendon that inserts at the tuberositas tibiae on the ventral side of the tibia (**Figure 2-7, A**). The patella is integrated within the tendon and guides it over the femoral condyles during flexion and extension. The patella thickness increases the lever arm for the quadriceps force with respect to the

centre of flexion (**Figure 2-7, B**). The patella itself is guided within the facies patellaris femoris. Relative position and contact area between patella and femur change over flexion-extension. Minor changes in the soft tissue structures around the knee joint may crucially affect the kinematics and loading conditions within the joint.⁴⁹

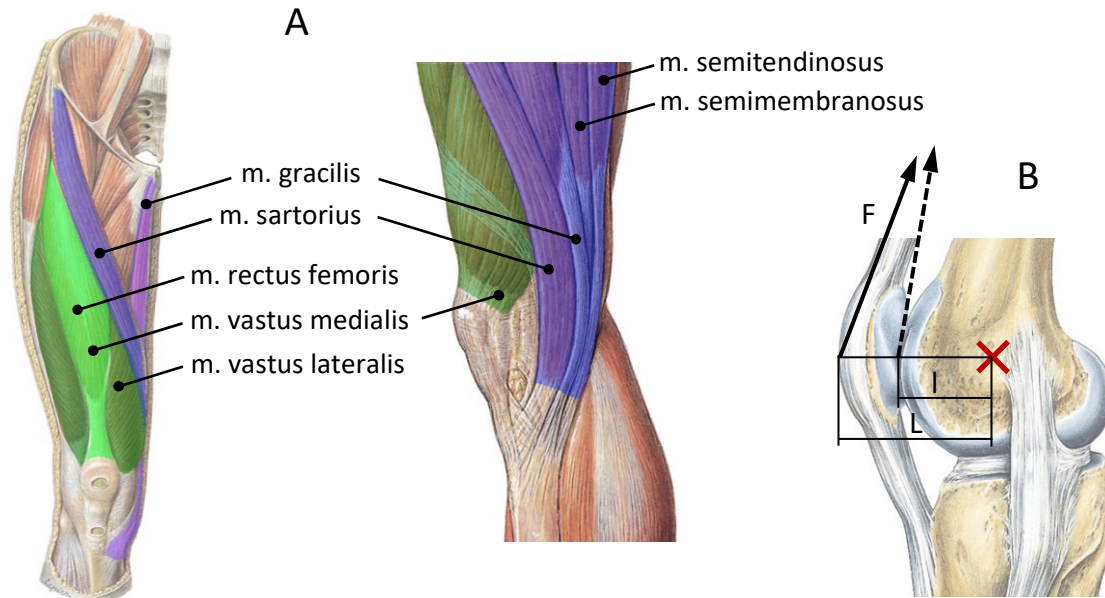


Figure 2-7: A: Muscles for flexion and extension of the knee joint, extension muscles are highlighted in green, flexion muscles are highlighted in blue. Left: Front view (m. semitendinosus, semimembranosus, vastus intermedius are not visible). Right: Medio-lateral view (m. rectus femoris, vastus lateralis, vastus intermedius are not visible). B: The patella increases the lever arm for the quadriceps extension force (F) with respect to the centre of flexion (red mark). [Adapted from Sobotta⁴⁸]

In full extension, an external rotation of the tibia with respect to the femur occurs, referred to as “terminal” rotation. This is due to the shape of the profile of the lateral condyle that is longer than the medial one, and the sagittally concave shape of the lateral tibial compartment. In addition, full tension of the medial collateral ligament is reached earlier from flexion to extension than full tension of the lateral collateral ligament, shifting the rotation centre to the lateral side. The terminal rotation is an axial external rotation of the tibia with respect to the femur of about 20° from knee flexion to extension. The range of anterior-posterior shift of the load transferring contact areas is larger on the lateral tibial compartment than on the medial, due to a multi-layered movement (flexion-extension and internal-external rotation)⁴⁹.

The motion of the femoral condyles relative to the tibial plateau in the sagittal plane is determined by the cruciate ligaments and inhibits rolling and sliding portions. From extension to flexion, first, the sliding range is restricted by the stiffness of the almost horizontal PCL and the femur predominantly rolls on the tibial plateau (**Figure 2-8, A left**). During flexion, the evolvent radius of the femoral condyles becomes smaller (smaller distance between rotational axis of the condyles and joint contact area) and the orientation of the PCL becomes more vertical, which enables sliding in a horizontal direction. The slide proportion within the movement becomes larger with progressing flexion. In deep flexion, sliding only is present⁴⁹ (**Figure 2-8, A right**). This movement is

referred to as rolling-sliding motion of the knee joint. Due to the rolling share, the contact point between femur and tibia is shifted to the posterior tibial plateau (**Figure 2-8, B**).

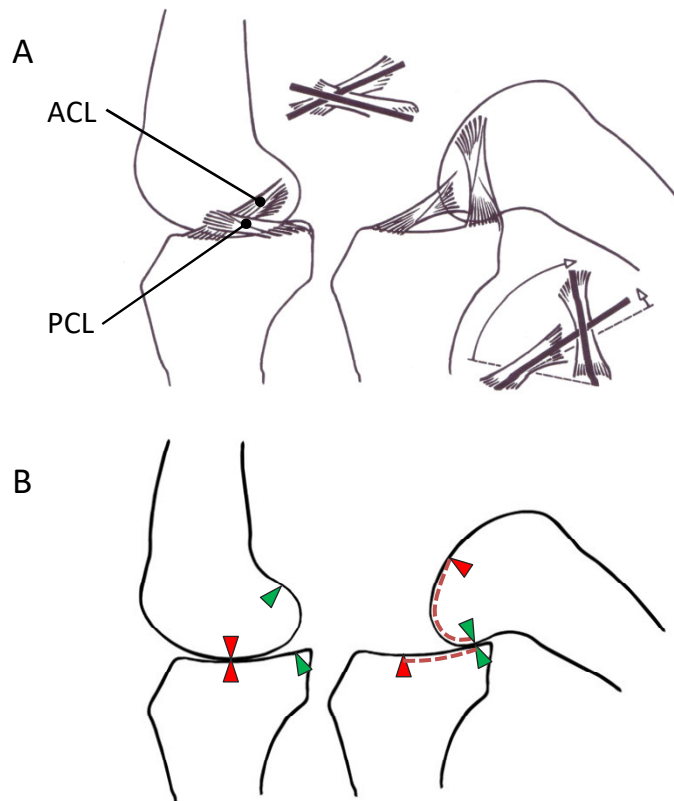


Figure 2-8: Sagittal view of the knee joint kinematics in extension-flexion. A: Cruciate ligaments. Left: In extension, the PCL is positioned almost horizontally and restricts further movement of the femur in the anterior direction: Right: In flexion, the PCL is positioned almost vertically; the ACL restricts further movement of the femur in the posterior direction. B: Contact point motion, the contact point is indicated by triangles (red in extension and green in flexion). The motion path is longer on the femur than on the tibia, indicating sliding portions during extension-flexion. [Adapted from Kapandji⁴⁹]

2.2.1 Anatomical and Mechanical Axis

For description of the knee joint, the mechanical and the anatomical axes are used. The mechanical axis (MA) is the straight line from the centre of the femoral head to the centre of the ankle joint. This line deviates about 3° from the vertical axis (therefore 87° to the horizontal by 87° , **Figure 2-9**). The anatomical axis (AA) is subdivided into a femoral and a tibial part, both aligned to the corresponding intramedullary canal. The femoral part therefore deviates 5° to 7° from the mechanical axis (80° to 82° to the horizontal), whereas the tibial part coincides with the mechanical axis. Both axes are used in endoprostheses positioning planning in the frontal plane (Section 2.3.2.3).⁵⁰

Consequently, the angle between the anatomical axes of tibia and femur is about 173° to 175° . Anatomically, the knee is in slight valgus position. A knee joint with smaller tibial-femoral angle is called valgus knee (genu valgum). Deviation in the other direction is referred to as a varus knee (genu varum). Another approach of this is based on the mechanical axis. Physiologically, it intersects the anatomical centre of the joint.

Mechanical and anatomical centre coincide. In a valgus knee, the knee is shifted medially with respect to the mechanical axis, with the load centre in the lateral compartment. In a varus knee, the knee joint is shifted laterally, with the load centre in the medial compartment.⁴⁹

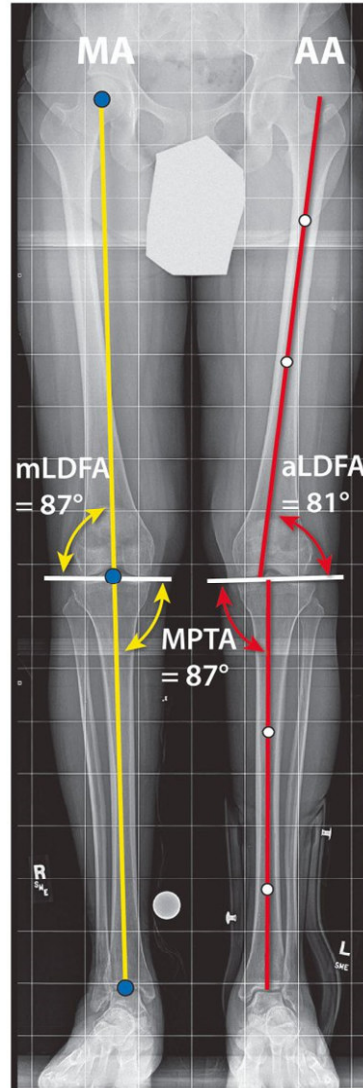


Figure 2-9: Mechanical axis (MA, yellow line) and anatomical axis (AA, red line) and corresponding angles (mechanical Lateral Distal Femoral Angle mLDFA, anatomical Lateral Distal Femoral Angle aLDFA, Medial Proximal Tibial Angle MPTA). [Reproduced from Cherian *et al.*⁵⁰]

2.2.2 Load on the Knee Joint

Load on the knee joint is shared between medial and lateral compartments. Due to the natural slight valgus position of the knee, the centre of pressure tends to lie in the medial compartment. Correspondingly, load during gait has been found to be predominantly transferred via the medial compartment^{51–53}. 55 % to 85 % medial load share has been determined in instrumented TKA during gait⁵³. This has also been shown for stair ascending and descending, although the medial share was 50 % to 72 % and thus lower than during normal gait⁵⁴. The medial load share being larger than the lateral coincides with the medial plateau area being larger than the lateral, resulting in similar bone stress

below the lateral and medial compartments. Based on biomechanical considerations, the overall maximum load on the tibial bearing areas during gait has been calculated, resulting in up to six times body weight (BW)⁵⁵.

Kutzner *et al.*⁵⁶ measured the load on a tibial component of a total knee replacement using an instrumented implant. A resultant load of 2.6 times body weight was determined for normal gait (**Figure 2-10**). Similar loads were reported for both healthy and osteoarthritic patients⁵². Shear force found by Kutzner *et al.*⁵⁶ was rather low at 26 % BW in a posterior direction and 18 % BW in an anterior direction, accounting for less than 10 % of the overall load.

Bergmann *et al.*⁵⁷ investigated several activities (walking, stairs ascending and descending, sitting on and rising from a chair and deep knee bend) using instrumented knee prostheses. The maximum values for the resulting force were reported for rising from a chair (280 %BW: ~3,800 N) and descending stairs (311 %BW: ~4,200 N). Values for deep knee bend were lower than for rising from a chair, although the flexion angle was larger. Cyclic anterior-posterior shear force was below 100 N in both directions in high-flexion activities and the maximum value was detected in a posterior direction. Medio-lateral shear forces were lower than those in the anteroposterior direction.

Shear loads on tibial trays are small compared to compression, even in high flexion. The focus of this study is on knees with arthroplasties, therefore consideration of the load data of Kutzner *et al.*⁵⁶ and Bergmann *et al.*⁵⁷ is appropriate.

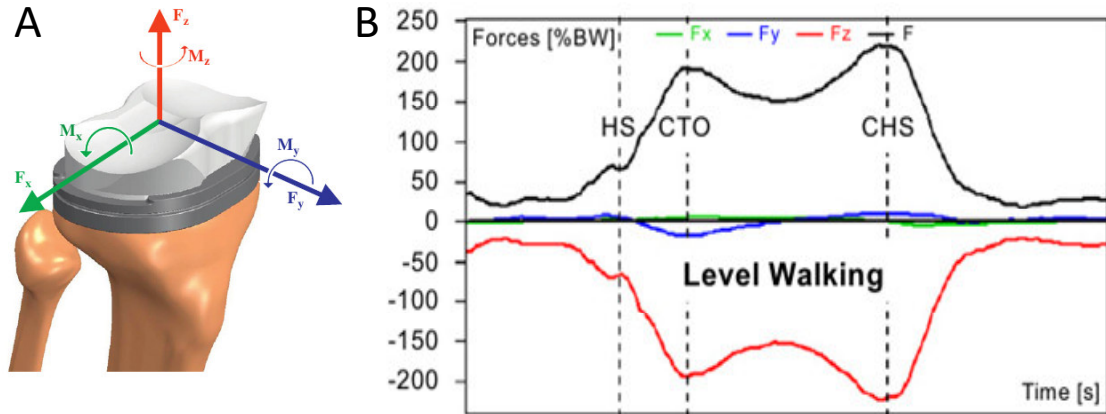


Figure 2-10: Load on the tibial component during gait. A: Coordinate system of the recorded load [adapted from Kutzner *et al.*⁵⁶]. B: Characteristic load pattern within a patient during level walking. The displayed diagram covers one gait cycle (peaks reflect swing phase of opposite leg and push-off for own swing phase). Major force component F_z is in axial compression direction. Shear force is considerably smaller. [Adapted from Kutzner *et al.*⁵⁶]

2.2.3 Indications for Total Knee Arthroplasty

Articular cartilage is not vascularised, so nourishment is provided by diffusion and via fluid flow due to pressure changes generated by knee joint loading. Decreased permeability of the tissue for nutrients leads to ensuing fissures and thinning of the cartilage. This degenerative process is called osteoarthritis and cannot be reversed. Osteoarthritis is a chronic process of joint cartilage erosion, which occurs due to aging, but is intensified to a pathological stage by mechanical factors, such as long-term

overload. One important factor in this is a primary or secondary^b injury of the meniscus that is accompanied by increased load on the cartilage^{58–60}. Varus and valgus deformations also lead to non-physiological loading.^{37,49,61}

The end stage of osteoarthritis is characterised by bone-on-bone articulation. In contrast to bone, healthy cartilage is not innervated, which enables pain-free movement of the joint. Even before the cartilage has completely degenerated, movement of the joint becomes extremely painful due to irritation of the bone nerves. When life quality is severely reduced due to local malfunction of the knee joint, the articulating surfaces are replaced by artificial materials. Osteoarthritis of the knee joint is reported as the major reason for knee replacement surgery (97 % to 98 % of the procedures)^{2,3}. Rheumatoid arthritis is another typical indication, but with a much lower incidence of less than 1 %². Further reasons for joint replacement are bone cancer resections and trauma¹.

In some cases, cartilage erosion is restricted to one of the joint compartments. Unicompartamental knee arthroplasty (UKA) may be sufficient. This study focuses on total knee arthroplasty (TKA) procedures that cover both compartments. The conclusions may be transferable to UKA.

Arthroplasty procedures are the gold standard for treating end-stage osteoarthritis. Quality regarding surgical technique and implant designs has to be assured, which has led to the introduction of Arthroplasty Registers in many countries worldwide. For assessment, the Registers comprise executed procedures in the respective country, along with detailed information about indication, implant and technique, particularly with regard to survival of the implant. Commonly consulted Registers with long observation periods are the Swedish¹ and the British² Registers, as well as the Australian Register³. The German Register was started in 2012. Reliable data analysis is expected within 5 to 7 years after initialisation⁶².

2.3 Total Endoprostheses in Knee Joint Reconstruction

In 2013, about 143 000 primary TKA procedures were carried out in Germany. The number increased steadily from 2005 to 2008 and, correspondingly, the number of revision surgeries^{63,64}. An international survey in 2011 found a steady increase of the combined number of primary and revision procedures per year (from 5.3 % in France to 17.0 % in Portugal)⁶⁵. A mean rate of 175 procedures per 100 000 inhabitants — 15 of these revisions — was reported on the basis of data from 18 countries⁶⁵. Data of the Statistisches Bundesamt indicate that the number of primary procedures in Germany has stagnated since 2009^{6,66–71} (**Figure 2-11**). This was also found by a study from the Deutsche Gesellschaft für Orthopädie und Orthopädische Chirurgie⁷², while the Swedish Register continues to report increasing numbers^{1,73–75}.

Both analyses of the German data are based on general hospital statistics, combining UKA and TKA to “primary knee reconstruction” (diagnostic code 5-822), whereas the Swedish Register reports data for TKA and a shift from UKA to more TKA procedures¹. TKA and its revision have a high incidence, both in Germany and internationally. Only detailed arthroplasty-specific Registers can provide sufficient data for quality assessment.

^b For example following ligament rupture

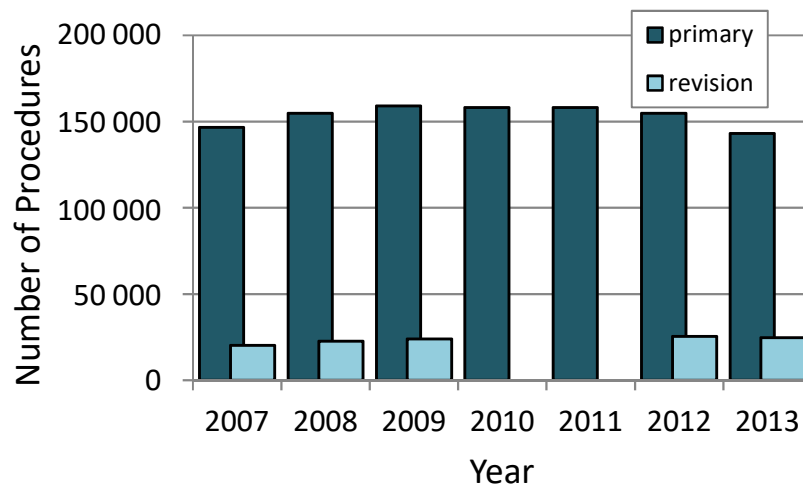


Figure 2-11: Number of diagnoses for primary and revision TKA procedures in Germany determined by application of diagnostic code, not differentiating between UKA and TKA. 2010 and 2011 reports were limited to the 50 most frequent surgical procedures, thereby excluding TKA revisions. [Data from Statistisches Bundesamt^{6,66-71}]

2.3.1 Evolution of Modern Implant Design

The first knee joint replacements were implanted in 1890 by Themistocles Gluck⁷⁶. They were hinged joints made from ivory and consisted of a femoral and a tibial component, both stemmed for fixation in the respective diaphysis (**Figure 2-12**, left). Infections required removal of the implants. Further evolution was triggered by the success of the hip joint replacement in the 1940s. In 1947, the Judet brothers developed several joint replacements made from acrylic resin — the developed knee joint was a hinged joint again — but had to capitulate to material failures.

The first metal implants were introduced by Walldius in 1951. The material was Vitallium, a chromium cobalt molybdenum alloy, which is still a standard material in artificial joints. The first actual surface replacement was implanted by Gunston in 1969 and was inspired by Sir John Charnley's introduction of tribologically favourable polyethylene (PE)-metal pairings and polymethyl methacrylate (PMMA) fixation for hip joints in 1961. These improvements led to Gunston's concept of an uncoupled femoral component that articulates with a tibial inlay, which is still the basis of modern implants (**Figure 2-12**, right).⁷⁷

The stems of the early implants were destined for anchorage within the diaphysis and were accordingly long. Increased shear resistance and reduced micromotion were shown for these stems⁷⁸. Direct load transfer to the diaphyseal bone may be directly to cortical bone, allowing stable anchorage even in low bone quality⁷⁸. However, this is accompanied by stress shielding of the proximal trabecular bone that may lead to bone resorption of the shielded but initially healthy bone stock⁷⁹. Loosening and migration may follow, so that long stems are rather used in revision procedures today, where the proximal bone is already impaired and stable anchorage is in the foreground (**Figure 2-13**, C).

Today's implants for primary TKR provide short stems in both femoral and tibial components. They are anchored in the metaphyseal bone in order to reduce stress

shielding of this region. Both components are made from metal, either titanium (Ti) or cobalt chromium (CoCr) alloys, less frequently ceramics or ceramic coating in the case of allergy.

The focus of the following is put on the tibial component — the tibial tray. The tray is placed on the bony plateau and the short stem secures the translational position. The implants may exhibit keels, which appear as reinforcing rib, perpendicular to the stem surface and tray surface and are intended to provide rotational stability (**Figure 2-13**, A and B). This design of the tibial tray enables transfer of all occurring loads within the metaphyseal region.

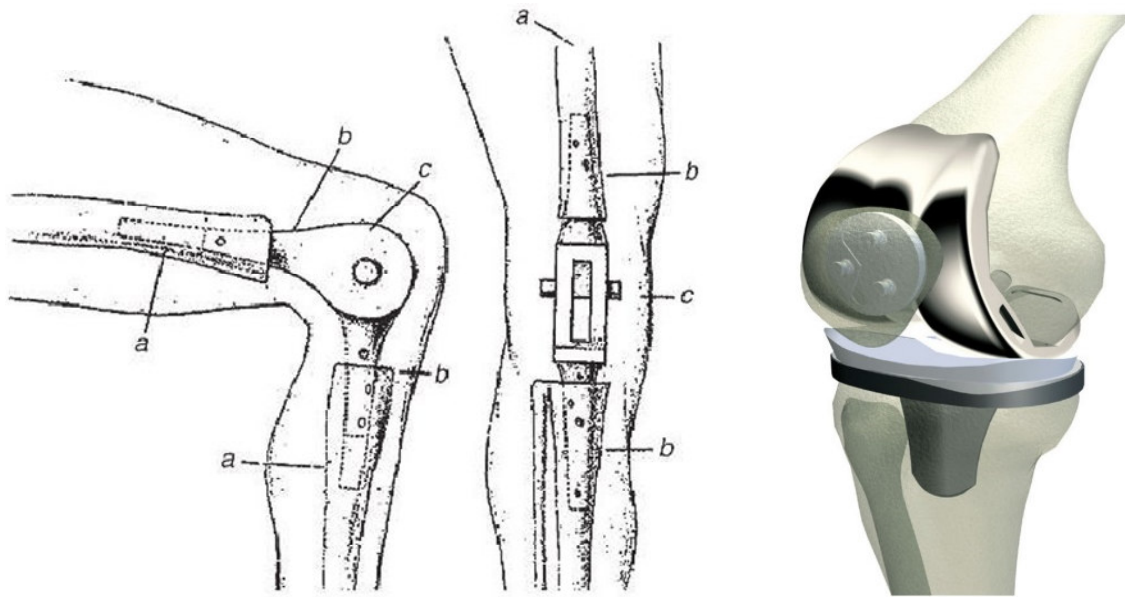


Figure 2-12: Development of knee joint replacement. Left: Ivory implant developed by Gluck in 1890 [adapted from Wirtz *et al.*⁷⁷]. Right: Modern surface replacement with femoral and tibial component, and a tibial inlay [adapted from bonesmart.org⁵]. The radius of the inlay articulation surface is larger than that of the condyles, allowing for anterior-posterior shift during flexion.

The soft-hard pairing between PE and metal in connection with the high loads described in Section 2.2.2 leads to a new challenge: wear of the PE inlay. PE particles provoke adverse immune reactions, the precise mechanisms of which are unclear but probably multi-layered⁸⁰. They lead to osteolysis and thereby to aseptic loosening of the implant⁸⁰. A worn PE surface even accelerates the wearing process, leading to cumulative adverse effects⁸¹. Ablation and cracks within the inlay lead to failure of the inlay. Wear-related degradation of the inlay appeared to be more severe in TKA than in THA, which probably reflects the larger contact stresses in TKA⁸¹.

In the late 1990s, reduction of the wear rates was achieved by introducing highly cross-linked PE, which was produced by high-energy irradiation of standard PE⁸⁰. However, particle-induced osteolysis remains a problem and, apart from material-related approaches, reduction of wear may be addressed by reducing the stress within the material.

Improvement of the load distribution in the tibial inlay was intended with new designs of the inlay that consider the physiological motion of the joint and/or reduce stress during

loading. Two design approaches were evolving at the same time: the anatomical and the functional approaches. In the anatomical approach, preferably all soft tissue structures are left and the artificial components are designed such as to prevent conflict with these structures. In the functional approach, emphasis is on the artificial structures, which requires either simplification of the knee kinematics — by resecting the cruciate ligaments — or transferring kinematics to the components of the arthroplasty. Two typical design types evolving from the anatomical and the functional approaches are the cruciate-retaining design and posterior-stabilised design, respectively.⁸²

In the cruciate-retaining design, the PCL is kept intact. TKA components exhibit recesses at the posterior side to leave the PCL kinematics unaffected (**Figure 2-13, A**). The prerequisite is a fully functional PCL. In a native knee, the PCL restricts anterior shift of the femur on the tibia and thereby introduces the rolling share in knee rolling-sliding motion during flexion.

If the PCL cannot be kept, this function has to be taken over by the prosthesis components. The femoral component posteriorly exhibits a horizontal rod between the condyles and the inlay surface is heightened in the central area, which results in a central peg (**Figure 2-13, B**). During flexion, the femoral rod abuts against the peg, thereby restricting the anterior shift of the femoral component on the tibial plateau. This design is referred to as posterior-stabilised. Both designs attempt to restore the rolling-sliding motion, now executed by the metallic femoral component on the PE inlay.

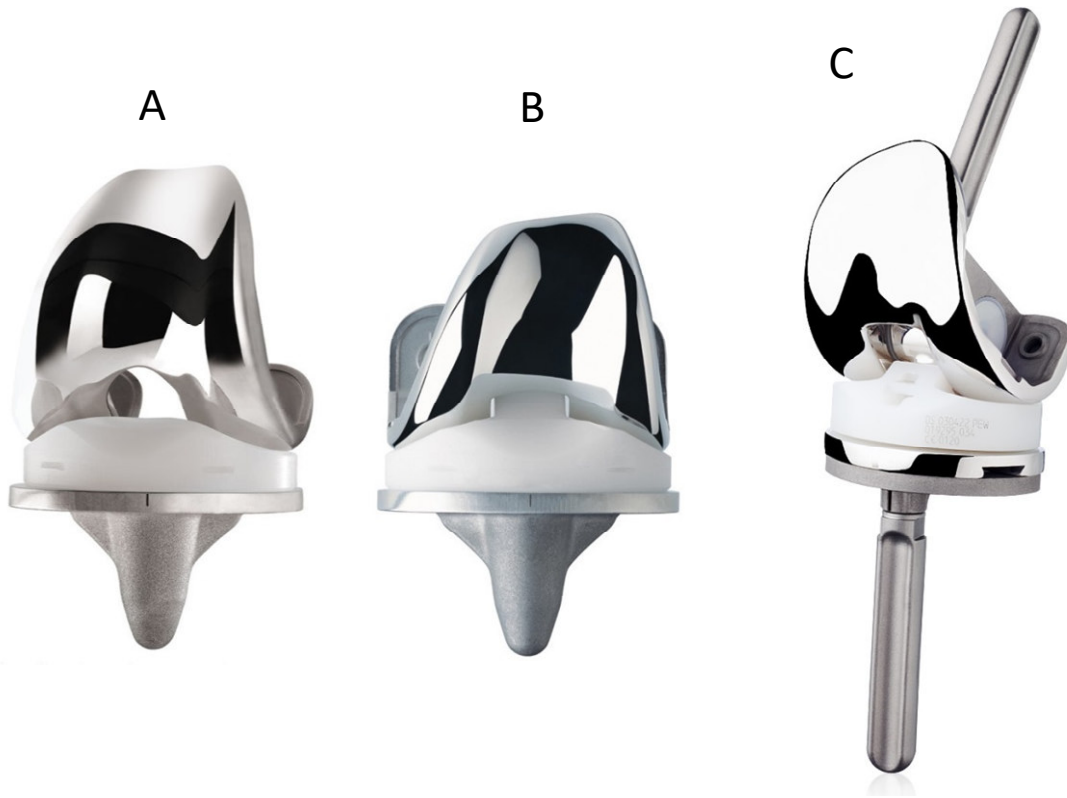


Figure 2-13: Implants with different degrees of freedom. A: Surface replacement with uncoupled femoral and tibial components [reproduced from kneereplacement.com⁸³], B: Posterior stabilised surface replacement with a central peg that constrains medial lateral shift [reproduced from depuyorthopaedics.com⁸⁴]; both A and B exhibit keels between stem and tray to provide rotational stability. C: Modern hinged implant for cases with lost ligaments. The stem is long for diaphyseal anchorage [reproduced from globalortho.com.au⁸⁵].

As mentioned before, knee kinematics is a multi-layered movement. During extension and flexion, simultaneous axial rotation occurs between tibia and femur. Motion on the PE is not uniform in anteroposterior direction, but rather overlain by a rotational movement, applying cross-shear to the PE surface. In a simulator study, cross-shear has been shown to increase PE wear⁸⁶. This has been attributed to the characteristic nature of PE molecules to orient towards a sliding direction⁸⁶. Load in a deviating direction shears the molecules and produces even more wear. An attempt to separate the overlying motion directions is the mobile-bearing or rotating-platform design. The inlay lies rotatably on the tibial tray, only fixed to it in the centre. The concave shape of the inlay compartments are formed to guide the femoral condyles without allowing for rotation. However, the mobile bearing design appears to be less forgiving to malpositioning of the implant components⁸⁷. The shape of the inlay plays an important role in the kinematics of a reconstructed knee.

Low congruence of femoral condyles and inlay surface shape decreases the contact area and thereby increases the stress in the PE inlay. Wear has been shown to be lower in low-congruence bearing, than in highly congruent bearings, which has been attributed to the lower contact area⁸⁸. The larger contact stress with smaller contact area appeared to be of low impact. Tribological behaviour of PE is multi-layered and the influences of such

design modifications on the clinical performance are often controversially discussed^{87,89,90}. Aspects of a specific design may only become negative when accompanied with inappropriate fixation or loading, or malpositioning of the components^{91,92}. In that manner, some implants may be more forgiving than others^{87,93,94}.

2.3.2 Fixation of the Tibial Tray in Total Knee Arthroplasty

In TKA and THA, cemented and cementless fixation methods are applied. Cementless fixation is based on press-fit between implant and bone and finally aims at bone ingrowth or ongrowth (**Figure 2-14, A**). Healthy bone stock is required as well as an unloaded period post-surgery. The implant surface is commonly structured and appears rough. It may be coated with hydroxyl apatite, which promotes bone ingrowth and ongrowth. In cemented fixation, PMMA is introduced between implant and bone in a doughy state. The dough cures within the body and forms an interlock with the porous trabecular bone, working as a grout (**Figure 2-14, B**). The surface of the implant is smooth. Cemented and uncemented implant fixation are based on different fixation concepts.

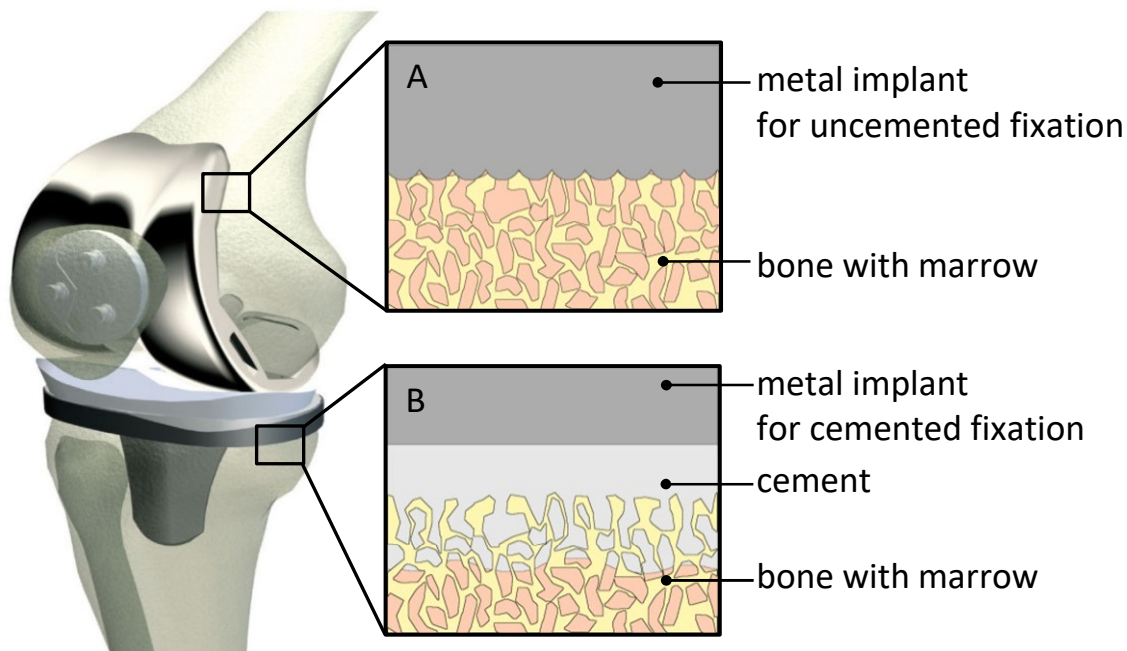


Figure 2-14: Fixation methods for joint implants. A: Uncemented, the implant surface is rough or porous to enable bone ingrowth or ongrowth [adapted from bonesmart.org⁵]. B: Cemented, bone cement penetrates the trabecular bone.

Cementless fixation is successful in THA, especially in patients under 65 years of age⁹⁵. In TKA, cementless fixation appears less favourable than cemented, in particular with regard to the tibial component: Early^c migration is larger for uncemented tibial trays than for cemented^{7,96}. However, the femoral component is more forgiving and may be inserted cementless, in combination with a cemented tibial tray, referred to as hybrid fixation⁹⁷⁻⁹⁹. The different outcome of femoral and tibial components regarding cemented fixation may be attributed to different loading. Loading on the femoral component is largely dependent on the flexion angle, which is also the case for THA components, but not for the tibial tray,

^c Commonly refers to a time period within 5 years after surgery²²⁵

which is loaded in compression (Section 2.2.2). Osseointegration in cementless fixation might be seriously impaired by predominant uniaxial loading. Nevertheless, cemented tibial trays are in about twice as much danger of aseptic loosening than uncemented trays⁹⁶. Summarising, cementation prevents migration of the tibial tray, but improvement is required regarding later aseptic loosening.

2.3.2.1 Properties of Bone Cement

Cemented fixation refers to fixation using a PMMA-based two-component polymer (Figure 2-15). In 1958, Charnley used PMMA for the first time to anchor femoral hip prostheses to the bone¹⁰⁰. This was a milestone in hip arthroplasty and promoted the development of arthroplasty in general. The two components are liquid methyl methacrylate (monomer) and a powder that contains pulverised PMMA and benzoyl peroxide that initialises the polymeric reaction. For visibility in radiographs, a radiopaque material is added, such as zirconium dioxide.

When the two components are combined, benzoyl peroxide initialises an exothermic polymerisation process. Adverse tissue reactions like necrosis and corresponding aseptic loosening have been associated to polymerisation heat¹⁰¹. The polymerisation temperature in bulk cement can reach up to 80°C¹⁰². However, maximum temperatures *in vivo* were measured as 48°C which is below protein-impairing temperature (56°C). Determining factors for the relatively low temperature are heat dissipation via the surroundings (interdigitated tissue, blood circulation, implant) and the short time period in which high temperatures are developed. Areas of pure cement where the heat could accumulate are very thin^{100,103}. The volume of introduced cement should be as small as possible to prevent development of high temperatures.

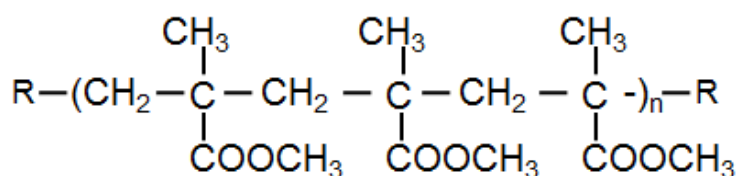


Figure 2-15: Chemical formula of polymethyl methacrylate (PMMA).

In the cured material, PMMA appears in the form of spheres of about 20 µm to 160 µm diameter that are embedded in a matrix of secondarily polymerised methyl methacrylate (Figure 2-16). The radiopaque additive zirconium dioxide is not part of the polymer but located between the PMMA beads. It does not affect the PMMA matrix. Although appearing homogeneous, PMMA is a composite of two phases.¹⁰⁴

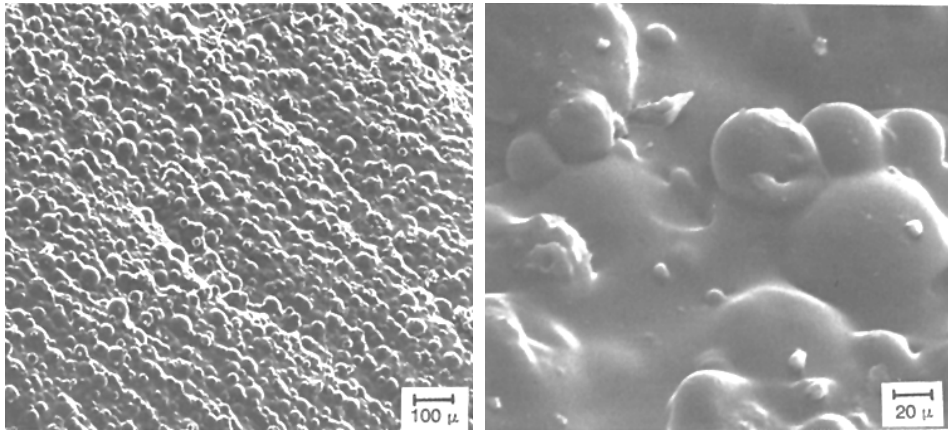


Figure 2-16: Electron microscope scans of bone cement that polymerised *ex vivo*. Spherical PMMA beads and smaller granules of additives are embedded within a matrix. The surface appears closed and continuous. [Adapted from Willert *et al.*¹⁰⁴]

Willert *et al.*¹⁰⁴ investigated PMMA samples that polymerised *in vitro* or *in vivo*. The surface of the *in vivo* polymerised samples exhibited a more inhomogeneous surface with occurring flattened beads or rough topology. They observed an open surface appearing as a rather porous structure and concluded that the PMMA polymerisation is influenced by the surrounding tissue. The effect of the modified surface remained unclear notwithstanding. A tendency to microfractures and breaking off of prominent polymer beads was suspected by the authors (**Figure 2-17**). Resulting free PMMA particles may provoke adverse tissue reactions, as already discussed for PE particles. This effect will be explained in more detail in the context of loosening in Section 2.3.3.

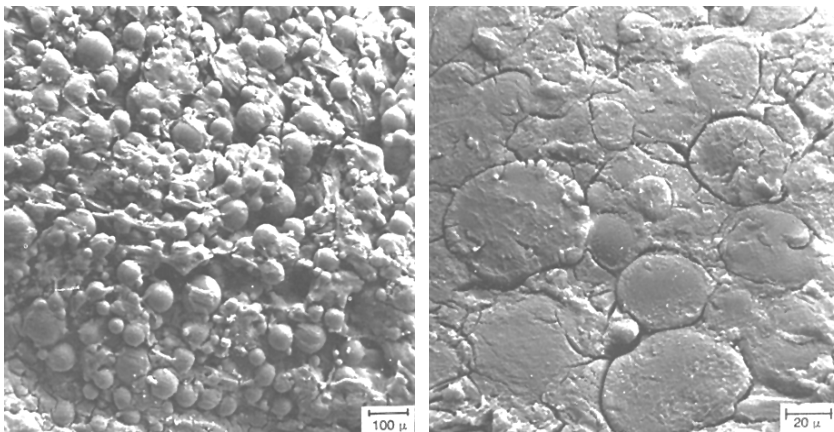


Figure 2-17: Surface of PMMA sample retrieved from surgical revision. Left: Surface appears porous with protruded beads that may break off when loaded. Right: Flattened beads. [Adapted from Willert *et al.*¹⁰⁴]

The mechanical properties of bone cement PMMA are standardised by ISO 5833:2002 “Implants for surgery — Acrylic resin cements”. In contrast to metals, polymers such as PMMA do not exhibit an endurance limit, which is the magnitude of cyclic stress below which infinite load cycles are possible without material failure¹⁰⁵. Thus, PMMA fails under fatigue load, regardless of load magnitude, but the actual number of cycles to failure decreases with increasing stress¹⁰⁶. Further, the fatigue crack growth rate in mechanical

testing has been found to increase with ageing of the material¹⁰⁷. As such, increasing time *in situ* reduces the fatigue limit of bone cement.

Today, high- and low-viscosity bone cements as well as intermediate types are offered for orthopaedic surgery. The time to setting is comparable between types (9 to 12 minutes). Low-viscosity cement offers low resistance to shear deformation and can be applied using syringes with small nozzles. It is commonly used for vertebroplasties where cement will be introduced into the vertebral body for fortification via a cannulated screw or a cannula. Low-viscosity cement is not suited for manual handling, since the doughy state is reached later, resulting in shortened working time. Low-viscosity cement was shown to penetrate less deeply in tibial TKA than high-viscosity cement. This is due to the lower pressure necessary for correct implant positioning (squeeze film effect^d)¹⁰⁸. In joint arthroplasty, high-viscosity cement is commonly used, but some intermediate types may also be appropriate.^{2,109–111}

2.3.2.2 Properties of Trabecular Bone in the Tibial Head

Trabecular bone is a porous network made up of connected rod- and plate-like elements in varying proportions^{30,31} (**Figure 2-18**). Rod-like structures are 0.05 mm to 0.30 mm thick and 0.50 mm to 1.50 mm long^{31,112}. The proportion of rods and plates, their geometry, as well as the orientation of the structure are pivotal for the mechanical properties of trabecular bone and depend on regional loading³⁰.

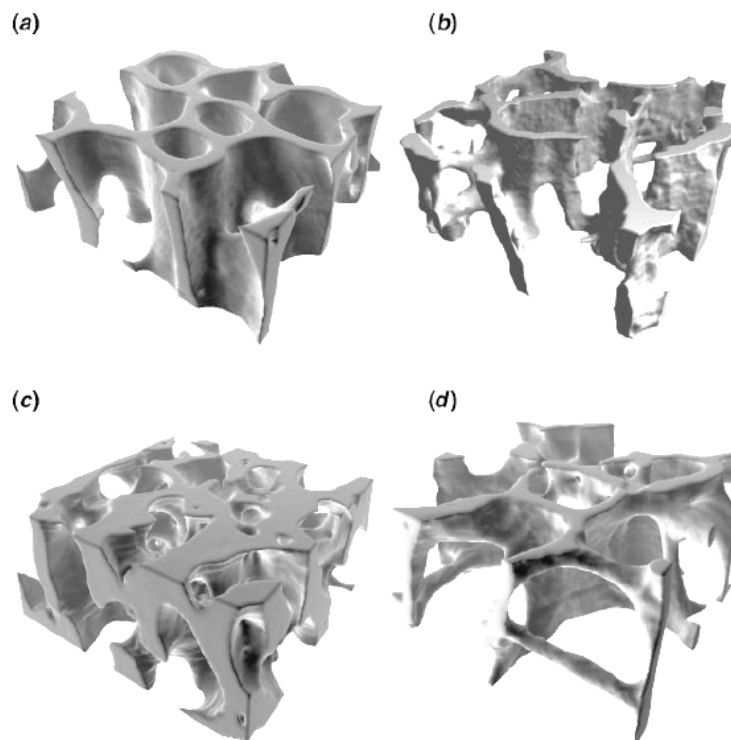


Figure 2-18: 3D reconstructions from micro-computed tomography (μ CT) scans of $3 \times 3 \times 1 \text{ mm}^3$ samples. a) Bovine proximal tibia. b) Human proximal tibia. c) Human femoral neck. d) Human vertebral trabecular bone. [Reproduced from Keaveny *et al.*¹¹³]

^d Squeeze film effect: A viscous fluid that is squeezed between two confined parallel plates will escape towards the peripheral region. The area through which it can escape becomes smaller while squeezing, so the pressure required for squeezing will increase with the viscosity of the liquid.

The bone quality in clinics can be rated, based on measurements of apparent bone mineral density (BMD) of the trabecular bone. The determined BMD value is ‘apparent’ because it covers the density of bony material, fat and marrow in the inter-trabecular spaces and non-mineralised structures. The patient or specimen is scanned using computed tomography (CT), together with a phantom with known density. The mean grayscale values in Hounsfield Units^e (HU) of a volume of interest (VOI) are calibrated using the phantom value. This technique is referred to as quantitative CT (qCT) and gives information about the overall bone quality, but not of the underlying trabecular architecture.¹¹⁴

Another measure for bone quality is the bone volume (BV) per total volume (TV) — commonly referred to as BV/TV — and its complement, the porosity (void volume per total volume). BV/TV can be calculated from CT scans with sufficient resolution. With regard to the lower geometric range of the trabecular thickness of 50 μm , imaging of the trabecular architecture requires a resolution of the scan device as precise as 50 μm . This is given for high-resolution CT (HR-CT) and micro-CT (μCT), that are currently applied in research^{33,115–117}. BV/TV is a measure of the architecture, but it merely reflects the bone proportion and not the architecture within the volume of interest (VOI). Complementing parameters are the pore size, thickness of the structure elements (rods and plates), the rod-plate proportion, and the orientation of the structure. Changes in mechanical compression properties have been found to be due to trabecular bone loss rather than changes in substance quality (collagen content)¹¹⁸, which would be reflected in architectural parameters. Trabecular architecture is determining for mechanical properties of trabecular bone. Determination of these architectural parameters is described in Chapter 5.

Gibson³⁰ has defined four basic types of trabecular structure: asymmetric rod-like, asymmetric plate-like, oriented^f rod-like and oriented plate-like. An oriented structure results in anisotropic mechanical behaviour with the greatest stiffness in orientation direction³⁰. In oriented plate-like structures, the plates are aligned to orientation direction, further increasing the stiffness. As already discussed in connection with Wolff’s Law (Section 0), bone structures are oriented according to the load on and resulting stress within the bone. Load on the bones is different at different anatomical sites, which is reflected by the trabecular orientation. Asymmetric structures have been found in the femoral head, which is loaded multidirectionally during extension-flexion³². Vertebral trabecular bone is oriented vertically, since only cranial-caudal loads occur³². Against the background of shown differences for different sites, relations between architecture and BMD from studies without site-specificity have to be treated with care^{32,33}.

A relationship of mechanical properties of proximal tibial trabecular bone to architectural parameters is not reported in literature. Merely one publication deals with the architecture of human trabecular bone in the proximal tibia³⁴. A change towards a more rod-like architecture and decreasing thickness of the trabecular elements was found for donors above 80 years. Below this age the investigated characteristics remained

^e Hounsfield Units, dimension of attenuation μ , $\mu_{\text{air}} = -1000$ HU, $\mu_{\text{water}} = 0$ HU

^f Gibson³⁰ used the term “columnar” instead of “oriented”.

unchanged. Other studies concentrate on mechanical properties and apparent BMD¹¹⁹. Rho *et al.*¹¹⁹ used density in terms of mass per volume as predictor for mechanical properties of the trabecular bone of lumbar vertebrae and proximal tibia (pooled data) in a power law:

$$E_{tibia} = 0.51 * \rho^{1.37} \quad (2-1)$$

where ρ is the density in kg/m^3 and E is Young's Modulus. Trabecular architecture characteristics of proximal tibial bone have not yet been exclusively related to the mechanical properties.

No difference was shown between tensile and compressive Young's Modulus and ultimate stress, respectively¹²⁰. Absolute values vary between studies (**Table 2-1**), which is probably due to the determination method. Density determination requires drying and subsequent re-moisturising for mechanical testing¹¹⁸. Compression parameter values from non-dried samples coincided with those from other studies^{120,121}. The mechanical properties of proximal tibial bone in axial orientation are independent of load mode direction (tensile or compression).

Table 2-1: Literature data for the mechanical properties of trabecular bone samples in the proximal tibia. Compression and tension are applied in longitudinal direction of the tibia. Standard deviation is given in brackets.

Authors	Donor age [years]	BMD [g/cm^3]	BV/TV [%]	Young's Modulus [MPa]		Ultimate stress [MPa]	
				Compression	Tension	Compression	Tension
Ding <i>et al.</i> , 1997 ¹¹⁸	60 to 83	0.4 (0.1)	18.4 (5.0)	613 (319)		7.27 (3.04)	
Røhl <i>et al.</i> , 1991 ¹²⁰	42 to 76			485 (333)	483 (323)	2.22 (1.42)	2.54 (1.18)
Odgaard <i>et al.</i> , 1989 ¹²¹	57 to 60	0.5 (0.1)		428 (228)		5.96 (3.13)	

Microscopic properties of individual trabeculae were postulated by some authors to be similar to those of cortical bone^{44,122-124}. Nevertheless, Young's Modulus of single trabeculae was found to be significantly lower than that of cortical bone (**Table 2-2**)¹²⁵⁻¹²⁷. The absolute values vary between studies, due to patient-specificity, local variances and specimen humidity¹²⁵. The length of initiated cracks in trabecular bone was found to be greater than in cortical bone¹²⁸. Extrapolation from cortical to trabecular bone due to BMD or porosity failed¹²⁴. The different mechanical behaviour of bone substance was found related to different collagen contents, although this was not compared between cortical and trabecular bone^{118,129,130}. The metabolic activity of trabecular bone is greater than that of cortical bone, ending up in overall 'younger' bone^{31,131}. The energy to fracture was shown to be greater than for 'old' bone in the sense of patient age¹¹². Trabecular bone substance is different from cortical bone substance, resulting in lower stiffness of the single trabecula.

Table 2-2: Overview of the mechanical properties Young's Modulus E , ultimate strength σ_u , ultimate strain ϵ_u of trabecular and cortical bone substance in literature. Standard deviation is displayed in brackets.

	Measurement	Sample state	Trabecular	Cortical
Rho <i>et al.</i> , 1997 ¹²⁷	nanoindentation	re-moisturised	$E = 13.4 \text{ GPa}$ (2.0 GPa)	Osteon $E = 22.5 \text{ GPa}$ (1.3 GPa)
Choi <i>et al.</i> , 1990 ¹²⁶	bending	kept moist	$E = 4.6 \text{ GPa}$ (1.6 GPa)	$E = 5.4 \text{ GPa}$ (1.3 GPa)
Mullins <i>et al.</i> , 2009 ¹²⁸ values estimated from diagram	nanoindentation	re-moisturised	$E \sim 14 \text{ GPa}$	$E \sim 17 \text{ GPa}$

2.3.2.3 Bone Preparation in Tibial Total Knee Arthroplasty

Preparation of the patient's native tibial plateau for inserting a tibial implant has an influence on the final axis alignment. The cut slopes are crucial in component alignment, which again is decisive for implant survival⁵⁰. Mechanical, anatomic or kinematic alignment is approached, depending on the philosophy of the surgeon. Mechanical alignment aims at restoration of the mechanical axis from femoral head to ankle joint in the frontal plane (**Figure 2-19**, right). In anatomic alignment, the joint line is intended to be recreated, likewise in the two-dimensional view (**Figure 2-19**, left). Kinematic alignment is a three-dimensional concept, taking into consideration all three axes of motion of the knee joint⁵⁰. Implant survival is better for the mechanical approach than for the anatomic⁵⁰. The kinematic approach has significantly better outcome after two years, also with regard to patient satisfaction¹³². The kinematic approach lacks long-term results, but with regard to the multi-layered 3D kinematics of the knee joint, this approach appears promising.

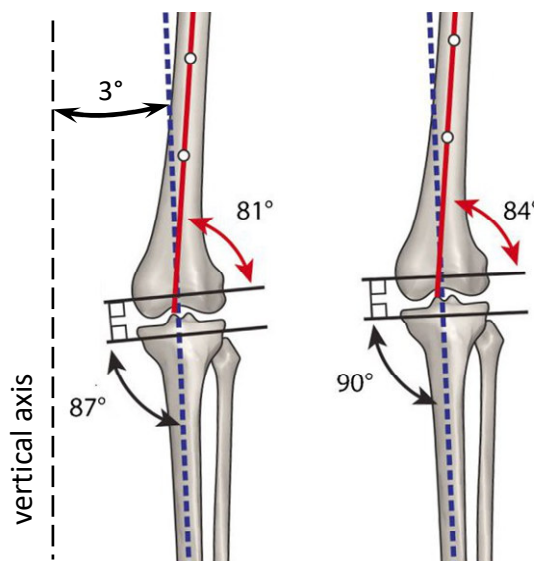


Figure 2-19: Component alignment in TKA according to anatomical (red line) and mechanical (blue dashed line) axis. Left: Anatomical approach with the joint line parallel to the ground (the mechanical axis is tilted by 3° to the vertical axis). Right: Mechanical alignment with joint line perpendicular to the mechanical axis. [Adapted from Cherian *et al.*⁵⁰]

Details of the procedure described in the following section refer to application of Sigma® High Performance (HP) implantation tools (DePuy Orthopaedics, Leeds, England). They vary for different manufacturers and implant designs. The Sigma® HP tools allow for implantation of Titanium Fixed Bearing and MBT Keeled (both P.F.C. Sigma®, DePuy Orthopaedics, Warsaw, IN, USA) — a fixed bearing and a mobile bearing (rotating platform) design, respectively (Section 2.3.1). Both exhibit a short central stem with keels (**Figure 2-20**). However, the general procedure is valid for all TKA procedures.



Figure 2-20: Two TKA designs with different inlay-to-tray concepts (both P.F.C. Sigma®, DePuy Orthopaedics, Warsaw, IN, USA). Left: Inlay is fixed on the tibial tray (fixed bearing) [reproduced from kneereplacement.com⁸³]. Right: Inlay is able to rotate on the tibial tray (mobile bearing, rotating platform) [reproduced from kneereplacement.com¹³³]. The tray designs require similar bone preparation procedures and are available in the same sizes.

Appropriate resection is achieved by using a cutting block positioned at the anterior tibial head. For alignment, a jig is clamped to the patient's ankle and fixed with a pin to the tibial head (**Figure 2-21**, left). It is used to adjust tibial slope in the sagittal plane and varus-valgus alignment in the frontal plane. Other systems may apply intramedullary alignment devices⁷⁷. Alignment is crucial for leg axis restoration, regardless of approach (anatomical, mechanical or kinematic).

The cut for resection of the tibial plateau is usually positioned about 9 mm below the plateau⁷⁷. Care has to be taken to completely resect the subchondral bone that is less porous than trabecular bone. Generally, the femoral resection is carried out before the tibial, but this can be done the other way around. The resected joint surfaces and corresponding gap between femur and tibia are assessed in extension concerning stress within the remaining ligaments. Re-working of the resected surfaces or soft tissue release may be necessary. The amount of resected material determines the distance between components and thereby the soft tissue stress.¹³⁴

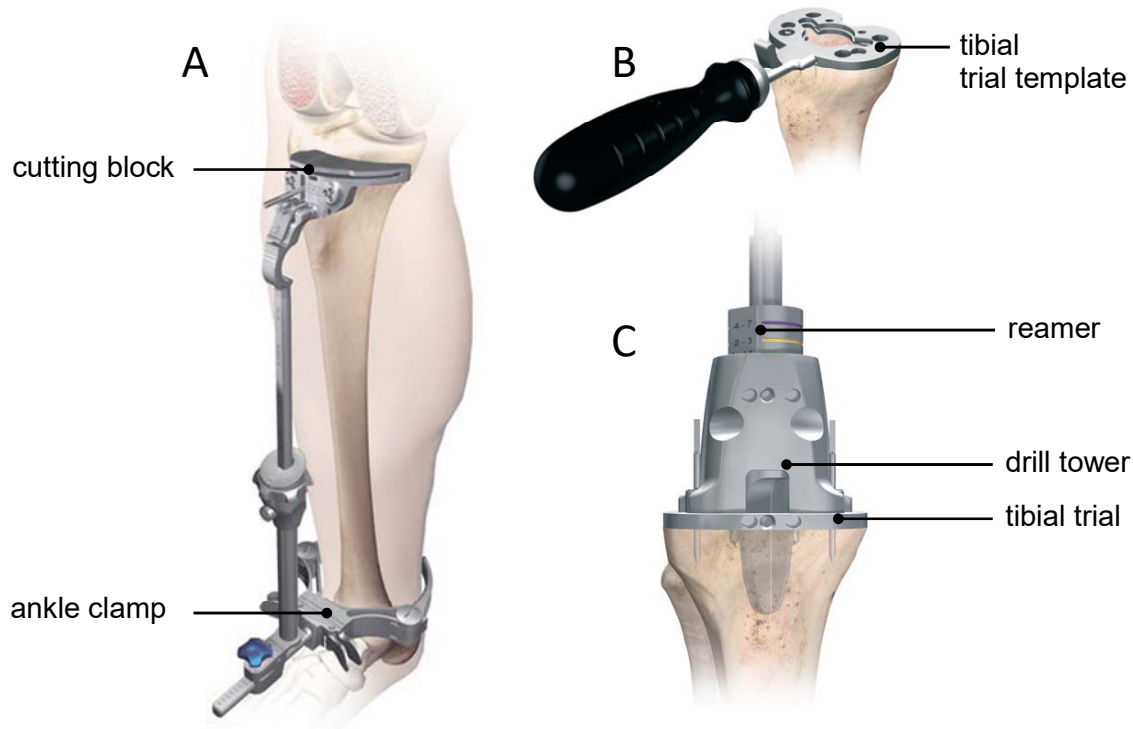


Figure 2-21: Tibial plateau preparation. A: Alignment for cutting block positioning using a jig. The jig components allow for planning of the cut slope in frontal (varus-valgus) and sagittal planes (tibial slope). B and C: Reaming of the surfaces. The tibial trial template is positioned on the resected surface and the implant cavity is reamed, guided by a drill tower. [Reproduced from DePuy Manual¹³⁴]

A tibial trial template is positioned on the resected bone surface (**Figure 2-21, B**). Rotational position of the tray with respect to the tibial axis is crucial to prevent patellofemoral complications^{93,135}. A drill tower is placed on the tibial trial template as a guide for reaming the cavity for the central stem (**Figure 2-21, C**). The cavities for the keels are inserted by a punch that is also guided by the drill tower. Design and size matching of femoral and tibial components define the rotational tolerance for the position of the tibial tray on the resection plateau (Sigma® series allows for 5° to 20°).¹³⁴

The resection surfaces are contaminated by fat, marrow and bone debris resulting from the cutting process. Cleansing is done by irrigation using saline solution. The fluid can either be applied by a syringe or an irrigation system that applies a pulsatile fluid jet to the porous surface. The jet is guided using a gun-like device that also exhibits a suction unit, to remove the contaminating material from the surgical area (**Figure 2-22**). Historically, pulsatile irrigation is an enhancement of syringe irrigation. It has been shown that pulsatile irrigation is more effective than syringe irrigation regarding debris removal¹³⁶. Cement penetration into the bone is increased after pulsatile irrigation compared to syringe irrigation, accompanied by increased strength of the interface¹². Pulsatile irrigation — also pulsatile “lavage” — of the stem cavity has been shown to decrease occurrence of fat embolisms in dogs when carried out in hip arthroplasty¹³⁷. Usage of a pulsatile lavage system is recommended for TKA as well as for THA^{12,77,136,138}. In THA, about 22 % of the centres in Germany apply techniques other than pulsatile lavage for the femoral side¹³⁹. For the more easily accessible acetabular surface, even 33 % non-

pulse-irrigation cleansing is reported in the same study. This coincides with the finding of an Australian survey that reports about 32 % of the responding surgeons applying syringe lavage in TKA or no lavage at all, the rest use pulsatile lavage¹⁴⁰. It appears that pulsatile lavage is not used on a principle basis, although its positive effect has been shown.



Figure 2-22: Pulsatile lavage system used to clean the porous bone surface of fat, marrow and bone debris using a pulsating fluid jet. [Adapted from juka-pharma.de¹⁴¹]

2.3.2.4 Cementation of the Tibial Tray

From merging to curing, bone cement undergoes four phases: mixing phase, waiting phase, working phase and setting phase. Cement mixing, the combination of the two components, is done in vacuum, using closed mixing systems. Conventional hand mixing in atmospheric pressure can result in air bubbles within the dough that remain detectable in the cured material. These remains have been shown to severely decrease the strength of the cement bulk¹⁴². Mixing conditions, such as velocity, ambient humidity and temperature may have both positive and negative effects on porosity, material homogeneity and shrinkage (lower than 7 %¹⁰⁰) during curing. Using closed vacuum mixing systems reduces the sensitivity of the mixing process to impairing effects of inappropriate mixing conditions, such as high mixing velocity, which would lead to increased porosity.^{143–145}

The duration of the working phase is crucial for the surgical procedure and may vary between 5 to 8 min, depending on the temperature and humidity of the surroundings¹⁴⁶. Reaching the end of this phase, the cement dough viscosity increases rapidly and does not allow for forming and intrusion into the trabecular bone anymore. Lower temperatures extend the working phase. Clinical practice often covers pre-chilling of the cement to extend the working phase. Cement application is a critical step during arthroplasty procedure, since it cannot be reversed without difficulty, from the moment the cement is applied to the bone, even if no pressure has yet been applied.¹⁰⁰

The cement application technique was shown to be of major importance in hip arthroplasty⁸. Usage of an intramedullary plug and retrograde introduction of cement to the stem cavity lead to a continuous cement mantle and improve the survival of the

cemented fixation. The technique enables a controlled introduction and predictable distribution of cement and is deemed responsible for a decrease of aseptic loosening and has become standard¹⁴⁷. Standardisation of the technique may also be advantageous in TKA.

Implant designs for cemented fixation do provide a gap between implant and bone surface for the cement layer in the stem-keel area¹³⁴. The system is designed for a full cement layer covering stem, keels and back side of the tray (**Figure 2-23**, left). Some authors argue that full cementation complicates the revision of failed implants disproportionately and increases the loss of bone that might be strongly attached to the stem by in- or ongrowth^{15,16}. They prefer to leave the stem cementless (**Figure 2-23**, right). Studies advocating full cementation found increased micromotion between bone and implant¹⁷ and more radiolucent lines¹⁸. Other authors found no difference in radiolucent line occurrence in a clinical study¹⁴⁸. The discussion regarding stem cementation remains controversial.

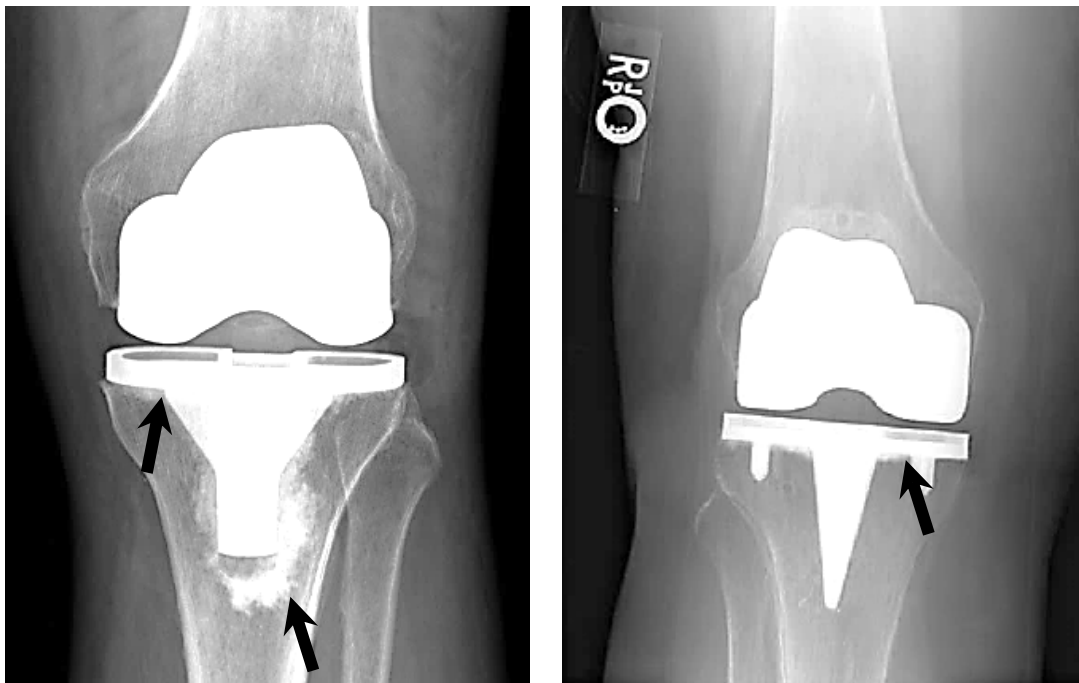


Figure 2-23: Radiographic scans of cemented tibial trays, cement is indicated with arrows. Left: Full cementation with cement layer covering stem, keels and back side of the tray [scan provided by University Hospital Heidelberg]. Right: Plateau-only cementation leaving the stem cementless [adapted from Hofmann *et al.*¹⁶].

Various techniques are commonly used to apply the cement to the bone¹⁴⁰. Cement is applied and pressed by hand, by spatula or cement gun. Cement dough can be positioned on the bone plateau and within the stem cavity, on the plateau and the back side of the implant or on the implant only.

Alongside conventional cement application by hand, cement guns or pistols are in use^{14,140}. They aim at cement application with reproducible pressure and cement distribution^{149,150}. Manual handling of the dough is decreased, predestining the method for medium viscosity cement¹³. However, no difference in cement layer characteristics was found in a retrospective clinical study of 77 patients treated with either finger

packing or gun application¹⁴. Since additional equipment is required for the latter and the benefit does not appear obvious, finger packing and gun application are both used with confidence^{13,14}.

2.3.3 Clinical Loosening of the Tibial Tray in Total Knee Arthroplasty

The Swedish and the British Register reported a survival probability of TKA of about 96 % at 9 years ^{2,3}. In Germany, about 25 000 patients underwent revision surgery in 2012⁶ (**Figure 2-11**) with increased infection risk. A retrospective clinical study reported 10-fold increased infection risk after revision compared to after primary surgery¹⁵¹. It appears that the tibial component is more frequently revised than the femoral. The Swedish Knee Register reports 1 % femur-only but 6 % tibia-only revisions for a 10-year period¹. Implants for revision exhibit long stems and component coupling with a decreased degree of freedom. This should compensate for the inevitable bone loss until and during revision surgery, which is due to bone resorption, as well as to removal of bone with the implant. Primarily stabilising structures, such as remaining ligaments might have to be removed in the second procedure. Revision surgery should be postponed as long as possible.

According to the Swedish Knee Register¹, the main reasons for revision are loosening (24 %) and infection (23 %), followed by patella-related complications (19 %) and instability (13 %) (**Figure 2-24**). Other reasons are migration of the implant or fracture and wear of the components¹. The analysis is based on the ultimate indication for surgery which, however, can be accompanied by other disorders. Loosening may occur caused by infection, but could also be wear particle-induced. The British Register differentiates between aseptic loosening and lysis and further covers pain as a revision reason². As in the Swedish Register, infection and loosening are the major revision indications in the British Register, but loosening refers to aseptic cases only, contrary to the Swedish Register numbers. Differentiation between septic and aseptic loosening is important for addressing the different underlying mechanisms, but is often not clearly definable.

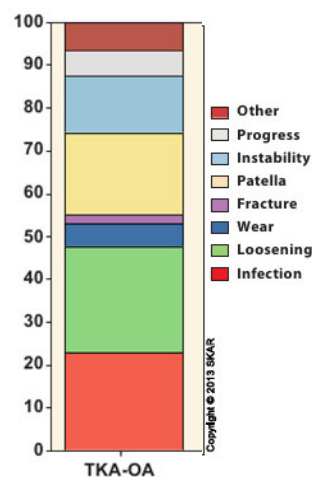


Figure 2-24: Distribution (%) of indication for revision of TKA due to osteoarthritis (OA). Loosening is a major reason for revision surgery¹

Infections occur due to peri-operative contamination or due to bacteria delivered by the blood or lymphatic system¹⁹. Infection-related loosening (septic loosening) often becomes manifest in radiographic signs similar to those of aseptic loosening, for example.

radiolucent lines, migration and osteolytic zones¹⁵² (**Figure 2-25**). Radionuclide scans and analysis of aspirated synovia are complementary diagnostic tools¹⁵². Cases of aseptic loosening are often hard to distinguish from a low-grade infection. Infection management is an intricate field in arthroplasty. Severe consequences of uncontrollable infection might be limb amputation or death of the patient. This study concentrates on aseptic loosening, which occurs due to a different mechanism.

On the one hand, aseptic loosening is attributed to body reaction to wear particles of the introduced artificial materials (PE, metal, bone cement). These activate macrophages that produce metabolic factors, stimulating bone resorption. Since the polymeric bone cement and PE alter *in vivo* and, in addition, are continuously loaded in fatigue mode, wear particles will occur sooner or later. On the other hand, insufficient initial stability of the implant fixation allows for micromotion in the interface between introduced material and bone. Micromotion is suspected of preventing osseointegration and thereby provoking formation of a soft tissue layer in the interface¹⁹. Successful implant ingrowth was shown to be achievable at 20 μm micromotion between implant and bone, but not at 40 μm ¹⁵³. Since polymer alteration cannot be completely prevented, improvement of the initial fixation and thereby reduction of micromotion to a level below 20 μm is a promising approach to postponing loosening processes.

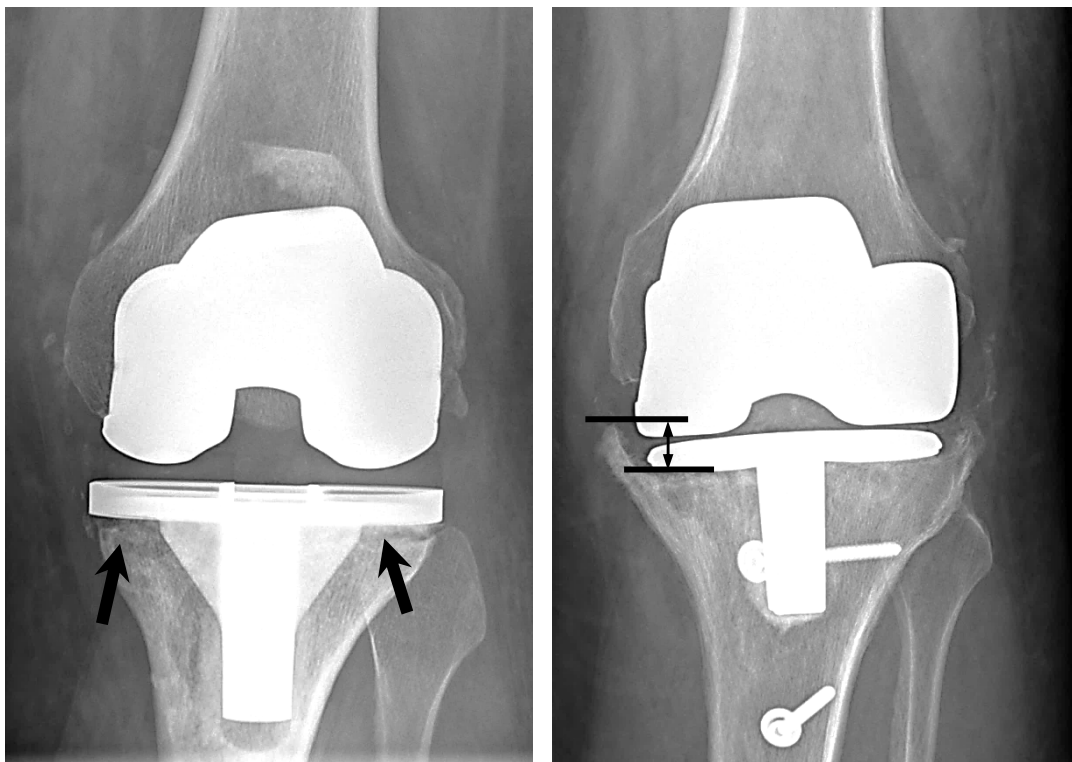


Figure 2-25: Radiographic scans showing signs of loosening. Left: Aseptic loosening with radiolucent lines and osteolytic zones below the tibial plateau (arrows); low-grade infection is possible. Right: Septic loosening with migration of the tibial and femoral component. Measure indicates original and current position of the tibial tray. [Scans provided by University Hospital Heidelberg]

2.4 *In Vitro* Testing of Cement-Bone Interfaces

Mechanical testing of implants concerns testing of the implant as such, on the one hand, and testing of the fixation to the body, on the other hand. In this thesis, the cemented fixation of the tibial tray to the tibial bone is investigated. This requires *in situ*[§] testing, which is usually done using PU foam as bone substitute, or cadavers. The elements under risk are the implant, the trabecular bone or respective substitute it is fixed to, the bone cement layer and the interfaces between implant and cement, as well as between cement and bone (**Figure 2-26**). Cement-bone interface failure appears in four modes: bone surfaces with no penetration, bone surfaces where the cement was pulled out of the porous trabecular bone, fracture of trabecular bone that remains at the removed cement and fracture of the cement¹⁵⁴. For mechanical testing of complete objects (bone, cement, implant), two basic failure modes can be assumed: failure at the cement-bone interface and failure at the cement-implant interface²⁹. Mixed failure modes have also been reported^{12,29}. This thesis focuses on the interface between cement and bone and the involved materials.

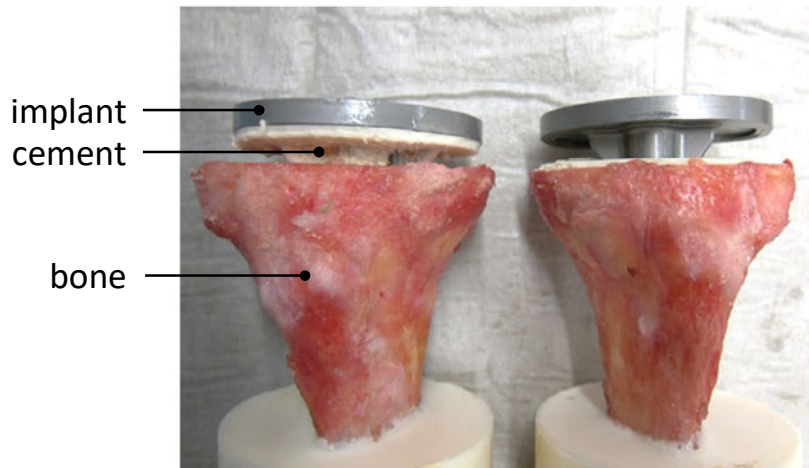


Figure 2-26: Interface failure modes of cemented tibial implants in mechanical testing. Left: Bone interface failure. Right: Implant interface failure. [Reproduced from Schlegel *et al.*¹²]

Several experimental studies focus on the analysis of initial stability of cemented fixation in TKA and UKA. This can be addressed using either entire implanted bones (human or artificial) or smaller samples from the cement-bone interface. Relative displacement or fixation strength, respectively, are documented. Some studies with respective parameters are listed in **Table 2-3**; a comprehensive overview is presented in Appendix C.1.

In implanted human tibiae, some authors measured cyclic displacement between bone and implant due to axial or off-axis load that mirrors load in a flexed knee joint^{15,17,155–157}. Others used Roentgen Stereometric Analysis (RSA) to analyse migration of the implant due to cyclic load^{158,159} (**Figure 2-27**). Although measuring micromotion, the cement-bone interface is not directly addressed.

[§] *In situ* = “at the designated site”, implies a more function-specific testing than ‘*in vitro*’, that not necessarily refers to a device that is actually implanted.

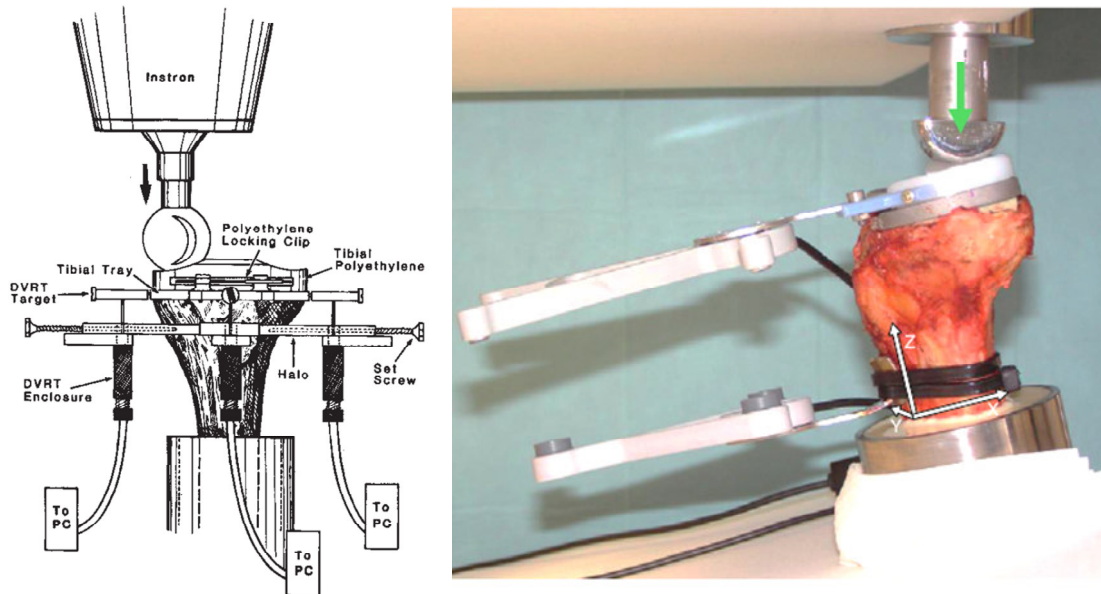


Figure 2-27: Representative setups for mechanical testing of tibial tray fixation. Left: Measurement of micromotion between implant and bone due to eccentric compression using inductive displacement transducers [reproduced from Peters *et al.*¹⁵]. Right: Measurement of micromotion between implant inlay and diaphyseal bone under compression in flexion using 3D motion analysis [reproduced from Grupp *et al.*¹⁵⁶].

Another approach is pull-out testing of the cement-bone interface^{12,29} (**Figure 2-28**). In contrast to the foregoing approaches, load mode is not in compression but in tension and therefore considered non-physiological. However, analysis of pull-out or push-out strength gives a qualitative impression of the fixation strength and is a common method¹⁶⁰. In pull-out testing, the fixation was stronger when cement penetration into the bone was greater^{12,29}.



Figure 2-28: Test setups for pull-out testing. Left: Load application in testing of lab-prepared cadavers using an adapter [reproduced from Schlegel *et al.*¹²]. Right: Load application in testing of post-mortem retrievals using a clamp [reproduced from Gebert de Uhlenbrock *et al.*²⁹].

Table 2-3: Mechanical testing of human or artificial bone implanted with cemented UKA or TKA. Type of specimen, load mode, measure and measurement site are listed. A comprehensive overview is supplied in Appendix C.1.

Authors	Type	Load mode	Measure	Measurement site
Sala <i>et al.</i> , 1999 ¹⁵⁵	lab-implanted cadaver	rotation	rotation	between implant and bone
Luring <i>et al.</i> , 2006 ¹⁷	synthetic composite tibiae	compression	lift-off	between implant and bone
Rao <i>et al.</i> , 2010 ¹⁵⁷	post-mortem retrievals	compression	lift-off depression	between implant and bone
Gebert de Uhlenbrock <i>et al.</i> , 2012 ²⁹	post-mortem retrievals	tensile	failure force	cement-bone cement-implant
Schlegel <i>et al.</i> , 2011 ¹²	lab-implanted cadaver	tensile	failure force	cement-bone cement-implant
Grupp <i>et al.</i> , 2013 ¹⁵⁶	lab-implanted cadaver	vertical compression (15° flexion)	failure force	between implant inlay and diaphyseal bone
Peters <i>et al.</i> , 2003 ¹⁵	lab-implanted cadaver	compression	micromotion	between implant and bone

Findings from macro-mechanical testing are complemented by micro-mechanical testing. Some studies are listed in **Table 2-4**, a comprehensive overview is presented in Appendix C.1. As in testing of whole implanted bones, testing of micro samples has shown that greater strength in tension corresponds to larger amount of cement-interdigitated bone and larger contact area between bone and cement^{29,161,162}. Micromotion in compression was found to be larger for smaller cement-bone contact zone²². As stated in Section 2.3.3, micromotion is decisive for development of fibrous tissue and the loosening progress^{19,22}. Tensile testing revealed lower stiffness of the interface zone when cement penetration is smaller¹⁶². Cement penetration is a key factor for fixation stability and strength.

Miller *et al.*⁴⁷ analysed micrographs of the cement-bone interface of cemented tibial trays that were retrieved post-mortem. They found cavities in the cement that they attributed to resorbed trabeculae (**Figure 2-29**, left). The resorption extent was smaller under the medial compartment. It was assumed that the force transferred to the bone in the medial compartment was greater, which kept the loading of the trabeculae physiological and thereby prevented resorption¹⁶³. In the lateral region, the initially cement-interdigitated trabeculae may be shielded from mechanical stimulus. Increased resorption with longer time *in vivo* results in decreasing effective interdigitation and contact area between bone and cement^{22,23}. Pull-out strength was found to be lower with shorter time *in vivo*²⁹, which may correspond to a lower effective interdigitation and therefore coincides with the micro-studies. Decrease of interdigitation due to progressing *in vivo* bone resorption is reflected by decreasing pull-out strength.

The remaining effective interdigitation was larger, when the initial interdigitation was larger²³ (**Figure 2-29**, right). The initial state was referred to as the primary interface. Lab-prepared cemented tibial trays do reflect this state and the encountered macro- and micro-mechanics can be regarded as early post-operative mechanics^{22,164}. The measured

fixation strength is the primary fixation strength, which should be large, considering that it decreases proportionally with time.

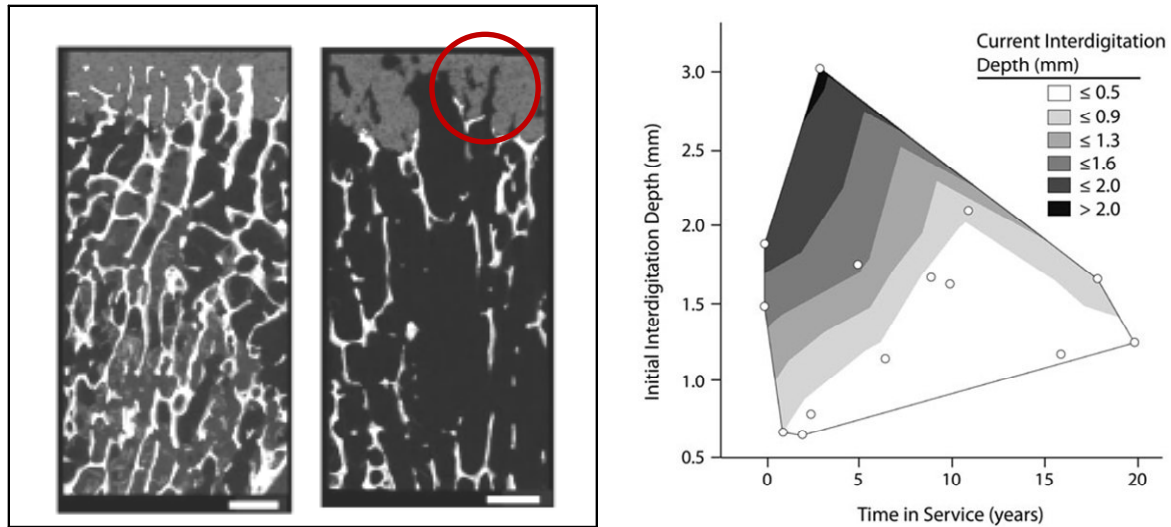


Figure 2-29: Bone resorption within the cement in *ex vivo* specimens retrieved from tibial TKAs. Left: μ CT scan of a freshly implanted (left) and post-mortem retrieval specimen (right). Top is cranial, bottom is caudal. The cement layer is visible in grey in the cranial region of the scan. Bone is white, and marrow and air are grey to black. Bone resorption cavities remain within the cement layer, where bone was resorbed (right within circle). The white bar in the lower right corner represents 1 mm. [Adapted from Goodheart *et al.*²²]. Right: The remaining effective interdigitation depth of cement and trabecular bone was larger, when the initial interdigitation depth was larger [reproduced from Miller *et al.*²³].

Table 2-4: Micro-mechanical testing of samples from the cement-bone interface. Sample origin, sample type, load mode, input and output measures are listed. Studies that are based on the same specimens are grouped. Lab-prepared specimens were cut from trabecular bone and merged with cement; lab-implanted specimens were cut from a cement-bone interface obtained from arthroplasties produced in the lab; post-mortem retrievals were cut from arthroplasties harvested from deceased donors. The terms 'tension', 'shear' and 'compression' refer to the approximate interface plane.

Authors	Origin	Type	Load mode	Input measure	Output measure
Askew <i>et al.</i> , 1983 ¹⁵⁴	tibia, femur	lab-prepared	tension	cement pressure penetration depth	interface strength bone area fraction
Janssen <i>et al.</i> , 2008 ¹⁶⁵	femoral THA	lab-implanted FE	tension compression	friction coefficient μ CT density cement stiffness	Interface stiffness
Waanders <i>et al.</i> , 2010 ¹⁶²	femoral THA	lab-implanted FE	tension shear	penetration contact μ CT density	contact area estimate strength stiffness
Miller <i>et al.</i> , 2010 ⁴⁷	femoral THA	post-mortem retrievals	tension compression	contact fraction	tensile strength stiffness
Miller <i>et al.</i> , 2014 ²¹ Goodheart <i>et al.</i> , 2014 ²²	tibial TKA	lab-implanted post-mortem retrievals	compression	<i>in vivo</i> time	penetration depth contact fraction micromotion
Graham <i>et al.</i> , 2003 ²⁸	bovine	lab-prepared	tension with crack initiation	porosity trabecular orientation cement pressure penetration depth	interface strength

Cement penetration depth is dependent on cement pressure²⁵ and surface preparation^{12,136,138}. Surface preparation implies irrigation to remove bone marrow and remaining bone particles generated during resection of the tibial plateau. Cement penetration depth was shown to be significantly larger after pulsatile lavage¹². The penetration can be influenced by specific bone preparation techniques.

Bone volume fraction (bone volume/total volume, BV/TV) is a measure of the bone proportion within the sample volume and is correlated to apparent BMD³³. (Pearson's r 0.903) Bone quality in terms of porosity was shown to influence cement penetration²⁴⁻²⁷. A strong negative correlation was found between cement penetration depth and BMD^{26,27}. At the same pressurisation, cement penetrates deeper in high-porosity bone than in low-porosity bone.

A strong positive relationship between BV/TV and compression strength has been shown²². In other studies, tensile strength of the interface was found to be independent of BMD^{12,29}. Bone strain is larger in lower BMD, than in higher BMD, indicating higher fracture risk¹⁶⁶. Assumingly, bone density of a cement-bone interface sample is positively correlated to the fixation strength in tensile as well as in compression testing, but there is remaining variance that is as yet unexplained.

2.5 Conclusion

Although a successful procedure, cemented TKA still exhibits a considerable portion of revision surgeries due to loosening of the tibial component. Loosening occurs sooner or later, but may be postponed by improvement of the initial fixation stability.

A crucial factor for loosening is micromotion between cement and bone. Micromotion provokes formation of a soft tissue layer and prevents osseointegration of the implant. Retrospective studies on post-mortem retrievals of TKA showed that low cement penetration depth corresponds to larger micromotion between cement and bone than large penetration depth. Experimental studies showed that the fixation strength of lab-prepared specimens with low cement penetration was lower than that with high penetration depth.

Several techniques have been proposed to achieve large cement penetration depth. Thorough irrigation of the trabecular bone before cement application was shown to increase cement penetration depth. Increased pressure by using application devices such as cement guns is also postulated to improve the cement penetration. However, over-penetration should be avoided. It may lead to increased stress-shielding and increased danger of heat accumulation in thick cement layers that may impair bone metabolism.

In revision all cement has to be removed and with it the enclosed trabecular bone. Thus, this removed bone is not available for anchorage of the revision prosthesis. With regard to revision surgery the volume of introduced cement should be reduced to a minimum.

Bone porosity has been stated as affecting cement penetration. Thus, low bone porosity restricts the cement flow into the trabecular bone. The achievable penetration depth may be larger than in high-porosity bone, thereby implying an interaction between cement penetration depth and bone quality. However, the influence of bone quality on fixation stability is unclear.

Detailed knowledge about the effect of cementation techniques on interlock mechanics and strength in cemented fixation is required to improve the fixation stability and successfully postpone loosening processes.

3

Impact of Cementation Techniques on Cement-Bone Interfaces in Total Knee Arthroplasty

3.1 Introduction

To date, only a few studies have been published that clearly analysed the cement-bone interface of cemented tibial trays in macroscopic testing while precluding the implant interface mechanics. An overview of these is given in Section 2.4. Pull-out testing of cemented tibial implants was recently carried out. Larger penetration depth of cement into the trabecular bone was found to correspond to larger tensile strength, although in non-physiological load mode^{12,29}. This was also found for small samples from the interface zone¹⁶¹. Micromotion in compression was smaller for larger cement penetration²². Micromotion under loading is considered a measure for implant stability and also a reason for development of a connective tissue layer in loosening processes. Literature on micro-mechanics of the interface is compiled in Section 2.4.

Bone mineral density (BMD) has been found to influence cement penetration depth, with higher densities leading to lower penetration^{26,27}. Bone strength is greater in the more peripheral regions of the metaphysis¹⁶⁷, which may be due to the proximity of the stronger corticalis. However, greater strength indicates increased bone density with less potential for cement penetration. At the same time, greater peripheral penetration appears favourable considering the greater strength. However, in a previous study, pull-out strength of tibial trays was independent of BMD²⁹. It is not clear in what way BMD and peripheral penetration have to be considered during cementation of implants and selection of cementation techniques.

Cement penetration depth may be influenced by the cement application technique. Various techniques are currently in use to apply the cement to the bone¹⁴⁰. Application may involve tools like a spatula or cement gun. Cement is applied to the bone plateau and within the stem cavity, on the plateau and the back side of the implant, or on the implant only. No difference in penetration depth of manual cement application and pressurisation (finger packing) compared to gun application was found in a clinical study¹⁴. A more controversial debate deals with the cementation of the stem, referred to as “full” cementation. Full cementation covers stem and plateau, but some authors argue that bone loss is greater and revision more complicated, when the stem is cemented in the primary procedure^{15,16}. This encourages the principle of introducing as little artificial material as possible into the body. Nevertheless, increased micromotion and radiolucent lines have been reported for plateau-only cementation when compared to full cementation^{17,18}.

Cement penetration depth has been shown to depend on both surface preparation and cement pressure^{12,25,136,138}. Application of pulsatile lavage increases the penetration depth and thereby the fixation strength^{12,25,162}. Maistrelli *et al.*¹³⁶ found that the reduced amount of bone debris after pulsatile lavage enables deeper penetration than after syringe lavage. The cleansing effect of pulsatile lavage leads to increased cement penetration depth¹³⁸. Cement penetration depth has been shown to increase when cement application pressure

generated by a mechanical testing apparatus was greater^{28,154}. In hip arthroplasty, cement pressurisation through the application of either gun or finger packing is a standard procedure that reduces pores within the cement and enables a more even cement layer^{8,168}.

Considering that both pressurisation and pulsatile lavage evidently increase penetration depth, these methods may be interchangeable. Although no clinical drawback is known about the usage of pulsatile lavage, an Australian survey reported that merely 68 % of surgeons applied pulsatile lavage¹⁴⁰. The remaining surgeons may expect comparable cleansing effects from other lavage techniques or suspect damage of trabeculae by the fluid jet, whose preservation may be valued higher than cement penetration depth. However, there is no evidence about the ability of specific pressurisation to compensate for the cleansing effect of pulsatile lavage.

The aim of this study was to determine whether the cement penetration depth and thereby the fixation strength can be increased by specific cementation techniques and if the penetration-increasing effect of pulsatile jet lavage can be compensated for by usage of a cement pressurisation tool.

3.2 Material and Methods

For this study, four cementation techniques that are used clinically were tested against a defined control technique in a pairwise design. The study design involved cemented implantation of tibial trays, followed by pull-out testing to determine fixation strengths. CT scans were used to reconstruct the cement layer and determine parameters describing the cement layer morphology.

3.2.1 Specimens

Experimental testing was performed on paired human cadavers to minimise the influence of the compositional characteristics of the bone, reflected by BMD. 18 pairs of tibiae were employed to accomplish this study. Overall, 19 pairs were collected by the Department of Legal Medicine of the University Medical Center Hamburg-Eppendorf. 7 of the donors were female and 11 male. One pair was originally implanted with a unicondylar replacement (patient 3018) and was therefore excluded from the study. Mean donor age was 74.2 years, standard deviation (SD) = 7.4 years (range 65 to 91 years). Specimens were assigned to the study groups, such that equal distribution of implant sizes was approached (Appendix C.2.1).

Donor age was 65 years and over. Gender was not restricted. Specimens were collected by the Department of Legal Medicine, University Medical Centre Hamburg-Eppendorf (Hamburg, DE) and stored below -21°C. Donor data were anonymised and no information apart from age and gender was passed on.

3.2.2 Bone Mineral Density

The BMD of the specimens in this project was determined by applying qCT method on pre-surgery CT scans (Mx8000 IDT 16, Philips Healthcare, Best, The Netherlands, voxel size 0.6x0.6x0.6 mm). CTs were processed in 3D visualisation software (Avizo 5.0, VSG, Merignac, France). Conversion factor between grey values in Hounsfield units (HU) and bone mineral density were derived from a dipotassium phosphate (K₂HPO₄) phantom.

More details about the applied method are given in Appendix C.2.1. The conversion factor was applied to a rectangular volume ($\sim 4\,000\text{ mm}^3$) within the tibial head, positioned parallel to the natural tibial plateau and about 10 mm below it (**Figure 3-1**).

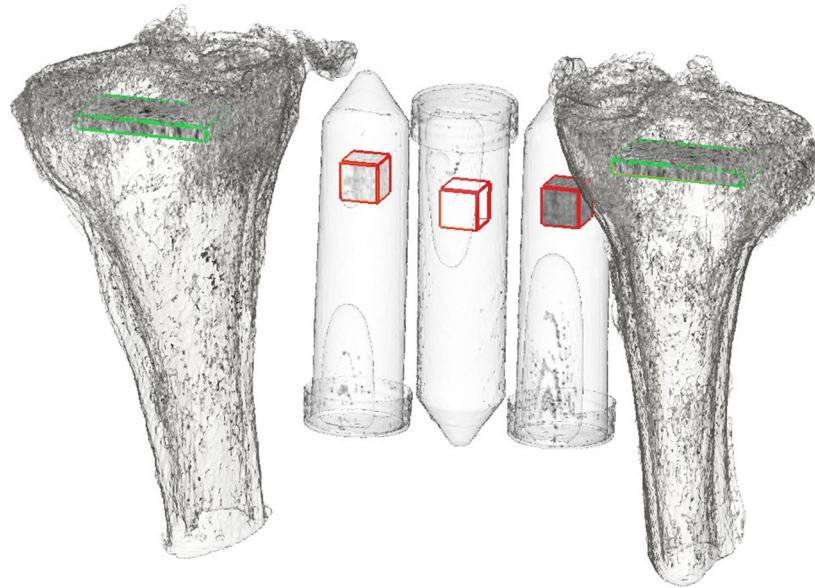


Figure 3-1: Bone mineral density determination from a rectangular volume positioned 10 mm parallel to the tibial plateau (green boxes). Calibration of the determined HU values was performed according to VOIs within a phantom that was scanned with the tibia pair (red boxes). The phantom covered three vials, each filled with a solution of different but known attenuation.

3.2.3 Tibial Tray Implant

P.F.C. Sigma® MBT Keeled tibial trays were used, which is a rotating platform design (**Figure 3-2**). Four implants of each size 2.5, 3, 4 and 5 were provided by DePuy Orthopaedics for the study.

The tray is made of cobalt chrome (CoCr) and the stem is taper-shaped with keels. The inlay-bearing surface of the implant exhibits a taper-shaped hole for inlay positioning. The implant was slightly modified to enable coupling to the machine actuator for pull-out testing, while leaving the back side of the implant unchanged. The tip of the stem was cut off by wire erosion and replaced by an anchor with an M6 outer thread and surface geometry matching the original stem tip. Anchor tip length and diameter of the inlay hole were dependent on implant size (Appendix A.2). A coupling device with a 40° taper was screwed to the implant. The coupling device was centred by its outer taper within the implant inner taper (**Figure 3-2**).



Figure 3-2: The P.F.C. Sigma® MBT Keeled tibial tray was tip-cut and equipped with an anchor in order to assemble a coupling device with a centring taper to the implant.

Inferior bearing area *bearA* between cement and implant (back side of the implant) was dependent on implant size. It is confined by the contour of the tray and the stem profile (Figure 3-3, Table 3-1).



Figure 3-3: The bearing area of the implant *bearA* (red region) is confined by the outer contour of the implant and the stem contour. *BearA* is dependent on implant size.

Table 3-1: Implant bearing area *bearA* of MBT implants.

Implant size	<i>bearA</i> [mm ²]
2.5	2008
3	2178
4	2507
5	2978

16 implants were available for implantation of 36 specimens (18 pairs); therefore implants had to be reused. Attached bone and cement were removed by submersion in an acetone bath for at least 12 h. Heat sterilisation was carried out, followed by repeated acetone baths and mechanical cleaning, using a brush until the back side of the implant was clean. After the last acetone bath, compressed air and lens paper were used for final drying.

3.2.4 Preparation and Implantation

The tibia pair to be tested was defrosted at room temperature during the night prior to preparation. All soft tissue was removed and the tibiae were prepared for implantation according to standard surgical instructions (Section 2.3.2.3, **Figure 3-6**, left). All implants were implanted using a 0° slope cutting block, corresponding punches (HP Instruments, DePuy Orthopaedics, Warsaw, Indiana, USA) and high viscosity bone cement (SmartSet® HV 40 g and Cemvac®, DePuy CMW, Blackpool, England). Bone cement was vacuum mixed for 60 s. After a waiting period of 120 sec at 21.2°C (SD = 1.1°C) and careful drying of the osseous surface using paper towels, the dough was applied to the tibial surfaces (**Figure 3-6**, middle). Cement was applied with clean and dry gloves when applied manually (finger packing).

In the first part of this study, three currently propagated cementation techniques were evaluated in a pairwise design, using three groups of tibia pairs (each n=4). In a pairwise design one side of a pair undergoes treatment, while the other side serves as control. Pulsatile jet lavage was performed on all 24 specimens using 1 800 ml of saline solution. One side of a pair was implanted using surface-only cementation and finger packing. Cement was applied to the bone side only. These specimens served as the control group (CONTROL, **Figure 3-4**) and provided the reference to determine effects of different techniques.



Figure 3-4: Bone preparation and cementation in CONTROL specimens. Left: Pulsatile jet lavage. Right: Finger packing cement application.

The treatment sides of the tibial pairs were implanted as follows:

- | | |
|---------------|--|
| Group FULL | Cement application to plateau and stem cavity (Figure 3-5 , A), n = 4. |
| Group GUN | Cement application using a commercially available cement gun (DePuy Orthopaedics, Warsaw, Indiana, USA) (Figure 3-5 , B), n = 4. |
| Group LAYERED | Cement application to implant and bone (Figure 3-5 , C), n = 4. |

In the second part, the combination of syringe lavage with gun cementation was compared to the CONTROL technique with pulsatile lavage and finger packing using n = 6 tibia pairs:

- | | |
|--------------|---|
| Group SYRGUN | Bone lavage by syringe and cement application using a cement gun (Figure 3-5 , D), n = 6. |
|--------------|---|

Syringe lavage was performed with 1800 ml saline solution. The sizes of the implanted trays were chosen to match bone sizes. In all techniques, excess cement was removed with a scalpel as in the *in vivo* procedure.

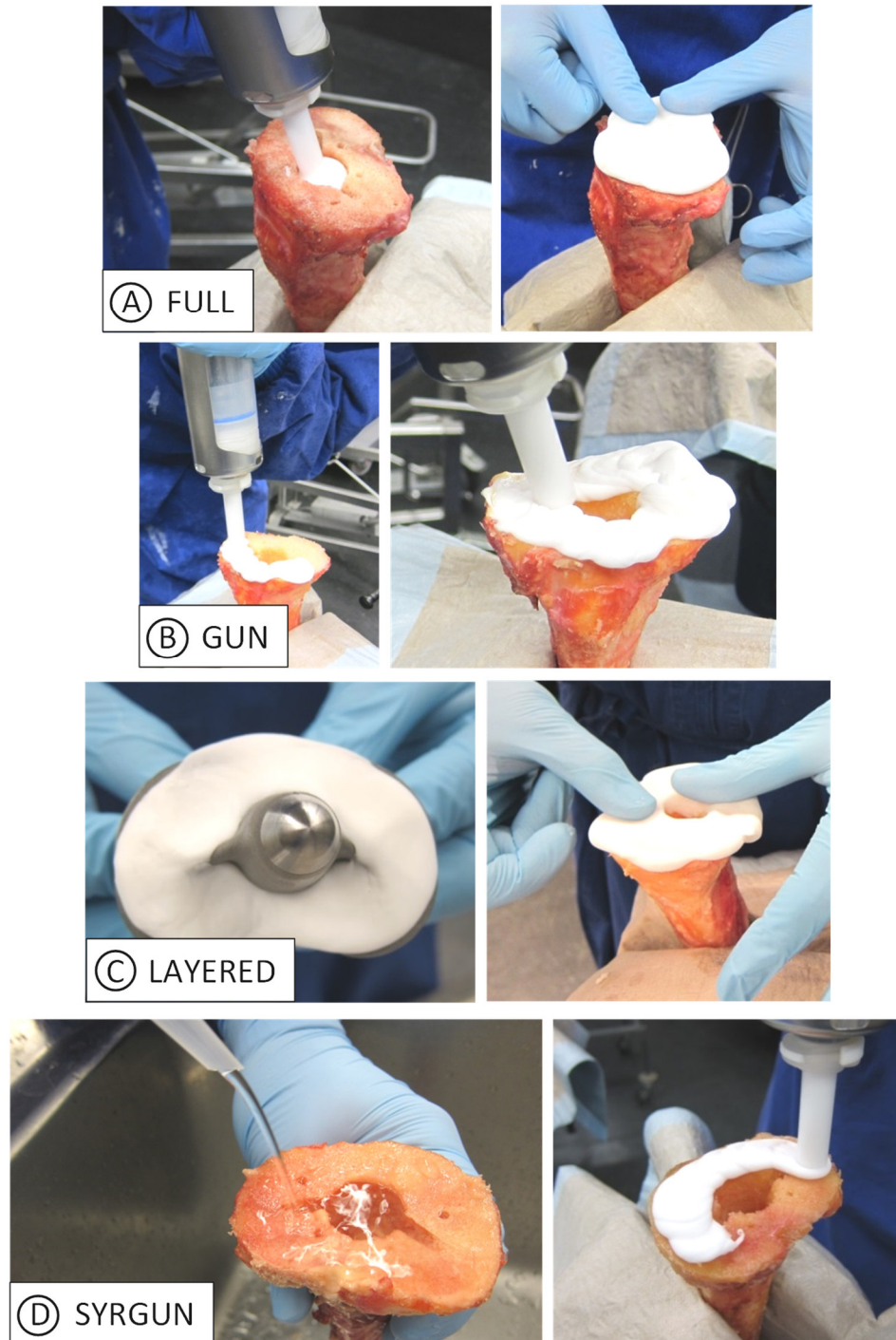


Figure 3-5: Preparation and cementation techniques applied in this study: A) Filling of stem cavity with cement for FULL cementation. B) Cement is applied to tibial plateau by a cement gun for GUN cementation. C) Cement is applied to back side of implant and to tibial plateau for LAYERED cementation. D) SYRGUN specimens underwent syringe lavage (left) and gun application (right).

The components were impacted with ten mallet blows. Following implantation, the implants were loaded with a dead weight of 50 N for 12 minutes to simulate leg extension during cement curing as practised in clinics (**Figure 3-6**, right).



Figure 3-6: Specimen preparation and implantation. Left: Example of a specimen prepared for implantation. Middle: Vacuum system for bone cement mixing. Right: Implanted specimen with positioned post-implantation loading device (weight below is not shown).

3.2.5 Computed Tomography and Re-gluing of Implant

Analysis of the cement-bone interface in this study was based on the cement layer morphology as obtained from 3D reconstruction of CT images. The scans had to be performed prior to pull-out testing of the implanted specimens, as pull-out induced damage to the interface. CoCr implants cause artefacts in CT scans that severely impair precision. In order to receive CT scans with reduced artefacts, CT scanning with the implant *ex situ* was required.

The design of the implant back side of the CoCr implant used in this study (**Figure 3-3**) enabled its removal from the cement bed for CT scanning without damaging the cement layer. In a pilot study, the implant design was pulled out at comparatively low forces (181 N to 719 N, Appendix A.1). However, adhesion between implant and cement could still be stronger than the cement-bone interface. For the actual study, the implant interface was weakened by applying a release agent to the implants before insertion (Vaseline®). After curing of the bone cement for at least 2 h, implants were removed at low forces. This process is referred to as "soft pull-out". The soft removal of implants was performed manually for CONTROL, GUN, LAYERED and SYRGUN specimens. Implants of FULL specimens could not be removed by hand. Instead a machine was used at 0.1 mm/s. Subsequent to implant removal, the specimens were re-frozen (< -21°C) and then CT-scanned with the implant *ex situ* (Brilliance CT 16-slice, Philips Healthcare, Best, The Netherlands). The voxel size was at least 0.46 mm in all three directions.

For testing, the specimens were defrosted and the tibial shafts were embedded in metal holders (Section 3.2.6). The free surface of the cement layer (implant removed) was cleaned, using a polymer cleaning agent (Kunststoffreiniger, MELLERUD®, Brüggen, DE), water and small amounts of acetone, applied with tissue and lens paper. The implant was cleaned as described in Section 3.2.3. It was re-attached to the cement mantle using industrial PMMA glue (Pattex® Stabilit Express, Henkel AG & Co., Düsseldorf, DE). At least 8 h of curing were needed to develop an interface with full strength. Each specimen was

re-implanted with its original device. In a pilot study, this method was shown to be appropriate (Appendix A.3). PMMA glue does not alter the cement and provides sufficient strength. The whole experimental procedure is illustrated in **Figure 3-7**.

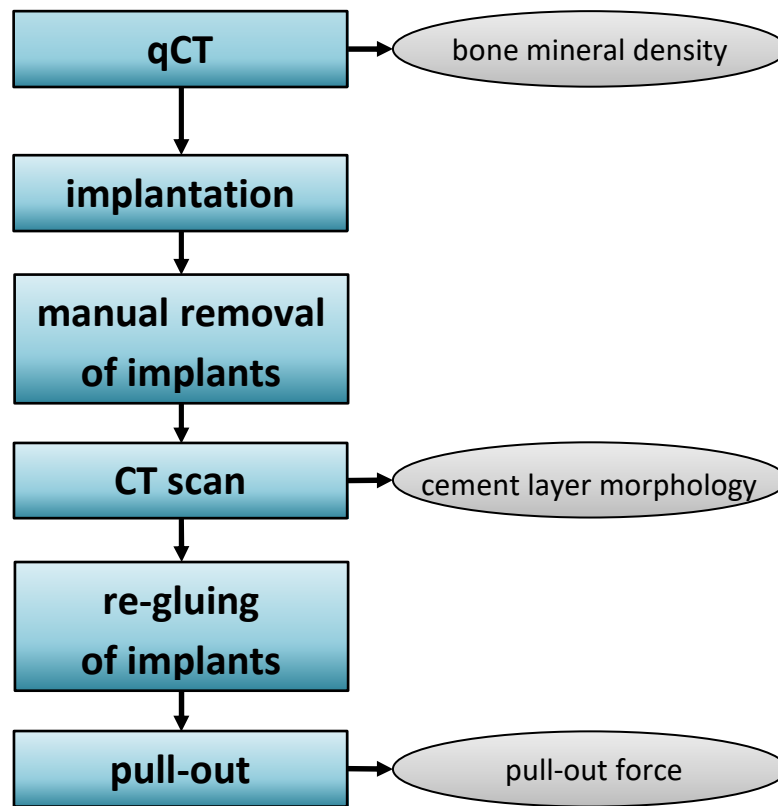


Figure 3-7: Experimental procedure applied to the specimens analysed in this chapter. The specimens were CT-scanned without implant and the implant were re-glued to the cement layer for mechanical testing (pull-out).

3.2.6 Pull-out Testing

Pull-out testing was performed, using a servo-hydraulic testing machine (MTSBionix, 858.2, MTS, Eden Prairie, MN, USA). The actuator and load cell capacities were 25 kN in the axial direction. Pilot testing revealed that the fixation strength of the tested implants may exceed 10 kN (Appendix A.3). The implanted specimens were embedded in metal holders, using PMMA resin (**Figure 3-8**, left). Embedding was enhanced by inserting screws into the tibial shaft (diaphysis) in a transverse direction. The specimen was positioned with the cement bed plateau plane horizontal at approximately 80 mm above the resin surface (**Figure 3-8**, left). The plateau was aligned to the holder base, using a spirit level. When the resin was cured, the implants were re-glued to the cement bed. The embedded specimen was mounted to the hydraulic testing system. An xy table was mounted below the metal holder to limit shear reaction forces in the transverse plane. The axial actuator of the machine was equipped with a Cardan joint and a machine adapter to enable unconstrained alignment of the load axis with the implant axis (**Figure 3-8**, left). All pull-out testing was performed quasi-statically at 0.5 mm/s and the data sampling rate was 50 Hz. During testing, seating processes occurred within the setup, for example, in the interlock of the implant-machine coupling and the Cardan joint. Each pull-out

experiment was filmed in order to assign occurring irregularities in the force-displacement curve to those seating events. The failure force F was defined as the first force peak with subsequent force decrease of more than 20 N that could not be assigned to a seating event visible in the documenting video (**Figure 3-8**, right). The determined failure force F was standardised to the effective area of the bone plateau to determine the strength of the interface S (Section 3.2.7).

Expected failure modes were failure at the cement-glue interface, the cement-bone interface, within the bone below the tibial plateau or failure of the embedding. The latter refers to failure of the embedding material with damage in diaphyseal or metaphyseal regions of the tibia that precluded repeated embedding.

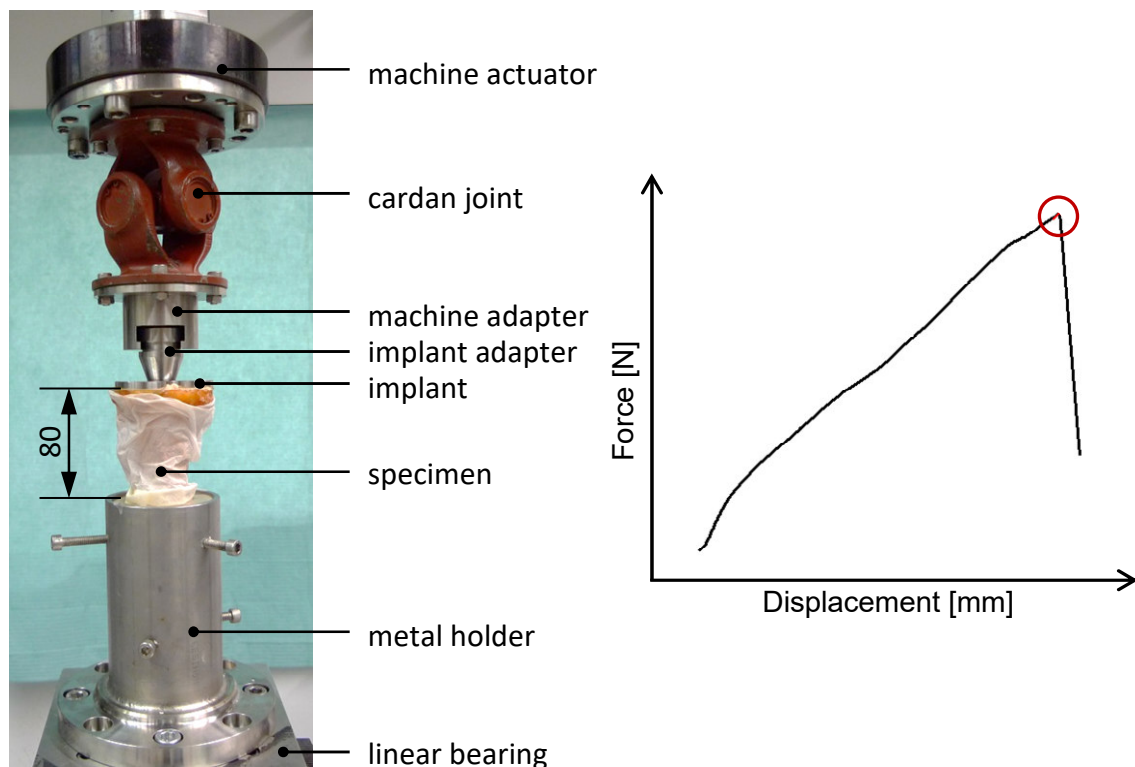


Figure 3-8: Experimental testing of tibial fixation. Left: Embedded specimen mounted to the testing machine. The plateau was positioned 80 mm above the resin surface. During embedding and pull-out, the specimens were wrapped in wet tissue paper to prevent the bone from drying out. Right: Characteristic force-displacement curve with marked failure event.

The whole testing procedure took 16 h (defrosting > 2 h, embedding curing > 1 h, glue curing > 8 h, alignment for embedding, cleaning for re-gluing). The specimens were tested about 24 h after being removed from the freezer. During the whole process, the specimens were wrapped in wet tissue paper and foil whenever possible to prevent drying out. This was essential, but led to increased humidity around the cement layer, which was shown to decrease the bonding strength of polymeric adhesives¹⁶⁹. Humidity was reduced by leaving the bony plateau with PMMA glue unwrapped. Due to the long testing procedure, wetting of the bone could not be omitted. This aspect is discussed in Section 3.4.5.

3.2.7 Cement Layer Morphology Analysis

The cement layer morphology was analysed using mathematical programming software (MATLAB®, The MathWorks Inc., Natick, MA, USA) and 3D reconstruction software (Avizo® 7, VSG, Burlington, MA, USA). A semi-automatic routine was developed for determination of morphology parameters. The algorithm is explained in the following paragraph and a flow diagram of the MATLAB® routine is given in Appendix B.1.

3D models were reconstructed based on the CT scans generated after soft pull-out of the implant (Avizo®, **Figure 3-9**). CT segmentation was performed according to HU values. The threshold between air and bone was set to -700 HU. The threshold for automatic segmentation between bone and cement was chosen as 500 HU, 600 HU or 700 HU. The decision as to which threshold was to apply was based on the differing HU range of the scan and corresponding capturing of the cement layer morphology. All applied segmentation thresholds are listed in Appendix B.2. Manual reworking after threshold-based segmentation was necessary regarding areas of highly dense bone that were assigned to the cement segment.

The cement layer model was aligned with the global coordinate system of the CT scanner, based on the centre of the implant stem cavity and parallel to the surface of the cement bed (**Figure 3-9**, right). This was performed using a MATLAB® module in the 3D reconstruction software.

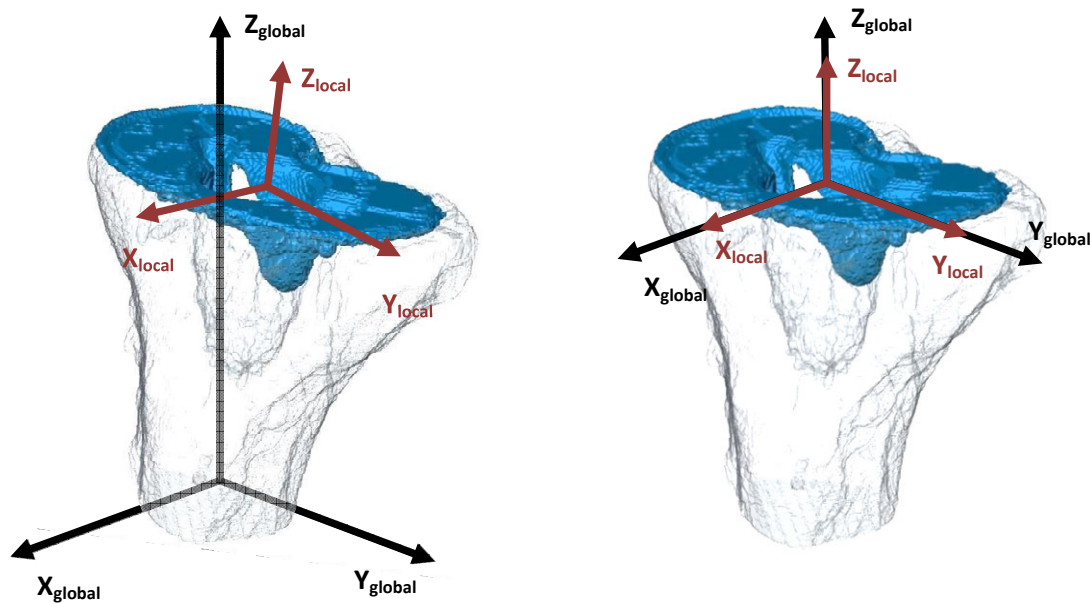


Figure 3-9: 3D model of a tibia with cement layer (blue) reconstructed from CT scans with corresponding coordinate system. Cementation was performed plateau-only. The cement-free stem cavity is visible in the metaphyseal region. Left: The global coordinate system (black, defined by the specimen position in the CT scanner) is different from the local coordinate system (red), defined by implant cavity and cranial surface of the cement bed. Right: Specimen position was aligned to the global coordinate system.

Alignment of the 3D model to the global coordinate system was performed as follows. For centre definition, the cement layer was virtually cut below the plateau. The cut level was chosen to provide sufficient reproduction of the inner stem geometry to fit an ellipse.

Sections of the received cross-sectional contour were deleted to reduce the data set to only those lines that reflect the stem cavity contour (**Figure 3-10**). Since the specimen's spatial position in the scanner was not axially aligned, the cut was not parallel to the cement layer surface and the cut profile of the stem was elliptical. The error due to the tapered shape of the stem was negligible for axis deviation of less than 5° . An ellipse was fitted to the contour lines and its centre was taken as origin of the z axis. The direction of the z axis was normal to the plane that was spanned by three markers on regions of the same level on the cranial cement layer surface, defining the xy plane (**Figure 3-10**).

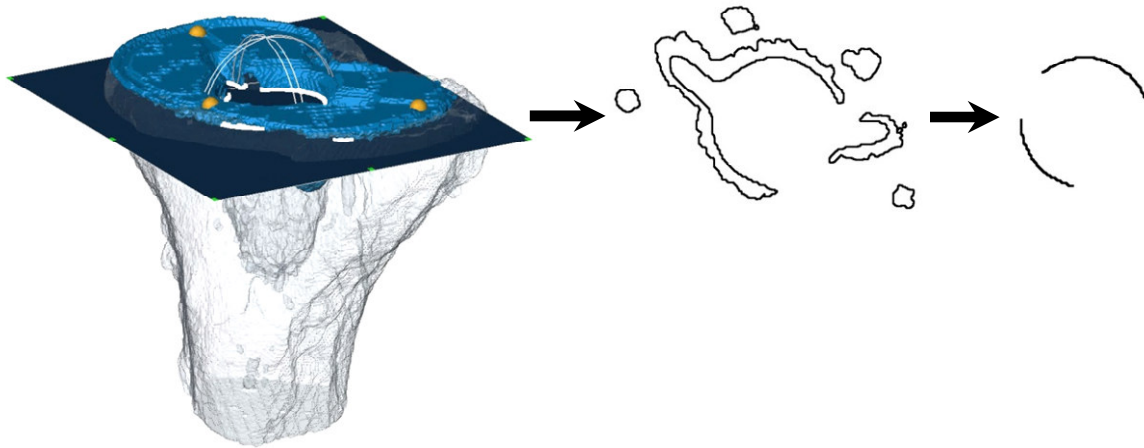


Figure 3-10: Determination of the position of the 3D model. From left to right: The 3D model was cut according to a cut plane. The white line in the model represents the cut line, which was then manually reduced to one or more bows representing the stem profile. Its centre point was used as temporary origin for the local coordinate system. Three markers were positioned on the cement layer to define the xy plane (yellow spheres on the blue cement layer).

Based on the local z axis, the model was aligned to the global z axis (**Figure 3-9**, right) and translated to the origin. The x and y axes are aligned in a subsequent step. The 3D model was converted to a triangle surface model and a tetrahedron volume model for further processing (**Figure 3-4**). Minimal edge length for both was 0.16 mm. The models were exported in ascii format and further processed in MATLAB®.

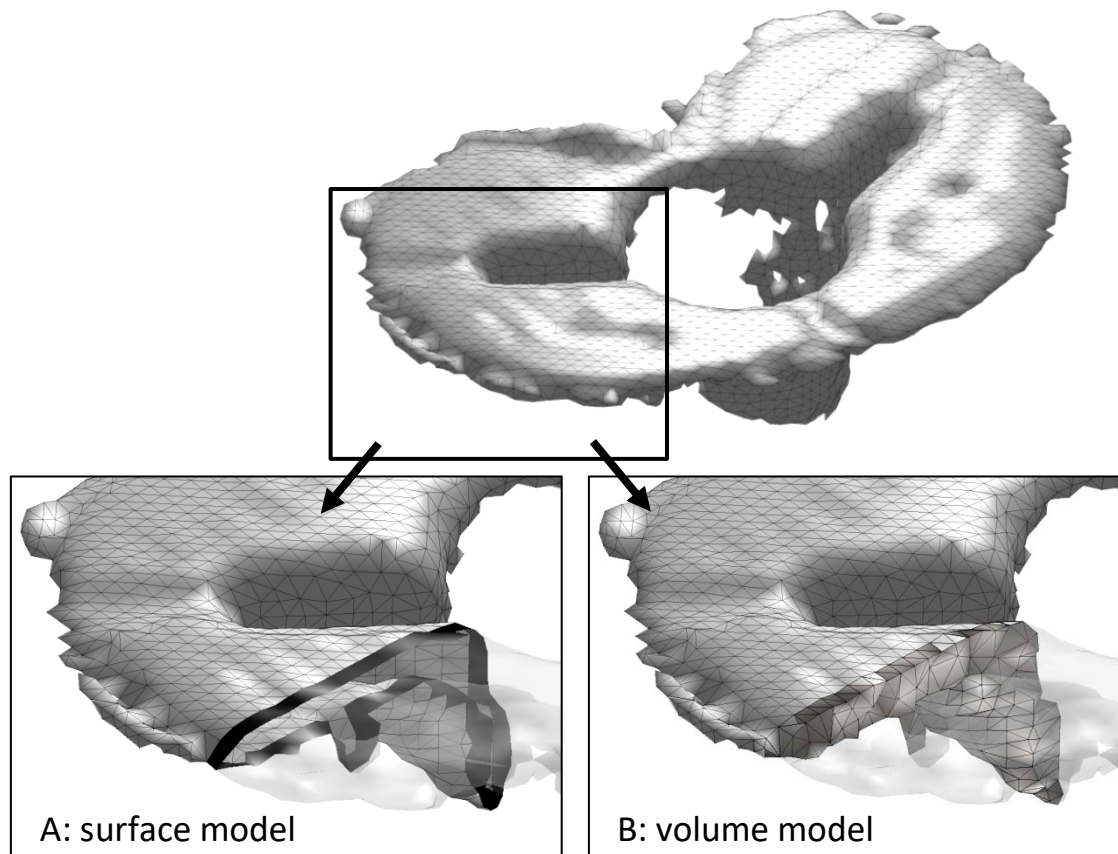


Figure 3-11: 3D models generated for each specimen; resolution of elements is enlarged for better visibility. A: 3D surface model composed of triangles. B: 3D volume model composed of tetrahedrons.

The resection plateau was defined by a best-fit plane of 10 landmarks positioned manually on the cortical rim and exported in MATLAB® data file format⁸ (**Figure 3-12**). The best-fit plane served as reference plane for processing. In MATLAB® the triangle and tetrahedron models were aligned according to x and y axes, with the x axis pointing anteriorly, the z axis pointing cranially. Left and right tibiae were not distinguished in analysis, therefore the y axis direction is of minor interest. The origin of the coordinate system was in the centre of the implant stem cavity ($x = 0$, $y = 0$) at the level of the tibial plateau after resection ($z = 0$, **Figure 3-12**).

⁸ File extension “.mat”

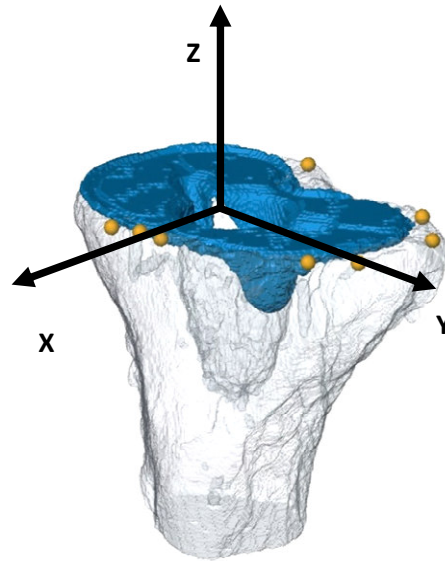


Figure 3-12: Determination of the resection plateau by 10 markers on the cortical rim (yellow spheres). The resection plateau was the reference plane for distinguishing between penetrating cement and cement between plateau and implant. The coordinate system displays the coordinate convention used in this study.

Two kinds of artefacts may bias the morphology analysis. Firstly, regardless of whether the stem was cemented or left cementless, there was cement within the stem cavity in any case, although to a differing extent. This cement penetrated the bone; however, the actual bone surface could not be defined as was performed with the resection plateau. Penetrating cement could not be distinguished from cement that merely filled in the gap between bone and implant. For the cement layer evaluation, the region around the stem was removed from the models (**Figure 3-13, A**). The cut contour was defined parallel to the stem contour. The distance was chosen in a specimen-specific fashion, such that all cement that might bias the results was removed.

Secondly, the excess cement at the outer rim of the implant during implantation was removed, but residues that did not penetrate the bone may have been left (**Figure 3-13, B**). These residues would affect the cement evaluation, despite not being involved in the pull-out mechanics. They were cut off, based on a contour parallel to the outer tray geometry. The distance of the parallel outer contour was directed inwards and chosen in a specimen-specific fashion (**Figure 3-13, C**).

Figure 3-13, D shows a top view of the data region from which the parameters were determined, the evaluation area *evalA*. Naturally, *evalA* was smaller than the actual bearing area *bearA* of the implant (**Figure 3-13, D**).

Diminishing of the 3D model data set according to the distances between original contour and evaluation contour chosen was performed automatically by the MATLAB® routine.

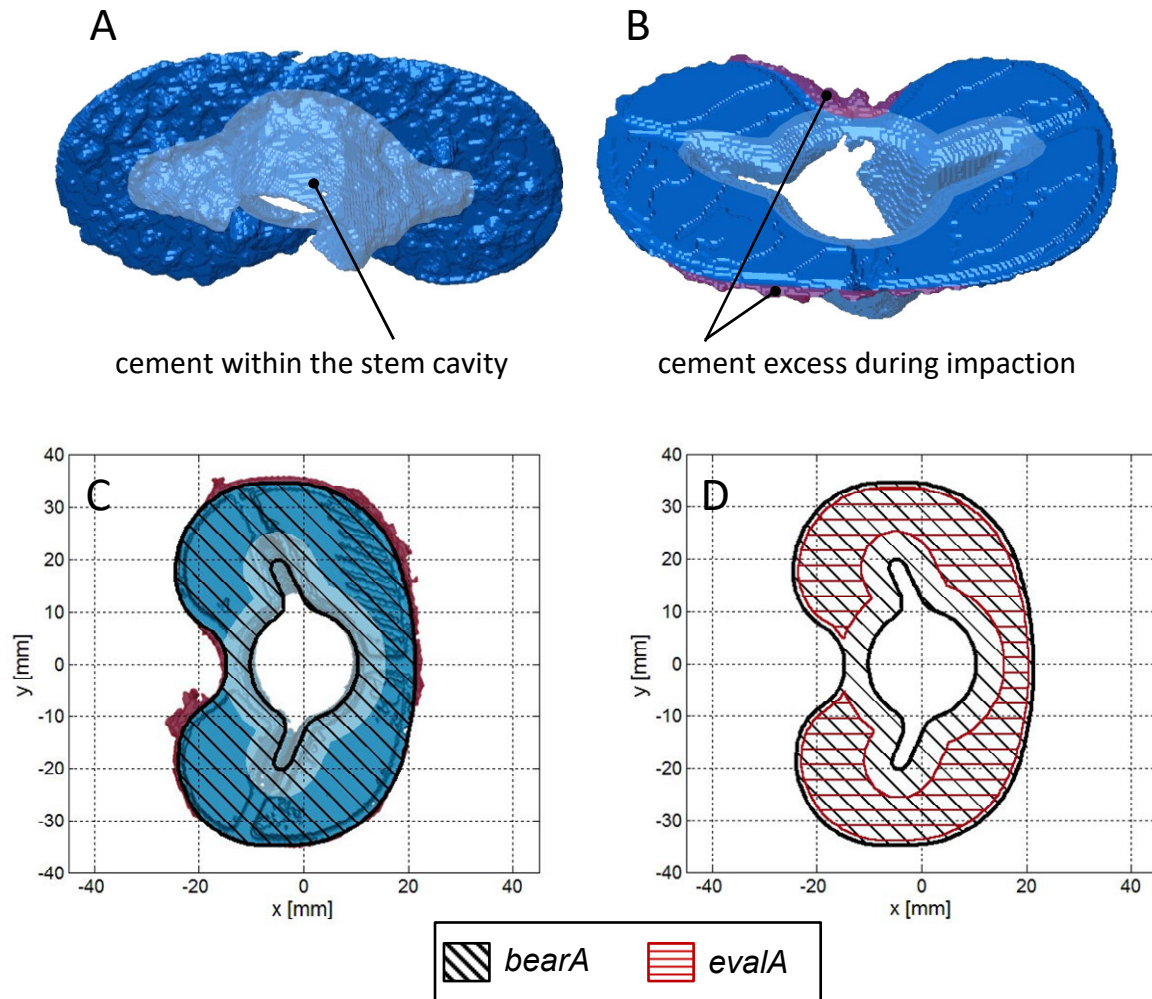


Figure 3-13: Data processing to reduce bias in the analysis. A: Cement region around the stem was removed from the model (light blue). B: Excess cement at the outer rim (red) was also removed from the model. C: Top view of the 3D model with delineated *bearA*, which is the bearing area between implant and cement, defined by size-dependent outer implant contour and stem contour. Removed regions of the cement layer are indicated in red and light blue. D: *BearA* and *evalA*. *EvalA* is confined by the combined parallel of the inner and outer *bearA* contour. Distance to the outer contour is exaggerated for better visibility.

Finally, the analysis was restricted to the cement geometry below the resection plateau (penetrating cement), i.e. data points with $z < 0$.

The penetration depth of the cement into the bone was determined in terms of the median of the distances of each data point to the bone plateau (*MedPen*), as done in previous studies^{12,29}. The volume (*Vol*) was calculated from the summed volumes of tetrahedrons, and the projected area (*Aproj*) was calculated from the surface triangles that were projected to a horizontal plane in the global coordinate system (**Figure 3-14**). The projected area was the basis for determining a reference area for the measured failure force to receive the strength of the fixation. The determination of this reference area and a volumetric characteristic of the cement layer are described in the following paragraphs. In order to minimise the unsystematic error due to removal of the stem cement, the interdigitation-related and therefore strength-effective parameter *Aproj* was normalised to *evalA* according to

$$Aproj_0 = \frac{Aproj}{evalA} , \quad (3-1)$$

where $Aproj_0$ reflects the actual cement-penetrated portion of the evaluated area. Vol was normalised to $Aproj$ according to:

$$Vol_{spec} = \frac{Vol}{Aproj} . \quad (3-2)$$

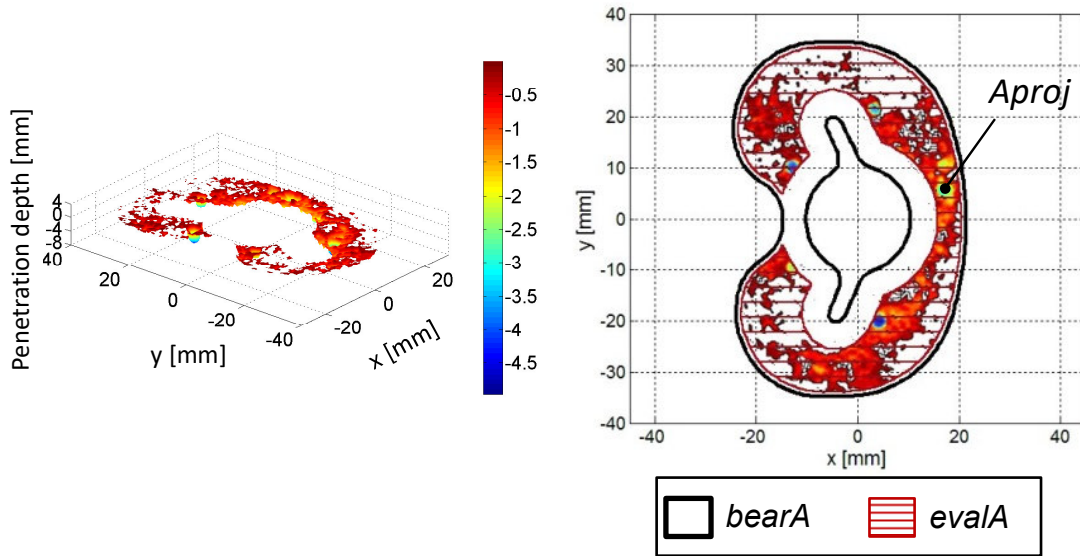


Figure 3-14: Characteristic cement layer of a specimen with low projected area $Aproj$, which is the area that is actually penetrated by cement. Left: 3D view of the surface model which is projected to the resection plane at $z = 0$. Right: The projected area was normalised by the area that was evaluated ($evalA$) to receive the proportion of penetrated area ($Aproj_0$), which is then extrapolated to the bearing area ($bearA$, black contour) to receive $AprojEx$.

$Aproj_0$ was applied to $bearA$ according to

$$AprojEx = Aproj_0 * bearA , \quad (3-3)$$

where $AprojEx$ was the cement-penetrated area with regard to the lower implant bearing area instead of the smaller region that was available for evaluation.

$AprojEx$ was used as reference area for the determined failure force F , resulting in failure strength S :

$$S = \frac{F}{AprojEx} , \quad (3-4)$$

Using S in the analysis instead of F controlled for the variation in the parameters that was due to the specimen-specific difference between $evalA$ and $bearA$.

Penetration increase in the peripheral region of the implant bearing area was considered influential on the overall strength of the fixation, since the bone in this area is generally stronger than in the central region. Therefore, the parameters $MedPen$, Vol and $Aproj$ were also determined for the peripheral region (RIM) only ($MedPen_{RIM}$, Vol_{RIM} and $Aproj_{RIM}$). The

width of the RIM was determined in an implant-specific fashion to receive a resulting RIM area covering 50 % of the bearing area (**Figure 3-15**, right). This portion-based approach was chosen to retain comparability between the different sizes. Stannage *et al.*¹⁷⁰ determined the cement penetration depth with regard to the percentile distance from implant contour to stem. Based on their results, an areal portion of 50 % was considered to capture relevant effects. Cement volume Vol_{RIM} and area $Aproj_{RIM}$ were standardised to the RIM evaluation area $evalA_{RIM}$:

$$Area_{0,RIM} = \frac{Area_{RIM}}{evalA_{RIM}} \quad . \quad (3-5)$$

Vol_{RIM} was normalised to $Aproj_{RIM}$ according to:

$$Vol_{spec,RIM} = \frac{Vol_{RIM}}{Aproj_{RIM}} \quad . \quad (3-6)$$

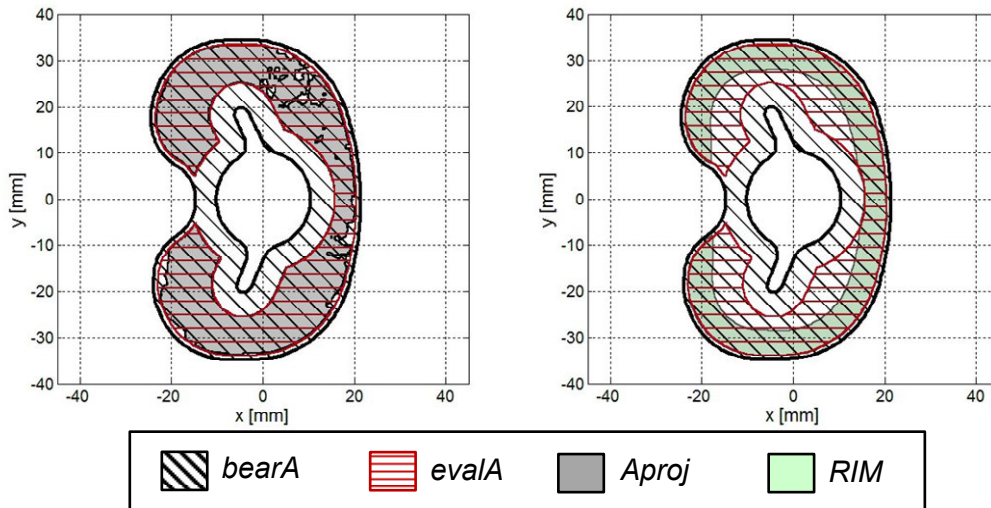


Figure 3-15: Different areas on the resected tibial bone surface. Left: Actually penetrated bone area $Aproj$. Right: RIM region, which made up 50 % of $bearA$ and was evaluated in an extra analysis.

3.2.8 Statistical Analysis

BMD as a structural parameter was controlled for by the paired design. However, BMD was compared overall between treated and CONTROL sides by a pairwise T test or a Related Samples Wilcoxon Signed Rank test, depending on the estimated distribution of the data.

Linear regressions were performed on the CONTROL side specimens to investigate the influence of BMD on bone cement penetration $MedPen$, $AprojEx$, F and S . Influence of $MedPen$ and $AprojEx$ on F was also tested by linear regressions, as well as influence of $MedPen$ on S . Adjusted R^2 was reported.

Comparison of $MedPen$, Vol_{spec} and $Aproj_0$, F and S between CONTROL and treatment side within each of the four groups was performed by a pairwise T test and a Related Samples Wilcoxon Signed Rank test where appropriate. $MedPen$, Vol_{spec} and $Aproj_0$, failure force F

and failure strength S were analysed over the evaluated area and for RIM region ($MedPen_{RIM}$, $Vol_{spec,RIM}$ and $Aproj_{0,RIM}$).

All statistical evaluations were performed using SPSS (IBM® SPSS® Statistics 21, IBM Corporation, Armonk, NY, USA) and applying a type-I error level of 0.05.

3.3 Results

Soft pull-out force for the FULL specimens ranged from 201 N to 951 N. In the following paragraphs, results for failure mode, BMD correlation and morphology parameters are given.

3.3.1 Failure Mode

In $n = 14$ cases, failure occurred in the trabecular bone with fractured bone remaining attached to the cement when the implant was pulled out (**Figure 3-16, A**). In $n = 5$ out of 36 cases, failure occurred directly at the cement-bone interface (**Figure 3-16, B**). Failure occurred either at the (re-attached) glue-implant interface or diaphyseal bone in $n = 17$ out of 36 cases (**Figure 3-16, C**). Failure modes are listed in Appendix C.2.3.

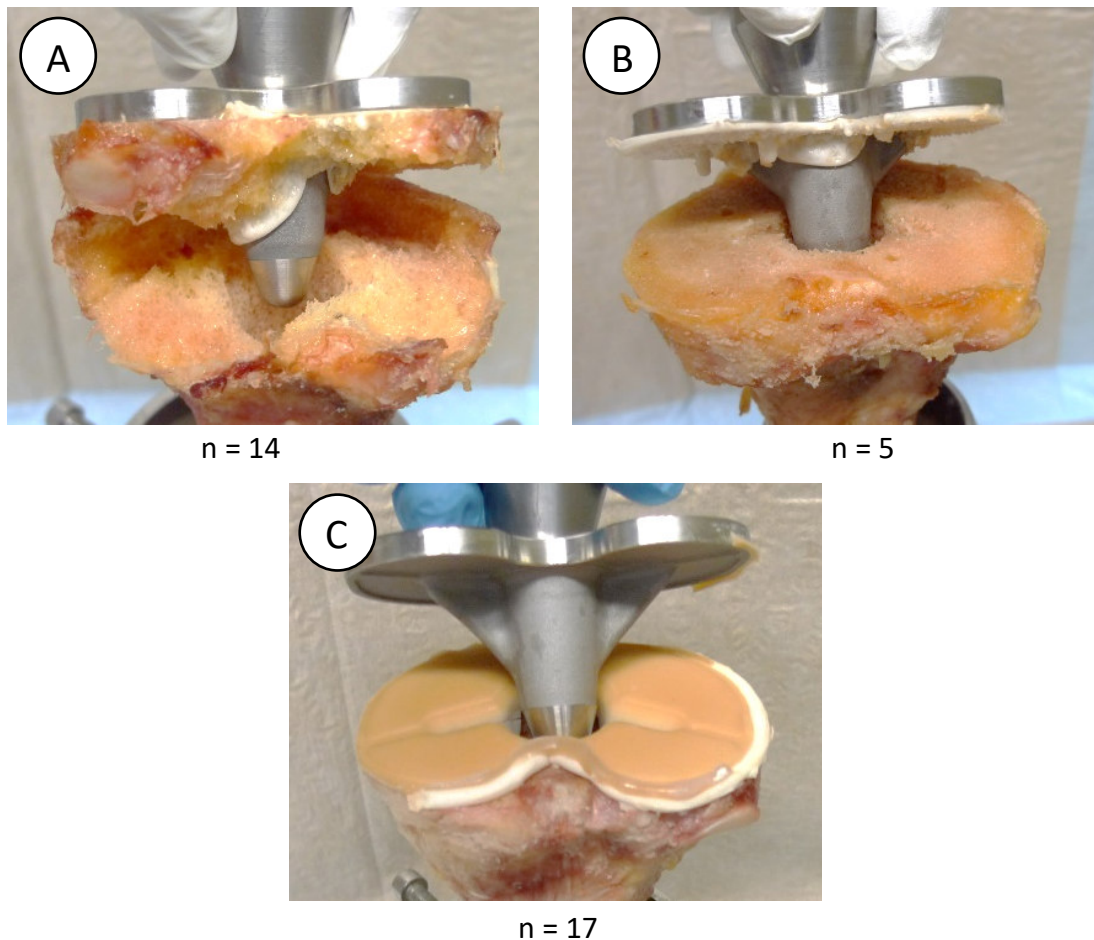


Figure 3-16: Failure modes in pull-out testing. A: Bulk bone failure (3006 L), B: Bone interface failure (3006 R), C: Glue interface failure (3023 R, brown-coloured layer is glue).

In one bulk bone failure case, it was not clear whether the interface was intact before pull-out (3008 R). The corresponding pull-out force was removed from the analysis, leaving $n = 13$ bulk bone failures and $n = 5$ cement-bone interface failures. All strength-related

evaluation was limited to these 18 specimens. Range of force F was from 469 N to 10 550 N (mean 4 766 N, SD 3 349 N) and corresponding S ranged from 0.36 MPa to 5.33 MPa (mean 2.62 MPa, SD 1.70 MPa). In the 17 glue/diaphysis failure cases, pull-out force was greater than 1 440 N (range 1 442 N to 9 941 N). The mean pull-out force F was 6 296 N (SD = 2 190 N), the mean strength S was 3.41 MPa (SD = 1.63 MPa).

Due to the frequent diaphyseal or glue interface failure, sample sizes within each group were too small for force-related comparison of FULL, GUN and LAYERED specimens to their CONTROL (Group FULL $n = 1$ vs. 1, Group GUN $n = 2$ vs. 2, Group LAYERED $n = 2$ vs. 1).

Comparison of SYRGUN to their CONTROLS showed a significant difference in both F and S (both $p = 0.028$, Related Samples Wilcoxon Signed Rank test).

3.3.2 Bone Mineral Density

BMD between treatment and CONTROL side was not significantly different ($p = 0.806$, paired T test).

Linear regression over all CONTROL specimens ($n = 18$, **Figure 3-17**) showed no significant relation between BMD and penetration parameters $MedPen$ ($p = 0.464$) or $AprojEx$ ($p = 0.939$).

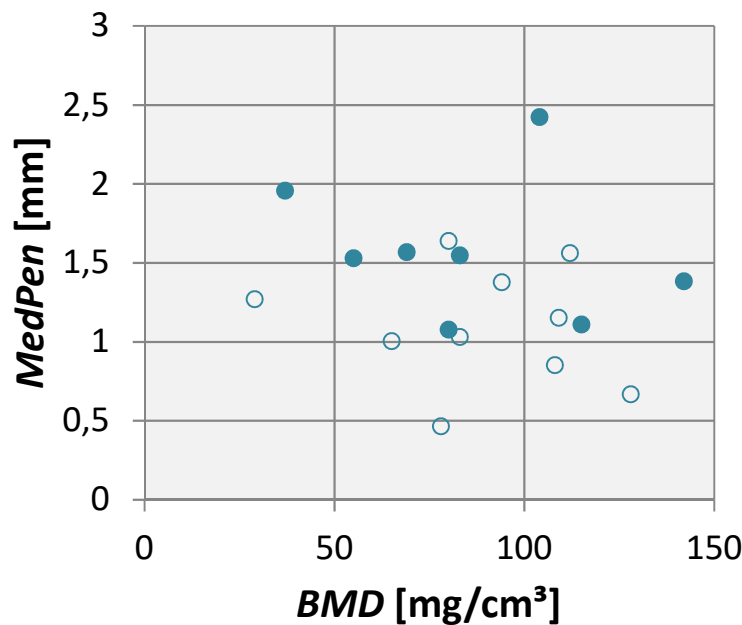


Figure 3-17: Median cement penetration depth $MedPen$ over BMD of CONTROL specimens. Linear regression shows no significant relation ($p = 0.464$, $n = 18$). There was likewise no relation of BMD to $AprojEx$ ($p = 0.939$, $n = 18$). Empty markers represent specimens that failed at the diaphysis / glue interface. Filled markers represent specimens that failed on the bone side.

$N = 8$ CONTROL specimens failed on the bone side and F and S were analysed. Failure force F did not significantly increase with increasing BMD ($R^2 = 0.22$, $p = 0.133$, **Figure 3-18**, left). The strength S significantly increased with increasing BMD ($R^2 = 0.65$, $p = 0.010$, **Figure 3-18**, right).

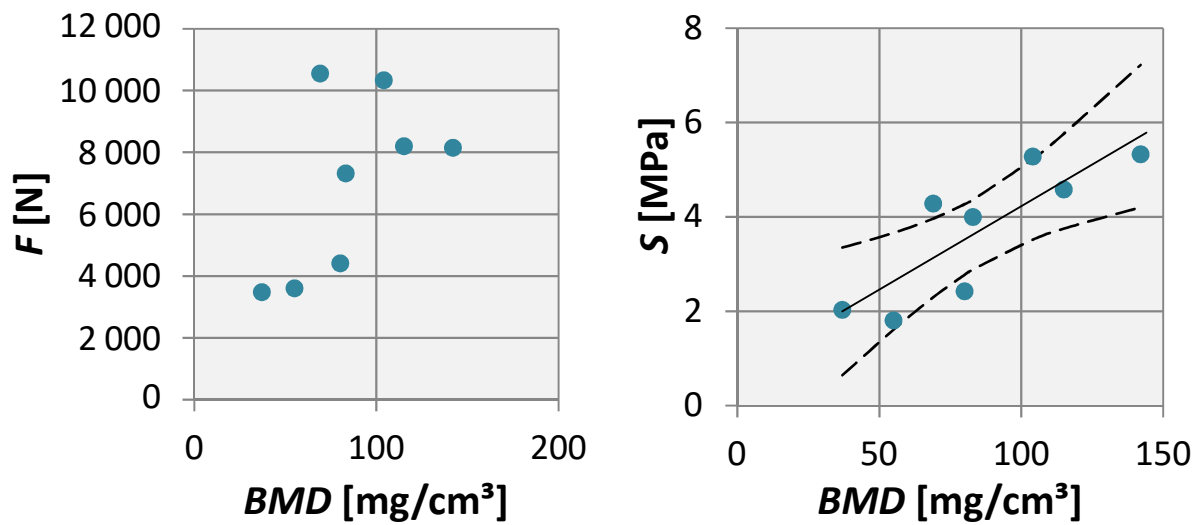


Figure 3-18: Failure force and strength over BMD of the CONTROL specimens that failed on the bone side of the cement (bulk and interface, $n = 8$). Left: Failure force F was not significantly related to BMD ($p = 0.133$). Right: Failure strength S significantly increased with increasing BMD ($R^2 = 0.65$, $p = 0.010$). 95 % confidence interval for the regression line is shown.

3.3.3 Cementation and Penetration-Increasing Techniques

Characteristic examples of the cement layers are displayed in **Figure 3-19**.

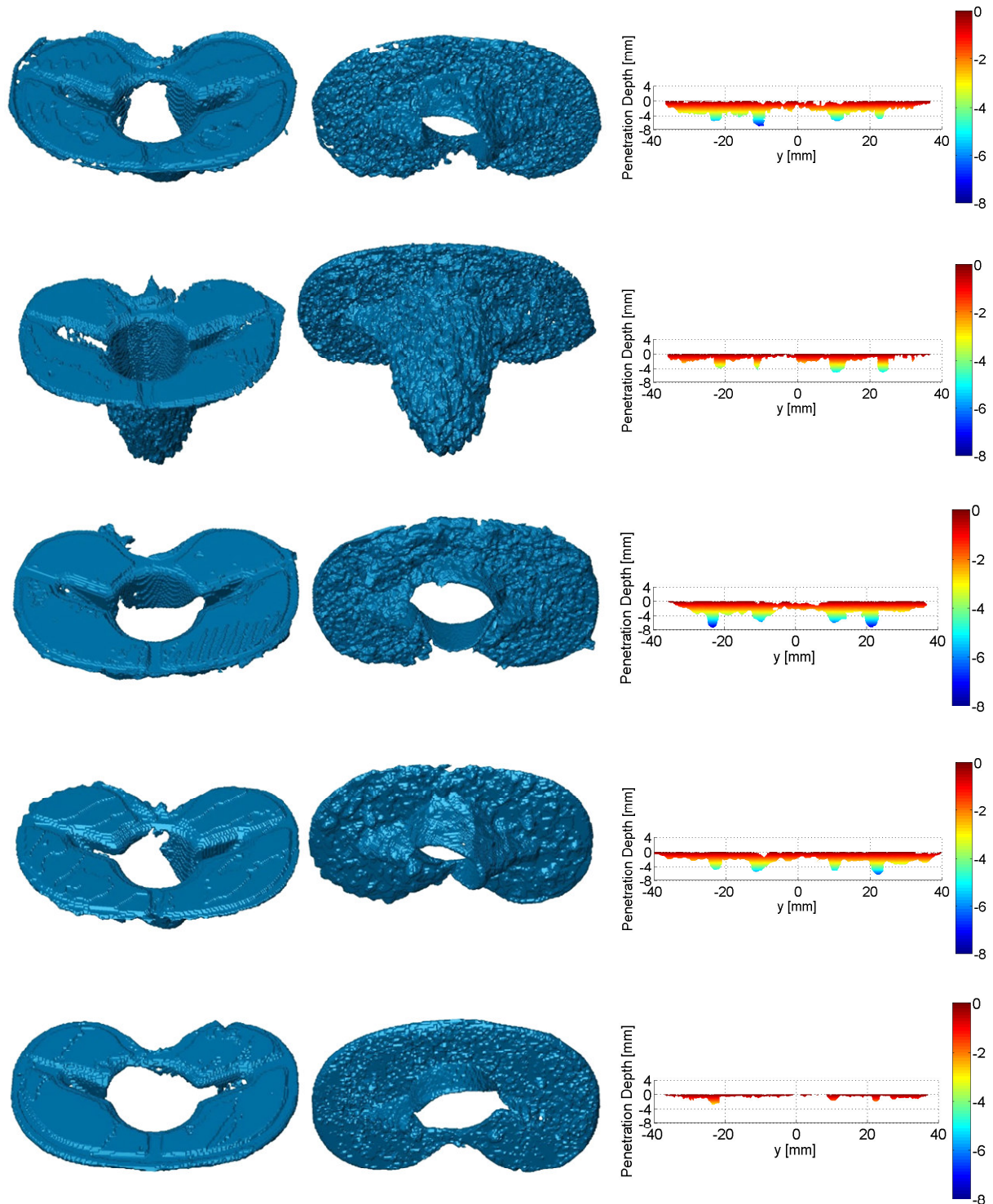


Figure 3-19: Characteristic 3D models of cement layers for the 5 applied cementation techniques. For each – top view and bottom view, as well as the anteroposterior view of the stem- and excessing-cement-reduced models with color-coded penetration depth is shown. The reduced model was the base for parameter determination. A: CONTROL cementation technique, B: FULL cementation technique, C: GUN cementation technique, D: LAYERED cementation technique, E: SYRGUN cementation technique.

Pull-out force F of the 8 bone failures in the CONTROL specimens was not significantly related to *MedPen* ($p = 0.569$) and *AprojEx* ($p = 0.338$). Also, pull-out strength S was not significantly related to *MedPen* ($p = 0.714$).

Mean *MedPen*, *Aproj_o* and *Vol_{spec}* were compared between treated and CONTROL side of each group (paired T test, **Table 3-2**, **Figure 3-20**). There was no significant difference between *Aproj_o* of FULL and LAYERED specimens and their CONTROL sides ($p_{\text{FULL}} = 0.690$, $p_{\text{LAYERED}} = 0.281$).

For GUN application, there was a trend towards larger *Aproj_o* for the treated side ($p = 0.059$). *MedPen* was significantly larger (2-fold) following GUN application ($p = 0.026$) as well as *Vol_{spec}* was significantly larger by 94 % ($p = 0.034$).

Within FULL and LAYERED groups, no significant difference for *MedPen* ($p_{\text{FULL}} = 0.910$, $p_{\text{LAYERED}} = 0.757$) and *Vol_{spec}* was found ($p_{\text{FULL}} = 0.837$, $p_{\text{LAYERED}} = 0.800$).

When comparing the different approaches for penetration increase, pulsatile lavage specimens had significantly larger *MedPen* (3.5-fold, $p = 0.006$), *Aproj_o* (38 %, $p = 0.011$) and *Vol_{spec}* (4.2-fold, $p = 0.004$).

Table 3-2: Group means and p values for within-group comparisons of *MedPen*, *Aproj_o* and *Vol_{spec}* (* indicates significant p values).

		Parameter		
		<i>MedPen</i>	<i>Aproj_o</i>	<i>Vol_{spec}</i>
FULL	CONTROL	1.10 (0.18)	0.79 (0.03)	0.99 (0.15)
	treated	1.12 (0.49)	0.76 (0.19)	1.04 (0.53)
	p	0.910	0.690	0.837
GUN	CONTROL	1.07 (0.35)	0.80 (0.15)	0.99 (0.38)
	treated	2.19 (0.82)	0.90 (0.02)	1.92 (0.74)
	p	0.026*	0.059	0.034*
LAYERED	CONTROL	1.50 (0.39)	0.85 (0.04)	1.33 (1.39)
	treated	1.41 (0.48)	0.85 (0.07)	1.26 (0.44)
	p	0.757	0.281	0.800
SYRGUN	CONTROL	1.49 (0.62)	0.80 (0.16)	1.30 (0.56)
	treated	0.43 (0.18)	0.58 (0.18)	0.31 (0.12)
	p	0.006*	0.011*	0.004*

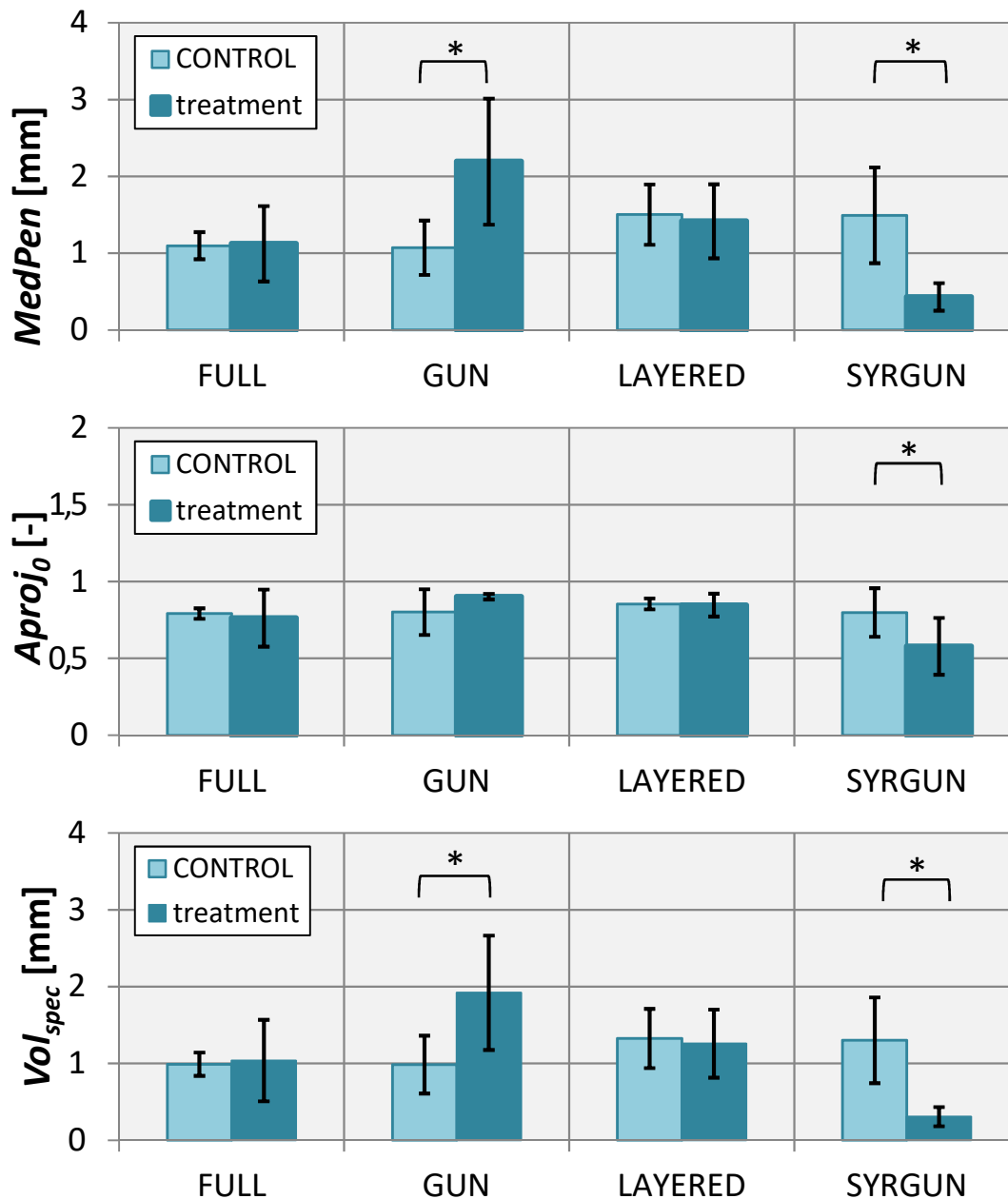


Figure 3-20: Mean values of $MedPen$, $Aprojo$ and Vol_{spec} sorted by group and CONTROL vs. treatment cementation technique (error bars indicate standard deviation).

Results of pairwise comparisons (paired T test) for the RIM region are displayed in **Table 3-3**. There was no significant difference in $MedPen_{RIM}$, $Aprojo_{RIM}$ and $Vol_{spec,RIM}$ between CONTROL and treated side of FULL, GUN and LAYERED cementation techniques with regard to the peripheral rim region. There was a trend to be larger on the GUN-treated side than on the CONTROL side for $MedPen_{RIM}$ ($p = 0.063$) and $Vol_{spec,RIM}$ ($p = 0.067$).

Pulsatile lavage led to significantly increased $MedPen_{RIM}$ (3-fold, $p = 0.012$) and $Vol_{spec,RIM}$ (4.5-fold, $p = 0.007$) in the rim region of the implant compared to gun application after syringe lavage. $Aprojo_{RIM}$ tended to be larger after pulsatile lavage than after gun application, however, this was not significant ($p = 0.071$). Corresponding diagrams are provided in Appendix C.2.4.

Table 3-3: Group means and p values of T test for within-group comparisons of *MedPen_{RIM}*, *Aprojo_{0,RIM}* and *Vol_{spec,RIM}* (* indicates significant p values).

		Parameter		
		<i>MedPen_{RIM}</i>	<i>Aprojo_{0,RIM}</i>	<i>Vol_{spec,RIM}</i>
FULL	CONTROL	0.86 (0.23)	0.66 (0.05)	0.71 (0.22)
	treated	0.83 (0.44)	0.62 (0.21)	0.71 (0.46)
	p	0.849	0.780	0.972
GUN	CONTROL	0.71 (0.23)	0.65 (0.16)	0.66 (0.29)
	treated	1.64 (0.86)	0.80 (0.05)	1.44 (0.74)
	p	0.063	0.150	0.067
LAYERED	CONTROL	1.08 (0.34)	0.72 (0.05)	0.92 (0.37)
	treated	1.06 (0.48)	0.71 (0.12)	0.89 (0.43)
	p	0.935	0.919	0.875
SYRGUN	CONTROL	1.12 (0.48)	0.68 (0.17)	0.94 (0.43)
	treated	0.36 (0.18)	0.48 (0.16)	0.21 (0.12)
	p	0.012*	0.071	0.007*

3.4 Discussion

Increased cement penetration depth into the bone has been shown to increase the strength of cemented fixation in tibial TKA^{12,25,29}. The cement layer morphology and thereby the cement penetration depth can be influenced by specific cementation techniques, although it is not known what technique in particular has a crucial effect. In this study, four techniques were investigated and compared to a defined control technique. Cement layer analysis revealed the effects of the cementation techniques on the cement layer. The analysis of failure strength was intended to evaluate the cement-bone interface strength. However, frequent failure of the implant-cement interface in mechanical testing prevented detailed insight into the relation between cement penetration depth and bone interface strength. Nevertheless, due to the strong relationship between the level of fixation strength and cement penetration depth, conclusions about the effectiveness of the cementation techniques were possible.

The discussion is structured in 5 sections, focusing on the effect of techniques on the cement penetration (Section 3.4.1) and considerations about the morphology analysis approach (Section 3.4.2), the relevance of the experimental penetration depth for clinics (Section 3.4.3), methodological aspects (Section 3.4.4) and general limitations (Section 3.4.5).

3.4.1 Effect of Cementation and Preparation Techniques on Cement Penetration

The occurring failure modes were bone interface failure and bulk bone failure, but also glue interface failure and diaphyseal bone failure.

Bone interface failures were present in the SYRGUN group only. Their CONTROLS failed within bulk bone (in the case of bone failure). This indicates a different failure mechanism, which may have been due to different lavage techniques applied in these sub-groups.

Hence, applying pulsatile lavage leads to failure in the bulk bone and not failure at the bone interface. The same pattern was observed by Walker *et al.*²⁵. Greater penetration that is achieved by pulsatile lavage, indicates that trabeculae are rather enclosed than only penetrated^{25,136}.

Glue / diaphyseal failures were undesired and the measured strength was considered as minimal strength of the corresponding fixation to the bone. Undesired failure was present in all the treatment and CONTROL specimens, but was less frequent in SYRGUN specimens and their CONTROLS (3 out of 12). However, two glue interface failures occurred in the SYRGUN group, while their CONTROLS failed at the bone interface at lower forces, which at least coincides with the expected direction of the effect towards larger force level for pulsatile specimens. The collateral specimen of the only glue interface failure in the CONTROL specimens exhibited the largest bone failure force measured in this study (10 550 N). Confidence is given that all three pairs follow the pattern of the remaining three.

There is no general recommendation regarding application of bone cement to the tibial surface, which leads to a notable variability in the techniques applied clinically.

In the present study, gun application doubled the median cement penetration depth and the volume of penetrating cement overall. This effect was significant even for the low sample size. This coincides with the results of Lutz *et al.*¹⁵⁰, who also found a doubling effect. Measurement in porcine bone showed a more uniform cement layer after gun cementation than after finger packing¹⁴⁹. The portion of penetrated area below the implant was not affected in the current study.

Gun cementation in combination with syringe lavage did not increase the cement penetration depth, compared to the control technique with pulsatile lavage and finger packing. Rather, penetration depth was only one-third compared to the control technique (0.49 mm and 1.49 mm, respectively) and even one-sixth in volume. It appears that the penetration-increasing aspect of gun pressurisation only comes into effect when pulsatile lavage is applied. This may be due to the plugging effect of bone debris in ineffectively cleansed bone¹³⁶, which may resist the pressure applied by the gun. According to the findings in other studies, lower penetration depth in the syringe (SYRGUN) specimens was accompanied by lower pull-out force and strength compared to the pulsatile specimens^{12,29}. Failure force and strength after pulsatile lavage were about 11 times and 8 times larger, respectively, than after syringe lavage. The effect of pulsatile jet lavage cannot be compensated for by usage of a cement gun.

No effect on the penetration was found for full cementation. However, the fixation stability was not intended to be increased by larger penetration depth in this setup, but rather to be affected by the larger cement mantle volume in the tibia. Indeed, the largest pull-out force was documented for a specimen from the FULL group (9.9 kN), being about 20 % larger than the largest force in the respective CONTROL specimen (8.2 kN), BMD was comparable. Nevertheless, in two of the four pairs in that group, pull-out strength for the CONTROL side was larger than in the fully cemented side, which is surprising, considering the smaller volume of cement around the stem compared to the fully-cemented treatment side (control side: 2 220 mm³, fully-cemented side 9 695 mm³). However, actual bone interface strength was determined for only 2 out of 8 specimens in Group FULL

(CONTROL and treatment); therefore effectiveness of full cementation on fixation strength remains unclear.

Likewise, layered cementation had no measurable effect on the cement penetration depth, although this has been demonstrated in artificial bones¹⁷¹. Hydrostatic pressure that counteracts the introduction of cement might be larger in cadavers than in dry artificial bone, since the distal pores of cadaveric specimens are still filled with fat and marrow despite any cleansing.

In the current study, there was no detectable correlation of cement penetration depth, volume, or penetrated area with force or strength, so the larger fixation strength in pulsatile specimens as found in other studies¹²¹³⁸ should not be contributed to the larger penetration depth offhandedly.

Considering the shown effect of pulsatile lavage regarding gun pressurisation, it appears likely that the effect of pulsatile lavage is large enough to generally override the effects of the cementation techniques. Pulsatile lavage has been shown to improve fixation strength in several studies and seems to be accepted as an important preparation step^{136,172-174}. Still, there are indications that about 30 % of surgeons do not apply pulsatile lavage in joint surgery^{139,140} (Section 2.3.2.3).

Cement penetration depth, volume and penetrated plateau area of CONTROL specimens were not related to bone density. Jones *et al.*²⁷ as well as Raiss *et al.*²⁶ found significant negative correlations between BMD and the achieved penetration depth. Nevertheless, both applied dual-energy X-ray absorptiometry (DXA) methods for BMD evaluation. Results from the DXA method are largely dependent on bone size, so that measurements from different sized bones can result in different values for *BMD*, although their real bone mineral content (BMC) may be similar¹⁷⁵. In another study, no relation between bone quality and cement layer morphology was found²⁹.

BMD contributes to failure strength and may be determining, since the failures of concern were bulk bone failures. Mechanical properties of bone were shown to correlate with BMD^{131,176}. However, the sample size for the regression was low ($n = 8$) and statistical power therefore limited.

3.4.2 Aspects in Cement Layer Analysis

Failure force was independent of bone density, whereas failure strength increased with increasing bone density. This difference was due to the four different implant sizes in the analysis. The bearing area of the largest size was almost 50 % larger than that of the smallest size (**Table 3-1**). Determination and analysis of fixation strength in terms of MPa is reasonable, since failure of materials is due to internal stress and therefore not directly related to external loading. Analysis of force may be biased by implant size.

Although CT scanning was performed without the metal implant, artefacts may still be present. The attenuation of the cement, the interpolation and smoothing processes during 3D reconstruction and, if nothing else, the segmentation process, are source for errors that may bias the results in a systematic or unsystematic way. In a validation study for the segmentation process, measures were obtained from sections of a specimen with intact cement fixation and compared to measures obtained from virtual sections at the 3D models at the same positions (Appendix B.4). There was a systematic error of 4 %

underestimation of lengths in the CT 3D models. The resulting model of the cement layer reflected the actual geometry of the cement layer in adequate quality.

In previous studies, a semi-automatic Avizo®- and MATLAB®-based procedure was used for determination of median cement penetration depth^{12,29}. Elements of this procedure were taken over in the algorithm developed for this study. Several steps were refined or added, such as consideration of implant size. Refinement of the Avizo®- and MATLAB®-based analysis algorithm from previous studies was accompanied by an increase of manual input, which probably increased the dependency of the result on the observer. An inter-rater reliability analysis was carried out (details are given in Appendix B.3) and showed that good reliability of the procedure was given. Deviations appeared to be systematic and were rather due to a slightly differing segmentation than due to different choice of evaluation area.

Analysis of the cement penetration in the RIM region, as defined in this study, did not reflect the same findings as analysis of the whole region. Merely the effect of pulsatile lavage in contrast to using syringe lavage combined with gun application became apparent in the RIM region. Data published by Stannage *et al.*¹⁷⁰ showed an effect of cementation technique on the cement penetration in the lateral compartment, which was about constant when approaching the implant centre. Likewise, the cementation techniques studied here do not specifically affect the RIM region. Effectiveness or ineffectiveness of cementation techniques are reflected sufficiently by analysis of the whole region.

The data point resolution was 0.16 mm and considered as capturing the relevant geometrical characteristics from the CT scans, as the CT resolution was 0.40 mm to 0.46 mm in all directions.

3.4.3 Relevance of the Cement Penetration Depth Range Measured

The range of median cement penetration depth determined in this study was 0.21 to 3.42 mm and within a similar range to specimens in a retrieval study²⁹. The optimum penetration depth suggested is 3 to 4 mm²⁵. This is larger than in the current study, but may be based on a different evaluation method. Cement penetration depth in clinics is commonly determined from X-rays and reported in terms of maximum or mean depth, rather than the median depth presented in the current study^{14,16,136,150,170}. Also, the appearance of the implant in X-rays overlies the penetrating cement. Finally, most studies do not distinguish between cement penetration into the bone and cement lying between implant and bony plateau^{14,16}. The reported values might be the sum of cement above the plateau and penetrating cement, which could be misleading, considering that the cement layer thickness above the plateau from a mechanical point of view does not decisively contribute to fixation strength and also widely depends on the design of the back side of the implant, cement viscosity and other factors. This study concentrated on the cement that actually penetrated the bone. Scuderi & Clarke¹⁷⁷ suggest 1 mm to 2 mm actual penetration depth, which is in accordance with the values measured in this *in vitro* project, so the cadaveric pull-out model reflects the clinical penetration depth.

It has been stated that cement penetration depths below 2 mm could lead to reduced fixation strength²⁵. Taking into account the level of penetration depth and the considerations about determination methods applied in other studies, there is doubt that this statement is still valid when exact CT-based measurements as proposed in this study are applied. Large failure force of more than 3 000 N was achieved at surprisingly low median penetration of ~ 1.5 mm. From a biomechanical point of view, this value was sufficient for an *in vitro* setup.

3.4.4 Challenges of the Experimental Method

Machine aid was necessary for “soft removal” of the fully cemented implants, since they could not be removed by hand, despite release agent. This might be attributed to the larger contact area between implant and cement. However, this area was covered with release agent and so exhibited minimised friction. The form locking between cement and implant tip due to very small but visible undercuts that evolved from the modified stem tip was more probable (**Figure 3-21**). Forces measured during soft pull-out of the stem-cemented specimens ranged from 201 N to 951 N and were therefore not considered as impairing the cement-bone interface.

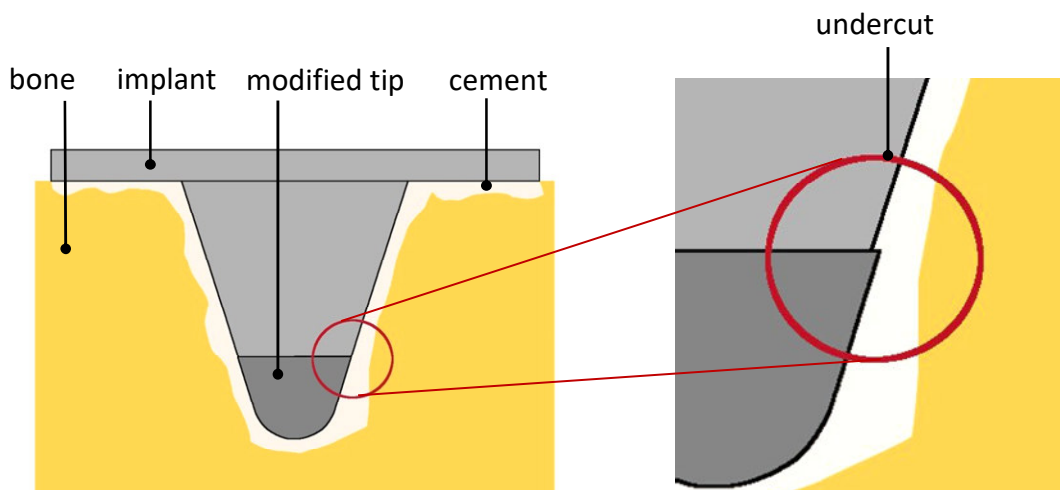


Figure 3-21: The modified tip resulted in undercuts, in some cases of full cementation. Left: Tip matches the implant geometry, no undercut. Right: Tip overlaps the implant geometry, undercuts increased interface strength in soft removal of the implant.

The overall lowest strength for a failing glue interface was 3 331 N. Previous pull-out studies concerning pulse lavage were limited to the level of implant interface strength (Schlegel *et al.*¹²: range 864 N to 1 391 N), lacking definite information about the improved bone interface strength. In a pilot study, it was shown that the pull-out forces for undercut-free implants can be even lower (Appendix A.1). This limitation was overcome by the applied re-gluing of the implant to the cement bed, although expected capacity of the glue interface was under-matched (Appendix A.3).

The CONTROL cementation technique was surface cementation, which is controversially discussed in clinics. A full cementation, as intended by most manufacturers, was reported to reduce micromotion and thus to improve long-term stability^{178–180}. Several studies did not find worrying differences between the two techniques, or even propose less bone resorption due to less stress-shielding^{15–17,180–183}. Furthermore, revision of a cemented

stem may increase bone loss during removal of the cement mantle, although *in vitro* data has challenged this argument¹⁸⁴. This study was based on CT segmentation of bone and bone cement, which becomes intricate and time-consuming with artefacts present. Less cement in the tibial head reduced artefacts, compared to fully cemented implants, while leaving the aim of comparing different techniques unaffected.

3.4.5 Limitations of the Study Design

The 3D models exhibited deeper penetration at positions where the pin holes from the implantation tools allowed deeper penetration (**Figure 3-22**). The axis of the “cement pins” was perpendicular to the plateau and therefore coinciding with pull-out direction. The shape was cylindrical, lacking interlocking structures, thus, the pin structure was not considered as contributing to pull-out strength. To reduce bias due to these outliers, the median cement penetration depth was determined and analysed, as performed in previous studies^{12,29}. Still, an influence of these maximum penetrations on strength cannot be completely precluded, which also applies to other aspects of the cement layer morphology as the lower surface topology and distribution of the penetration depth values. It is not yet clear what aspect of cement layer morphology is most determining for strength.

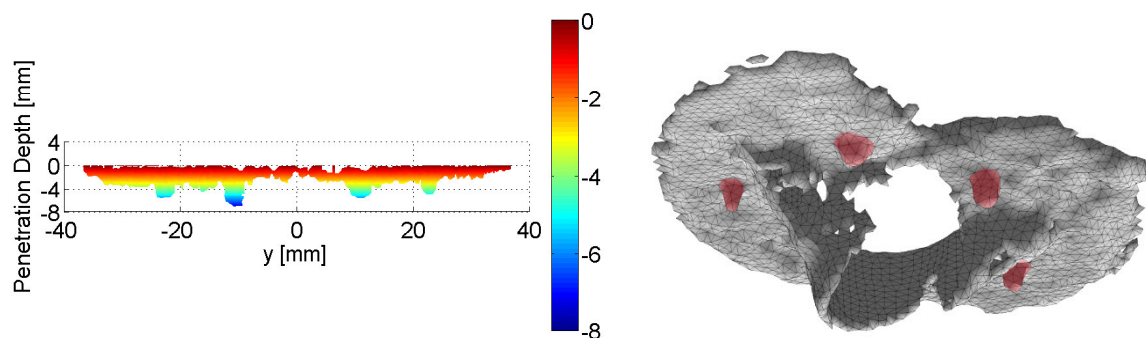


Figure 3-22: 3D model of the cement layer with protruding cement “pins”. Left: Anteroposterior view of the evaluated 3D model. There is clear evidence of deeper penetration at the position of the four pin holes that were produced during bone preparation. Right: Perspective view of the lower cement layer with cement pins (red).

The test setup enabled movement of the specimens in horizontal translation when loaded, but widely restricted rotational movement. Torsion and shear loads could have occurred. Their effect cannot be quantified and increases the variance in the data. Effects with regard to pull-out strength may have been missed. Still, the effect of BMD on pull-out strength of specimens that failed on the bone side could be shown, and group comparisons could not be carried out due to the low number of bone-side failures. The conclusions of this study are not affected.

The statistical power of the study was limited, since the three groups consisted of merely four pairs each. In connection with inhomogeneous standard deviations of the group means as given for the CONTROL groups (e.g. 0.18 mm – 0.62 mm for *MedPen.*), power is expected to be low. Yet, the median cement penetration depth values were low (overall mean *MedPen* 1.25 mm). For $n = 4$ and a difference of 1 mm (SD = 0.5 mm) between CONTROL and treated group, as determined in this and other works^{12,171}, a power of 0.75

was calculated (G*Power 3.1.9.2¹⁸⁵). However, a smaller effect of 0.5 mm with the same SD and sample size results in a power of merely 0.29. The minimum increase in penetration depth to achieve a significant effect on fixation strength is unclear, but considering that a linear correlation between *MedPen* and strength could not be shown in this study, an increase of less than 1 mm is of negligible effect. The sample size was appropriate to find effective differences.

The large number of samples with undesired failure mode (and therefore excluded from failure force evaluation) might have increased proportionally to increasing sample size. The necessary sample size would have been very large and - in terms of human cadaver testing - unethical, considering the number of samples with restricted information output.

An absolute requirement with regard to cadaver testing is the improvement of implant re-bonding to the cement mantle that lacked strength in testing. Since the time-to-testing was about 24 h long, wetting of the bone to retain its mechanical properties — in particular close to the resection plateau — was essential and could not be omitted to keep the humidity low for glue curing.

There is as yet no alternative to enable analysis of the cement-bone pull-out fixation strength. Mechanical strengthening of the attachment could be realised by implementing interlock structures at the back side of the implant, but this would also require CT scanning with the CoCr implant *in situ*. Extensive metal artefacts would occur and prevent cement layer analysis. In addition, even attachment with special interlock design features has limitations. Implants with undercuts at the implant back side have been shown to detach from the cement at $\sim 1\,500\text{ N}^{12}$, which is far below the pull-out force measured in the current study. The majority of the time to testing involved the curing of the PMMA glue (8 h). This process may be shortened by warming-up of the implant preceding implantation. Thereby, the humidity-induced impairment of the polymerisation would be antagonised. Warming-up of the implant may also vaporise remaining liquids from cleansing of the back side of the implant.

The stem region of the cement layer was virtually removed for parameter determination, because MATLAB® evaluation of these data points would have resulted in delusive values. However, although the stem cement penetrates in the central region of the tibial plateau that has lower density and strength compared to the peripheral regions¹⁶⁷, an influence of the cement around the stem cannot be precluded. This aspect will be analysed in the following chapter.

Finally, pull-out testing appears to be a non-physiological load mode, which restricts transfer to clinical conditions. The clinically required pull-out strength is not known. Pull-out strength is merely an indicator for primary strength immediately after implantation. This is discussed in more detail in Section 6.3 of this thesis.

3.4.6 Conclusion

In summary, gun pressurisation of the cement increases penetration depth, but only after pulsatile lavage is applied. Gun application of cement would not replace pulsatile lavage as penetration-increasing technique in surgery. However, the penetration depth achieved

with mere finger packing after pulsatile lavage appeared to result in sufficient strength, since failure occurred in the bone in most cases.

The effect of full stem cementation on the pull-out strength remains unclear, however a general analysis of the cement volume around the stem will be performed in the following chapter and may reveal a tendency. Layered cementation did not have a detectable effect in this setting.

Strength of the fixation was greater after pulsatile lavage than after syringe lavage and was accompanied by greater cement penetration depth and bulk bone failure. Notwithstanding, there was no linear correlation between strength and penetration depth, but between strength and bone density.

The conclusion is that pulsatile lavage has an effect on cement penetration depth that brings bone density into effect. The basic mechanism of this crucial aspect of penetration depth has to be clarified in order to improve cemented fixation.

A promising approach is a more detailed analysis of the cement layer. Other aspects of the cement morphology could be as, or more, crucial than the median cement penetration depth.

This will be addressed in the following chapter, as well as the different mechanisms of failure for pulsatile and syringe lavage that were found here.

4

Failure of Cement-Bone Interfaces in Total Knee Arthroplasty

4.1 Introduction

Failure of cemented tibial implant fixation in pull-out testing occurs at four different locations: in the diaphysis close to or within the embedding resin, at the cement-implant interface, at the cement-bone interface, or within bulk bone below the cement layer. In this thesis, both bone interface and bulk bone failures were observed in mechanical testing (Chapter 3). They were classified as bone side failures, and they are the subject of the current chapter.

Application of pulsatile lavage has been shown to increase the pull-out force of cemented tibial trays¹². Increased pull-out force has been attributed to increased median cement penetration depth, determined from CT-based 3D models of the cement layer^{12,29}. A significant correlation between pull-out force and median penetration depth has been reported by Gebert de Uhlenbrock *et al.*²⁹ in a study with retrieved specimens. Data of Schlegel *et al.*¹² matched the proposed regression model (**Figure 4-1**). However, the measured failure force was analysed disregarding the failure mode. Causality of the detected correlation is in question, since failure on the implant side and failure on the bone side are probably not due to the same failure mechanism. In the previous chapter no significant relation between *MedPen* and pull-out strength could be shown ($p = 0.714$). The regression model proposed by Gebert de Uhlenbrock *et al.*²⁹ should not be transferred to bone interface failures without further investigation of bone side failure.

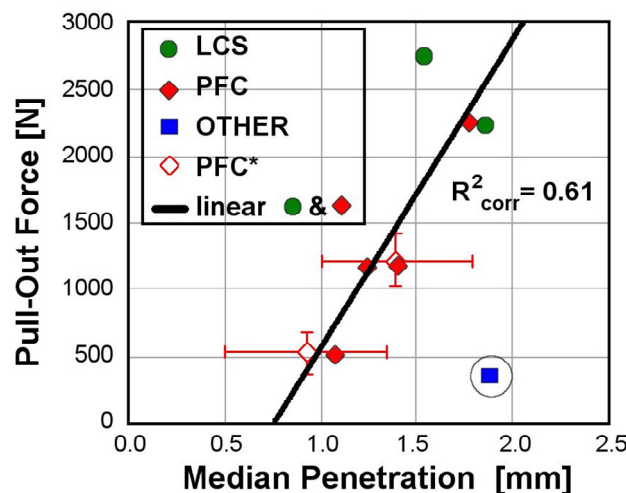


Figure 4-1: Pull-out force in dependence on median penetration depth [adapted from Gebert de Uhlenbrock *et al.*²⁹]. Linear regression was significant. LCS and PFC reflect implant designs LCS® COMPLETE™ and P.F.C. Sigma® Fixed Bearing (DePuy Orthopaedics). PFC* is data from Schlegel *et al.*¹².

In mechanical testing in the current study, larger bone interface strength of a specimen after pulsatile lavage was accompanied by larger median cement penetration depth

compared to syringe lavage (Chapter 3). A corresponding linear correlation was not detected when looking at pulsatile specimens only. Instead, there was a clear increase in strength with increasing bone density (**Figure 3-18**). Failure occurred in bulk bone, rather than at the bone-cement interface, in all pulsatile cases, probably due to the large strength of the bone fixation. Thus, fixation failure strength was related to cement penetration depth, but not in a proportional fashion, while fixation strength appears to be proportionally related to bone density.

Failure strength is considered an indicator for fixation stability and bulk bone failure in the current study was accompanied by larger failure strength than bone interface failure. Since the failure mode appears to flag large and low levels of fixation stability, risk assessment of cemented fixation may be based on prediction of failure mode. Two pending issues have to be addressed to predetermine the failure mode.

Firstly, the parameter median penetration depth potentially lacks information about a specific morphological aspect of the cement layer. This aspect may be crucial for strong fixation and is minor or absent in syringe cement layers, but as yet unrevealed. This omitted parameter may also be determining for the resulting failure mechanism. A so far disregarded characteristic is the surface area of the lower surface of the cement layer, which may be considered as contact area between cement and bone and thus as important for strength. Further, as discussed in the previous chapter, the cement layers exhibit four protruding elements. They arise from holes drilled into the tibial plateau for tool positioning during bone preparation. They are filled with cement during cementation and their relevance for fixation strength is not clear. Another neglected structure is the cement volume around the stem that was not considered in the previous chapter, since the cement penetration depth in this region could not be defined clearly. Interlock between cement and trabecular bone around the stem may contribute to strength. Investigation of such geometric characteristics of the cement layer appears essential to provide thorough insight into the mechanics of cemented fixation in order to improve fixation stability.

Secondly, it has been postulated that high bone density restricts cement penetration and hence leads to lower fixation strength^{26,27}. Since high bone density also appears to increase strength after pulsatile lavage, it could confound the relation between penetration depth and fixation strength. The same cement penetration depth may result in low fixation strength in low-density bone and in high fixation strength in high-density bone. Investigation and determination of the confounding effect is necessary in order to control it.

The aim of this study was to relate the observed failure modes to characteristic parameters of cemented tibial fixations. The relation of median cement penetration depth to failure strength and failure mode was compared to the relation of other characteristics of the cement layer to failure strength and failure mode. These characteristics were volumetric measures of the cement layer, the distribution of penetrating cement and also the topology of the lower cement layer surface. The influence of bone density on the characteristics and failure strength was also investigated. The characteristics were analysed regarding the prediction capability for failure strength and discriminant ability regarding failure mode.

4.2 Material and Methods

For the analysis of bone failure mechanism, data from three pull-out studies were pooled. The total data set was partitioned according to failure mode. The influence of morphological characteristics of the cement layer on pull-out strength and the influence of bone density on morphological characteristics and strength were investigated.

4.2.1 Specimens and Implants

Analysis was based on lab-implanted tibiae from the current thesis ($n = 36$, Section 3.2.4), a pilot study on tibial implant design described in Appendix A.1 ($n = 8$), and $n = 12$ lab-implanted tibiae from previous experimental series¹². This study focused on specimens that failed on the bone side in pull-out testing (bulk bone or cement-bone interface).

Two different P.F.C. Sigma® implant designs (DePuy Orthopaedics), modified for testing, were used in the projects (**Figure 4-2**): “Ti Fixed Bearing” and “CoCr MBT Keeled”. The Fixed Bearing was made from titanium with a hole for inlay positioning in the bearing surface. An M8 thread was cut into this hole. A coupling device was screwed to the implant and then mounted to the adapter of the testing machine for pull-out testing. The MBT Keeled modification was similar (Section 3.2.3). The pilot study on implant design showed that the cement layer morphology in terms of cement penetration depth was comparable between both implant types (Appendix A.1). The semi-automatic analysis routine developed in Chapter 3 requires input of the design- and size- specific contour of the implant to consider it in evaluation. The routine is therefore appropriate for analysis of cement layers of both implant types. The specific implant-bone bearing area *bearA* is listed in **Table 4-1**.

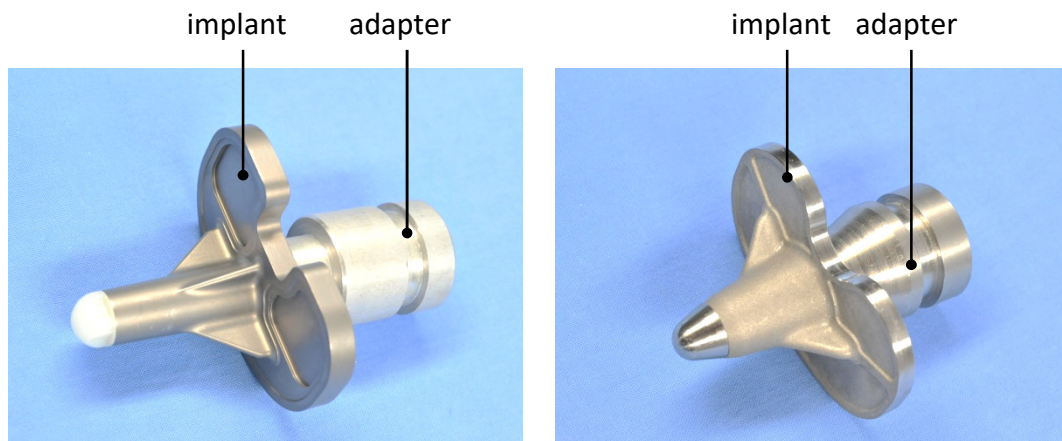


Figure 4-2: P.F.C. Sigma® implants used in the pooled lab-implanted specimens. Both implants are equipped with an adapter for coupling to the test machine. Left: Ti Fixed Bearing tibial tray was equipped with a thread in the surface to fix the device for machine coupling. The design of the back side of this implant provided undercuts for cement-implant interlock. Right: CoCr MBT Keeled was tip-cut and provided with an anchor that could be screwed to a coupling device with a centring taper. The back side of this design was undercut-free.

Table 4-1: Implant bearing area *bearA* of implant designs used in this study.

size	<i>bearA</i> [mm ²]	
	Ti Fixed Bearing	CoCr MBT Keeled
2.5	-	2008
3	2426	2178
4	2784	2507
5	3370	2978

The data available for each specimen were bone density measured by qCT, CT scans of the cement layer with maximum resolution of 0.46 mm in all directions, implant design and size, pull-out failure force and failure mode. Details about the specimens with implants and sizes are given in Appendix C.3.1.

4.2.2 Computed Tomography and Evaluated Parameters

The cement layer morphology was analysed, applying the routine described in Section 3.2.7. It comprised CT segmentation and xy plane alignment of the 3D models in Avizo® (version 7, VSG, Burlington, MA, USA), followed by rotation alignment of the 3D models and determination of cement layer parameters in MATLAB® (version R2013a, The MathWorks Inc., Natick, MA, USA). The back sides of the two implant designs were different: the Ti Fixed Bearing provided undercuts for a cement-implant interlock, while the CoCr exhibited an undercut-free back side (**Figure 4-2**). The CT scans of Ti Fixed Bearing specimens had to be generated with the implant *in situ*, since manual removal, as carried out in the mechanical testing procedure described in Chapter 3 (**Figure 4-3**) was not feasible, due to the interlock between the implant undercuts and the cement.

CT data sets from the previous study were already available¹² (Brilliance 40-channel CT, Philips Healthcare, Best, The Netherlands). The corresponding specimens (n = 12) were implanted with Ti Fixed Bearing implants, so a smoothing kernel filter was used to reduce artefacts in the CT scans due to the *in situ* metal implant¹². It has been shown that with modern scanners, *in situ* scanning of Ti implants is feasible with negligible loss of information due to artefact filtering¹⁸⁶, so the Ti Fixed Bearing specimens from the pilot study were CT-scanned with implant *in situ* and no subsequent image filtering (Appendix A.1, n = 4, Brilliance 16-slice, Philips Healthcare, Best, the Netherlands).

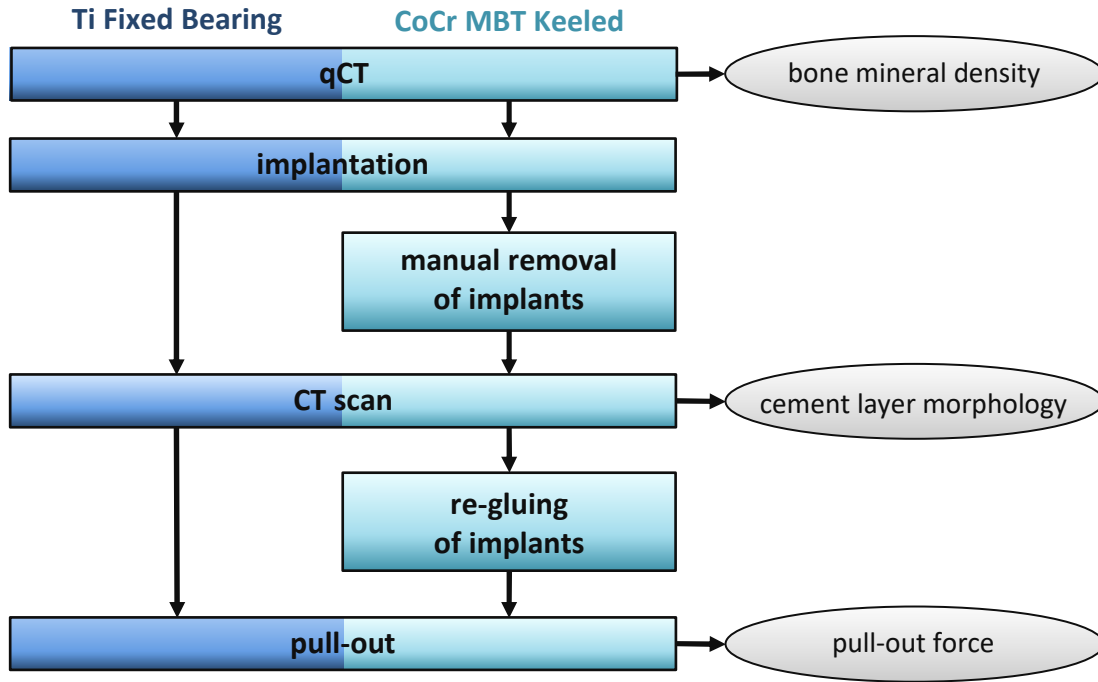


Figure 4-3: Experimental procedure applied to the specimens analysed in this chapter. The blue sequence was applied to specimens with implanted Ti Fixed Bearing and included CT scanning with implant *in situ*. The green sequence was applied to specimens implanted with CoCr MBT Keeled and included CT scanning with the temporarily-removed implant.

Segmentation of the CT scans to obtain the 3D models of the cement layers was described in Section 3.2.7. Segmentation of the CT scans without implant required two thresholds for segmentation, one between exterior and bone and one between bone and cement. For segmentation of the CT scans with implant *in situ*, an additional threshold had to be set between cement and implant. This threshold was determined by an iterative procedure in Avizo^{®12}. The known volume of the implant was the command variable and approximated by changing the threshold. Segmentation thresholds are listed in Appendix B.2.

Two 3D models were generated for further processing, a surface model made up from triangles and a volume model made up from tetrahedrons (Section 3.2.7). The models formed the base for parameter determination. The corresponding MATLAB[®] routine is presented in more detail in Appendix B.1.

In total, 20 parameters were determined for analysis. From these 20, 12 morphology parameters and 4 auxiliary measures were determined from the 3D models of the cement layers. Auxiliary measures were primarily used to calculate other parameters. Another 4 variables in the analysis were the output parameters of mechanical testing failure load F , failure strength S , as well as the categorical parameter failure mode and, lastly, the bone density BMD of the specimens. The morphology parameters were later evaluated regarding their classification potential, with reference to failure mode and their contribution to fixation strength (**Table 4-2**). The 4 auxiliary measures and 2 out of 12 morphology parameters were defined in the previous chapter and are also analysed here: auxiliary measures *bearA*, *evalA*, *AprojEx* and *Aproj0*, and morphology parameters Vol_{spec}

and *MedPen*. The remaining 10 morphology parameters were defined in the current study as follows:

The volume of the cement in the stem region that was excluded from parameter determination in the previous chapter was analysed separately in the current study; Analogous to Vol_{spec} , the absolute volume was normalised by the corresponding projected area (**Figure 4-4**):

- Stem volume $Vol_{Stem_{spec}}$

The penetration depth of the cement into the bone, determined by calculating the distance of each data point (node) of the triangle surface model to the bone plateau:

- Maximum penetration depth $MaxPen$
- Mode penetration depth $ModePen$
- Mean penetration depth $MeanPen$

Further descriptives of the penetration depth distribution:

- Standard deviation of the penetration depth distribution $SDPen$
- Skewness of the penetration depth distribution $SkewPen$
- Kurtosis of the penetration depth distribution $KurtPen$
- Cumulated penetration depth $CumPen$

The topology of the cement layer, represented by two measures:

- Root mean square of the tilt of the surface triangles of the lower cement layer surface in terms of their angle to the resection plateau Ang_{RMS}
- Ratio between surface area and projected area (A_{proj}) of the lower cement layer (*Folding*)

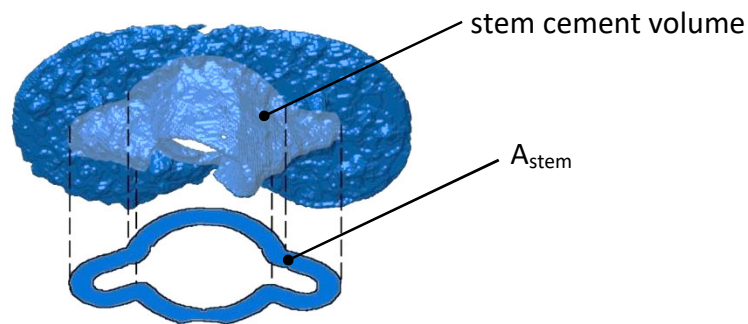


Figure 4-4: The cement around the stem was normalised by its projected area for evaluation.

Strength S was calculated according to equation (3-4) from the determined failure force and reference area A_{projEx} . Failure modes in pull-out testing were determined for all specimens. Analysis was restricted to specimens that failed on the bone side (bone interface or bulk bone failure). The measured force of the remaining failure modes (implant / glue interface, diaphysis) referred to the cement-implant interface, precluding direct conclusions about the failure force on the cement-bone side. These failure modes are therefore “undesired” failure modes. An indirect conclusion in this case would be that the cement-bone fixation was stronger than the cement-implant fixation (lower-bound

observation). Cases with “undesired” failure mode were used for cross-validationⁱ of the derived regression models, taking their failure strength as lower bound for the strength estimated by the derived models. A summary of all the parameters in the analysis is given in **Table 4-2**.

Table 4-2: Parameters retrieved from specimens, mechanical testing and cement layer morphology models. The first 12 parameters describe the cement morphology.

	Description	Symbol	Origin
Morphology	specific volume	Vol_{spec}	equation (3-2)
	maximum penetration depth	$MaxPen$	cement layer model
	median penetration depth	$MedPen$	cement layer model
	mode penetration depth	$ModePen$	cement layer model
	mean penetration depth	$MeanPen$	cement layer model
	standard deviation of penetration depth	$SDPen$	cement layer model
	skewness of penetration depth distribution	$SkewPen$	cement layer model
	kurtosis of penetration depth distribution	$KurtPen$	cement layer model
	cumulated penetration depth	$CumPen$	cement layer model
	root mean square of the surface triangle angles with respect to the resection plateau	Ang_{RMS}	cement layer model
	ratio between penetration surface and projected area	$Folding$	$\frac{\text{surface area}}{A_{proj}}$
	stem volume	$VolStem_{spec}$	$\frac{\text{stem cement volume}}{\text{projected area around stem}}$
Auxiliary	bearing area of the tibial tray	$bearA$	implant geometry
	region from which the parameters were determined	$evalA$	manual settings in cement layer processing
	standardised projected area	A_{proj0}	equation (3-1)
	extrapolated projected area	A_{projEx}	equation (3-3)
Other	failure force	F	mechanical testing
	failure strength	S	equation (3-4)
	failure mode	-	mechanical testing
	bone mineral density from CT scans	BMD	measured

4.2.3 Statistics

Analysis of the parameters was performed with regard to three aspects: classification potential regarding bone failure mode, contribution to measured strength of single parameters and strength prediction capability of combined parameters. Some specimens underwent cementation techniques that were shown to affect or suspected of affecting the analysed parameters (Chapter 3). Specimens that were treated with combined gun cementation and pulsatile lavage ($n = 4$) were excluded from the analysis of the relation

ⁱ Cross-validation: Confirming a derived model by applying it to an independent data set.

between bone density and morphology, since the morphology was shown to be influenced by gun application. An effect of full cementation on pull-out failure force has not been disproved, so the corresponding specimens ($n = 4$) were excluded from analysis of fixation strength.

Means of all 12 morphology parameters, *Aprojo*, *S*, *BMD*, *evalA* and *bearA* of bone interface and bulk failure groups were compared, using the T test for independent samples or the Mann-Whitney U test. In Chapter 3, bulk bone failures showed larger strength than bone interface failures, therefore morphology parameters with significantly different values for bone failure modes were considered as potentially classifying for failure mode and potentially predictive for fixation strength. Accordingly, further analysis was focused on such parameters. *VolStem_{spec}* was of specific interest, as it was stated in the previous chapter that it should not be disregarded.

In order to identify parameters that were determining for failure mode, receiver operating characteristic (ROC) analysis was carried out on morphology parameters, *S* and *BMD* to determine measures discriminating the failure mode of bone failures and corresponding thresholds. In ROC analysis, a continuous variable is analysed according to its ability to act as a marker for two occurring categories, wherein one category is 'positive' and corresponds to presence of a signal and the other 'negative', corresponding to absence of a signal. The positive category is commonly unfavourable, such as presence of a disease. A threshold for the marker is determined, based on a desired minimum rate of correctly classified positive cases (sensitivity) and a maximum rate of wrongly classified negative cases (error rate).

In the current study, failure at the bone interface was defined as the 'positive' category in the analysis, since it indicates lower fixation strength (Chapter 3). Desired classification ability was at sensitivity^j above 99.9 %, to ensure identification of all cases with low fixation strength, and corresponding minimal error rate^k to keep the number of cases with underestimated fixation strength as low as possible. An error rate below 0.1 % represented correct classification in all cases and therefore correct discrimination between the failure modes. The value of the respective parameter at which sensitivity was above 99.9 % and error rate was as low as possible, was considered the threshold between risk of bone interface failure and risk of bulk bone failure.

Morphology parameters with desired discriminating ability were further analysed regarding their predictive relation to strength and dependency on bone density using simple linear regression.

Relation of *Aprojo* to strength was not analysed using regression, since *Aprojo* was involved in calculating the reference area for determining failure strength from failure force. In regressions, *BMD* was divided by 10^3 when analysed, to receive a similar scale for the coefficients in different models.

Morphology parameters with classification potential with less than 10 % error (ROC analysis) were regarded as relevant for resulting failure mode. Multiple regressions with an interaction term and forced entry were carried out to further analyse the relation of

^j Sensitivity = statistical power $1 - \beta$

^k Error rate = type-I error rate α

the relevant morphology parameters and *BMD* to failure strength. Regression models were of the form

$$S = a_0 + predictor * a_1 + BMD * a_2 + predictor * BMD * a_3 \quad , \quad (4-1)$$

where a_i were the coefficients and “predictor” was the respective morphology parameter. Predictors were centred, according to their overall mean to control for collinearity effects due to the interaction term¹⁸⁷. As before in simple regression analysis, *BMD* was divided by 10^3 when analysed.

Cross-validation of the multiple-regression models was performed on the specimens that did not fail on the bone side in pull-out testing (Appendix C.3.1). Gun-and-pulsatile specimens were excluded as in model determination. Ratios between estimated and measured strength were calculated. Values below 1 showed that the estimated strength was lower than the measured, indicating underestimation. A binomial test with a group separation (cut-off point) at 1 was carried out. It tests for the probability that a dichotomous measure follows a given distribution of category frequency. In the current study, the test criterion for the proportion of underestimated cases was set to 10 %¹.

All statistical evaluations were performed using SPSS (IBM® SPSS® Statistics 21, IBM Corporation, Armonk, NY, USA) and applying a type-1 error level α of 0.05.

4.3 Results

The total data set covered 56 specimens. One of the CT data sets from the previous experimental series¹² was not available. In the current thesis, the failure mode of one specimen from mechanical testing could not be clearly identified (3008 R, Appendix C.3.1). The respective data were removed from analysis. Of the remaining 54 specimens, 24 failed on the bone side (**Table 4-3**). 10 specimens failed at the bone interface and 14 within the bulk bone. All specimens of the interface failure group were prepared using syringe lavage and all specimens from the bulk bone failure group were prepared using pulsatile lavage, apart from one syringe –prepared specimen. One specimen from the bulk failure group was full-stem-cemented and excluded from *VolStem_{spec}* analyses. Two specimens were prepared by combined pulsatile lavage and gun cementation, which was shown to influence the cement layer (Chapter 3). They were excluded from bone density analyses.

¹ Not to be confused with the significance level. A significant p value meant that, with a probability of less than 5 % (α level), occurrence of more than 10 % (test criterion) of underestimated cases appeared by chance.

Table 4-3: Sample size and implant design of the combined studies; corresponding number of bone interface and bulk bone failures is displayed in brackets.

Origin of CT data sets	Sample size n (bone interface failure / bulk bone failure)	Implant design
previous experimental series ¹²	11 (5 / 0)	Ti Fixed Bearing
current thesis (Chapter 3)	35 (5 / 13)	CoCr MBT Keeled
pilot study (Appendix A.1)	8 (0 / 1)	Ti Fixed Bearing + MBT Keeled
Total	54 (10 / 14)	

4.3.1 Classification Potential of Parameters

SkewPen and *KurtPen* were not significantly different between bone interface and bulk bone failures ($p = 0.229$ and $p = 0.275$, respectively). *CumPen* was significantly smaller in the interface failure group by 58 % ($p < 0.001$). *AngRMS* was significantly smaller in the bulk failure group by 7 % ($p < 0.001$). There was a trend of *bearA* and *evalA* being smaller in the bulk failure group by 11 % and 13 %, respectively ($p = 0.070$ and $p = 0.052$, respectively). *BMD* was not significantly different between bulk and interface failure specimens ($p = 0.305$). All other parameters had significantly larger values in the bulk failure group ($p < 0.001$, **Table 4-4**): *Aprojo* of bulk failure cases was larger by 62 %, *Vol_{spec}* was 3-fold in the bulk group, *MaxPen* was 82 % larger, *MedPen* 3-fold larger, *ModePen* was 4.5-fold larger, *MeanPen* was 2.6-fold larger, *SDPen* was larger by 83 %, *Folding* was larger by 7 %, *Volstem_{spec}* was 2.5-fold larger and strength was 6.7-fold larger in the bulk group.

Table 4-4: Bone density and morphology parameters for the bone interface and the bulk bone failure groups (standard deviation is given in brackets). Corresponding p values from independent T test are listed.

Parameter	n	Mean interface	Mean bulk	p
<i>Aprojo</i> [-]	10vs.14	0.53 (0.19)	0.86 (0.06)	< 0.001
<i>Vol_{spec}</i> [mm]	10vs.14	0.45 (0.22)	1.36 (0.40)	< 0.001
<i>MaxPen</i> [mm]	10vs.14	3.87 (0.99)	7.04 (0.8)	< 0.001
<i>MedPen</i> [mm]	10vs.14	0.51 (0.21)	1.51 (0.43)	< 0.001
<i>ModePen</i> [mm]	10vs.14	0.29 (0.22)	1.32 (0.69)	< 0.001
<i>MeanPen</i> [mm]	10vs.14	0.66 (0.21)	1.70 (0.4)	< 0.001
<i>SDPen</i> [mm]	10vs.14	0.60 (0.17)	1.10 (0.13)	< 0.001
<i>SkewPen</i> [-]	10vs.14	-1.90 (0.83)	-1.54 (0.35)	0.229
<i>KurtPen</i> [-]	10vs.14	8.22 (4.28)	6.60 (1.35)	0.275
<i>CumPen</i> [mm]	10vs.14	11175.74 (8766.84)	26507.91 (7642.91)	< 0.001
<i>Ang_{RMS}</i> [°]	10vs.14	161.20 (5.81)	150.51 (4.93)	< 0.001
<i>Folding</i> [-]	10vs.14	1.26 (0.07)	1.47 (0.12)	< 0.001
<i>VolStem_{spec}</i> [mm]	10vs.13	1.93 (1.18)	4.85 (1.39)	< 0.001
<i>S</i> [MPa]	10vs.14	0.48 (0.18)	3.21 (1.44)	< 0.001
<i>BMD</i> [mg/cm ³]	10vs.14	86.04 (33.23)	70.77 (36.31)	0.305
<i>bearA</i> [mm ²]	10vs.14	2464.00 (398.46)	2203.50 (273.73)	0.070
<i>evalA</i> [mm ²]	10vs.14	1946.84 (359.7)	1684.53 (265.79)	0.052

ROC analysis showed that *MaxPen* and *MeanPen* are classification predictors for bone failure mode (sensitivity > 99.9 %, error rate < 0.1 %, **Table 4-5**), with a threshold to bulk bone failure of 5.57 mm and 1.06 mm, respectively. *MedPen* showed an error rate of 7.1 % bulk bone failures, wrongly predicted to fail at the bone interface at a threshold of 0.93 mm cement penetration. Likewise, classification using *SDPen*, *Vol_{spec}*, *Folding* and *S* resulted in an error rate of 7.1 % (thresholds of 0.90 mm, 0.88 mm, 1.34, and 1.17 MPa, respectively, **Figure 4-5, A**). Classification based on *Aprojo*, *CumPen*, *BMD* and *VolStem_{spec}* had an error rate of 42.9 %, 64.3 %, 71.4 % and 38.5 % false positive, respectively (**Figure 4-5, B**). Supplementary data are given in Appendix C.3.2.

Table 4-5: Parameters with error rates below 10 % and corresponding thresholds with regard to failure mode classification (ROC analysis with > 99.9 % sensitivity).

Parameter		Threshold	Error rate [%]
<i>SDPen</i>	[mm]	0.90	7.1
<i>Vol_{spec}</i>	[mm]	0.88	7.1
<i>MaxPen</i>	[mm]	5.57	< 0.1
<i>MedPen</i>	[mm]	0.93	7.1
<i>MeanPen</i>	[mm]	1.06	< 0.1
<i>Folding</i>	[-]	1.34	7.1
<i>S</i>	[MPa]	1.17	7.1

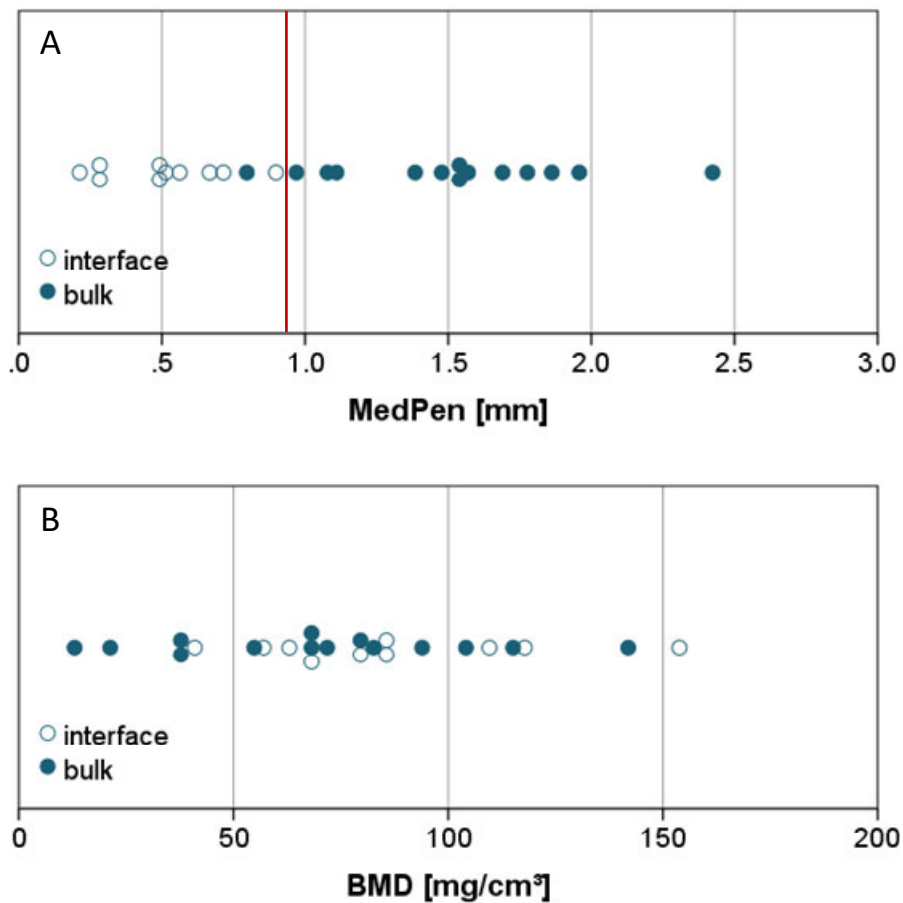


Figure 4-5: Characteristic data distributions for results in ROC analysis of bone failure mode classification. A) Characteristic distribution for an error rate of 7.1 %, *MedPen*; red line indicates threshold of 0.93 mm, B) Characteristic distribution for error rate > 99.9 %, *BMD*; no classification threshold.

4.3.2 Contribution of Cement Layer Characteristics and Bone Density to Fixation Strength

Aprojo, *Vol_{spec}*, *MaxPen*, *MedPen*, *MeanPen*, *SDPen* and *Folding* were not significantly related to *BMD*, neither overall nor within failure mode groups (*p* values are given in Appendix C.3.2).

Strength *S* was not significantly related to *BMD* in the overall data, but *S* in both interface failure group and bulk failure group significantly increased with increasing *BMD* ($R^2 = 0.45$, $p = 0.020$ and $R^2 = 0.68$, $p = 0.001$, respectively, **Table 4-6**, **Figure 4-6**, left).

VolStem_{spec} significantly decreased with increasing *BMD* in the bone interface failure group, ($R^2 = 0.45$, $p = 0.021$, **Figure 4-6**). No relation was found in the overall data and within the bulk failure group ($p = 0.266$).

Table 4-6: Determined regression models for dependence of strength *S* and cement volume around the stem on bone density, overall and within failure mode groups (*n* is the sample size). Regression models are of the form $dependent = a_0 + BMD * a_1$. (The adjusted value for R^2 is reported; Non-significant models are not reported.)

	Dependent							
	<i>S</i> [MPa]				<i>VolStem_{spec}</i> [mm]			
	<i>a</i> ₀ [MPa]	<i>a</i> ₁ [MPa cm ³ 10 ³ /mg]	<i>R</i> ²	<i>p</i>	<i>a</i> ₀ [mm]	<i>a</i> ₁ [mm cm ³ 10 ³ /mg]	<i>R</i> ²	<i>p</i>
Overall n = 21	-	-	-	0.231	-	-	-	0.156
Interface failure n = 10	0.139	3.956	0.45	0.020	4.10 4	-25.280	0.45	0.021
Bulk failure n = 11	0.915	33.596	0.68	0.001	-	-	-	0.833

In the overall data, *S* significantly increased with increasing *Vol_{spec}*, *MaxPen*, *MedPen*, *MeanPen*, *SDPen* and *Folding* ($p < 0.001$, R^2 is given in **Table 4-7**, **Figure 4-6**, right). No significant relation between *S* and these parameters was detected within the failure mode groups (*p* values are given in Appendix C.3.2).

VolStem_{spec} was significantly related to *S* in the overall data ($R^2 = 0.43$, $p < 0.001$, **Table 4-7**). There was no significant relation between *S* and *VolStem_{spec}* within the failure mode groups (Appendix C.3.2).

Table 4-7: Determined regression models for dependency of strength S on Vol_{spec} , $MaxPen$, $MedPen$, $MeanPen$, $SDPen$, $Folding$ and $VolStem_{spec}$ in the overall data (n is the sample size). Regression models are of the form $S = a_0 + predictor * a_1$. (The adjusted value for R^2 is reported; Non-significant models are not reported; “dim” denotes the dimension of the respective predictor.)

	Overall n = 23			
	a_0 [MPa]	a_1 [MPa/dim]	R^2	p
Vol_{spec}	-0.045	2.266	0.46	< 0.001
$MaxPen$	-2.264	0.770	0.61	< 0.001
$MedPen$	-0.146	2.103	0.49	< 0.001
$MeanPen$	-0.593	2.183	0.53	< 0.001
$SDPen$	-1.682	4.222	0.47	< 0.001
$Folding$	-9.689	8.539	0.51	< 0.001
$VolStem_{spec}$	-0.116	0.618	0.43	< 0.001

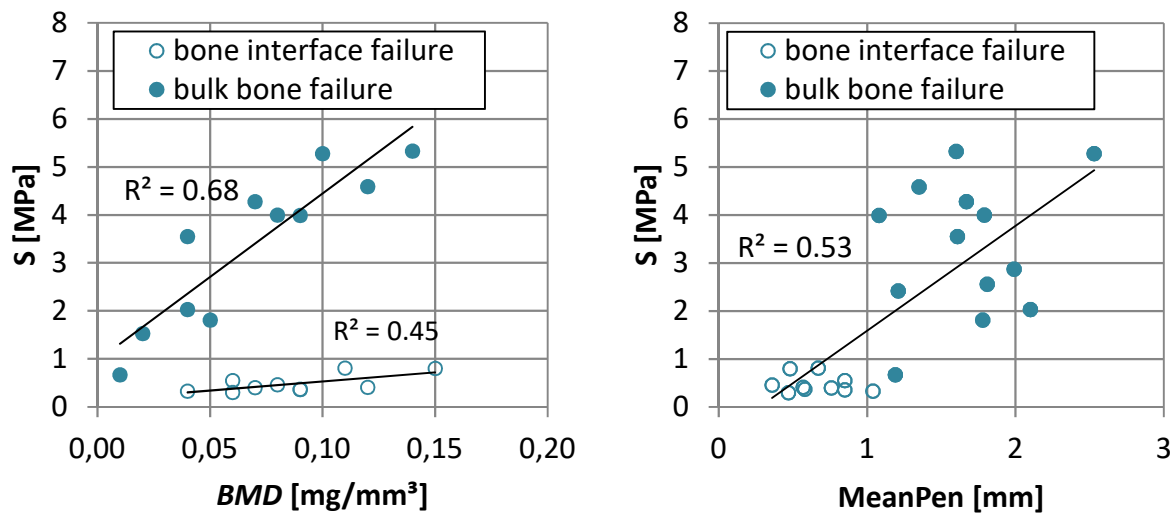


Figure 4-6: Relation between fixation strength and predictors. Left: The relation between fixation strength (S) and mean cement penetration depth was significant for both interface and bulk bone failure specimens; there was no relation to strength in the overall data. According to ROC analysis, groups were separated at 1.06 mm mean penetration depth. Right: The relation between fixation strength (S) and bone density (BMD) was significant in the overall data, but not within groups.

4.3.3 Prediction Capacity of Combined Parameters

Vol_{spec} , $MaxPen$, $MedPen$, $MeanPen$, $SDPen$ and $Folding$ fulfilled the criteria for potential predictors of S in multiple regressions. These major parameters and bone density were centred to their overall means (Table 4-8).

Table 4-8: Overall means of the predictors in multiple regressions. The values were used for centring of data.

Predictor	Mean (n=54)
Vol_{spec} [mm ³]	0.98
$MaxPen$ [mm]	6.16
$MedPen$ [mm]	1.08
$MeanPen$ [mm]	1.27
$SDPen$ [mm]	0.94
$Folding$ [-]	1.40
BMD [mg/10 ³ cm ³]	0.08

Multiple regression with the respective interaction term resulted in significant models for strength estimation ($p < 0.001$, R^2 values are given in **Table 4-9**). Due to exclusion of $n = 2$ gun-and-pulsatile and $n = 1$ full cemented specimens, sample size was $n = 21$. The largest amount of explained variance was 74 % in regression with $MeanPen$ and BMD as predictors. The smallest amount of explained variance was 60 % with $Folding$ and BMD as predictors (**Table 4-9**). The coefficient a_3 of the interaction term was not significant (confidence interval crosses 0). Influence of the interaction term changes direction. This also applied to all coefficients of the $Folding$ model.

Table 4-9: Multiple regression models with an interaction term for dependence of strength on cement morphology characteristics and bone density. Models are of the form $S = a_0 + predictor * a_1 + BMD * a_2 + predictor * BMD * a_3$. (The adjusted value for R^2 is reported; Confidence intervals are given in brackets; “dim” denotes the dimension of the respective predictor.)

Predictor	a_0 [MPa]	a_1 [MPa/dim]	a_2 [MPa cm ³ 10 ³ /mg]	a_3 [MPa/dim]	R^2	p
Vol_{spec}	2.361 [1.870 2.852]	2.678 [1.738 3.617]	26.234 [12.004 40.464]	20.482 [-7.480 48.444]	0.70	< 0.001
$MaxPen$	2.575 [2.092 3.059]	0.791 [0.522 1.060]	17.756 [4.584 30.928]	4.183 [-3.642 12.008]	0.72	< 0.001
$MedPen$	2.288 [1.808 2.769]	2.454 [1.615 3.292]	24.392 [10.338 38.446]	16.256 [-8.097 40.608]	0.70	< 0.001
$MeanPen$	2.347 [1.898 2.796]	2.472 [1.697 3.247]	23.974 [10.945 43.090]	19.493 [-4.104 43.090]	0.74	< 0.001
$SDPen$	2.525 [2.026 3.025]	4.664 [2.910 6.418]	0.019 [0.005 0.032]	57.412 [-1.439 116.262]	0.70	< 0.001
$Folding$	2.291 [1.737 2.846]	9.171 [-3.876 27.907]	12.015 [-3.876 27.907]	75.206 [-44.664 195.076]	0.60	< 0.001

Cross-validation was done based on $n = 30$ undesired failure mode cases (implant / glue interface, diaphysis). From these cases, $n = 1$ case was combined pulsatile-prepared and

gun-cemented and $n = 3$ were stem-cemented. They were excluded from analysis. The probability of underestimation of fixation strength was significantly greater than 10 % for all six models ($p < 0.040$; $n = 26$, binomial test, Appendix C.3.2). Each 8 underestimated cases occurred for the statistical models based on *MaxPen* and *MeanPen*. 9 cases were underestimated with the statistical models based on *Folding* and *SDPen*, and each 10 cases were underestimated with the models based on *Vol_{spec}* and *MedPen*.

4.4 Discussion

The relevance of bone quality in terms of mineral density for tibial tray fixation strength was hypothesised to be attributed to the bone's porosity and strength in Section 4.1. On the one hand, large porosity in low-density bone has been suspected of allowing deeper cement penetration than low porosity in high-density bone^{26,27}, which has been shown to result in increased fixation strength. On the other hand, cemented fixation in low-density bone has been shown to provide low strength in tensile testing²⁸. The apparently contrasting effects of bone density in the two findings were investigated here by analysing the effect of bone density with regard to fixation strength and cement layer morphology. Occurrence of different failure modes within the analysed data set enabled attribution of the failure mode to particular cement layer morphology characteristics and, eventually, to a specific fixation mechanism.

In order to provide a throughout analysis, all parameters evaluated are discussed regarding their relevance for fixation strength and failure mode (Section 4.4.1). The potential interaction between bone density and cement penetration depth is discussed in Section 4.4.2. The failure mechanism and the corresponding modelling are discussed in Section 4.4.3. General limitations are discussed in Section 4.4.4.

4.4.1 Relation of Cement Layer Characteristics to Fixation Strength and Failure Mode

Several studies have shown that cement penetration depth is an important aspect in fixation stability^{12,29,162}. Cement penetration depth in bulk bone failures was larger than in bone interface failures, which was reflected in the larger values of all depth parameters (*MaxPen*, *MedPen*, *MeanPen*, *ModePen*, *CumPen*, *SDPen*). The median value of a distribution is more robust to outliers than the mean value. Outliers may be due to inadequate model geometry caused by roentgen artefacts, but also due to the cement filling of the pin holes in the bony plateau originating from the surgical procedure (Section 2.3.2.3 and **Figure 4-7**) or the stem cement being removed. The maximum penetration is a measure for the pin holes. Mean and maximum cement penetration depth were shown to classify between bone failure modes with an error rate of less than 0.1 %, which is less than the error rate of 7.1 % determined for median penetration depth. Classification using the standard deviation of the depth also results in 7.1 %. The mode of the penetration depth even resulted in about 30 % classification error. The cement pin structures are assumed to contribute to fixation strength, because mean and maximum penetration depth — that consider these structures — exhibit a strength prediction capability superior to that of the median, mode and SD of the penetration depth. However, classification ability of median and SD of penetration depth — that exhibit a reduced influence of the pin structures — was still acceptable.

Although mean and maximum penetration depth performed better as predictor than the other depth parameters, there is no clearly predominant one. Correlation between the parameters and potentially biasing structures confounded the analysis. Additional controlled studies are necessary to rule out the influence of pin and stem cement.

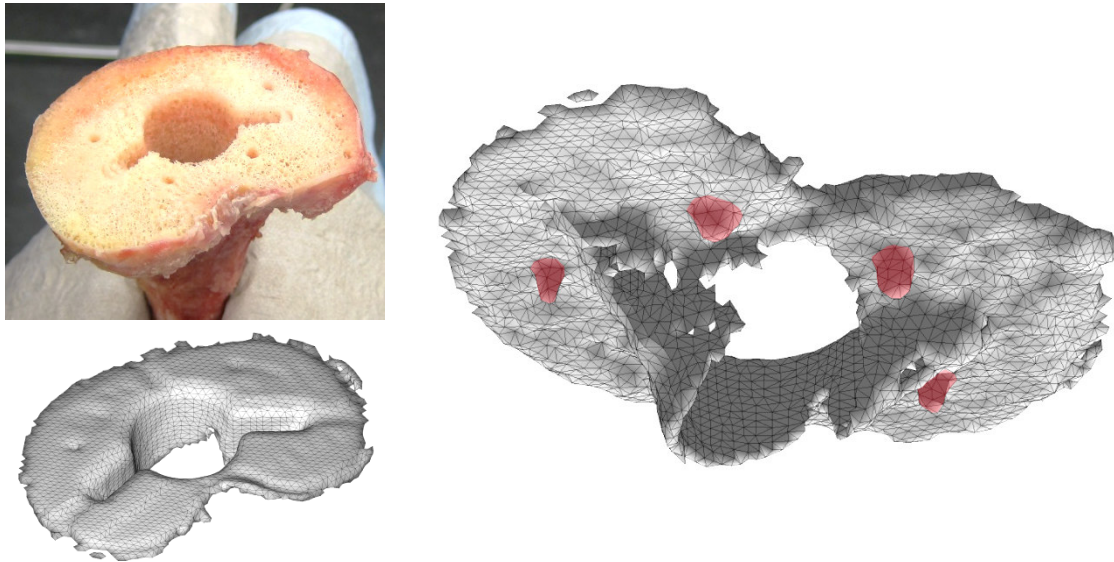


Figure 4-7: Origination of cement fillings at the lower cement layer surface. Left: Tibial plateau with four pin holes introduced during bone preparation and 3D model of the corresponding cement layer. Right: Bottom view of the cement layer model with cement fillings of the pin holes (red).

Areal and volumetric morphology parameters have been used in literature to compare cement layers between different treatment groups^{26,27,29,162}. The portion of penetrated area (*A_{projo}*) of the bulk failures was larger than that of interface failures and exhibited less variance (SD_{bulk} 0.06, $SD_{interface}$ 0.19). However, the error rate in classification was greater than 40 %. The portion of cement-penetrated area of the tibial contact area is not related to the observed failure mode of cemented fixation and therefore not a suitable predictor for failure mode.

The specific cement volume (Vol_{spec}) actually reflected the cement penetration depth, if the cement was distributed homogeneously below the evaluation area. The error rate of failure mode classification based on the specific volume was equal to that of the median penetration depth, and larger than that of the mean and the maximum penetration depth. The specific volume is a potential predictor for failure mode of cemented tibial fixation.

The cumulated penetration depth (*CumPen*) is biased by the number of data points that depends on implant size and penetrated area. Large penetration depth with low penetrated area may result in the same value as low penetration depth with large penetrated area. Normalisation of *CumPen* to the number of data points would equal *MeanPen* and normalisation to the penetrated area of the cement layer still inhibits bias, due to possibly different data resolution (lowest and largest resolution differed by a factor 2). Conclusions about the cement layer morphology are more valid based on the

mean, median or maximum cement penetration depth than based on the cumulated depth.

Both skewness (*SkewPen*) and kurtosis (*KurtPen*) of the penetration distribution showed less variance in the bulk group than in the interface failure group, which indicates different data distribution. Although a larger frequency of large penetration depth values may be mirrored by skewness and kurtosis, no difference between failure mode groups was shown. Therefore, importance of skewness and kurtosis of the penetration depth distribution for fixation strength is not assumed and the two parameters were not further analysed.

The topology of the lower cement layer surface was investigated in terms of the surface angle (*AngRMS*) and the ratio of surface area to cement-penetrated area (*Folding*). The amount of cement was neglected by these parameters and focus was put on how 'rough' the lower surface of the cement layer was. The angle was determined with respect to the tibial resection plane (**Figure 4-8, A**) and was merely 6° smaller in the bulk failure group. The surface angle is related to cement penetration depth. Pearson's *r* between mean penetration depth and the surface angle is -0.690. In cement layers that penetrate deeper, a larger proportion of steeper surface triangles was given (**Figure 4-8, B**). An increase in angle does not imply steeper flanks, but rather indicates longer flanks and therefore reflects the same aspect of cement layer morphology as mean cement penetration depth. The surface angle is not an appropriate measure of topology in the context of this study.

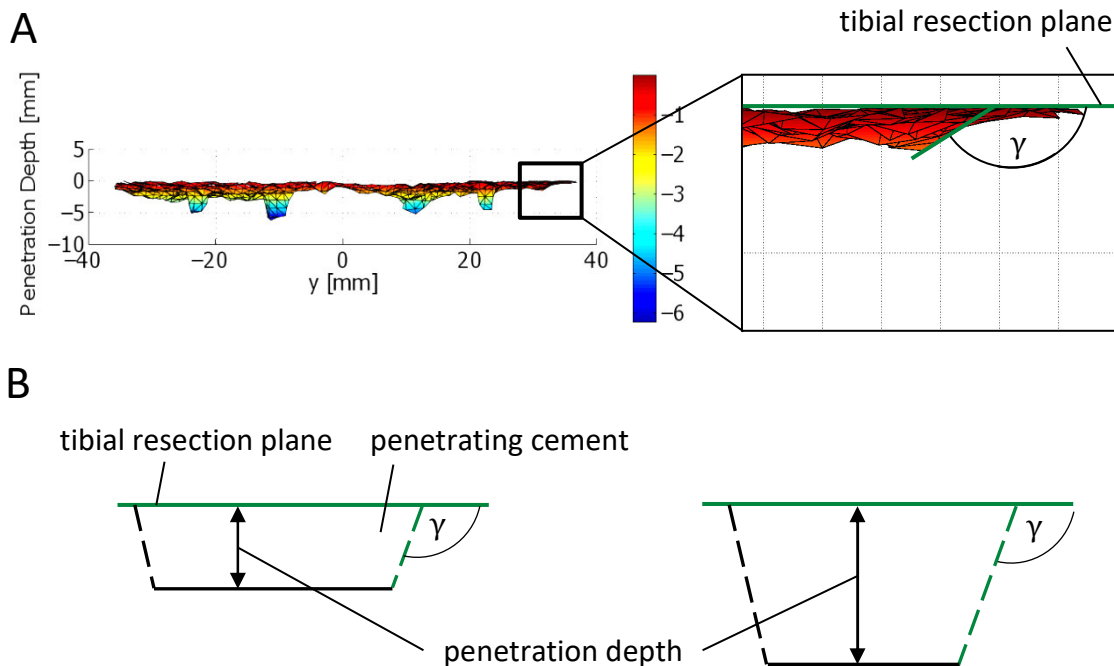


Figure 4-8: Triangle tilt γ of penetrating surface. A) Anteroposterior view of the 3D surface model with detail view of the tilted triangles (model was down-sampled for better illustration). B) Left: Low penetration with short flanks. Right: Larger penetration, although triangle tilt γ stays the same, more elements contribute to the RMS of angles *DevAng*.

Folding also reflected the topology of the lower cement layer surface. It was related to strength and showed classification potential for bone failure mode with 7.1 % error rate. A larger folding corresponds to a larger cement-bone interface area, which may imply a

larger area for load transfer from the cement to the bone. The relation of *Folding* to strength is similar to that of cement penetration depth (mean, median and maximum). It is a potential predictor for failure mode.

The cement volume around the stem ($VolStem_{spec}$) was larger for bulk failures, as well as the fixation strength. However, failure mode classification due to the stem volume resulted in almost 40 % of wrongly classified cases. These cases showed high strength (bulk failure mode) with rather low stem cement volume. The variance in stem cement volume accounted for merely 43 % of variance in strength. There was no relation between $VolStem_{spec}$ and fixation strength within the failure mode groups (INTERFACE $R^2 = 0.23$, BULK $R^2 < 0.01$). The increased stem cement volume in bulk bone failure specimens was probably not determining for strength, but a corollary of the simultaneously larger general cement volume that was shown to inhibit classification potential regarding failure mode. The volume of the cement around the stem decreased with increasing bone density for interface failures, but model quality was rather low ($R^2 = 0.45$). In addition, the stem cement penetrates in the central region of the tibial plateau, which has lower density and strength compared to the peripheral regions¹⁶⁷, and therefore cement-bone interlock in this region may be less effective. Considering this aspect, full cementation of the stem as performed in the previous chapter may not be as effective on fixation strength as assumed by some authors^{17,18}. All determined relations of $VolStem_{spec}$ to bone density or fixation strength have to be handled carefully, since $VolStem_{spec}$ depended on trimming of the 3D model for parameter determination. The amount of cement that was pulled into the stem cavity when the implant was inserted is assumed to depend on the overall amount of cement that had been placed on the bony plateau before. Since the applied cement volume was not controlled in the current study, it may bias the analysis of $VolStem_{spec}$ conducted here and with regard to the low R^2 . The influence of the stem cement volume on the strength was considered of minor importance in the current study.

4.4.2 Relation between Bone Density, Cement Layer Morphology and Fixation Strength

The hypothesised interaction between bone density and cement penetration depth was based on the assumption of restricted cement penetration in high-BMD bone. Contrasting the hypothesis, bone density did not influence the morphology of the cement layer in this study (**Figure 4-9**). *Aprojo* was independent of bone density, so smaller pores do not prevent cement penetration. This contradicts the findings of two other studies^{26,27}. However, as discussed in Section 3.4.1, in these studies the density was determined using the DXA method, which remains a controversial technique with regard to absolute values, since the size of bone influences the output value. Both measured the cross-sectional area of cement under the implant. DXA methods were used for density evaluation, which raises doubt about the measured values. Despite bone density having an influence on strength, there was no interaction with the cement layer morphology in the data of this study.

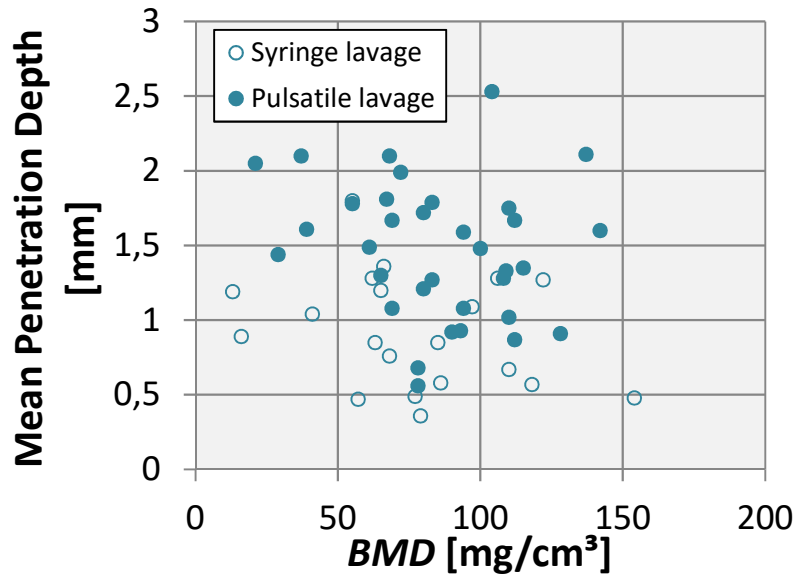


Figure 4-9: Data set evaluated in the current analysis ($n = 54$), separated by lavage technique, since this substantially influences the cement penetration depth. There was no relation between bone density (BMD) and mean penetration depth for both syringe lavage specimens and pulsatile lavage specimens ($R^2 = 0.03$ and $R^2 = 0.04$).

Penetration depth parameters *MaxPen*, *MedPen* and *MeanPen*, as well as parameters *Vol_{spec}* and *Folding* significantly correlated with fixation strength in the overall data, but not within the failure mode groups. This phenomenon is referred to as “Simpson’s Paradox”: measures of subgroups of a data set contradict a measure found for the combined data¹⁸⁸. It indicates a variance contributor that was not investigated (omitted variable bias) or a causality issue¹⁸⁹. In analysis of the relation between cement layer morphology and strength, bone density was omitted. The contribution (regression slopes) of bone density to strength is about 4 MPa per 1 mg/mm³ in the interface group, but about 34 MPa per 1 mg/mm³ in the bulk group. Variance in bone density accounted for 45 % and 68 % of variance in strength in interface and bulk failures, respectively. The contribution of bone density to fixation strength is significant, but different between the failure mode groups.

The calculated mean strength was 0.48 MPa (SD 0.18 MPa) for bone interface failure and 3.21 MPa (SD 1.44 MPa) for bulk bone failure. The total range of fixation strength was similar to that observed by Walker *et al.*²⁵ (0.5 MPa to 3 MPa). Bulk failure strength was similar to the ultimate tensile stress of trabecular bone of 2.54 MPa (SD 1.18 MPa) that was measured by Røhl *et al.*¹²⁰. The failure strength of bulk bone failure measured in this study corresponds to literature data for failure of trabecular bone. The determining influence of bone density on bone strength has been shown before for bone-only samples¹²², as well as for cement-bone interface samples²⁸. The strength of bulk bone failure in this study is the strength of the corresponding trabecular bone, reflected by the strong relationship of strength to bone density in this group.

The other issue in Simpson’s Paradox is causality of the analysed relation, here dependency of fixation strength on cement penetration depth (mean, median, standard deviation and maximum). Fixation strength was hypothesised in a previous study to

increase linearly with increasing penetration depth²⁹, although Walker *et al.*²⁵ found only minimal evidence for such a relation, even when the failure mode was respected. Previous studies were limited to a small window of the data range (**Figure 4-10**). From the current data, it appears that the effect of cement penetration depth is a classifying one.

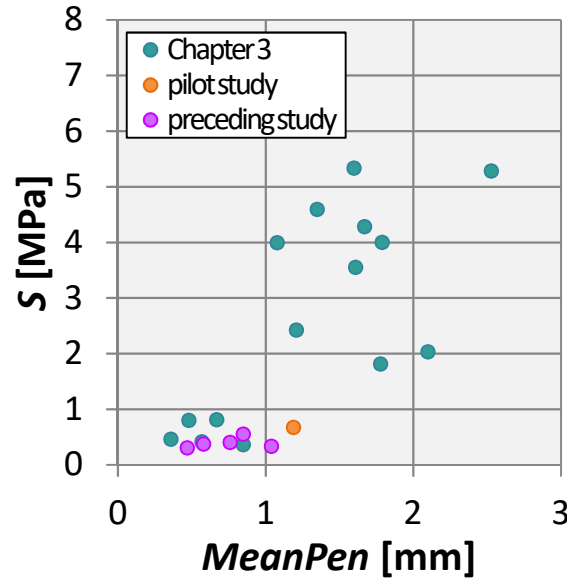


Figure 4-10: Pull-out strength S over mean cement penetration depth ($MeanPen$). Bone failures analysed in this study comprised three data subsets of specimens: from the current thesis ($n = 14$, Chapter 3), from a pilot study on implant design ($n = 1$), and from a previous study¹² ($n = 5$). The relation of fixation strength to bone density and cement penetration depth could not be shown based on the isolated subsets.

Bulk bone failure specimens underwent pulsatile lavage in all cases but one, whereas all interface failures underwent syringe lavage. However, the failure mode is not directly due to the lavage method, but via its increasing effect on the cement penetration depth. The only syringe lavage specimen in the bulk bone failure group had a very low bone density of 13 mg/cm^3 . While the bulk bone failed, the interface stayed intact, which indicates that its bulk bone was weaker than the interface. The penetration depth achieved by syringe lavage was large enough to transfer the load to the bulk bone. The penetration depth in that case was similar to that of another specimen that exhibited about 6-fold bulk failure strength at a BMD of 94 mg/cm^3 . From a specific penetration depth, bone density is determining for strength.

4.4.3 Mechanism and Mathematical Modelling of Cement-Bone Interface Failure

The mechanical phenomenon resulting from a cement penetration depth threshold from which the BMD comes into effect, also causes the failure mode. Load in interlock connections is transferred via a load-transfer area causing stress in the interlocking materials. According to

$$\sigma = \frac{F}{A} , \quad (4-2)$$

where F is a load and A is the load-transfer area, a small transfer area leads to large stress and a large transfer area results in low stress. The load-transfer area is the contact area

between bone and cement within the interlock zone, which is a different concept than the projected or the surface area discussed before. The load-transfer area cumulatively increases when penetration is deeper, which does not necessarily apply to the projected area and to only a minor extent to the area of the lower cement layer surface.

Referring to the bone failure modes in this analysis, bone interface failure occurred when the load-transfer area was too small, deformation of the pore-forming trabeculae was large and ultimate stress of the few interlocking trabeculae was exceeded (**Figure 4-11**, left).

In bulk bone failures, the load-transfer area was large enough to keep the local material stress in the interdigitating structures below ultimate stress and transfer the load to the bulk bone (**Figure 4-11**, right). The cement penetration depth is a measure of the amount of interdigitated trabeculae, as already stated by Walker *et al.*²⁵, so it is related to fixation strength, although not linearly.

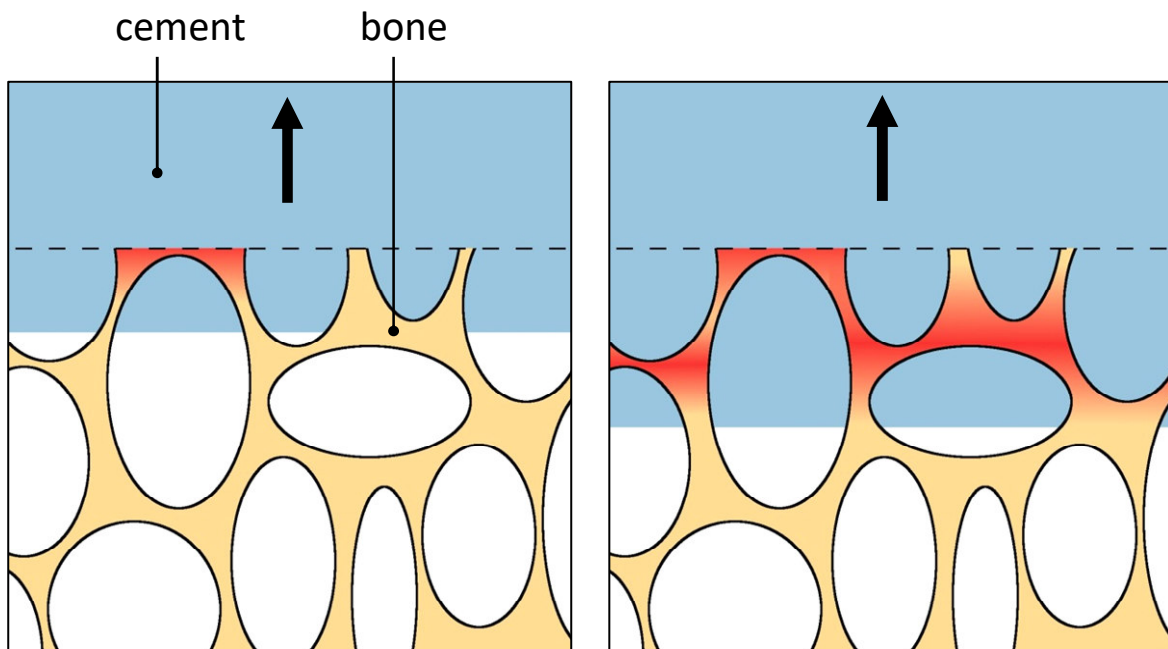


Figure 4-11: Schematic of the trabecular structure with penetrating cement; black arrow indicates load direction, red bone area forms an interlock with the cement. Left: At low penetration depth, only few transverse trabeculae are engaged. Right: At large penetration depth, more transverse trabeculae are engaged and enable load transfer to bulk bone, while the projected area of the cement remains the same as in low penetration.

Modelling using multiple regression with an interaction term was done, based on failure mode classifying parameters Vol_{spec} , $MaxPen$, $MedPen$, $MeanPen$ and $Folding$, as well as on bone density, that determines the strength in the case of sufficient cement penetration. Coefficients of the interaction terms were not significant, so the term could increase or decrease the strength within its variance range. There was no interaction between bone density and the cement layer morphology that significantly influenced strength, which confirms the previous finding of no relation between bone density and cement layer morphology.

The statistical model with $MeanPen$ showed the largest R^2 of 0.74. R^2 of models with Vol_{spec} , $MaxPen$, $MedPen$ and $SDPen$ was marginally lower, not finally eliminating these

approaches. However, cross-validation showed that none of the models was able to predict strength with presumed reliability of less than 10 % error. About one-third of the specimens' fixation strengths were underestimated. This may be attributed to the strict threshold criterion of > 99.9 % sensitivity for interface failure mode. This criterion must be kept, since missing a weak fixation by overestimation of strength would be more severe for the patient than wrongly assigning a case with strong fixation to the interface failure group. Modelling of strength based on mean cement penetration depth and bone density appears a promising approach.

It was implied by Walker *et al.*²⁵ that impaired trabecular structure, as in osteoporotic bone, may influence the interlock capacity. It is known that the trabecular architecture can vary widely at different locations or for different bone density^{32,167,190,191}. Inclusion of the tibia-specific trabecular architecture in an approach for modelling of fixation strength appears reasonable and may be a step towards patient-specific risk analysis of implant fixations.

4.4.4 Limitations of the Analysis

Overall, more than half ($n = 30$) of the specimens in the data pool did not fail on the bone side and were used for cross-validation only. The fixation strength of these specimens is unknown. It remains unclear whether the bone failure specimens had generally lower fixation strength than the cross-validation group. This would bias the statistical model towards low bone interface strength, underestimating the fixation capacity. As stated above, underestimation is the less severe threat in the context of risk assessment, since no weak fixations are missed. However, the bone failure specimens that were the base for the model covered strengths from 0.33 MPa to 5.33 MPa. The largest bone density in the bone failure group was 142 mg/cm³ and thereby in the same range as the largest bone density in the cross-validation group (137 mg/mm³). A substantial difference between the groups is not expected.

4.4.5 Conclusion

In the context of this analysis mean cement penetration depth was superior to median in predicting pull-out failure mode, although both were shown to be good predictors. Volume- and topology-based measures were also related to failure mode. Nevertheless, measures that described the distribution of penetration depth were not pivotal.

Although large cement penetration depth was accompanied by large fixation strength, it was revealed that strength increase was not proportional to penetration depth increase. Instead, fixation strength increased with increasing bone density. This effect was magnified many times if mean cement penetration depth exceeded about 1.1 mm. Penetration depth has a classifying rather than a linear effect on fixation strength.

Failure mechanism of cement-bone interfaces is based on the interlock character of the fixation. Low cement penetration results in a low amount of interdigitated trabeculae. The load-transfer area is small, so the local deformation is large enough to enable pull-out of the cement from the bone pores and stress exceeds the ultimate strength of bone at a relatively low applied load. It was found in classification analysis that a mean penetration depth greater than about 1.1 mm changes the failure mode from bone interface to bulk bone failure. From this depth, the cement interdigitates a sufficient number of trabeculae

and a correspondingly large area to transfer the applied load to the bulk bone. Bulk bone quality therefore becomes determining for pull-out strength. Accordingly, prediction of failure mode and corresponding strength of cement-bone fixation can be approached, based on cement penetration depth and bone quality by use of the models derived in this chapter.

Pulsatile lavage appears pivotal to exceed the critical penetration depth. In all but one case, specimens in the bulk bone failure group underwent pulsatile lavage. Penetration depth and the portion of cement-penetrated area were larger in this group than in the interface failure group, which increases the amount of interdigitated trabeculae and thereby the load-transfer area.

The four most promising models for strength estimation according to equation (4-2) and **Table 4-9** reflected the load-transfer area and the bone strength in their components. While the load-transfer area is indicated by *MeanPen*, *MaxPen*, *MedPen* or *Vol_{spec}* — all being measures for the cement penetration depth — the bone strength was reflected by *BMD*. The best model was based on the mean cement penetration depth and bone density (centred values) and is given as

$$\begin{aligned}
 S = & 2.347 \text{ MPa} + 2.472 \frac{\text{MPa}}{\text{mm}} * \text{MeanPen} \\
 & + 23.974 \frac{\text{MPa mm}^3}{\text{mg}} * \text{BMD} \\
 & + 19.493 \frac{\text{MPa mm}^2}{\text{mg}} (\text{MeanPen} * \text{BMD}) ,
 \end{aligned}$$

which, in a more general formulation, can be expressed as

$$\text{fixation strength} = f(\text{cumulative load-transferring area, bone strength}) ,$$

where f is a function.

The derived models for strength prediction tended to underestimate the strength. A more precise formulation of the interlock capacity may be based on the trabecular structure, which will be investigated in the next chapter.

5

Role of Trabecular Architecture in Cement-Bone Interfaces in Total Knee Arthroplasty

5.1 Introduction

In the previous Chapter 4, the interlock character of cemented fixation was revealed to become manifest in either bone interface or bulk bone failure mode. Since the primary fixation strength of cemented tibial implants is based on an interlock mechanism, it was hypothesised in the previous chapter that modelling of the fixation has to consider the trabecular structure. The idea of the number of engaged trabeculae being strongly related to fixation strength was indeed already stated in 1984 by Walker *et al.*²⁵.

Two approaches may be equivalent: on the one hand, a mean cement penetration depth of 1.1 mm was shown to differentiate between bone interface and bulk bone failure. Given the interlock character of the fixation and the trabecular length of 0.5 mm to 1.5 mm (Section 2.3.2.2), 1.1 mm might be the depth where sufficient transverse trabeculae are interdigitated to transfer the applied load to the bone. The amount of interdigitated trabeculae at a specific penetration depth depends on the porosity of the bone. In low-porosity bone, more trabeculae are interdigitated than in high-porosity bone at the same depth. The porosity P of bone is defined as

$$P = 1 - BV/TV, \quad (5-1)$$

where BV/TV is the bone volume fraction within the sample volume, which is correlated to BMD ($r = 0.90$)³³. The pore size may represent the cement penetration depth that is necessary to exceed in order to engage at least one layer of transverse trabeculae. The penetration depth required to exceed the pore size was lower in high-density bone and higher in low-density bone. Inclusion of a pore-size parameter may lead to more precise assessment of fixation strength of a specific TKA.

On the other hand, a closer look at interlock mechanics reveals that the interface area, across which load applied to one interlock partner is transferred to the other, is crucial for the stress within the material. It follows from

$$\sigma_{interface} = \frac{F}{A_{transfer}} \quad (5-2)$$

that the stress $\sigma_{interface}$ at the interface is smaller when the load transfer area $A_{transfer}$ of the interlock is larger at constant normal load F . $A_{transfer}$ is perpendicular to the applied load. It appears reasonable that the area becomes larger at larger penetration depths with more interdigitated trabeculae, matching Walker's hypothesis.

Furthermore, when load is transferred from one material to another, deformation and the ultimate strength of the weaker structure limits the strength of the coupling. In this context, 'structure' refers to the combined geometry and material properties of an interlock partner. Trabecular bone substance (trabeculae) is stiffer by a factor 3 and stronger by about three orders of magnitude than bone cement in static tensile mode,

which corresponds to the quasi-static pull-out testing performed in the current thesis (**Table 5-1**). However, porous structures are less stiff and strong than single-phase bodies of the same material. Young's Modulus of a sample of trabecular bone is about 5 % of that of a single trabecula and ultimate strength is about 2 %^{41,120,125}. An ultimate tensile strength of 2.54 MPa has been measured for trabecular bone samples¹²⁰, which corresponds to the strength measured for bulk bone failures in the previous chapter (3.21 MPa, Section 4.4.2). Donors were of the same age range as in this study, so bone density was probably about the same. The ultimate strength of a material is defined analogously to equation (5-1):

$$\sigma_U = \frac{F_U}{A_{bone}} \quad , \quad (5-3)$$

which means that the ultimate strength σ_U is smaller when the cross-sectional area A_{bone} of the trabecular structure normal to the applied load is larger for a given ultimate force F_U . The porosity as well as the load-transfer area may pre-determine the fixation failure strength by bringing the cross-sectional area of the bulk bone into effect.

Table 5-1: Quasi-static tensile properties of bone cement, trabecular bone samples and single trabeculae (standard deviation is given in brackets). Tensile strength of a single trabeculae was determined for $n = 1$.

	Trabecular bone ¹²⁰	Bone cement ¹¹⁰	Trabeculae ^{41,125}
Tensile Young's Modulus [MPa]	483 (323)	3 033 (263)	10 400 (3 500)
Tensile strength [MPa]	2.54 (1.18)	40 (8)	166.89 (-)

However, clinical relevance of fixation strength estimation based on the trabecular architecture is limited, since determination of architectural characteristics requires μ CT scanning, which is accompanied by high radiation exposure and limited size of the sample. Although radiation exposure is expected to decrease with improved technical advances, application of μ CT to human patients is not yet possible. Conventional qCT scanning provides lower resolution, but is applicable in clinics. It has already been shown that the mechanical properties of trabecular bone can be estimated from apparent density^{30,119,192,193} that can be determined using qCT. Linear relations as well as power functions are applied¹⁹¹. However, estimation validity is limited due to the anisotropic character of trabecular bone¹⁹¹. It has been stated that the estimation of mechanical properties for oriented structures, such as present in vertebrae, exhibits a larger variance in the transverse direction³⁰. This may also apply to tibial trabecular bone. Estimating equations for mechanical properties of tibial bone have been established. Hvid *et al.*¹⁹³ analysed HU values from qCT at different energy levels and found linear relations between strength and Young's Modulus. Rho *et al.*¹¹⁹ used density in terms of mass per volume as a predictor for the mechanical properties of trabecular bone of lumbar vertebrae and proximal tibia in a power law (Equation (2-1)). The trabecular architecture may likewise be estimable from apparent bone density using models, as long as the principal orientation of the architecture is known.

The aim of this study was to determine pore size, bone volume fraction, as well as the load-transfer area and cross-sectional area of tibial trabecular bone and relate them to apparent bone density below the tibial plateau. Trabecular pore size, mechanical interlock area and bone strength were implemented into formulations of fixation strength of the cement-bone interlock, using the specimen-characteristic trabecular architectural parameters estimated from bone density.

5.2 Methods

This study addressed the influence of trabecular structure in the tibia on fixation strength and failure mechanism. This was done by an analysis of tibial trabecular bone samples and further analysis of the mechanically tested specimens in the preceding Chapter 4. Cubic samples of tibial trabecular bone were prepared and the trabecular architectural characteristics of pore size, bone volume fraction, number and distance of trabeculae as well as rod-plate composition and orientation were determined. In addition, the trabecular interlock parameters load-transfer area and cross-sectional area were derived and determined to characterise interlock aspects of cement-trabeculae compounds. Results were related to global BMD measured below the tibial plateau. A statistical model for strength prediction was developed, based on the parameters and BMD bone side failures from pull-out testing.

5.2.1 Preparation of Trabecular Bone Samples

Cube-shaped samples from trabecular bone were produced from 3 pairs of human tibiae. The tibiae were CT-scanned and BMD was determined applying a qCT method (Avizo 7, VSG, Merignac, France). Conversion factor between grey values in Hounsfield units (HU) and bone mineral density were derived from a commercially available calibration hydroxyl apatite (HA) phantom (QRM, Moehrendorf, DE). More details about the applied method are given in Appendix C.4.1. Tibiae were collected to reflect a range of BMD values as wide as possible (about 20 to 100 mg/cm³, Department of Legal Medicine of the University Medical Center Hamburg-Eppendorf). Samples were taken from the region of interest below the subchondral bone. In the first step, the tibial plateau was resected according to the recommendations for tray implantation (Section 2.3.2.3), using a diamond-coated band saw (EXAKT 3031 CP/N, EXAKT Advanced Technologies GmbH, Norderstedt, Germany). Further cutting of the cubes was performed, using a diamond circular saw that enabled clamping and processing of small samples (**Figure 5-1**, left, Isomet I000, Buehler, Lake Bluff, IL, USA). 6 samples with cube edge length of 10 mm were produced from each tibia, and cranial and anterior directions were marked on the cubes (**Figure 5-1**, right). Samples were excluded when their bone structure was not stiff enough to enable clamping in the saw holder without damaging the bone cube.

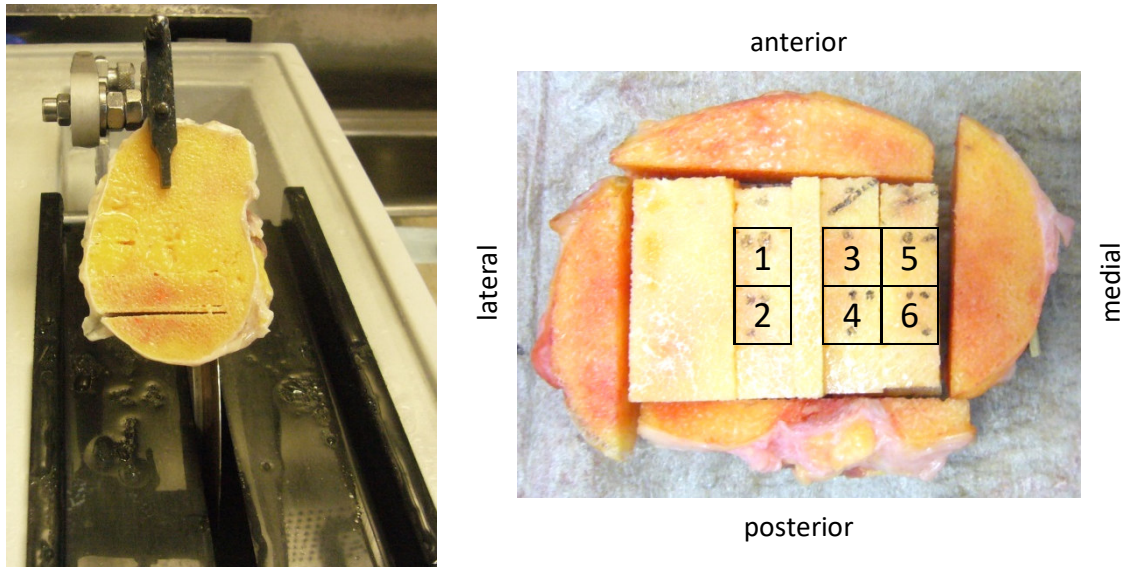


Figure 5-1: Preparation of trabecular bone samples. Left: Cutting of pre-processed tibial plateaus with a diamond circular saw. Right: Bone sample cubes within the tibial plateau from which they originate. Orientation within the plateau is marked on the cranial surface of the cube.

5.2.2 Architectural Parameters of Tibial Trabecular Bone

All trabecular bone samples were scanned in a μ CT scanner ($10 \times 10 \times 10 \mu\text{m}^3$, Scanco Medical AG, Brüttisellen, CH). Cubes were positioned in the μ CT sample holder with the cranial face approximately pointing in z direction of the scanner coordinate system. The μ CT scanner provided a global coordinate system in which the sample cube provided a local coordinate system. A dentine rod was used as marker for the position in the μ CT scanner (**Figure 5-2**). Segmentation of the μ CT scans to bone and exterior material was performed by a bone-specific algorithm provided by the scanner software. Calibration to an HA phantom was supplied by the manufacturer.

The cranial face of the bone cube reflected the cemented tibial resection surface. Considering the experimental setup of mechanical testing (axial pull-out), virtual load is pointing cranially.

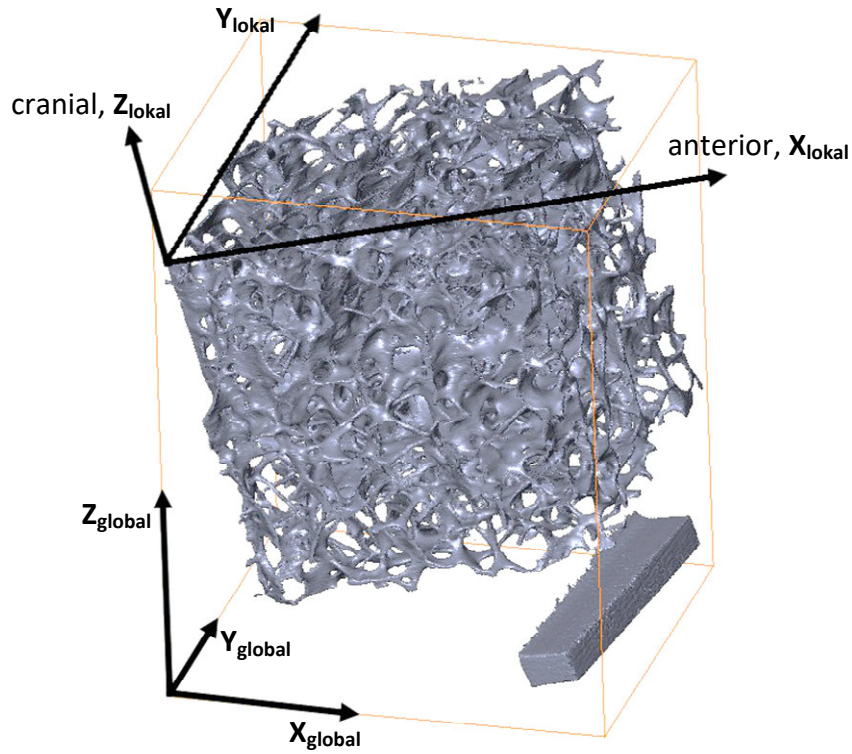


Figure 5-2: Position of the bone sample within the scanner holder. A dentine rod is positioned below the sample at the anterior edge.

Trabecular architecture was evaluated by analysis of architectural parameters that are well described in the literature^{32,33,194–198}. Measures in this study were taken directly from the 3D model of a trabecular sample, which was shown to outmatch the original stereological approach^{32,199,200}. The stereological approach comprised random distribution of a number of lines over 2D cross-sections of the sample (CT scans) and analysis of the structures passed by the lines.

A measure for density was the bone volume density, which was the fraction of bone volume (BV) in the total sample volume (TV) and referred to as BV/TV . In contrast to BMD , BV/TV neglected marrow and fat densities.

The width of the intertrabecular space is referred to as trabecular spacing $Tb.Sp$ in mm. It reflects the pore size of the bone. Determination was based on the 3D models. The intertrabecular space was filled with maximal spheres from which the mean spacing was derived. The number of trabeculae $Tb.N$ per mm is a measure of how many trabeculae are within the sample per unit length. It is determined based on the distances of the mid axes of the rod- and plate-like structural elements.^{32,33}

The structure model index (SMI) was an indicator for the characteristic rod-plate proportion of the trabecular structure (Section 2.3.2.2) according to

$$SMI = 6 \left(\frac{BV}{BS^2} \frac{dBS}{dr} \right), \quad (5-4)$$

where BS is the surface area and r the radius of the trabecular structures (half thickness). The derivative of BS by r reflects the geometry of the bone phase. The factor 6 in the formula has been implemented to receive simple values for ideal geometrical forms

(plates, rods and spheres). An *SMI* of 0 indicates an ideal plate structure. For *SMI* = 3, the structure is ideally rod-like (**Figure 5-3**).³²

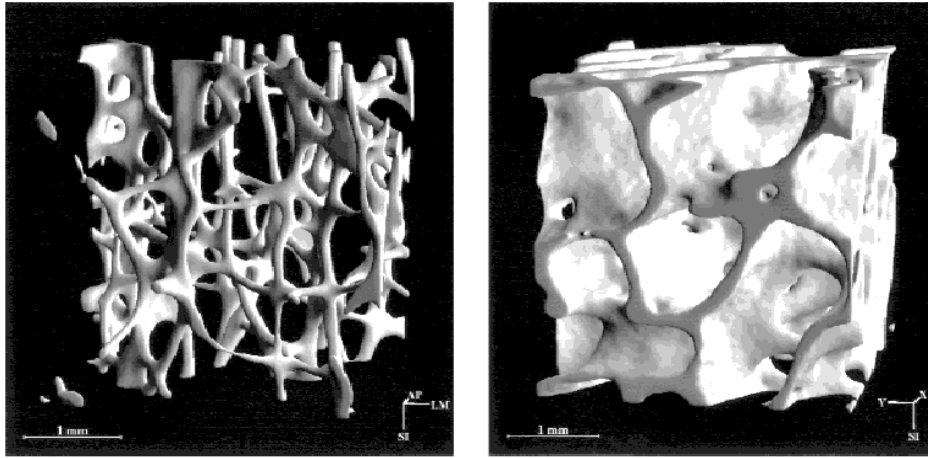


Figure 5-3: 3D models of trabecular structures. Left: Rod-like structure from the lumbar spine. Right: Plate-like structure from the femoral head. [Adapted from Hildebrand *et al.*³²]

The trabecular orientation (*DevAng*) was determined in terms of deviation from the caudal-cranial axis (local *z* axis) of the cube (*DevAng* = 0° refers to a caudal-cranial orientation). It was derived from the mean intercept length (MIL), a measure for the anisotropy based on stereological methods³³. A number of parallel straight lines is distributed over a 2D cross-sectional image of the sample along a defined angle (**Figure 5-4**, left). For each reference line, the number of intersections between line and bone contour is counted. The total length of lines is divided by the total number of intersections to receive an average distance between bone-exterior interfaces. This was repeated for angle increments over a range of 0° ≤ angle ≤ 180°. When plotted on a polar plot, an elliptical shape appeared (**Figure 5-4**, right). In three-dimensional space, an ellipsoid would be formed, which can be expressed by a 2nd rank tensor²⁰¹. The ellipsoid can be approximated by

$$\frac{1}{MIL(\bar{m})^2} \approx \bar{m} M \bar{m} \quad , \quad (5-5)$$

with \bar{m} as unit vector in direction of the reference line and *M* as the 2nd order tensor from the ellipsoid^{33,198,201}.

M can be transformed into a fabric tensor *H* following the relation²⁰²

$$H = M^{-1/2} \quad . \quad (5-6)$$

The columns of *H* were the principal axes of the ellipsoid, in which the longest vector reflects the direction of the trabecular structure with regard to the global coordinate system. In Avizo® (version 7, VSG, Burlington, MA, USA), three virtual markers were placed on the resection surface of the corresponding 3D model of the bone sample to define the corresponding surface plane. *DevAng* was calculated in terms of deviation of the longest vector in *H* from the normal vector of the cranial plane of the bone cube.

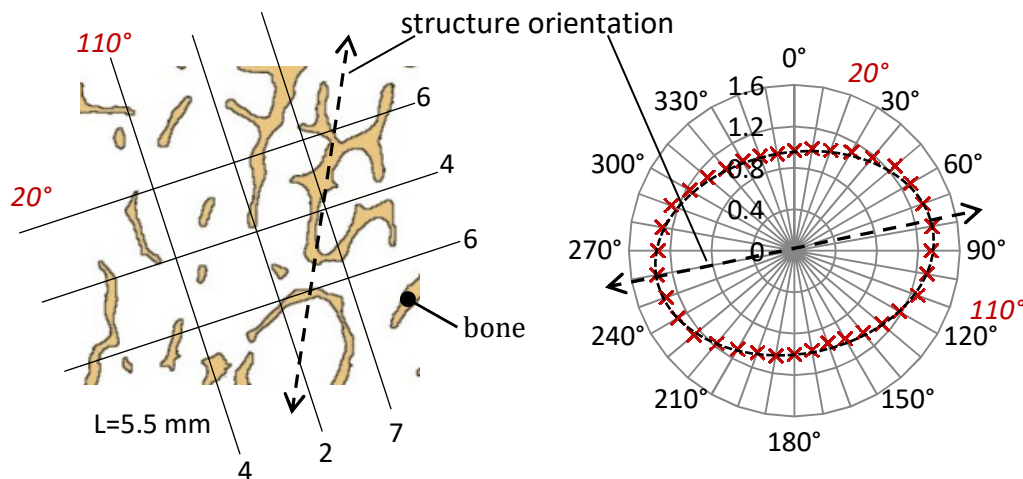


Figure 5-4: Stereological approach to determine the orientation of a porous structure. Left: Parallel lines in defined angles (red) are distributed over a cross-sectional image of the sample. The total length of lines is divided by the number of intersections with the bone contour. Right: Polar plot of the determined intersection length over line angle.

Established bone architectural parameters BV/TV , SMI , $Tb.Sp$, $Tb.N$ and fabric tensor H were determined using the software of the μ CT scanner. Thus, the volume of interest (VOI) was defined in the global coordinate system, while the sample's local coordinate system was unaligned with the cube axes. $DevAng$ was determined from H , using a MATLAB® routine that expresses the orientation in terms of the local coordinate system of the sample cube, with respect to the local z axis.

5.2.3 Interlock Parameters of Tibial Trabecular Bone

Two additional parameters were developed for this study that allow for analysis of the interlock capacity, based on how much of the trabecular structure was engaged in cement-bone interlock. The resection surface of the bone cube was assumed to be penetrated homogeneously by cement that thereby interdigitates with the trabeculae (**Figure 5-6**). On the one hand, fixation strength depended on the load-transfer portion of the interlock interface between bone and cement phase. The load-transfer portion of the interface area was assumed to be smaller than the total interface area between bone and cement. Compression load is applied to the area of the bone cavity's cranial surface, projected on to a plane parallel to the resection plane. Contact is lost caudally since the adhesion-free contact cannot transfer tensile load. The sum of all (**Figure 5-5**) projected load-transfer areas was referred to as the interlock area (IA , **Figure 5-6**, right).

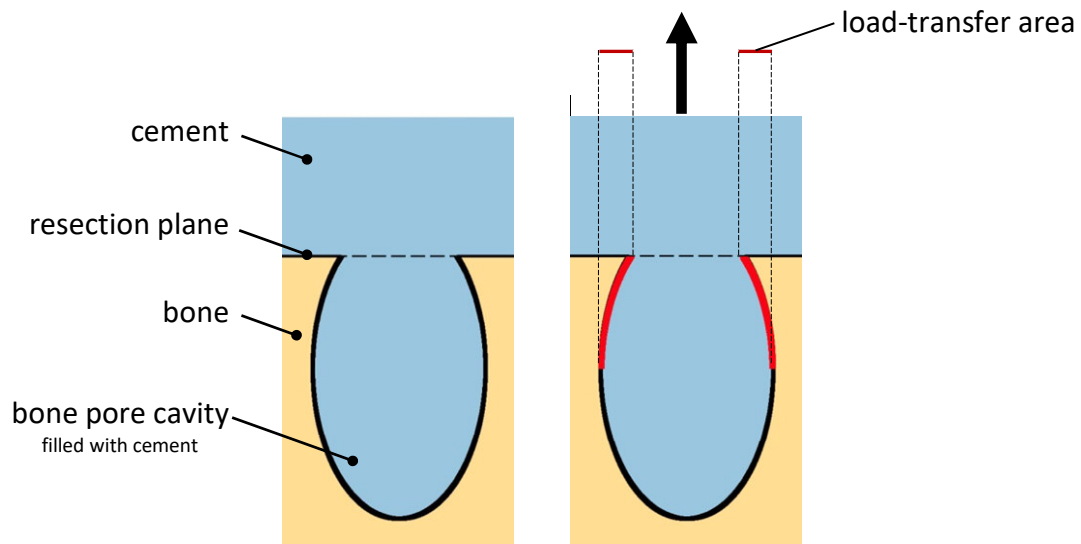


Figure 5-5: Cement-bone interlock under load. Left: Unloaded state; contact area between bone and cement corresponds to interface between bone and cement. Right: Loaded state (black arrow); load is transferred via the area of the projected cranial surface of the bone pore (red marks).

On the other hand, fixation strength was governed by the load capacity of the involved materials. It was shown in Chapter 4 that bulk bone failure occurred when a particular cement penetration depth was exceeded and all load was transferred to the bulk bone below the cement. The strength of trabecular bone limited the strength of the fixation. According to equation (5-3), ultimate load F_U for a given bone material strength σ_U was dependent on the cross-sectional area of the bone at the interface between cement-bone and bone-only region. For this analysis, the cross-sectional area (CSA) of trabecular bone perpendicular to the applied load was determined (**Figure 5-6, right**).

Cement penetration depth was identified as a pre-determining measure of strength in the previous chapter, so interlock parameters were determined in dependency on the negative z coordinate of each bone cube, referred to as PEN.

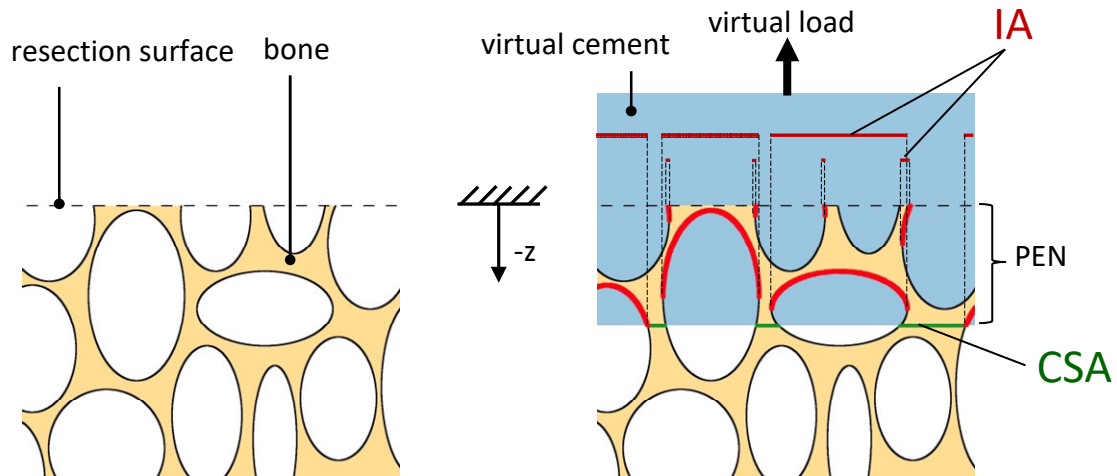


Figure 5-6: Schematic of the trabecular structure simplified from 3D to 2D. Left: Native, with resection level indicated by a dashed line. Right: With cement (blue) penetrating the trabecular structure with a particular penetration depth; red marks indicate the contact surface in deformed (loaded) state that was projected on to a plane parallel to the resection plane, to cumulate to the interlock area (*IA*); green marks indicate the cross-sectional area (*CSA*).

Determination of interlock parameters *IA* and *CSA* was performed, using reconstruction software (Avizo® 7, VSG, Burlington, MA, USA) and numerical computing software (MATLAB® R2013a, The MathWorks Inc., Natick, MA, USA). Digital 3D surface models of the trabecular structure were generated from the μ CT scans of each sample in Avizo® 7 (Figure 5-7, left). The threshold for automatic segmentation between bone and exterior material was set to 7 000 HU. The surface between the two materials was generated using triangles with a minimum edge length of 0.02 mm. The 3D model was manually pre-aligned to the global coordinate system, according to the dentine marker position set for cranial and anterior directions. The resection plane was defined by three virtual markers that were also used to determine *DevAng*. 3D surface models and markers were exported and further processed in MATLAB®.

The 3D model was aligned so that the resection plane coincided with the xy plane of the global coordinate system. *IA* and *CSA* were determined from a VOI within the 3D model of the sample, to control for edge artefacts from sawing and irregularities of the cube shape (Figure 5-7).

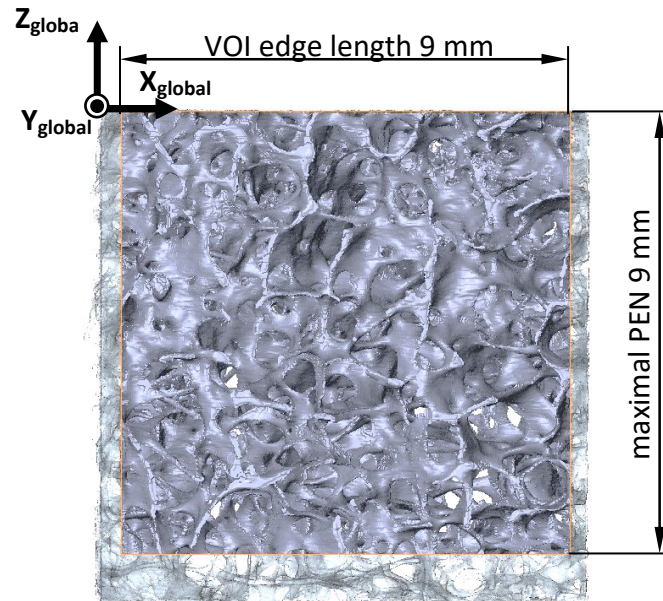


Figure 5-7: VOI within a 3D model of a trabecular bone sample for *IA* and *CSA* determination.

VOI edge length for interlock parameter determination was 9 mm. The VOI model was virtually cut at planes parallel to the cranial face of the cube, whereby each cut represented a particular cement penetration depth PEN. At each cut level, *IA* and *CSA* were determined, based on the triangles of the 3D surface models of the samples (**Figure 5-8**). PEN progressively increased, so *IA* and *CSA* were determined as a discrete series of values. Cut increment size was 0.06 mm and maximum depth was 9 mm.

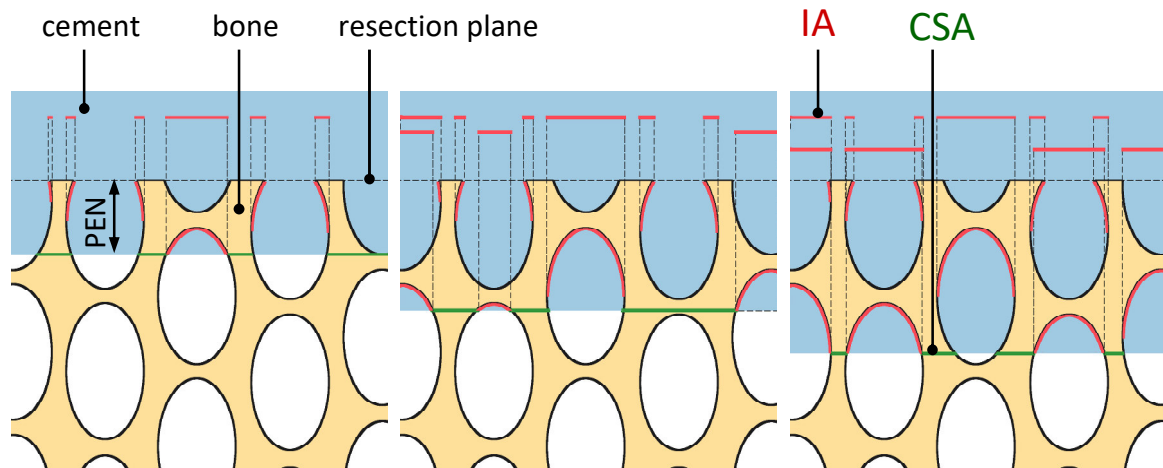


Figure 5-8: Determination of interlock area (*IA*) and cross-sectional area (*CSA*) in a 2D simplification of the interlock. Penetration depth PEN increases from left to right as well as *IA*. *CSA* is about constant.

IA was calculated from surface triangles with the normal vector pointing caudally. The triangles were projected onto a plane parallel to the assumed resection plane. All triangles cranially to the respective cut level were included. *CSA* was determined from the cross-sectional profile at the PEN level.

Values were normalised to the VOI reference area of $9 \times 9 \text{ mm}^2 = 81 \text{ mm}^2$ forming two discrete series of dimensionless data: Specific interlock area IA_0 and specific cross-

sectional area CSA_0 . Index “0” denotes the normalised values. IA_0 was expected to increase with increasing PEN, so the slope sIA_0 of a corresponding linear regression was reported (**Figure 5-9**, upper row). The regression model constant was neglected, since IA_0 at $PEN = 0$ mm was assumed to equal zero:

$$IA_0 = constant + sIA_0 * PEN \quad , \quad (5-7)$$

$$\rightarrow IA_0 \approx sIA_0 * PEN \quad . \quad (5-8)$$

sIA_0 is defined in mm^{-1} . CSA_0 was expected to stay constant with increasing PEN, so the mean value $mCSA_0$ was reported as characteristic parameter (**Figure 5-9**, lower row).

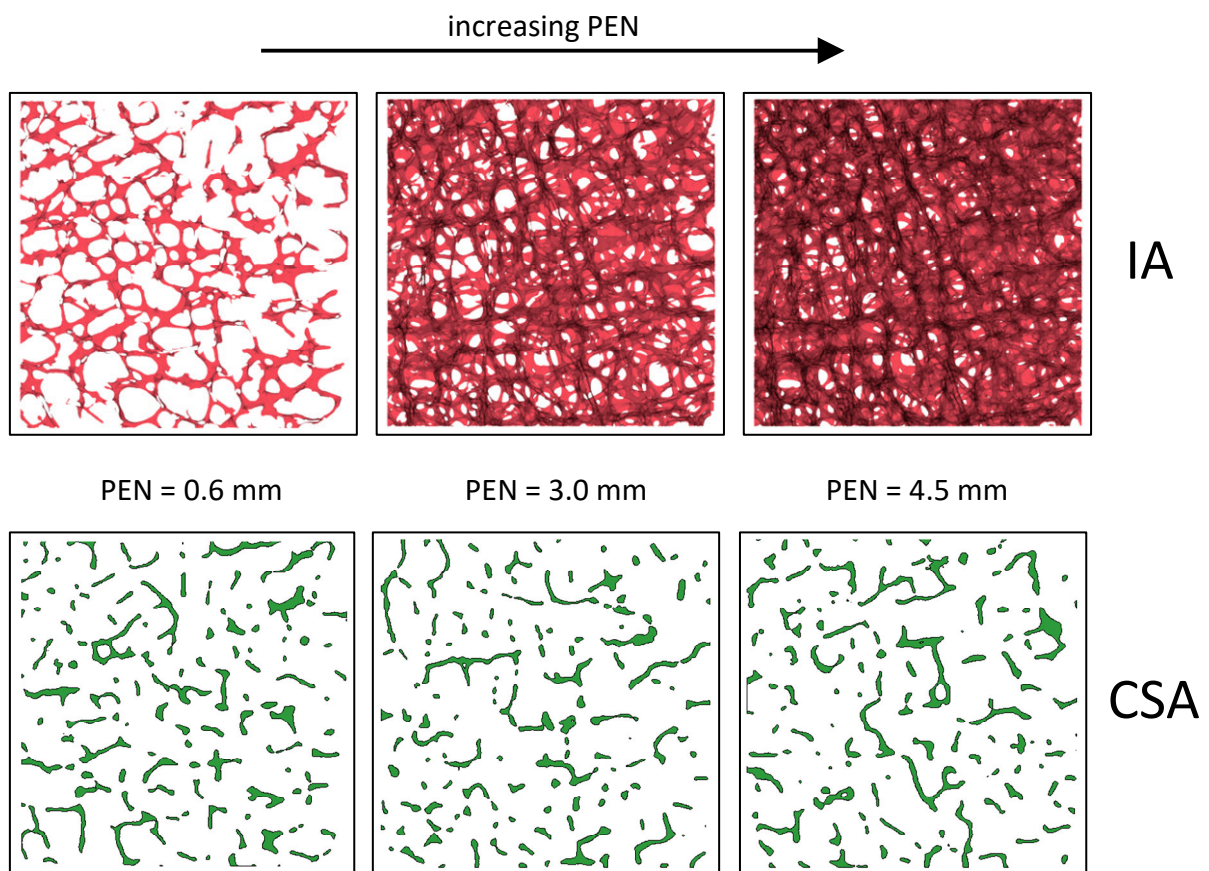


Figure 5-9: Dependency of IA and CSA on PEN for a characteristic sample cube. Upper row: Images from MATLAB interlock area (IA) determination routine. IA increases with increasing PEN . Lower row: Corresponding images from MATLAB cross-sectional area (CSA) determination routine. CSA is approximately constant with increasing PEN .

Three bone cubes with characteristic BV/TV values (low- BV/TV , medium- BV/TV , high- BV/TV) were subject to convergence analyses regarding required cube edge length and inclination of the cube. Inclined cubes depicted deviation of the structure orientation or inclined resection planes. sIA_0 and $mCSA_0$ were determined for cube edge lengths of VOIs of 0.5, 1, 2, 3, 5, 7 and 9 mm (**Figure 5-10**, A). A VOI of 9 mm edge length was taken from 3D cube models inclined by 22.5°, 45°, 67.5° and 90° (**Figure 5-10**, B). sIA_0 and $mCSA_0$ were determined at each angle. Both convergence parameters were determined in

increments of 0.06 mm to maximum $PEN = 5$ mm in edge length variation and $PEN = 3$ mm in inclination variation. In the convergence studies, regression slope sIA_0 and its R^2 as well as $mCSA_0$ and its standard deviation (SD) were compared between parameters of edge length and inclination.

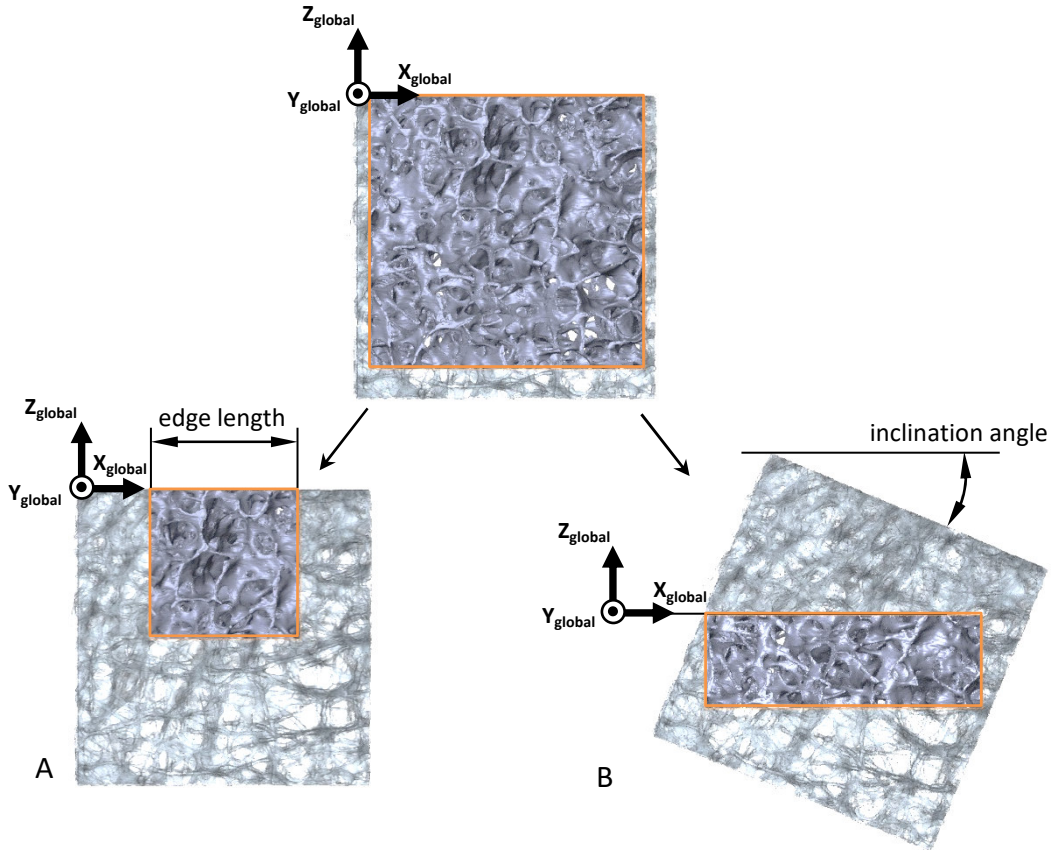


Figure 5-10: Definition of VOIs for convergence analysis. A: VOIs of different edge lengths. B: VOI in inclined cube.

5.2.4 Statistical Modelling of Bone Failure Based on the Trabecular Structure

It was hypothesised in Chapter 4 that statistical modelling of the fixation strength has to consider the trabecular architecture. The load-transfer area within the interlock (Equation (5-2)) and the cross-sectional area of the structure the load is transferred to (Equation (5-3)) were assumed to be crucial for fixation strength.

In Chapter 4, exceedance of a critical cement penetration depth was found to pre-determine the failure mode, by resulting in a load-transfer area within the interlock that is large enough to transfer the load to the bulk bone. In Chapter 3, strength in bulk bone failure was shown to be independent of the cement penetration depth. The specific interlock area IA_0 is proportional to the penetration depth (equation (5-8)), so the classifying effect of penetration depth can also be assumed for IA_0 .

A statistical model was derived, based on this hypothesis and 24 specimens that failed on the bone side in mechanical testing (Chapter 4).

In the current study, the interlock capacity was represented by either the specific interlock area IA_0 or — in an alternative approach — by the cement penetration depth with respect to the porosity.

Given a significant relation of sIA_0 to BMD

$$sIA_0 = sIA_0(BMD) \quad , \quad (5-9)$$

IA_0 was derived based on Equation (5-8) according to

$$IA_{0,i} = sIA_{0,i}(BMD_i) * MeanPen_i \quad , \quad (5-10)$$

using the mean penetration depth $MeanPen$ from the previous chapters.

As already indicated, the critical mean penetration depth found in Chapter 4 corresponds to the approximate pore size of trabecular bone. Exceeding the pore size may enable load transfer to the bulk bone, so the absolute penetration depth is probably less determining for strength than the mere statement of whether the penetration depth is larger or smaller than the given pore size. Analogous to IA_0 , a relative penetration depth with respect to the pore size (PEN_0) was calculated and was assumed to classify between bone interface and bulk bone failure by providing a critical value. It has been stated that the pore size of a trabecular structure $Tb.Sp$ is inversely related to BV/TV according to

$$Tb.Sp = \frac{1 - BV/TV}{Tb.N} \quad 203. \quad (5-11)$$

A strong linear correlation between BV/TV and BMD was found by Goulet *et al.*³³, so pore size in terms of $Tb.Sp$ is predictable from BMD . The cement penetration depth with respect to the porosity was calculated using the pore size $Tb.Sp$, given a significant relation between $Tb.Sp$ and BMD :

$$Tb.Sp = Tb.Sp(BMD) \quad , \quad (5-12)$$

Used to calculate the relative penetration depth PEN_0

$$PEN_{0,i} = \frac{MeanPen_i}{Tb.Sp(BMD_i)} \quad . \quad (5-13)$$

The functions $sIA_0(BMD)$ and $Tb.Sp(BMD)$ were the statistical models for estimating the trabecular parameters of a specimen i and $MeanPen$ was the corresponding mean penetration depth.

Both IA_0 and PEN_0 were continuous dimensionless variables determined for each of the 24 bone failure specimens. Bone failure mode was dichotomous and shown to be based on pre-determination by the penetration depth in Chapter 4. IA_0 and PEN_0 were derived using the penetration depth, so they are assumed to exhibit classifying behaviour regarding failure mode as the mean cement penetration depth. A threshold was determined, as explained in Section 5.2.5 ("Statistics"), and two categorical variables, $CLASS_{IA}$ and $CLASS_{PEN}$, were introduced as classifying parameters. The variables were 0 for specimens whose parameter value was smaller than the respective threshold of IA_0 and PEN_0 and 1 for parameter values greater than the threshold. The determination of the two thresholds was based on statistical methods described in the subsequent Section 5.2.5.

Given a significant relation of $mCSA_0$ to BMD

$$mCSA_0 = mCSA_0(BMD) \quad , \quad (5-14)$$

statistical modelling of fixation strength was performed. Four multiple regressions with $mCSA_0$, representing the specific cross-sectional area and each one of the four parameters IA_0 , PEN_0 , $CLASS_{IA}$ and $CLASS_{PEN}$, representing the load-transfer area of the bone structure were applied. A corresponding interaction term was also introduced:

$$S = a_0 + IA_0 * a_1 + mCSA_0 * a_2 + mCSA_0 * IA_0 * a_3 \quad , \quad (5-15)$$

$$S = a_0 + PEN_0 * a_1 + mCSA_0 * a_2 + mCSA_0 * PEN_0 * a_3 \quad , \quad (5-16)$$

$$S = a_0 + CLASS_{IA} * a_1 + mCSA_0 * a_2 + mCSA_0 * CLASS_{IA} * a_3 \quad , \quad (5-17)$$

and

$$S = a_0 + CLASS_{PEN} * a_1 + mCSA_0 * a_2 + mCSA_0 * CLASS_{PEN} * a_3 \quad . \quad (5-18)$$

5.2.5 Statistics

Data sets and subsets were tested for normality, applying Kolmogorov-Smirnov tests. In the case of small sample size ($n < 12$) or occurrence of non-Gaussian distribution in subsets, non-parametric analysis was reported.

Tibiae were numbered in ascending order with increasing BMD (Tibia 1 has the lowest BMD).

It was hypothesised that parameters describing the trabecular architecture were related to BMD and could be estimated from it. This would enable clinical application of a potential influence of trabecular parameters on the implant fixation strength, because BMD can be measured directly in the patient, in contrast to trabecular parameters. The architectural and interlock parameters were averaged for each tibia and simple linear regression with BMD as predictor was performed on the tibia by means of each parameter. BMD was divided by 10^3 when analysed, to receive a similar scale for the coefficients in regression models. The estimation equation was formed as follows:

$$parameter = a_0 + a_1 * BMD \quad . \quad (5-19)$$

Architectural and interlock parameters were compared between the 6 tibiae, applying one-way ANOVA with *a priori* control of the familywise type-I error probability. *A priori* control was achieved by planned comparisons created to compare between tibial pairs and within the pairs and to be independent of each other (details in Appendix C.4.2). In the case of non-parametric data of independent samples, the Kruskal-Wallis test was performed with subsequent Mann-Whitney U tests on each planned comparison.

IA_0 and PEN_0 were determined according to equations (5-10) and (5-13), respectively. Their classification potential was analysed, using receiver operating characteristic (ROC, Section 4.2.3). Since $mCSA_0$ was used to reflect the bone strength in statistical modelling,

ROC analysis was applied to support the assumption that this parameter had no classification potential for the failure mode groups. Requested classification ability in ROC was at sensitivity^m above 99.9 % and corresponding minimum error rateⁿ. An error rate of 0.1 % represented correct classification in all cases and therefore correct discrimination between the failure modes. Failure at the bone interface was considered as a 'positive' category. The value of the respective parameter at which sensitivity was above 99.9 % and error rate was as low as possible, was considered the threshold between risk of bone interface failure and risk of bulk bone failure.

For multiple linear regressions, $mCSA_0$ was centred to its overall mean. Specimens with full stem cementation were excluded from analysis.

Cross-validation of these regression models was carried out on the specimens that did not fail on the bone side in pull-out testing (Appendix C.3.1). Ratios between estimated and measured strength were determined for all regression models. A ratio below 1 indicated that the estimated strength was lower than the measured strength, so the strength was underestimated. A binomial test was carried out with a cut-off point of 1. The test criterion for the proportion of underestimated cases was set to 10 %^p. However, wrongly assigning a case with strong fixation to the interface failure group is acceptable if the danger of missing a weak fixation by overestimation of strength is reduced.

All statistical evaluations were performed using statistics software (IBM® SPSS® Statistics 21, IBM Corporation, Armonk, NY, USA) and applying a type-1 error level α of 0.05.

5.3 Results

The results for architectural and interlock parameters are reported in Section 5.3.1. Statistical modelling of the strength dependence on trabecular parameters is documented in Section 5.3.2.

BMD of the tibiae from which the bone samples were cut ranged from 26 mg/cm³ to 115 mg/cm³.

5.3.1 Characterisation of Tibial Trabecular Bone

The VOI within the trabecular bone samples from which the architectural parameters (BV/TV , $Tb.Sp$, $Tb.N$, SMI , $DevAng$) were determined was 6 x 6 x 6 mm³ in each cube. The interlock parameters (sIA_0 , $mCSA_0$) were determined from VOIs of 9 x 9 x 9 mm³ volume. Two sample cubes could not be clamped in the last sawing step, due to low substance content and were excluded from analysis, therefore $n = 34$ cubes were analysed.

Increase of IA_0 with increasing PEN was approximately linear in all cases. sIA_0 was determined in terms of regression slope (**Figure 5-11**, A). Regression slopes and R^2 are given in Appendix C.4.3. CSA_0 alternated around a mean value (**Figure 5-11**, B). Means of *BMD* and all trabecular parameters of each tibia are displayed in **Table 5-2**.

^m Sensitivity = statistical power 1- β

ⁿ Error rate = type-1 error rate α

^p Not to be confused with the significance level. A significant p value meant that, with a probability of less than 5 % (α level), occurrence of more than 10 % (test criterion) of underestimated cases appeared by chance.

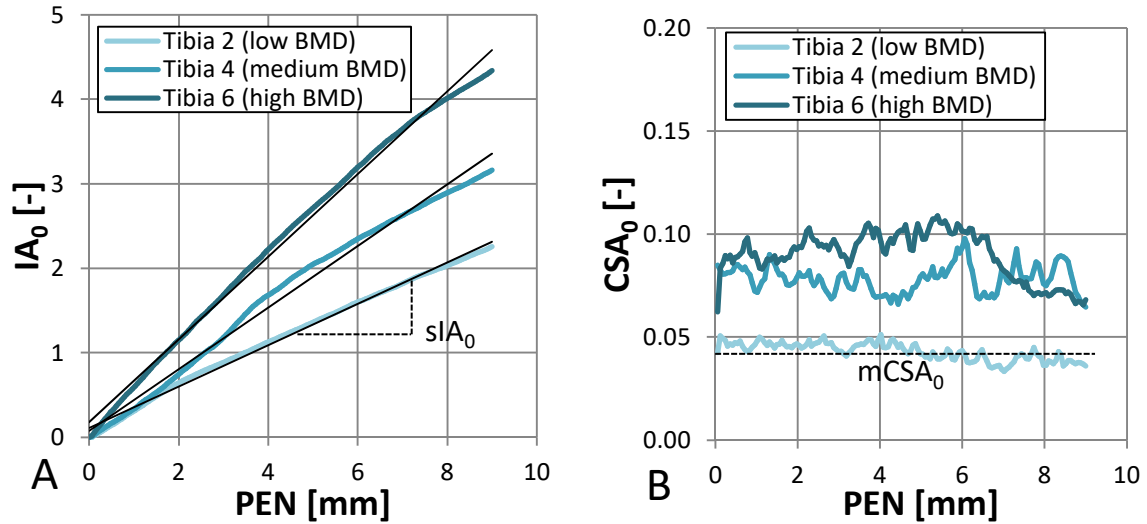


Figure 5-11: Characteristic curves for interlock parameters, dependent on penetration depth PEN. One characteristic curve per *BMD* level is displayed. A) IA_0 with corresponding slope (sIA_0) for further analysis is displayed. B) CSA_0 and corresponding mean ($mCSA_0$) for further analysis is displayed.

Table 5-2: Mean value and standard deviation (SD, given in brackets) of architectural and interlock parameters for each tibia.

		Low-BMD Pair		Medium-BMD Pair		High-BMD Pair	
		Tibia 1 n = 5	Tibia 2 n = 6	Tibia 3 n = 6	Tibia 4 n = 6	Tibia 5 n = 6	Tibia 6 n = 5
Architecture	<i>BMD</i> [mg/cm ³]	26	32	64	64	98	115
	<i>BV/TV</i> [-]	0.072 (0.023)	0.056 (0.025)	0.082 (0.009)	0.092 (0.022)	0.101 (0.023)	0.109 (0.026)
	<i>Tb.Sp</i> [mm]	1.022 (0.217)	0.981 (0.081)	1.022 (0.059)	0.994 (0.101)	0.592 (0.043)	0.601 (0.054)
	<i>Tb.N</i> [1/mm]	1.008 (0.213)	1.013 (0.08)	0.986 (0.058)	1.03 (0.124)	1.65 (0.104)	1.613 (0.133)
	<i>SMI</i> [-]	1.516 (0.529)	1.793 (0.475)	1.286 (0.167)	1.175 (0.228)	1.69 (0.17)	1.653 (0.183)
	<i>DevAng</i> [°]	12.7 (4.5)	14.9 (3.8)	21.7 (9.2)	18.4 (6.1)	18.2 (12.2)	13.1 (7.6)
Interlock	sIA_0 [1/mm]	0.227 (0.060)	0.211 (0.047)	0.352 (0.037)	0.330 (0.024)	0.497 (0.096)	0.523 (0.026)
	$mCSA_0$ [-]	0.067 (0.024)	0.051 (0.024)	0.076 (0.008)	0.088 (0.026)	0.095 (0.021)	0.100 (0.023)

Mean *Tb.Sp* for a tibia significantly decreased with increasing *BMD* ($R^2 = 0.70$, $p = 0.023$, **Figure 5-12**, A), whereas *BMD* significantly increased with increasing *BV/TV* ($R^2 = 0.82$, $p = 0.008$). Likewise, mean *Tb.N* significantly increased with increasing *BMD* ($R^2 = 0.70$, $p = 0.024$) as well as $mCSA_0$ ($R^2 = 0.78$, $p = 0.013$, **Figure 5-12**, B). The regression model for predicting sIA_0 from *BMD* was highly significant ($R^2 = 0.97$, $p < 0.001$, **Figure 5-12**, C).

BMD of a tibia was not significantly related to mean *DevAng* ($p = 0.814$) and *SMI* ($p = 0.858$) of the trabecular bone.

Regression model coefficients, R^2 and p values are listed in Appendix C.4.3.

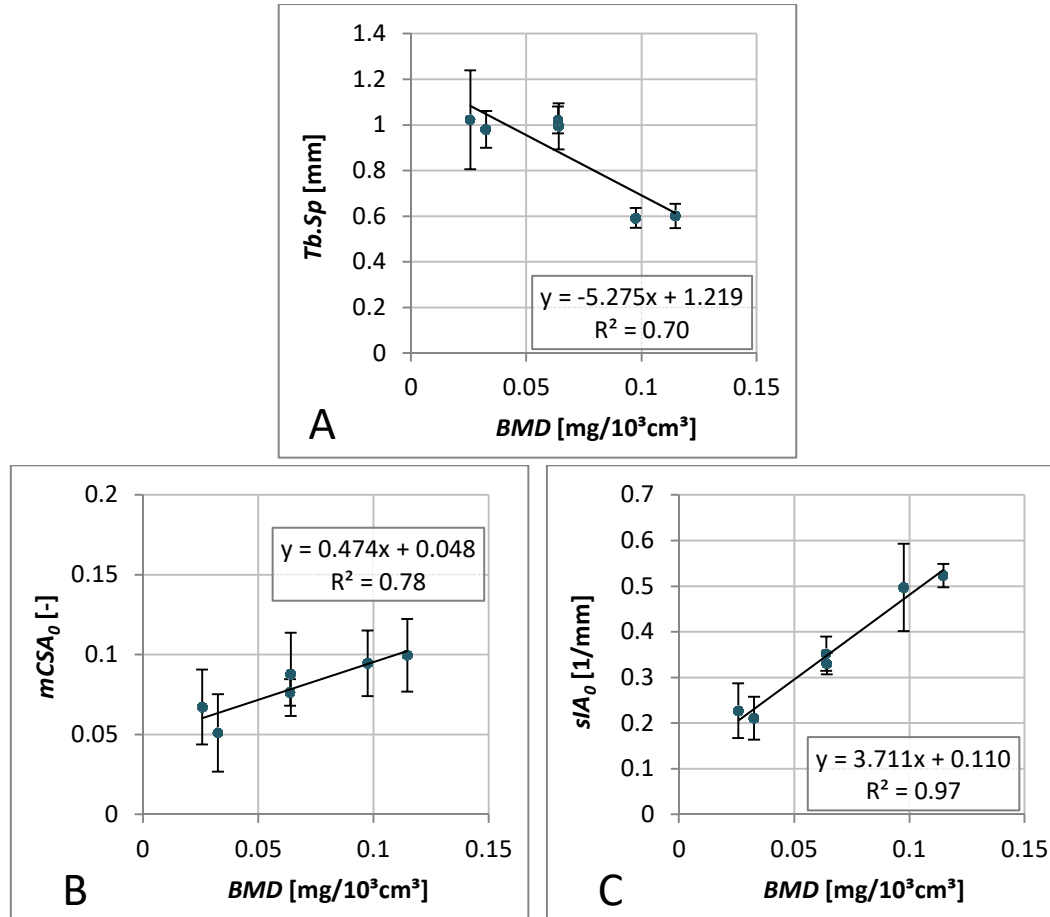


Figure 5-12: Significant regression models for *BMD* in relation to trabecular parameters ($n = 6$, error bars indicate tibia-specific standard deviation; regression models were derived from the mean values).

The results from architectural and interlock parameters of sample cubes were not significantly different within a tibial pair (p values are presented in Appendix C.4.3).

BV/TV significantly increased with *BMD* from low-BMD pair to high-BMD pair ($p < 0.016$).

Tb.Sp was lower and *Tb.N* was larger in the high-BMD pair than in the low- and medium-BMD pairs ($p < 0.001$, **Figure 5-13**, A). No difference between medium- and low-BMD pairs was found for *Tb.Sp* and *Tb.N* ($p = 0.928$, $p = 0.091$, respectively).

SMI was significantly larger in the high-BMD pair than in the medium- and low-BMD pairs ($p = 0.008$, **Figure 5-13**, B) and significantly larger for low- than for medium-BMD pair ($p = 0.027$).

There was no significant difference in *DevAng* between tibial pairs ($p = 0.563$).

*sIA*₀ significantly increased from low- to high-BMD pair ($p < 0.001$, **Figure 5-13**, C).

*mCSA*₀ significantly increased from low- to medium-BMD pair ($p = 0.027$) and to high-BMD pair ($p = 0.037$, **Figure 5-13**, D).

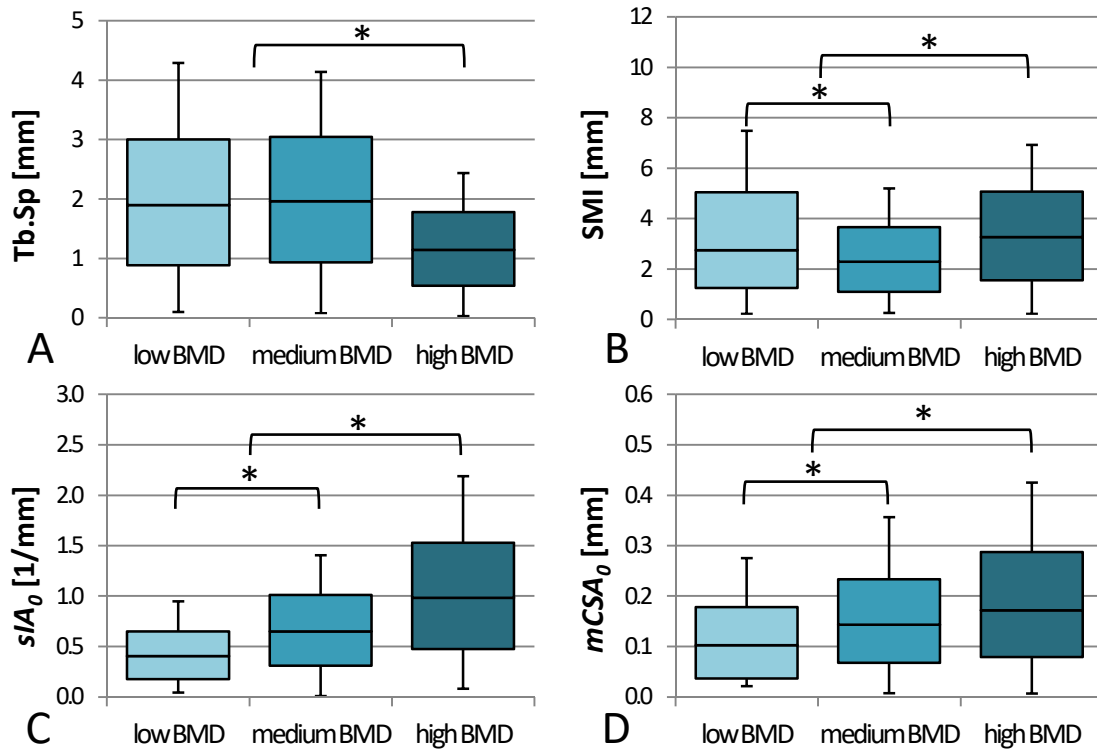


Figure 5-13: Mean values of architectural and interlock parameters for each tibial pair (* indicates p values < 0.05). Sample size: low-BMD n = 11, medium-BMD n = 12, high-BMD n = 11.

All three samples in convergence analysis showed constant sIA_0 and corresponding R^2 , as well as $mCSA_0$ from a VOI with edge length larger 5 mm. This lower bound was determined by the medium-BMD cube (convergence curves in Appendix C.4.4). $mCSA_0$ for the medium- and high-BMD samples was constant from 2 mm edge length. SD of $mCSA_0$ was constant from 5 mm edge length.

sIA_0 was different at all inclination angles, with the minimum between 0° and 45° and maximum between 45° and 90° . Deviation of $mCSA_0$ at different inclinations was small. Variance due to different BMD was larger for 0° and 90° and smaller around 45° .

5.3.2 Modelling of Fixation Strength Based on Trabecular Parameters

Estimated values of dimensionless parameters IA_0 , $mCSA_0$ and PEN_0 for the bone failure specimens from mechanical testing are presented in Appendix C.4.5.

In ROC analysis, PEN_0 and IA_0 showed an error rate of 7.7 % wrongly classified bulk bone failure cases, when applying thresholds 1.33 and 0.38, respectively. $mCSA_0$ did not show classification potential (error rate > 99.9 %) (Table 5-3).

Dimensionless IA_0 , PEN_0 and $mCSA_0$ were centred to their overall means (Table 5-3).

Table 5-3: Results from ROC analysis and overall means of the predictors in multiple regressions. Mean values were used for centring of data.

Predictor	Threshold	Error rate [%]	Mean (n=54)
IA_0 [-]	-	> 99.9	0.52
PEN_0 [-]	1.33	7.7	1.72
$mCSA_0$ [-]	0.38	7.7	0.098

Multiple regression with the respective interaction term resulted in significant models for strength estimation ($p < 0.001$, R^2 values are given in **Table 4-9**). Due to exclusion of $n = 1$ full cemented specimens, sample size was $n = 23$. The largest amount of explained variance was 89 % in regression with $CLASS_{IA}$ or $CLASS_{PEN}$ as well as $mCSA_0$ as predictors. The smallest amount of explained variance was 72 % with PEN_0 and $mCSA_0$ as predictors (**Table 4-9**). In both models that consider a continuous effect of IA_0 and PEN_0 on strength, the coefficients in $mCSA_0$ terms were not significant ($p = 0.773$ and 0.777 , respectively) as well as the interaction terms ($p = 0.740$ and 0.948 , respectively).

Classification to interface and bulk bone failure group based on $CLASS_{PEN}$ and $CLASS_{IA}$ was identical (**Table C-21** in Appendix C.4.5). Both $CLASS_i$ variables resulted in the same significant model (**Table 5-1**). The $mCSA_0$ term was not significantly affecting strength ($p = 0.722$). The interaction term was significant ($p = 0.002$).

Table 5-4: Multiple regression models with an interaction term for dependence of strength on continuous or dichotomous specific interlock area (IA_0) or relative penetration depth (PEN_0) as well as bone density $mCSA_0$. Models are of the form $S = a_0 + predictor * a_1 + mCSA_0 * a_2 + predictor * mCSA_0 * a_3$. (The adjusted value for R^2 is reported; Confidence intervals are given in brackets)

Predictor	a_0 [MPa]	a_1 [MPa]	a_2 [MPa]	a_3 [MPa]	R^2	p
IA_0	2.250 [1.808 2.692]	5.650 [4.020 7.281]	-4.089 [-33.283 25.105]	16.461 [-85.902 118.824]	0.73	< 0.001
PEN_0	2.343 [1.896 2.791]	1.805 [1.275 2.335]	3.799 [-23.830 31.428]	1.077 [-33.165 35.320]	0.72	< 0.001
$CLASS_{IA}$	0.513 [0.119 0.908]	3.316 [2.767 3.866]	3.800 [-18.205 25.805]	60.126 [25.881 94.371]	0.89	< 0.001
$CLASS_{PEN}$	0.513 [0.119 0.908]	3.316 [2.767 3.866]	3.800 [-18.205 25.805]	60.126 [25.881 94.371]	0.89	< 0.001

In cross-validation of the PEN_0 model for predicting the fixation strength, the probability of underestimating the fixation strength was 30 % and significantly greater than 10 % ($p = 0.001$; binomial test). Using IA_0 for predicting the fixation strength resulted in 40 % and significantly greater than 10 % probability of underestimating the fixation strength ($p < 0.001$; binomial test). This corresponds to 9 and 11 underestimated cases, respectively.

The probability of underestimation of the fixation strength was 30 % and significantly greater than 10 % for the model with classifying $CLASS_{PEN}$ ($p = 0.004$; binomial test), and 20 % and significantly greater than 10 % for the model with classifying $CLASS_{IA}$ ($p = 0.004$; binomial test). In 8 and 6 out of 30 cases, respectively, the fixation strength was underestimated, which was less than for the continuous predictors IA_0 and PEN_0 .

5.4 Discussion

It was hypothesised that the interlock capacity of a cement-bone fixation depends on the underlying trabecular structure. Architectural and areal interlock parameters with respect to cement penetration depth were investigated in the current study and related to failure mode and strength of cemented fixations. Relations between the determined architectural parameters corresponded to those found in the literature and relations between bone density and the trabecular parameters were significant, despite low statistical power. Based on these relations, conclusions about the failure mechanism of cement-bone fixations could be introduced to the statistical model for fixation strength derived in this study.

The discussion of the presented data is divided into investigation of trabecular architecture in tibial bone in Section 5.4.1 and strength modelling in Section 5.4.2. Limitations are discussed in Section 5.4.3.

5.4.1 Architectural and Interlock Parameters of Tibial Trabecular Bone

BV/TV is an indicator for apparent BMD as measured in this study. R^2 was 0.82, which coincides with the results of Goulet *et al.*³³ ($R^2 = 0.81$). Absolute BV/TV in this study ranged from 0.02 to 0.15 and was comparable to the range of 0.04 to 0.23 that was measured by Ding *et al.*¹¹⁸. The results for trabecular architecture are consistent with the literature data, so there is confidence that the conclusions derived from the current data can be transferred to other samples.

When applying the relation between BV/TV , $Tb.Sp$ and $Tb.N$ according to equation (5-11)²⁰³, a linear regression between calculated and measured $Tb.Sp$ resulted in $R^2 = 0.98$ ($p < 0.001$). Thus, the applied formula holds for the current data and $Tb.Sp$ and $Tb.N$ are inversely related to each other and both linearly to BV/TV . According to Goulet *et al.*,³³ BV/TV is linearly related to BMD , so regression modelling of $Tb.Sp$ and $Tb.N$ based on assuming a linear relation to BMD ($R^2 = 0.70$) was suitable. sIA_0 and $mCSA_0$ clearly increased with increasing BMD ($R^2 > 0.78$), which can be attributed to the increased amount of bone substance that provides larger interlock area (IA) and larger bone area within the cross-sectional plane (CSA) (**Figure 5-14**).

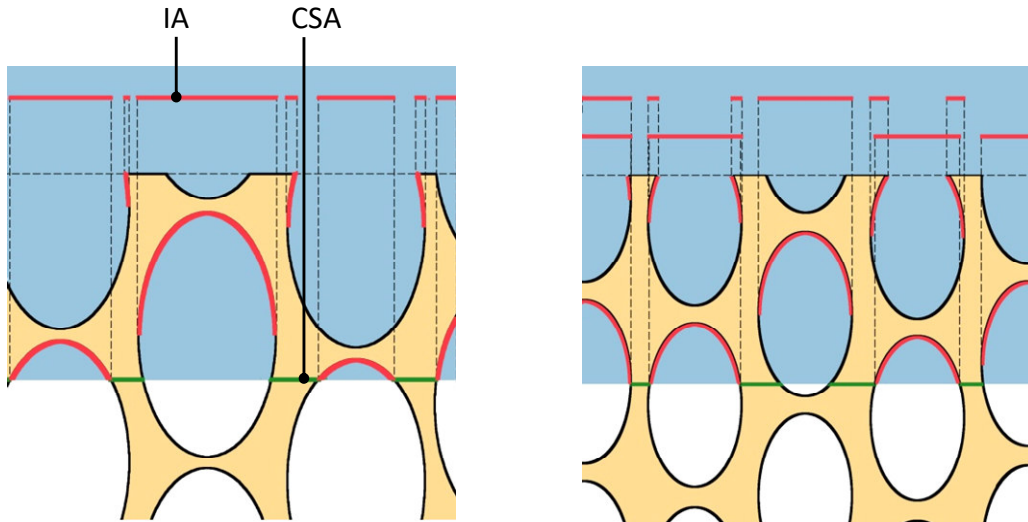


Figure 5-14: Interlock area (IA , red) and cross-sectional area (CSA , green) in different bone densities. Left: Low-density bone. Right: High-density bone; IA and CSA are larger than in low-density bone.

IA_0 linearly increased with increasing cement penetration depth (PEN). The extent of increase (sIA_0) was dependent on BMD . If less bone material was added per PEN increment, the interlock area increased less. The contribution of the longitudinal trabeculae (plates) can be considered steady, since they form rather continuous columns^{30,204}. In contrast, transverse trabeculae are not arranged on specific, but on varying levels, which leads to constant increase of IA with increasing PEN (**Figure 5-15**). In a structure with periodically arranged transverse trabeculae increase of IA may be rather stepwise.

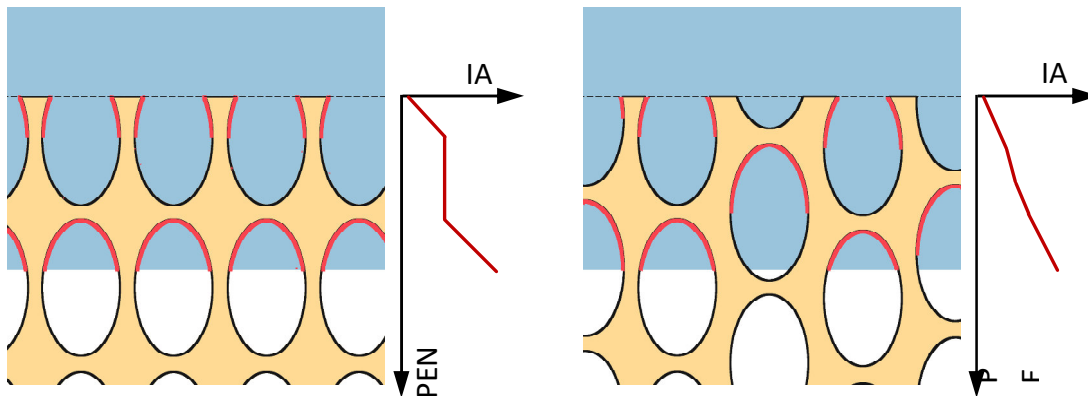


Figure 5-15: Effect of transverse trabeculae in trabecular bone on the determined interlock area (IA). Left: Qualitative increase of IA with increasing penetration depth (PEN) in regularly structured bone; the increase of IA is stepwise. Right: Qualitative increase of IA in bone with transverse trabeculae at varying levels; the increase is steady.

The determined tibia-specific structure model index SMI was between 1.29 and 1.79, indicating that the trabecular structure below the tibial plateau is composed of rods and plates at equal volume shares ($SMI = 0 \rightarrow$ ideal plate-like structure, $SMI = 3 \rightarrow$ ideal rod-like structure). Plate-like elements within a trabecular structure have been shown to be aligned with the principal direction of loading, which coincides with the principal

orientation of the structure^{44,205}. A plate-like element has a larger cross-sectional area than a rod-like element, which increases the stiffness normal to the cross-sectional area and reduces local material stress: the strength of the trabecular bone in plate-orientation is larger than transversally to it, where rod-like elements dominate.

The orientation of the structure was given by *DevAng* and was within 1.3° to 37.3° with respect to the cranially pointing z axis (confidence interval 13.9° to 19.5°). It remains unclear whether the deviation from z-axis orientation was due to sample processing or naturally varying structure orientation within tibial bone under the plateau. Tibial cuts reveal that the structure is dominantly oriented in a caudal-cranial direction, but deviates slightly from the axis when approaching the peripheral regions of the plateau (**Figure 5-16**). In terms of axial pull-out testing of cemented tibial fixation, the geometry of the predominantly vertically-aligned plates are of limited influence on interlock mechanics, but provide increased strength of the trabecular bone compared to the transverse direction³⁰.

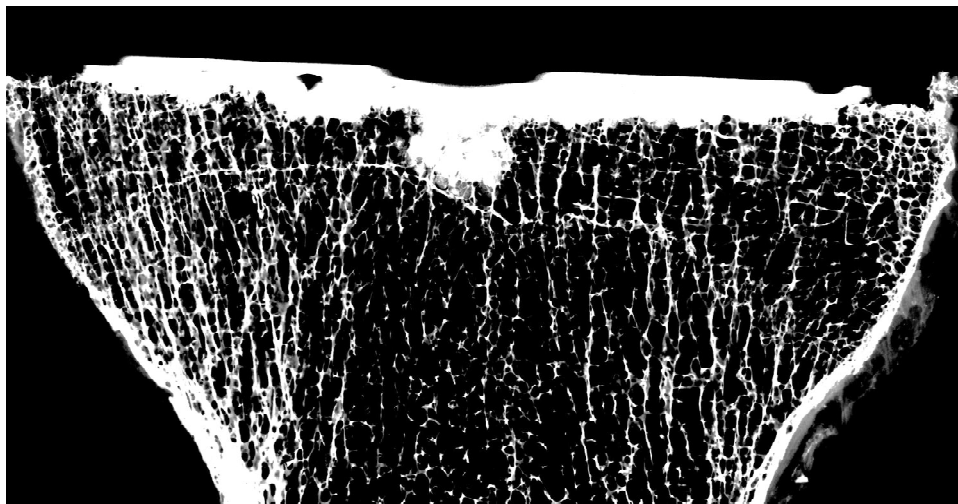


Figure 5-16: Contact radiographic scan of a cut through a tibial plateau with cement layer from preceding cemented implantation of a tibial tray. Dominant structures were accentuated by a contrast-increasing filter. The dominant orientation is caudal-cranial, but orientation at the rim of the plateau may deviate slightly from the vertical axis. The specimen is from the current study. (Scan was generated by M. Hahn, Department of Osteology and Biomechanics, University Medical Center Hamburg-Eppendorf, Hamburg, DE)

The effect of the plate-like elements on interlock parameters was revealed by incremental inclination of the sample. sIA_0 was expected minimal when determined in a plane deviating from the structure orientation and maximal when determined in a plane aligned to the structure orientation. Correspondingly, in the inclination study, the maximum was determined for sample inclination of 90° and about $0.2 \text{ mm}^2/\text{mm}^2$ larger than the minimum at about 20° inclination (**Figure 5-17**). Inclinations larger than 90° have not been evaluated; hence the maximum sIA_0 may be reached at 110° , perpendicular to the minimum value. Considering Equation (5-2), the stress within the trabecular bone is decreased in an inclined structure compared to aligned structure orientation, since the load-transfer area is larger, indicated by larger sIA_0 . Therefore, the interlock capacity was larger when the structure orientation deviated from perfect axis alignment. This would

result in rather underestimated fixation strength, which is preferable to an overestimation of strength. In clinics, the required tibial slope is pre-determined by the knee kinematics to restore, so consideration of tibial slope to improve fixation strength is not feasible. Moreover, the flow of cement into the bone may be restricted by the plate structures in inclined structures, so the strength-increasing and penetration-restricting effects may cancel each other out. Nevertheless, resection planes that are slightly inclined with respect to the orientation of the trabecular structure do not deteriorate fixation strength.

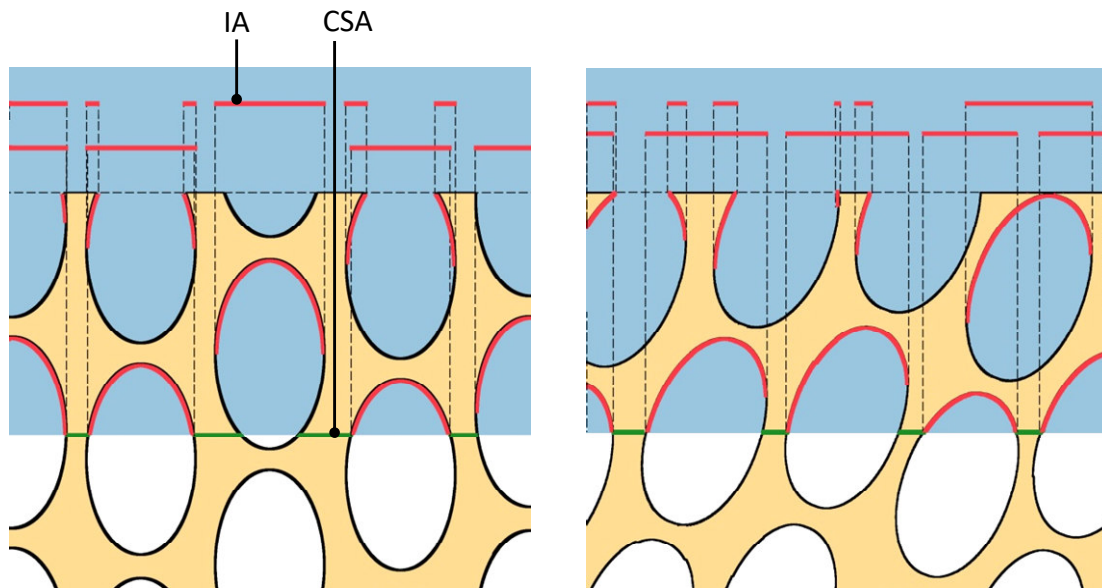


Figure 5-17: Effect of inclined resection plane on IA (red) and CSA (green). Left: Resection plane is perpendicular to the structure orientation. Right: Resection plane is at an angle of about 20° to the resection plane. IA is larger at the same penetration depth.

5.4.2 Statistical Modelling of Strength Based on Trabecular Architecture and Interlock

Modelling of strength was approached by including the cement penetration depth in terms of *MeanPen* (Chapter 3). In the first approach, *MeanPen* was related to the pore size *Tb.Sp*, expecting that when *MeanPen* was greater than the pore size, transverse trabeculae are engaged over the whole cementation area. A relative penetration depth greater than 1 indicated engagement of at least one layer of transverse trabeculae over the whole penetration area. In the second approach, *MeanPen* was multiplied by determined penetration-depth-dependent increase of interlock area of the respective specimen (sIA_0) to obtain the respective interlock area IA_0 . Hence, in both relative penetration depth and specific interlock area, bone density and penetration depth were reflected.

In the previous chapter, bone density and penetration depth were shown to classify between bone interface failure and bulk bone failure. Classification analysis regarding bone failure mode showed that the critical penetration depth in the current study was about 1.3-fold pore size and the critical specific interlock area was 38 % of the area penetrated by cement below cemented tibial trays. Combining each threshold with the compositional parameter $mCSA_0$ in the form of categorical classification parameters, resulted in a large explained variance of 89 %. Considering IA_0 and PEN_0 as continuous

predictors resulted in less explained variance (72 % and 73 % for IA_0 and PEN_0 , respectively) and larger number of cases with underestimated strength. Both relative penetration depth and specific interlock area were appropriate predictors for successful load transfer to the bulk bone, but only when used to classify the influence of the cross-sectional area of trabecular bone. In cross-validation, classification according to the specific interlock area resulted in fewer underestimated cases than classification using the relative penetration depth.

Several studies have investigated the contact area in cement fixations on a microlevel and have shown large relevance for strength and stability. In an experimental study, the tensile strength of cement fixations has been found to correlate with the cement-bone contact area estimated from μ CT scans²⁰⁶, which matches the current results. However, the contact area was estimated without consideration of load deformation. Miller *et al.*²¹ introduced a stereologically-obtained cement-bone contact fraction. This was based on distributing a number of straight lines over a cross-sectional image and dividing the number of cement-bone interface contours crossed by the lines by the overall number of bone contours. Smaller micromotion at the contact interface has been found to be correlated to a larger contact fraction. Micromotion promotes, but can also initiate loosening processes¹⁹. Therefore, the contact area might be a crucial indicator for the initiation of loosening processes. It may therefore be a useful parameter to consider in the assessment of loosening risk.

5.4.3 Limitations of the Analysis

Sample size was low for modelling of BMD dependency of trabecular parameters. R^2 was at least 0.70, resulting in a statistical power of 0.79 ($n = 6$; G*Power, version 3.1.9.2¹⁸⁵). This was considered sufficient.

Samples with low bone quality were excluded since they could not be further processed, so the ultimately processed samples may be biased towards large bone density. Therefore, the estimating models were derived from tibia-specific means, with the exclusion of samples of very low bone quality. This may result in overestimation of architectural parameters in low-BMD bone when applying the models. However, the excluded samples were obtained from the central plateau region, which is extracted during bone preparation. Therefore, one could likewise argue that bias may rather concern the high-BMD tibiae whose strength may be underestimated. As already mentioned, underestimation of fixation strength is not considered a crucial issue.

The increment of PEN at which CSA and IA were determined, was 0.06 mm. The 3D surface model of the trabecular structure was built up from triangles. In MATLAB® processing, triangles (and tetrahedrons) that crossed the current PEN level, were removed. Due to the small triangle edge length, applied incrementation was considered appropriate to reflect model geometry with minimum bias due to element removal.

Architectural parameters were determined from a VOI within the sample cube by means of the μ CT scanner software. The VOI was defined in alignment with the global coordinate system of the scanner, whereas the sample could be slightly tilted or rotated within its sample holder. Therefore, the edge length of the globally positioned VOI was restricted, when it should not exceed the actual sample region. The edge length for determination of

architectural parameter was therefore only 6 mm in contrast to 9 mm in interlock parameter determination. The VOI was assumed to be similarly influential on architectural parameters as on interlock parameters that were analysed in a convergence analysis. A minimum sample edge length of 5 mm was determined for the interlock parameters. Yan *et al.*²⁰⁷ suggested a 6 mm edge length for reliable analysis. Therefore VOIs in the current study were in accordance with both convergence analysis and the literature.

Surprisingly, the minimum sample edge length was set by the medium-BMD cube and not by the low-BMD cube (minimum edge length 2 mm). It was also found that the mineral density of the bone volume of the medium-BMD pair appeared larger than that of the other two (low-BMD pair: 863 mg/cm³, medium-BMD pair: 926 HA/cm³, high-BMD pair: 873 HA/cm³), while *Tb.Sp* of the medium-BMD pair was comparable to that of the low-BMD pair, i.e. smaller than expected. This may be due to a subject-specific aspect related to pathophysiological processes. However, since the medium pair was concerned, the more influential boundary areas of the data range were considered unaffected, keeping the corresponding bias low.

5.4.4 Conclusion

Architectural parameters of tibial trabecular bone were determined and were in accordance with the literature. The structure is oriented normally to the tibial plateau, which matches Wolff's Law of structural adaptation to the predominant loading direction⁴⁴.

In the previous chapter, tensile fixation strength was attributed to a parameter that pre-determines the failure mode and brings the bone strength itself into effect. In the current chapter, this approach is extended by the trabecular structure. In addition to architectural parameters, interlock parameters were developed to describe the two basics of fixation strength in interlock: load-transfer area and material strength.

Regression models were derived to estimate architectural and interlock parameters from the apparent bone density below the tibial plateau. Two parameters were derived from the architectural and interlock parameters and the implanted tibiae from the previous chapter: the specimen-characteristic penetration depth with respect to the pore size and the specimen-characteristic interlock area at a particular penetration depth. Both reflected the amount of load-transfer area. A penetration depth of about 1.3-fold pore size and a specific interlock contact area of about 38 % of the cement-penetrated plateau area were the critical values above which the load is transferred to the bulk bone.

In combination with the specific cross-sectional area of the respective trabecular bone as strength determining parameter, each of the two parameters' combinations according to

$$\begin{aligned}
 S = & 0.513 \text{ MPa} + 3.316 \text{ MPa} * CLASS_i \\
 & + 3.800 \text{ MPa} * mCSA_0 \\
 & + 60.126 \text{ MPa} * CLASS_i * mCSA_0
 \end{aligned}
 \tag{5-20}$$

explained almost 90 % of variance in fixation strength (i indicates whether dichotomous variable $CLASS_i$ was derived based on PEN_0 or IA_0).

The proposed model achieved a high explained variance proportion. Also, assuming a critical minimum cement penetration depth, whose absolute value depends on the underlying trabecular structure, is causal given the fact that the fixation is a pure interlock fixation. Thus, the statistical model for fixation strength is valid and may improve risk assessment of cemented fixations based on patient-specific parameters.

6

Conclusions

The overall study aim was to improve the cement-bone interlock mechanics of cemented tibial fixations with regard to loosening. This was approached basically by evaluation of the mechanical response of the fixation to tensile load.

6.1 Characterisation of Cement-Bone Fixation

The following section separately answers the three study questions. The findings are summarised in bullet points in each section.

First study question: Can the penetration of cement into the bone be increased by particular cementation techniques?

- Gun application increases cement penetration depth, if pulsatile lavage is applied beforehand, but not after syringe lavage.
- Due to the increasing effect of pulsatile lavage on cement penetration depth, this procedure ensures strong fixation, regardless of application technique.
- Pulsatile lavage in cemented fixation allows the mechanical properties of bone to play a role in fixation strength. However, fixation strength is independent of cement penetration depth when pulsatile lavage is used.

Increased strength of cemented fixation has been shown to be related to increased cement penetration depth into the trabecular bone²⁹, so a clinically favoured cementation technique may be a tool to increase penetration depth. In this study, an increasing effect of a cement application using a cement gun was shown, but only after application of pulsatile lavage. The penetration depth after gun application combined with pulsatile lavage was larger than after manual cement application and pulsatile lavage, and also larger than after gun application and syringe lavage. Nevertheless, since the strength measured after pulsatile lavage was larger than after syringe lavage and was also independent from cement penetration depth, the cement application method appears to be of minor importance for strong fixation, as long as pulsatile lavage is applied. Pulsatile lavage resulted in failure of the bulk bone in mechanical testing, whereas syringe lavage specimens failed at the cement-bone interface¹². Thus, the failure strength of pulsatile lavage specimens was strongly related to the underlying bone quality in terms of bone density. Pulsatile lavage in cemented fixation brings the bone strength into effect.

Second study question: How do cement layer morphology and bone mineral density influence fixation strength?

- The effect of bone density on fixation strength is larger when mean cement penetration depth is greater than 1 mm.
- The morphology of the cement layer is independent from bone density.
- Cement penetration depth is an indicator for the load-transfer contact area between cement and bone within the interlock.

Bone density appears to interact with cement penetration depth with regard to their effect on fixation strength. So, the linear correlation between penetration depth and strength^{12,25,29} and the decreasing effect of bone density on penetration depth^{26,27} stated in the literature appear debatable. Further investigation of the cement layer morphology in this thesis revealed that penetration depth was not related to bone density, and that cement penetration depth increases fixation strength, as hypothesised. However, this effect was not linear but rather dichotomous. In the mechanical testing of this thesis, mean cement penetration depth of less than about 1.1 mm resulted in bone interface failure, at low force, with low relation to bone density. Mean cement penetration depth of greater than about 1.1 mm led to failure of the bulk bone, at high forces, with a strong relation to bone density. At a large penetration depth, the applied load was transferred to the bulk bone without overloading the interlock between cement and trabeculae. At a low penetration depth, the load led to failure close to the cement, due to stress concentration at the few locations where load-transfer takes place. Pore-forming trabeculae deform under load, so the cement mantle is pulled out of the pores (**Figure 6-1**). The few enclosed trabeculae are overloaded.

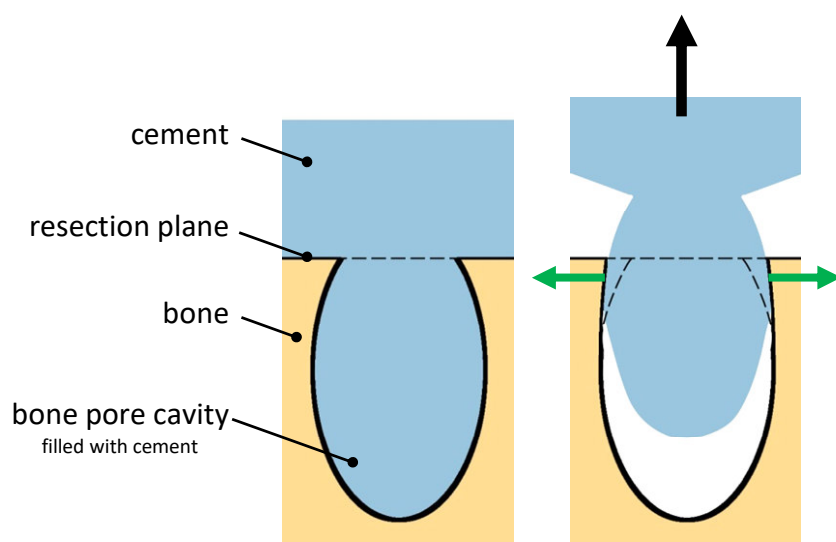


Figure 6-1: Cement-bone interlock under load. Left: Unloaded state without deformation. Right: Deformation under load (load is indicated by black arrow, deformation by green arrows).

Loading of the cement is transferred to the bone via the so-called load-transfer area within the interlock between trabeculae and cement. The transferred load causes stress within the bone that may exceed the ultimate stress of the loaded structures, leading to failure of the fixation. If the load-transfer area is large enough to transfer the load to the bone

without exceeding the ultimate stress of the loaded structure, the fixation stays intact. The loaded structure, in the case of low penetration depth, is limited to a low number of engaged trabeculae. In the case of high penetration depth, the number of engaged trabeculae is larger, force is transferred via a larger area and local stresses are lower than in low penetration depth. This was already hypothesised as a basic concept by Walker *et al.*²⁵. Thorough cleansing of the resection surface is important to achieve the critical cement penetration depth that then provides the critical load-transfer area. Fixation strength is then determined by the load-transfer area and the strength of the underlying bone.

Third study question: How does the structure of the trabecular bone influence fixation mechanics?

- Trabecular pore size and load-transfer contact area (specific interlock area) within the interlock depend on bone density and can be estimated from it.
- The fixation strength is maximal when the specific interlock area is greater than 38 % of the cement-penetrated area.
- The fixation strength is maximal, when the cement penetration depth is larger than about 1.3-fold pore size.
- A statistical model based on the thresholds of specific interlock area and specific penetration depth as well as the cross-sectional area of the trabecular bone explains almost 90 % of the variance in fixation strength.

With disregard of the bone density, the critical mean penetration depth in cemented tibial trays of this study was just under 1.1 mm, which coincides with the length of trabeculae¹¹² (0.5 mm to 1.5 mm). Since the trabecular length is considered to represent the pore size of the structure, exceedance of the critical penetration depth marks exceedance of the trabecular pore size, which results in engagement of at least one transverse layer of trabeculae.

The architecture of trabecular bone in the tibial head is composed of rod-like and plate-like elements forming an oriented structure. The composition may influence the load-transfer area in cement-bone interlock. It was found in this thesis that the trabecular spacing (pore size) is predictable from the apparent bone mineral density. The trabecular architectural parameters as investigated in this study are assessable by μ CT scans only, which precludes studies with living human subjects due to high radiation exposure. Therefore, predictability of the trabecular architecture based on clinically retrievable parameters, such as apparent bone density, is a prerequisite for the clinical application of findings about an influence of the trabecular structure on the fixation mechanism.

Trabecular samples were used to estimate the projected load-transfer area of an interlock with bone cement, as well as the cross-sectional area of the trabecular bone to reflect the material strength. Like the trabecular spacing (pore size), these interlock parameters were predictable from the apparent bone mineral density. A relative penetration depth with respect to the estimated pore size was defined, based on the trabecular pore size and a specific interlock area based on the load-transfer area. In consideration of the dichotomous character of the cement penetration depth found in this study, thresholds for sufficient load transfer within the interlock were determined. A specific interlock area

greater than 38 % of the cement-penetrated resection area and a penetration depth greater than 1.3-fold bone pore size was found to result in bulk bone failure and thus, load-transfer to the bulk bone. The determined fixation strength was depending on BMD and thus on the strength of the bulk bone.

Four models were derived including either the relative penetration depth as continuous or dichotomous predictor or the specific interlock area, likewise as continuous or dichotomous predictor. All four models included the cross-sectional area of the trabecular bone. Compared to the statistical models with continuous specific interlock area IA_0 and relative penetration depth PEN_0 the statistical models with dichotomous predictors were of superior quality. The two models with dichotomous $CLASS_{IA}$ and $CLASS_{PEN}$ each exhibited almost 90 % of explained variance in strength. The specific interlock area and the relative penetration depth are rather digital switches for the mechanical influence of bone quality on strength than continuous predictors for strength. The model equations form to

$$\begin{aligned} S = & 0.513 \text{ MPa} + 3.316 \text{ MPa} * CLASS_i \\ & + 3.800 \text{ MPa} * mCSA_0 \\ & + 60.126 \text{ MPa} * CLASS_i * mCSA_0, \end{aligned} \quad (6-1)$$

where i denotes, whether variable $CLASS$ was derived based on PEN_0 or IA_0 , so either based on achieved mean penetration depth or on resulting interlock area. Derivation base was shown to be equivalent in this thesis.

6.2 Relevance for Aseptic Loosening

In the following paragraphs, the findings of this thesis will be related to the process of aseptic loosening, which remains a challenge in arthroplasty.

Stability of cemented fixation is commonly reported in terms of relative motion between cement and bone phases on the trabecular level, also referred to as micromotion. It is agreed that micromotion is a crucial factor in aseptic loosening initiation^{19,20} (Section 2.3.3). The general process of late aseptic loosening cannot be prevented, since the polymeric bone cement underlies altering processes. Fatigue strength of bone cement is reduced continuously due to increasing crack growth rate with increasing time *in vivo*¹⁰⁷. When fatigue resistance decreases the cement starts to mechanically release particles, provoking adverse immune reactions. However, since micromotion appears to be critical in aseptic loosening initiation, reduction of early occurring micromotion within 2 years after surgery is essential in order to postpone stability-impairing processes.

Micromotion has been found to be reduced in post-mortem retrievals with larger cement penetration depth²¹. It could be concluded that the penetration should be as deep as possible to minimise micromotion. However, the interdigitated trabecular bone is stress-shielded and will be inevitably resorbed. In a post-mortem retrieval study, cavities left by resorbed trabecular bone have been found in all cement layers²³. Absolute bone loss is larger when more trabeculae are interdigitated, since more trabeculae are shielded from mechanical stimulus and may resorb. Especially in patients with low bone quality, resorption of the engaged bone deteriorates the conditions in potential revision surgery. Besides, remaining cement-enclosed trabeculae are removed in revision surgery along

with the cement. The bone stock for fixation of the secondary device is smaller, while poor bone quality requires a larger fixation interface for sufficient stability. Furthermore, bone cement cures by polymerisation within the human body, thereby releasing free radicals that may induce harmful processes due to their high reactivity and cytotoxicity. In cell culture, PMMA bone cement has been shown to result in local toxic reactions within fibroblast tissue²⁰⁸. Considering the potential accumulation of polymeric reaction heat in thick cement layers, as it has been shown in cadaver and FE studies^{209,210}, the bone cement volume introduced to the bone should be kept as small as possible. The statistical model derived in this study can be used to determine an optimal cement penetration depth based on known bone density.

However, the current thesis addresses aseptic loosening processes initiated by micromotion. Force transfer from the cement to the bone with minimum local stress within the trabeculae, as found for the bulk bone failure specimens in this study, is not necessarily accompanied by reduced micromotion. The required interlock area may have to be larger for an effect on micromotion than for adequate load transfer.

Miller *et al.*²¹ investigated the cement-bone interface of lab-implanted and post-mortem retrieved TKAs on the micro-mechanical level, looking at micromotion between cement and bone under compression loading of the tibial tray and corresponding interdigitation. Cement-enclosed trabeculae within a cement-bone interlock are resorbed with increasing *in vivo* time, so lab-implanted specimens reflect the initial fixation mechanics after surgery, which also applies to the specimens in the current study. Miller *et al.*²¹ measured micromotion between 0.82 μm and 2.54 μm at an interdigitation depth of 1.51 mm to 1.61 mm in lab-implanted TKAs, which was within the range of cement penetration depth in the current thesis. The corresponding micromotion of Miller *et al.*²¹ was low compared to 20 μm , which has been shown to still allow for bone ingrowth¹⁵³. Miller *et al.*²¹ proposed an inverse power law for the relation between interdigitation depth and micromotion, based on their total data pool data of $n = 23$ interface samples from 12 TKAs (**Figure 6-2**).

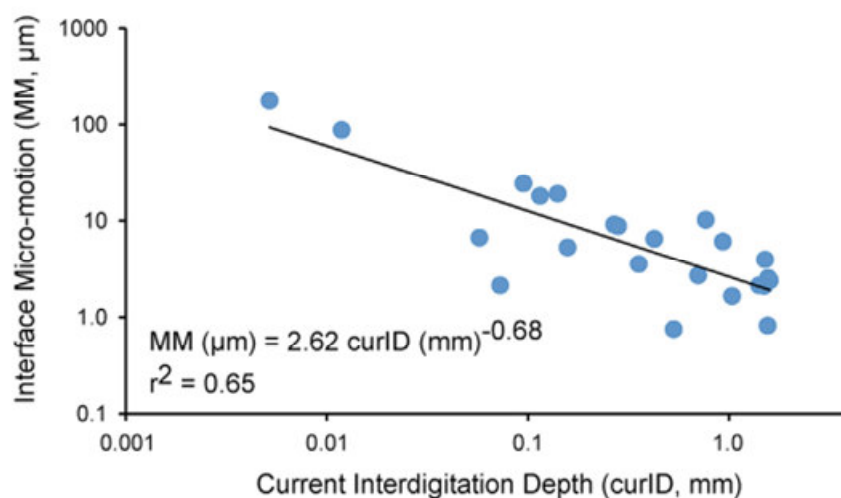


Figure 6-2: Inverse power law for dependency of micromotion on interdigitation depth. [Adapted from Miller et al.21]

According to Miller's inverse power law (**Figure 6-2**), an interdigitation depth greater than 1 mm results in micromotion of less than 2.62 μm . The definition of the mean interdigitation depth by Miller *et al.*²¹ is comparable to that of the mean cement penetration depth in the current study. The mean value of Miller *et al.*²¹ (0.65 mm, SD = 0.60 mm) is lower than the mean value from the current study (1.27 mm, SD = 0.62 mm), since their data pool included post-mortem retrieval TKAs that exhibited a declined interdigitation due to bone resorption within the interface, which was respected in the data analysis.

The critical value of 1.1 mm penetration depth determined in Chapter 3 of the current study corresponds to micromotion that are considerably lower (**Figure 6-2**) than the bone-ingrowth-allowing 20 μm . Transfer from interdigitation depth to specific interlock area may be performed based on the proportionality between critical relative penetration depth and critical specific interlock area found in this study: Determined thresholds resulted in identical failure mode classification of the specimens (Chapter 5 and Appendix C.4.5). The specimens in this study with specific interlock area greater than 38 % do also exhibit a mean penetration depth of more than 1.3-fold pore size. Even in case of a small pore diameter of 0.5 mm resulting in 0.65 mm mean penetration depth, which corresponds to an uncritical level of micromotion of less than 10 μm , based on Miller's inverse power law (**Figure 6-2**).

Exceeding the critical specific interlock area (or penetration depth) leads to bulk bone failure in pull-out. In conclusion, achieving a penetration depth that leads to bulk bone failure in a pull-out test corresponds to accomplishing minimal micromotion within the cement-bone interface. Aseptic loosening of implants is commonly attributed to micromotion within the implant fixation and the potential for loosening or loosening itself is even measured in micromotion. However, there is no clinical proof that micromotion is actually initiating aseptic loosening. It may rather be an indicator for instable fixation that marks insufficient contact between the interfacing materials and thereby low mechanical stimulus.

The specific interlock area can be easily determined for compression loading instead of tensile, however, the signalling failure modes bone interface and bulk bone failure do not have equivalents in compression. Nevertheless, in cyclic loading there might be a difference between force transfer to the bulk bone below and above a critical specific interlock area. In bone interface failure, the load-transfer area was smaller than in bulk bone failure, which resulted in larger local stress and strain. Deformation of the trabecular pores is large enough to pull the cement out of the pores. In compression mode, small load-transfer area indicates low region of mechanical stimulus for bone remodelling. Trabecular regions with no load uptake do not receive mechanical stimulus (**Figure 6-3**). Bone resorption may follow in the unloaded regions. If, in contrast, compression load is transferred to the bone below the plateau in a more equally-distributed fashion, supported by deeper cement penetration, mechanical stimulus is given more uniform and stress-shielding is reduced. So, low load-transfer area as given by low penetration depth is unfavourable in compression and also in tensile loading. Nevertheless, the critical value of specific interlock area in compression may deviate from that in tensile loading.

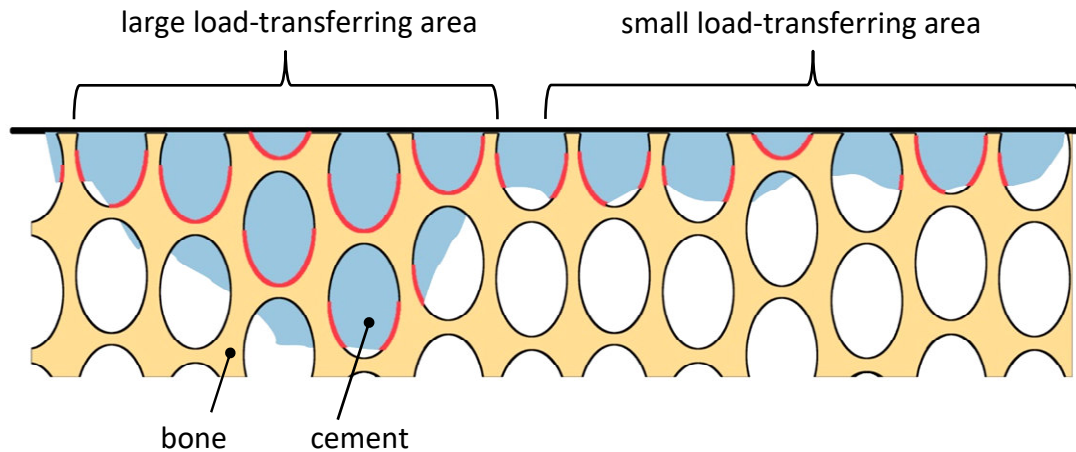


Figure 6-3: Uneven cement distribution below the resection plateau. Locally, very large cement penetration offers a large area for load transfer in compression (red lines), which may allow for mechanical stimulus of the trabecular bone for bone remodelling, while low cement penetration receives low stimulus due to smaller specific interlock area.

Considering the findings of Miller *et al.*²¹, micromotion in cement-bone interlock specimens with merely 38 % specific interlock area is smaller than 10 μm (see above), which questions even more the need for further increasing the specific interlock area by deeper penetration. However, it is not certain that micromotion continuously decreases with increasing specific interlock area.

The two specimens that exhibited fixation strength greater than 5 MPa were the only two specimens exhibiting a specific interlock area above 1 (**Figure 6-4**). While the strength was similar in the two cases (5.33 MPa and 5.28 MPa), the specific interlock area was different (1.02 and 1.26). The case with larger specific interlock area should have larger strength, which was not the case. This may indicate a saturation limit of specific interlock area, after which further increase is no longer effective, irrespective of whether resulting from the given bone density or increased penetration depth.

A finite element (FE) study published by Waanders *et al.*¹⁶² contains evidence of a saturation limit for interdigitation between cement and trabecular bone. They determined the contact area between cement and trabecular bone from the whole surface in contact. Strength in tensile and shear testing initially increased with increasing contact area, but subsequently stagnated with a further increase in contact area.

If a saturation limit of specific interlock area is given, fixation strength may be more appropriately modelled using a sigmoidal (logistic) model than a linear one as this kind of model more distinctly mirrors two different states (**Figure 6-6**). The total of only two available data sets in the upper range of strength and cement penetration depth is limiting, so a more general linear model with fewer assumptions appears more appropriate to achieve a conservative model. However, increased data may be obtained using FE models of the interlock zone. This is further discussed in Section 6.4 (Future Work).

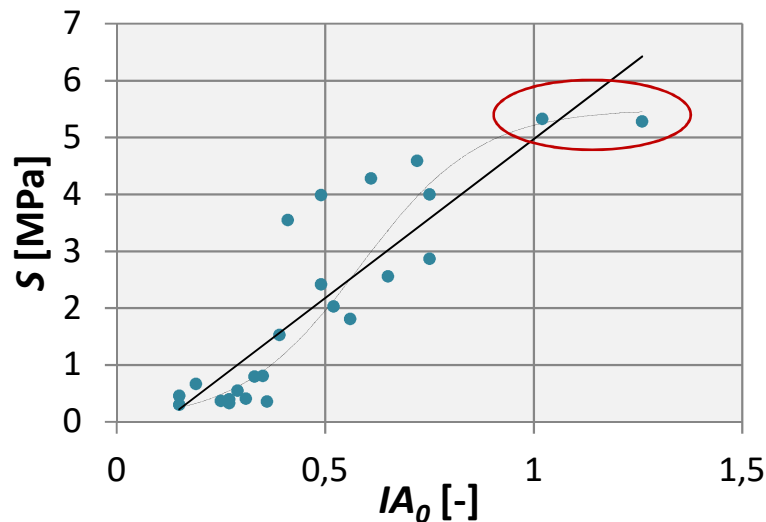


Figure 6-4: Distribution for strength over specific interlock area for the bone failure specimens of the current study with corresponding regression lines. Linear regression results in $R^2 = 0.76$ (straight line); a logistic approach ($R^2 = 0.83$, dotted curve) may be applied when a minimal and a saturation specific interlock area exists.

The extent of micromotion within the interface and strength of cemented fixation in tibial TKA largely depends on the specific interlock area within the cement-bone interlock that can be derived from the penetration depth and the bone density of a patient. In critical cases with low penetration depth, the loosening risk in terms of tendency to large or small micromotion can be predicted, based on the cement-bone interlock mechanism revealed in this thesis and by Miller *et al.*²¹. This requires the determination of bone density of the patient for pore size estimation and the penetration depth, which is derived from a 3D cement layer reconstruction. If penetration depth exceeds the estimated pore size, micromotion can be expected to be small enough to enable bone-ingrowth.

The clinically necessary fixation stability in terms of micromotion is probably reached at critical specific interlock area, which is warranted by irrigation of the prepared tibial plateau using pulsatile lavage, no matter how the cement is subsequently applied. Bone quality is determining for strength, when the critical cement penetration depth is exceeded. Further increase of penetration depth, as intended by techniques, such as suction cementation⁹ and increased cement pressurisation, may increase bone loss due to resorption, while primary stability remains the same.

6.3 Limitations

In this study, fixation was characterised in terms of fixation pull-out strength, which represents a non-physiological loading condition regarding TKA, since tensile forces on the interface rarely occur. In instrumented prostheses, the major loading direction during gait was compression with a low fraction of shear (5 % to 10 % of compression load⁵⁶). However, in an *in vivo* radiological study, temporary lift-off of the femoral component from the tibial tray was observed in 30 out of 40 patients during deep knee bend (flexion

⁹ Suction cementation: Inducing underpressure below the tibial plateau during cementation by two cannulated needles inserted into the proximal tibia, and a connected vacuum.¹⁷⁰

from 0° to 90°), and has also been found in lower flexion angles²¹¹. Femoral lift-off occurred mostly in one compartment only, which implies that all loading is transferred via the contralateral compartment. Due to the resulting moment with respect to the anteroposterior axis the tray must be lifted from the unloaded compartment, thereby applying tensile load on the implant fixation in this region (**Figure 6-5**). Non-native tensile load on the implant fixation could be a crucial factor in fixation loosening. Pull-out reflects this load case.

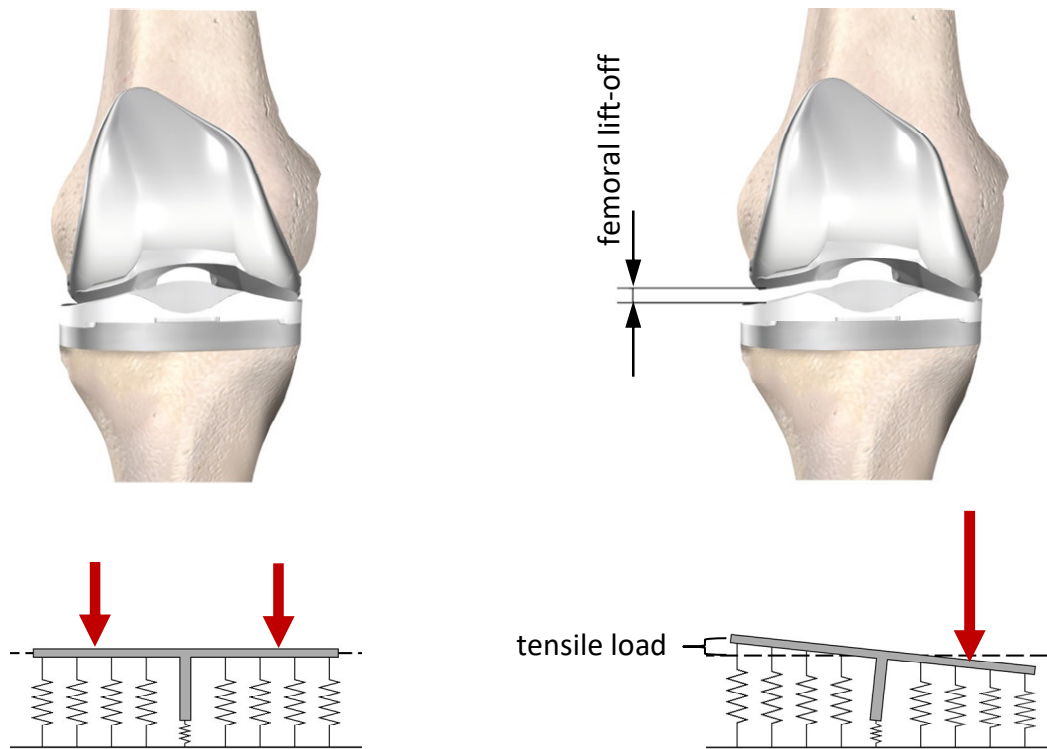


Figure 6-5: Load on the tibial tray resulting from femoral lift-off in one compartment of the knee joint. Springs in the lower pictures represent the fixation. Left: normal load. Right: Femoral lift-off. The moment on the tray that results from the one-compartmental lift-off may induce tensile load on the implant fixation.

Clinical failure is related to dynamic loading. However, decreasing interface strength with time in situ²⁹ in post-mortem retrievals has been shown by applying static tensile loading. Static strength of lab-implanted specimens in another study was larger than that of post-mortem retrievals, which reflects resorbed trabeculae that were found in the same study²². This shows that failure strength determined in non-dynamic load mode can be used as indicator for fixation strength. However, it is not known what the clinically necessary fixation strength may be in context of dynamic loading. Concludingly, tensile loading is clinically relevant and destructive testing is a realistic indicator for the capacity of the interface.

Several studies attempt to investigate either micromotion or failure displacement in implanted tibiae^{17,155-159}. In these studies, sensor partners and load actuators were assembled to bone and implant, or to bone and tibial insert. The setups therefore covered two or three interfaces offering potential for micromotion and also undetermined elastic deformation of several materials, including bone. These setups provided valuable results

to address the respective study questions. Nevertheless, they did not enable observation of the cement-bone interface mechanics in intact objects and required intricate sensor technology and subsequent data processing. Against the background of these technical considerations, pull-out testing of intact TKAs provides comparatively clear data about the interface capacity.

The transferability of *in vitro* studies with lab-implanted cadavers to *in vivo* conditions is clearly restricted to primary stability, since physiological processes within the body such as resorption of stress-shielded bone can be decisive for implant survival. It was shown by Goodheart *et al.*²² that the cement-bone interface continuously degenerates from the beginning of loading. Engaged bone is resorbed and leaves cavities in the cement, which reduce the contact area between cement and bone¹⁶³. The clear restriction of the findings to primary stability has to be respected in any risk assessment approach based on the presented findings

For statistical modelling, the cement volume was assumed to be evenly distributed below the tibial tray, which is not the case in reality. The critical area may also be achieved by local and extremely deep penetration, which may still allow for critical micromotion due to low contact area in the surrounding regions. A more detailed map of the load-transfer regions may be derived from the 3D surface data of the cement layers. Mapping the pore size (mm) on the penetration depth data, a map of the regions where the estimated pore size is exceeded can be produced. In the current study, this aspect was neglected, since data of this kind derived from uncontrolled settings are merely of informative character. Conclusions would be hard to draw due to the wide range of possible characteristics and confounding variables.

6.4 Future Work

In this thesis, manual removal and re-gluing of the CoCr implants were essential to obtain the cement layer morphology by CT imaging. Although resisting high pull-out load larger than 5 MPa in some cases, the glue connection failed at 2 MPa in other cases, which ultimately prevented determination of the corresponding cement-bone fixation strength. An alternative approach to gluing would be to generate interlock between implant and cement by modification of the implant. However, as far as CoCr implants are concerned, CT scanning for cement layer reconstruction is not feasible without considerable loss of information. The Ti implant used in this study provided an undercut on its back side that induces an interlock with the cement. The interlocked cement-implant interface commonly failed below 1 MPa and was hence not strong enough to shift failure to the bone side. The respective cement-implant interlock also prevented manual removal of the implant to obtain artefact-free CT scans of the cement layer. Cement layer reconstruction was manageable with the Ti implant *in situ*, but unfeasible with CoCr implants.

Therefore enlargement of interlock in the Ti implants or usage of custom-made implants has to be achieved. Custom-made implants for experimental purposes could be produced from polymers using rapid prototyping, such as selective laser sintering, which would enable introduction of undercuts and also CT scanning with the implant *in situ*.

The final strength model in the current thesis does not address a potential saturation limit of specific interlock area, since cement penetration depth was too low. Specimens with

large penetration depth would need to be tested to obtain additional information about relative specific interlock areas greater than 1. Considering the challenge of implant re-fixation, this should be done using a numerical approach.

It was shown that the trabecular architecture of the tibial head has a specific orientation and, although not ideally regularly structured, the architecture and corresponding properties may be reflected by an FE model based on the ideal arrangement of rod- and plate-like structures. Hexagonal sub-structures of trabecular bone were investigated analytically by Gibson³⁰ and found to match experimentally determined relations between mechanical properties (Young's Modulus, ultimate compressive strength) and bone density (**Figure 6-6**). An FE model could be derived from these structures and used to estimate the behaviour of cemented fixations with large specific interlock area. In addition, different load directions may be analysed.

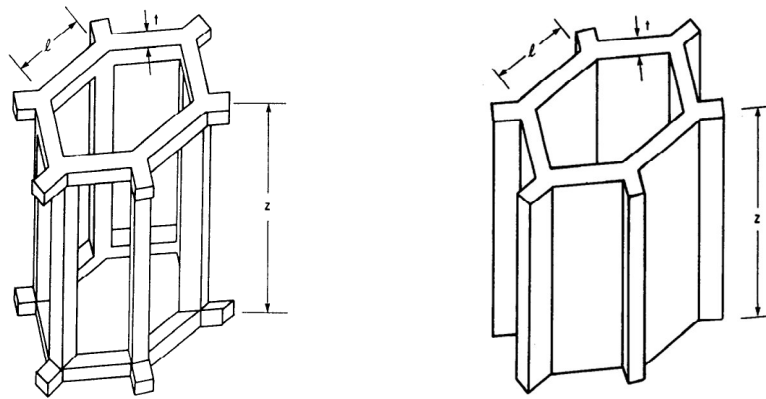


Figure 6-6: Hexagonal sub-structures of oriented trabecular bone investigated by Gibson[] that may serve as a base for finite element analysis of trabecular bone. Left: Open cell rod-like structure. Right: closed cell plate-like structure. [Reproduced from Gibson³⁰]

Based on the approach for determining the interlock area portion of the trabecular surface (specific interlock area), the risk of loosening initiation by micromotion may be assessed in clinics. However, the approach is based on bone density measurements from qCT, while post-surgery monitoring in arthroplasty is performed using 2-dimensional roentgenography.

In order to establish loosening risk assessment algorithms based on the findings of the current thesis, an extension to clinically applied imaging methods is required. This concerns determination of bone density as well as imaging of the cement layer.

7

Literature

1. Swedish Knee Arthroplasty Register (2013). *Annual Report 2013*. Online: <http://www.myknee.se/en/>.
2. National Joint Registry (2013). *National Joint Registry for England and Wales - 10th Annual Report*. Online: www.njrreports.org.uk.
3. Australian Orthopaedic Association (2013). *National Joint Replacement Registry - Annual Report*. Online: <https://aoanjrr.dmac.adelaide.edu.au>.
4. *TKA resection surfaces*. Online: <http://www.phamy-medical.com.vn/MBMCMS/files/82/82b8c1cf-936f-4de8-ab85-487c8cbe40d3.jpqm>, retrieved: 11.04.2015.
5. *3D Knee Prothesis*. Online: <http://bonesmart.org/wp-content/uploads/2010/10/3DKnee.jpg>, retrieved: 08.04.2015.
6. Statistisches Bundesamt (2013). *Fallpauschalenbezogene Krankenhausstatistik (DRG Statistik) - Operationen und Prozeduren der vollstationären Patientinnen und Patienten in Krankenhäusern*. Online: <https://www.destatis.de/DE/Publikationen/Publikationen.html>.
7. Springer Medizin Verlag Heidelberg (2005). *Total knee arthroplasty - A guide to get better performance*. Bellemans, Johan and Ries, MD and Victor, JMK (ed.). Springer Medizin Verlag Heidelberg.
8. Breusch, SJ and Malchau, H (2005). *What is modern cementing technique?* In: Breusch, Steffen J and Malchau, Henrik (ed.). *The well-cemented total hip arthroplasty*. Springer Medizin Verlag Heidelberg: 146–149.
9. Hirose, S; Otsuka, H; Morishima, T and Sato, K (2012). *Outcomes of Charnley total hip arthroplasty using improved cementing with so-called second-and third-generation techniques*. *Journal of Orthopaedic Science*. **17**(2): 118–123.
10. Mulroy, R and Harris, W (1990). *The effect of improved cementing techniques on component loosening in total hip replacement. An 11-year radiographic review*. *Journal of Bone & Joint Surgery, British Volume*. **72**(5): 757–760.
11. Sutherland, CJ; Wilde, A; Borden, L and Marks, K (1982). *A ten-year follow-up of one hundred consecutive Müller curved-stem total hip-replacement arthroplasties*. *The Journal of Bone & Joint Surgery*. **64**(7): 970–982.
12. Schlegel, UJ; Siewe, J; Delank, KS; Eysel, P; Püschel, K; Morlock, MM and Gebert de Uhlenbrock, A (2011). *Pulsed lavage improves fixation strength of cemented tibial components*. *International Orthopaedics*. **35**(8): 1165–1169.

13. Cawley, DT; Kelly, N; McGarry, J and Shannon, F (2013). *Cementing techniques for the tibial component in primary total knee replacement*. Bone & Joint Journal. **95**(3): 295–300.
14. Kopeck, M; Milbrandt, JC; Duellman, T; Mangan, D and Allan, DG (2009). *Effect of hand packing versus cement gun pressurization on cement mantle in total knee arthroplasty*. Canadian Journal of Surgery. **52**(6): 490–494.
15. Peters, CL; Craig, MA; Mohr, RA and Bachus, KN (2003). *Tibial component fixation with cement: Full-versus surface-cementation techniques*. Clinical Orthopaedics and Related Research. **409**: 158–168.
16. Hofmann, AA; Goldberg, TD; Tanner, AM and Cook, TM (2006). *Surface cementation of stemmed tibial components in primary total knee arthroplasty: Minimum 5-year follow-up*. The Journal of Arthroplasty. **21**(3): 353–357.
17. Luring, C; Perlick, L; Trepte, C; Linhardt, O; Perlick, C; Plitz, W and Grifka, J (2006). *Micromotion in cemented rotating platform total knee arthroplasty: Cemented tibial stem versus hybrid fixation*. Archives of Orthopaedic and Trauma Surgery. **126**(1): 45–48.
18. Chon, J; Lombardi Jr, A and Berend, K (2003). *Hybrid stem fixation in revision total knee arthroplasty (TKA)*. Surgical Technology International. **12**: 214–220.
19. Morawietz, L; Classen, R; Schröder, J; Dinybil, C; Perka, C; Skwara, A; Neidel, J; Gehrke, T; Frommelt, L; Hansen, T; and Oto, M; Barden, B; Aigner, T; Stiehl, P; Schubert, T; Meyer-Sholten, C; König, A; Ströbel, P; Rader, C; Kirschner, S; Lintner, F; Rüther, W; Bos, I; Hendrich, C; Kriegsmann, J and Krenn, V (2006). *Proposal for a histopathological consensus classification of the periprosthetic interface membrane*. Journal of Clinical Pathology. **59**(6): 591–597.
20. Sundfeldt, M; V Carlsson, L; B Johansson, C; Thomsen, P and Gretzer, C (2006). *Aseptic loosening, not only a question of wear: a review of different theories*. Acta Orthopaedica. **77**(2): 177–197.
21. Miller, MA; Terbush, MJ; Goodheart, JR; Izant, TH and Mann, KA (2014). *Increased initial cement-bone interlock correlates with reduced total knee arthroplasty micro-motion following in vivo service*. Journal of Biomechanics. **47**(10): 2460–2466.
22. Goodheart, JR; Miller, MA and Mann, KA (2014). *In vivo loss of cement-bone interlock reduces fixation strength in total knee arthroplasties*. Journal of Orthopaedic Research. **32**(8): 1052–1060.
23. Miller, MA; Goodheart, JR; Izant, TH; Rimnac, CM; Cleary, RJ and Mann, KA (2014). *Loss of cement-bone interlock in retrieved tibial components from total knee arthroplasties*. Clinical Orthopaedics and Related Research. **472**(1): 304–313.
24. Noble, PC and Swarts, E (1983). *Penetration of acrylic bone cements into cancellous bone*. Acta Orthopaedica. **54**(4): 566–573.

25. Walker, PS; Soudry, M; Ewald, F and McVickar, H (1984). *Control of cement penetration in total knee arthroplasty*. Clinical Orthopaedics and Related Research. **185**: 155–164.
26. Raiss, P; Pape, G; Kleinschmidt, K; Jäger, S; Sowa, B; Jakubowitz, E; Loew, M; Bruckner, T and Rickert, M (2011). *Bone cement penetration pattern and primary stability testing in keeled and pegged glenoid components*. Journal of Shoulder and Elbow Surgery. **20**(5): 723–731.
27. Jones, CW; Lam, L-O; Butler, A; Wood, DJ and Walsh, WR (2009). *Cement penetration after patella venting*. The Knee. **16**(1): 50–53.
28. Graham, J; Ries, M and Pruitt, L (2003). *Effect of bone porosity on the mechanical integrity of the bone-cement interface*. The Journal of Bone & Joint Surgery. **85**(10): 1901–1908.
29. Gebert de Uhlenbrock, A; Püschel, V; Püschel, K; Morlock, MM and Bishop, NE (2012). *Influence of time in-situ and implant type on fixation strength of cemented tibial trays - A post mortem retrieval analysis*. Clinical Biomechanics. **27**(9): 929–935.
30. Gibson, LJ (1985). *The mechanical behaviour of cancellous bone*. Journal of Biomechanics. **18**(5): 317–328.
31. Rho, J-Y; Kuhn-Spearing, L and Zioupos, P (1998). *Mechanical properties and the hierarchical structure of bone*. Medical Engineering & Physics. **20**(2): 92–102.
32. Hildebrand, T; Laib, A; Müller, R; Dequeker, J and Rüegsegger, P (1999). *Direct three-dimensional morphometric analysis of human cancellous bone: microstructural data from spine, femur, iliac crest, and calcaneus*. Journal of Bone and Mineral Research. **14**(7): 1167–1174.
33. Goulet, RW; Goldstein, SA; Ciarelli, MJ; Kuhn, JL; Brown, M and Feldkamp, L (1994). *The relationship between the structural and orthogonal compressive properties of trabecular bone*. Journal of Biomechanics. **27**(4): 375–389.
34. Ding, M and Hvid, I (2000). *Quantification of age-related changes in the structure model type and trabecular thickness of human tibial cancellous bone*. Bone. **26**(3): 291–295.
35. *Bone types*. Online: http://cnx.org/contents/14fb4ad7-39a1-4eee-ab6e-3ef2482e3e22@6.27:37/Anatomy_&_Physiology, retrieved: 17.04.2015.
36. Platzer, W (1975). *dtv-Atlas der Anatomie. Band 1: Bewegungsapparat*. Georg Thieme Verlag Stuttgart.
37. Reuter, P (2004). *Springer Lexikon Medizin*. Reuter, Peter (ed.). Springer-Verlag Berlin.
38. Netter, FH and Mühlbauer, R (2011). *Atlas der Anatomie*. Elsevier, Urban & Fischer.

39. *Femur Cut*. Online: http://etc.usf.edu/clipart/15400/15407/femurxsectn_15407.htm, retrieved: 12.05.2015.
40. Roux, S and Orcel, P (2000). *Bone loss. Factors that regulate osteoclast differentiation: An update*. Arthritis Research. **2**(6): 451–456.
41. Carretta, R; Stüssi, E; Müller, R and Lorenzetti, S (2013). *Within subject heterogeneity in tissue-level post-yield mechanical and material properties in human trabecular bone*. Journal of the Mechanical Behavior of Biomedical Materials. **24**: 64–73.
42. Pietschmann, P; Rauner, M; Sipos, W and Kersch-Schindl, K (2009). *Osteoporosis: An age-related and gender-specific disease-a mini-review*. Gerontology. **55**(1): 3–12.
43. *Trabecular Bone*. Online: <http://www.ectsoc.org/gallery/>, retrieved 15.05.2015.
44. Wolff, J (1892). *Das Gesetz der Transformation der Knochen*. DMW-Deutsche Medizinische Wochenschrift. **19**(47): 1222–1224.
45. Mullender, M and Huiskes, R (1995). *Proposal for the regulatory mechanism of Wolff's law*. Journal of Orthopaedic Research. **13**(4): 503–512.
46. Rumpler, M; Würger, T; Roschger, P; Zwettler, E; Peterlik, H; Fratzl, P and Klaushofer, K (2012). *Microcracks and osteoclast resorption activity in vitro*. Calcified Tissue International. **90**(3): 230–238.
47. Miller, MA; Eberhardt, AW; Cleary, RJ; Verdonschot, N and Mann, KA (2010). *Micromechanics of postmortem-retrieved cement-bone interfaces*. Journal of Orthopaedic Research. **28**(2): 170–177.
48. Sobotta, J (1993). *Atlas der Anatomie des Menschen - Band 2 Rumpf, Eingeweide, untere Extremität*. Putz, R. and Pabst, R. (ed.). Urban & Schwarzenberg.
49. Kapandji, IA (1985). *Funktionelle Anatomie der Gelenke*. Schematisierte und kommentierte Zeichnungen zur menschlichen Biomechanik - Band 2 Untere Extremität. Ferdinand Enke Verlag Stuttgart.
50. Cherian, JJ; Kapadia, BH; Banerjee, S; Jauregui, JJ; Issa, K and Mont, MA (2014). *Mechanical, anatomical, and kinematic axis in TKA: Concepts and practical applications*. Current Reviews in Musculoskeletal Medicine. **7**(2): 89–95.
51. Johnson, F; Leitzl, S and Waugh, W (1980). *The distribution of load across the knee. A comparison of static and dynamic measurements*. Journal of Bone & Joint Surgery, British Volume. **62**(3): 346–349.
52. Kumar, D; Manal, K and Rudolph, K (2013). *Knee joint loading during gait in healthy controls and individuals with knee osteoarthritis*. Osteoarthritis and Cartilage. **21**(2): 298–305.

53. Halder, A; Kutzner, I; Graichen, F; Heinlein, B; Beier, A and Bergmann, G (2012). *Influence of limb alignment on mediolateral loading in total knee replacement*. The Journal of Bone & Joint Surgery. **94**(11): 1023–1029.
54. Kutzner, I; Küther, S; Heinlein, B; Dymke, J; Bender, A; Halder, AM and Bergmann, G (2011). *The effect of valgus braces on medial compartment load of the knee joint-in vivo load measurements in three subjects*. Journal of Biomechanics. **44**(7) Elsevier: 1354–1360.
55. Maquet, PG (1976). *Biomechanics of the knee: with application to the pathogenesis and the surgical treatment of osteoarthritis*. Springer Medizin Verlag Heidelberg.
56. Kutzner, I; Heinlein, B; Graichen, F; Bender, A; Rohlmann, A; Halder, A; Beier, A and Bergmann, G (2010). *Loading of the knee joint during activities of daily living measured in vivo in five subjects*. Journal of Biomechanics. **43**(11): 2164–2173.
57. Bergmann, G; Bender, A; Graichen, F; Dymke, J; Rohlmann, A; Trepczynski, A; Heller, MO and Kutzner, I (2014). *Standardized loads acting in knee implants*. PLOS ONE. **9**(1).
58. Abermann, E; Hoser, C; Benedetto, K-P; Hepperger, C and Fink, C (2015). *Arthroseentwicklung nach vorderer Kreuzbandruptur*. Arthroskopie. **28**(1): 26–30.
59. Daniel, DM; Stone, ML; Dobson, BE; Fithian, DC; Rossman, DJ and Kaufman, KR (1994). *Fate of the ACL-injured patient - A prospective outcome study*. The American Journal of Sports Medicine. **22**(5): 632–644.
60. Murray, JR; Lindh, AM; Hogan, NA; Trezies, AJ; Hutchinson, JW; Parish, E; Read, JW and Cross, MV (2012). *Does anterior cruciate ligament reconstruction lead to degenerative disease? Thirteen-year results after bone-patellar tendon-bone autograft*. The American Journal of Sports Medicine. **40**(2): 404–413.
61. Helminen, H; Jurvelin, J; Kiviranta, I; Paukkonen, K; Saamanen, A and Tammi, M (1987). *Joint loading effects on articular cartilage: A historical review*. Joint Loading: Biology and Health of Articular Structures. : 1–46.
62. *Endoprothesenregister Deutschland erfolgreich etabliert*. Online: <http://www.eprd.de/meldungen/endoprothesenregister-deutschland-erfolgreich-etabliert/>, retrieved: 18.04.2015.
63. Boy, O; Hahn, S and Kociemba, E (2009). *Knie-Endoprothesenwechsel und -Komponentenwechsel*. Qualität Sichtbar Machen—BQS Qualitätsreport 2008. BQS Bundesgeschäftsstelle Qualitätssicherung gGmbH. : 168–174.
64. Boy, O; Hahn, S and Kociemba, E (2009). *Knie-Totalendoprothesen-Erstimplantation*. Qualität Sichtbar Machen—BQS Qualitätsreport 2008. BQS Bundesgeschäftsstelle Qualitätssicherung gGmbH. : 161–167.

65. Kurtz, SM; Ong, KL; Lau, E; Widmer, M; Maravic, M; Gómez-Barrena, E; de Pina, M de F; Manno, V; Torre, M; Walter, WL; de Steiger, R; Geesink, R; Peltola, M and Röder, C (2011). *International survey of primary and revision total knee replacement*. International Orthopaedics. **35**(12): 1783–1789.
66. Statistisches Bundesamt (2008). *Fallpauschalenbezogene Krankenhausstatistik (DRG-Statistik) Operationen und Prozeduren der vollstationären Patientinnen und Patienten in Krankenhäusern*. Online:
<https://www.destatis.de/DE/Publikationen/Publikationen.html>.
67. Statistisches Bundesamt (2009). *Fallpauschalenbezogene Krankenhausstatistik (DRG-Statistik) Operationen und Prozeduren der vollstationären Patientinnen und Patienten in Krankenhäusern*. Online:
<https://www.destatis.de/DE/Publikationen/Publikationen.html>.
68. Statistisches Bundesamt (2010). *Fallpauschalenbezogene Krankenhausstatistik (DRG-Statistik) Operationen und Prozeduren der vollstationären Patientinnen und Patienten in Krankenhäusern*. Online:
<https://www.destatis.de/DE/Publikationen/Publikationen.html>.
69. Statistisches Bundesamt (2011). *Fallpauschalenbezogene Krankenhausstatistik (DRG-Statistik) Operationen und Prozeduren der vollstationären Patientinnen und Patienten in Krankenhäusern*. Online:
<https://www.destatis.de/DE/Publikationen/Publikationen.html>.
70. Statistisches Bundesamt (2012). *Fallpauschalenbezogene Krankenhausstatistik (DRG-Statistik) Operationen und Prozeduren der vollstationären Patientinnen und Patienten in Krankenhäusern*. Online:
<https://www.destatis.de/DE/Publikationen/Publikationen.html>.
71. Statistisches Bundesamt (2014). *Fallpauschalenbezogene Krankenhausstatistik (DRG-Statistik) Operationen und Prozeduren der vollstationären Patientinnen und Patienten in Krankenhäusern*. Online:
<https://www.destatis.de/DE/Publikationen/Publikationen.html>.
72. Lüring, C; Niethard, F-U; Günther, K-P; Schäfer, T; Hannemann, F; R, P; Maier, W and Kirschner, S (2013). *Regionale Unterschiede und deren Einflussfaktoren – Schwerpunkt Knieendoprothetik*. Deutsche Gesellschaft für Orthopädie und Orthopädische Chirurgie.
73. Swedish Knee Arthroplasty Register (2010). *Annual Report 2010*. Online:
<http://www.myknee.se/en/>.
74. Swedish Knee Arthroplasty Register (2011). *Annual Report 2011*. Online:
<http://www.myknee.se/en/>.
75. Swedish Knee Arthroplasty Register (2012). *Annual Report 2012*. Online:
<http://www.myknee.se/en/>.
76. Brand, RA; Mont, MA and Manring, M (2011). *Biographical Sketch: Themistocles Gluck (1853-1942)*. Clinical Orthopaedics and Related Research. **469**(6): 1525–1527.

77. Wirtz, DC (2011). *AE-Manual der Endoprothetik: Knie*. Wirtz, Dieter C (ed.). **3** Springer Heidelberg.
78. Scott, C and Biant, L (2012). *The role of the design of tibial components and stems in knee replacement*. Journal of Bone & Joint Surgery, British Volume. **94**(8): 1009–1015.
79. Chong, DY; Hansen, UN and Amis, AA (2011). *The influence of tibial prosthesis design features on stresses related to aseptic loosening and stress shielding*. Journal of Mechanics in Medicine and Biology. **11**(01): 55–72.
80. Brach del Prever, EM; Bistolfi, A; Bracco, P and Costa, L (2009). *UHMWPE for arthroplasty: past or future?* Journal of Orthopaedics and Traumatology. **10**(1): 1–8.
81. Landy, MM and Walker, PS (1988). *Wear of ultra-high-molecular-weight polyethylene components of 90 retrieved knee prostheses*. The Journal of Arthroplasty. **3**: 73–85.
82. Robinson, RP (2005). *The early innovators of today's resurfacing condylar knees*. The Journal of Arthroplasty. **20**: 2–26.
83. *Sigma MBT*. Online: https://www.kneereplacement.com/DePuy_technology/DePuy_knees/rotating_knees, retrieved: 28.03.2015.
84. *Sigma RP CS*. Online: http://patients.depuyorthopaedics.com/docs/patient_ed/patient_education/knee_prod_images.html, retrieved: 28.03.2015.
85. *S.Hi.V.A.* Online: <http://www.globalortho.com.au/orthopaedic-product.php?s=shivatm&cat=Knee>, retrieved: 28.03.2015.
86. Schwenke, T and Wimmer, M (2013). *Cross-shear in metal-on-polyethylene articulation of orthopaedic implants and its relationship to wear*. Wear. **301**(1): 168–174.
87. Huang, C-H; Liao, J-J and Cheng, C-K (2007). *Fixed or mobile-bearing total knee arthroplasty*. Journal of Orthopaedic Surgery and Research. **2**.
88. Galvin, AL; Kang, L; Udofia, I; Jennings, LM; McEwen, HM; Jin, Z and Fisher, J (2009). *Effect of conformity and contact stress on wear in fixed-bearing total knee prostheses*. Journal of Biomechanics. **42**(12): 1898–1902.
89. Verra, WC; van den Boom, L; Jacobs, W; Clement, DJ; Wymenga, A and Nelissen, R (2013). *Retention versus sacrifice of the posterior cruciate ligament in total knee arthroplasty for treating osteoarthritis*. The Cochrane Library. **10**.
90. Jacobs, W; Anderson, PG; Limbeek, J and Wymenga, A (2004). *Mobile bearing vs fixed bearing prostheses for total knee arthroplasty for post-operative functional status in patients with osteoarthritis and rheumatoid arthritis*. The Cochrane Library. **2**.

91. Hothan, A; Morlock, M and Hoenig, E (2013). *The effect of body weight on the choice of material for the bearing couple in artificial hip joints*. *Seminars in Arthroplasty*. **24**(4): 218–239.
92. Bonnin, M (2008). *Failure mechanisms in total knee arthroplasty*. In: Bonnin, Michel and Pierre, Chambat (ed.). *Osteoarthritis of the Knee*. Springer Verlag Paris: 205–224.
93. Schindler, OS (2012). *Basic kinematics and biomechanics of the patellofemoral joint. Part 2: The patella in total knee arthroplasty*. *Acta Orthopaedica Belgica*. **78**(1): 11–29.
94. Matziolis, G; Adam, J and Perka, C (2010). *Varus malalignment has no influence on clinical outcome in midterm follow-up after total knee replacement*. *Archives of Orthopaedic and Trauma Surgery*. **130**(12): 1487–1491.
95. Mäkelä, KT; Matilainen, M; Pulkkinen, P; Fenstad, AM; Havelin, L; Engesaeter, L; Furnes, O; Pedersen, AB; Overgaard, S; Kärrholm, J; Malchau, H; Garellick, G; Ranstam, J and Eskelinen, A (2014). *Failure rate of cemented and uncemented total hip replacements: register study of combined Nordic database of four nations*. *British Medical Journal*. **348**.
96. Nakama, GY; Peccin, MS; Almeida, G; Lira Neto Ode, A; Queiroz, A and Navarro, RD (2012). *Cemented, cementless or hybrid fixation options in total knee arthroplasty for osteoarthritis and other non-traumatic diseases*. *The Cochrane Library*. **10**.
97. Lombardi, AV; Berasi, CC and Berend, KR (2007). *Evolution of tibial fixation in total knee arthroplasty*. *The Journal of Arthroplasty*. **22**(4): 25–29.
98. McLaughlin, JR and Lee, KR (2014). *Hybrid total knee arthroplasty: 10-to 16-year follow-up*. *Orthopedics*. **37**(11): 975–977.
99. Vielgut, I; Kastner, N; Pichler, K; Holzer, L; Glehr, M; Gruber, G; Leithner, A; Labek, G and Sadoghi, P (2013). *Application and surgical technique of total knee arthroplasties: a systematic comparative analysis using worldwide registers*. *International Orthopaedics*. **37**(8): 1465–1469.
100. Kühn, K (2005). *Properties of bone cement: What is bone cement?* In: Breusch, Steffen J. and Malchau, Henrik (ed.). *The well-cemented total hip arthroplasty*. Springer: 86–92.
101. Completo, A; Coutinho, M; Schiller, M; Ramos, A; Relvas, C; Simões, J and Meireles, S (2011). *A device to control implant and bone-cement temperatures in cemented arthroplasty*. *Journal of Medical Devices*. **5**(2).
102. Wiltse, L; Hall, R and Stenehjem, J (1957). *Experimental studies regarding the possible use of self-curing acrylic in orthopaedic surgery*. *The Journal of Bone & Joint Surgery*. **39**(4): 961–972.
103. Reckling, F and Dillon, W (1977). *The bone-cement interface temperature during total joint replacement*. *The Journal of Bone & Joint Surgery*. **59**(1): 80–82.

104. Willert, H-G; Mueller, K and Semlitsch, M (1979). *The morphology of polymethylmethacrylate (PMMA) bone cement*. Archives of Orthopaedic and Traumatic Surgery. **94**(4): 265–292.
105. Lee, C (2005). *Properties of bone cement: The mechanical properties of PMMA bone cement*. In: Breusch, Steffen and Malchau, Henrik (ed.). The well-cemented total hip arthroplasty. Springer: 60–66.
106. Hoey, D and Taylor, D (2009). *Comparison of the fatigue behaviour of two different forms of PMMA*. Fatigue & Fracture of Engineering Materials & Structures. **32**(3): 261–269.
107. Ayre, WN; Denyer, SP and Evans, SL (2014). *Ageing and moisture uptake in polymethyl methacrylate (PMMA) bone cements*. Journal of the Mechanical Behavior of Biomedical Materials. **32**: 76–88.
108. Silverman, EJ; Landy, DC; Massel, DH; Kaimrajh, DN; Latta, LL and Robinson, RP (2014). *The effect of viscosity on cement penetration in total knee arthroplasty, an application of the squeeze film effect*. The Journal of Arthroplasty. **29**(10): 2039–2042.
109. Furnes, O; Havelin, LI and Espehaug, B (2005). *Properties of bone cement: Which cement should we choose for primary THA?* In: Breusch, S. & Malchau, H. (ed.). The well-cemented total hip arthroplasty. Springer Medizin Verlag Heidelberg.
110. Spierings, PT (2005). *Properties of bone cement: testing and performance of bone cements*. In: Breusch, Steffen and Malchau, Henrik (ed.). The well-cemented total hip arthroplasty. Springer: 67–78.
111. Kopeck, M; Milbrandt, JC; Kohut, N; Kern, B and Allan, DG (2009). *Effect of bone cement viscosity and set time on mantle area in total knee arthroplasty*. The American Journal of Orthopedics. **38**(10): 519–522.
112. Keaveny, TM; Morgan, EF and Yeh, OC (2003). *Bone mechanics*. In: Kutz, Myer (ed.). Standard handbook of biomedical engineering and design. McGraw-Hill New York.
113. Keaveny, TM; Morgan, EF; Niebur, GL and Yeh, OC (2001). *Biomechanics of trabecular bone*. Annual Review of Biomedical Engineering. **3**(1): 307–333.
114. Engelke, K; Adams, JE; Armbrrecht, G; Augat, P; Bogado, CE; Buxsein, ML; Felsenberg, D; Ito, M; Prevrhal, S; Hans, DB and others (2008). *Clinical use of quantitative computed tomography and peripheral quantitative computed tomography in the management of osteoporosis in adults: The 2007 ISCD official positions*. Journal of Clinical Densitometry. **11**(1): 123–162.
115. Cohen, A; Dempster, D; Müller, R; Guo, X; Nickolas, T; Liu, X; Zhang, X; Wirth, A; Van Lenthe, G; Kohler, T; McMahon, D; Zhou, H; Rubin, M; Bilezikian, J; Lappe, J; Recker, R and Shane, E (2010). *Assessment of trabecular and cortical architecture and mechanical competence of bone by high-resolution peripheral computed tomography: Comparison with transiliac bone biopsy*. Osteoporosis International. **21**(2): 263–273.

116. Engelke, K; Libanati, C; Fuerst, T; Zysset, P and Genant, H (2013). *Advanced CT based in vivo methods for the assessment of bone density, structure, and strength*. Current Osteoporosis Reports. **11**(3): 246–255.
117. Lowitz, T; Chappard, C; Laouisset, L; Museyko, O; Bousson, V; Laredo, J and Engelke, K (2014). *Advanced knee structure analysis (AKSA) for osteoarthritis (OA): Comparison of BMD and texture in trabecular structure of the knee by QCT and HR-PQCT*. Osteoarthritis and Cartilage. **22**: S269–S270.
118. Ding, M; Dalstra, M; Danielsen, CC; Kabel, J; Hvid, I and Linde, F (1997). *Age variations in the properties of human tibial trabecular bone*. Journal of Bone & Joint Surgery, British Volume. **79**(6): 995–1002.
119. Rho, J-Y; Hobatho, M and Ashman, R (1995). *Relations of mechanical properties to density and CT numbers in human bone*. Medical Engineering & Physics. **17**(5): 347–355.
120. Røhl, L; Larsen, E; Linde, F; Odgaard, A and Jørgensen, J (1991). *Tensile and compressive properties of cancellous bone*. Journal of Biomechanics. **24**(12): 1143–1149.
121. Odgaard, A; Hvid, I and Linde, F (1989). *Compressive axial strain distributions in cancellous bone specimens*. Journal of Biomechanics. **22**(8): 829–835.
122. Carter, DR and Hayes, WC (1977). *The compressive behavior of bone as a two-phase porous structure*. The Journal of Bone & Joint Surgery. **59**(7): 954–962.
123. Townsend, PR; Rose, RM and Radin, EL (1975). *Buckling studies of single human trabeculae*. Journal of Biomechanics. **8**(3): 199–201.
124. Keller, T; Mao, Z and Spengler, D (1990). *Young's modulus, bending strength, and tissue physical properties of human compact bone*. Journal of Orthopaedic Research. **8**(4): 592–603.
125. Rho, J-Y; Ashman, RB and Turner, CH (1993). *Young's modulus of trabecular and cortical bone material: Ultrasonic and microtensile measurements*. Journal of Biomechanics. **26**(2): 111–119.
126. Choi, K; Kuhn, JL; Ciarelli, MJ and Goldstein, SA (1990). *The elastic moduli of human subchondral, trabecular, and cortical bone tissue and the size-dependency of cortical bone modulus*. Journal of Biomechanics. **23**(11): 1103–1113.
127. Rho, J-Y; Tsui, TY and Pharr, GM (1997). *Elastic properties of human cortical and trabecular lamellar bone measured by nanoindentation*. Biomaterials. **18**(20): 1325–1330.
128. Mullins, L; Sassi, V; McHugh, P and Bruzzi, M (2009). *Differences in the crack resistance of interstitial, osteonal and trabecular bone tissue*. Annals of Biomedical Engineering. **37**(12): 2574–2582.

129. Burstein, AH; Zika, J; Heiple, K and Klein, L (1975). *Contribution of collagen and mineral to the elastic-plastic properties of bone*. The Journal of Bone & Joint Surgery. **57**(7): 956–961.
130. Wang, X; Bank, RA; TeKoppele, JM and Agrawal, C (2001). *The role of collagen in determining bone mechanical properties*. Journal of Orthopaedic Research. **19**(6): 1021–1026.
131. Rice, J; Cowin, S and Bowman, J (1988). *On the dependence of the elasticity and strength of cancellous bone on apparent density*. Journal of Biomechanics. **21**(2): 155–168.
132. Dossett, H; Estrada, N; Swartz, G; LeFevre, G and Kwasman, B (2014). *A randomised controlled trial of kinematically and mechanically aligned total knee replacements Two-year clinical results*. The Bone & Joint Journal. **96**(7): 907–913.
133. Sigma FB. Online:
https://www.kneereplacement.com/DePuy_technology/DePuy_knees/fixed_knee/,
retrieved: 29.03.2015.
134. DePuy Orthopaedics (2008). *Measured Resection Classic Surgical Technique*. DePuy Orthopaedics.
135. Berger, R; Crossett, L; Jacobs, J and Rubash, H (1998). *Malrotation causing patellofemoral complications after total knee arthroplasty*. Clinical Orthopaedics and Related Research. (356): 144–153.
136. Maistrelli, GL; Antonelli, L; Fornasier, V and Mahomed, N (1995). *Cement penetration with pulsed lavage versus syringe irrigation in total knee arthroplasty*. Clinical Orthopaedics and Related Research. **312**: 261–265.
137. Wheelwright, E; Byrick, R; Wigglesworth, D; Kay, J; Wong, P; Mullen, J and Waddell, J (1993). *Hypotension during cemented arthroplasty. Relationship to cardiac output and fat embolism*. Journal of Bone & Joint Surgery, British Volume. **75**(5): 715–723.
138. Weiss, RJ; Heisel, C and Breusch, SJ (2003). *Patellar component stability improves with pulsatile lavage in total knee arthroplasty*. International Orthopaedics. **27**(1): 18–21.
139. Fischer, C; Kaszap, B; Drexler, C; Lehner, B and Clarius, M (2012). *Stand der zementierten Hüftendoprothetik in Deutschland 2010*. Zeitschrift für Orthopädie und Unfallchirurgie. **150**(3): 309–317.
140. Lutz, MJ and Halliday, BR (2002). *Survey of current cementing techniques in total knee replacement*. ANZ Journal of Surgery. **72**(6): 437–439.
141. PulseLavage. Online: <http://www.juka-pharma.de/produktportfolio/spuelsysteme/>,
retrieved: 14.04.2015.
142. Lidgren, L; Drar, H and Möller, J (1984). *Strength of polymethylmethacrylate increased by vacuum mixing*. Acta Orthopaedica. **55**(5): 536–541.

143. Draenert, K and Draenert, Y (2005). *Properties of bone cement: The three interfaces*. In: Breusch, S. & Malchau, H. (ed.). *The well-cemented total hip arthroplasty*. Springer Medizin Verlag Heidelberg.
144. Muller, SD; Green, SM and McCaskie, AW (2002). *The dynamic volume changes of polymerising polymethyl methacrylate bone cement*. *Acta Orthopaedica*. **73**(6): 684–687.
145. Wang, J-S; Franzén, H; Jonsson, E and Lidgren, L (1993). *Porosity of bone cement reduced by mixing and collecting under vacuum*. *Acta Orthopaedica*. **64**(2): 143–146.
146. DePuy CMW & DePuy (2007). *SmartMix™ CEMVAC + SmartSet® HV*. DePuy CMW & DePuy.
147. Mulroy, WF and Harris, WH (1996). *Revision total hip arthroplasty with use of so-called second-generation cementing techniques for aseptic loosening of the femoral component. A fifteen-year-average follow-up study*. *The Journal of Bone & Joint Surgery*. **78**(3): 325–30.
148. Gililland, JM; Gaffney, CJ; Odum, SM; Fehring, TK; Peters, CL and Beaver, WB (2014). *Clinical & radiographic outcomes of cemented vs. diaphyseal engaging cementless stems in aseptic revision TKA*. *The Journal of Arthroplasty, Supplement*. **29**(9): 224–228.
149. Bauze, A; Costi, J; Stavrou, P; Rankin, W; Hearn, T; Krishnan, J and Slavotinek, J (2004). *Cement penetration and stiffness of the cement-bone composite in the proximal tibia in a porcine model*. *Journal of Orthopaedic Surgery*. **12**(2): 194–198.
150. Lutz, MJ; Pincus, PF; Whitehouse, SL and Halliday, BR (2009). *The effect of cement gun and cement syringe use on the tibial cement mantle in total knee arthroplasty*. *The Journal of Arthroplasty*. **24**(3): 461–467.
151. Mortazavi, SJ; Schwarzenberger, J; Austin, MS; Purtill, JJ and Parvizi, J (2010). *Revision total knee arthroplasty infection: incidence and predictors*. *Clinical Orthopaedics and Related Research*. **468**(8): 2052–2059.
152. Brown III, E; Clarke, HD and Scuderi, GR (2006). *The painful total knee arthroplasty: Diagnosis and management*. *Orthopedics*. **29**(2): 129–136.
153. Jasty, M; Bragdon, C; Burke, D; O'Connor, D; Lowenstein, J and Harris, WH (1997). *In vivo skeletal responses to porous-surfaced implants subjected to small induced motions*. *J Bone Joint Surg Am*. **79**(5): 707–14.
154. Askew, MJ; Steege, JW; Lewis, JL; Ranieri, JR and Wixson, RL (1983). *Effect of cement pressure and bone strength on polymethylmethacrylate fixation*. *Journal of Orthopaedic Research*. **1**(4): 412–420.
155. Sala, M; Taylor, M and Tanner, K (1999). *Torsional stability of primary total knee replacement tibial prostheses: A biomechanical study in cadaveric bone*. *The Journal of Arthroplasty*. **14**(5): 610–615.

156. Grupp, TM; Pietschmann, MF; Holderied, M; Scheele, C; Schröder, C; Jansson, V and Müller, PE (2013). *Primary stability of unicompartmental knee arthroplasty under dynamic compression-shear loading in human tibiae*. *Clinical Biomechanics*. **28**(9): 1006–1013.
157. Rao, AS; Engh, JA; Engh, GA and Parks, NL (2010). *Mechanical stability of well-functioning tibial baseplates from postmortem-retrieved total knee arthroplasties*. *The Journal of Arthroplasty*. **25**(3): 481–485.
158. Skwara, A; Figiel, J; Knott, T; Paletta, J; Fuchs-Winkelmann, S and Tibesku, C (2009). *Primary stability of tibial components in TKA: in vitro comparison of two cementing techniques*. *Knee Surgery, Sports Traumatology, Arthroscopy*. **17**(10): 1199–1205.
159. Turgay, E; Figiel, J; Danek, S; Tibesku, CO; Paletta, JR and Skwara, A (2011). *Initial stability of tibial components in primary knee arthroplasty. A cadaver study comparing cemented and cementless fixation techniques*. *Interface*. **29**(15): 50.
160. Dhert, W; Verheyen, C; Braak, L; De Wijn, J; Klein, C; De Groot, K and Rozing, P (1992). *A finite element analysis of the push-out test: Influence of test conditions*. *Journal of Biomedical Materials Research*. **26**(1): 119–130.
161. Mann, KA; Ayers, D; Werner, F; Nicoletta, R and Fortino, M (1997). *Tensile strength of the cement-bone interface depends on the amount of bone interdigitated with PMMA cement*. *Journal of Biomechanics*. **30**(4): 339–346.
162. Waanders, D; Janssen, D; Mann, KA and Verdonschot, N (2010). *The mechanical effects of different levels of cement penetration at the cement-bone interface*. *Journal of Biomechanics*. **43**(6): 1167–1175.
163. Mann, KA; Miller, MA; Pray, CL; Verdonschot, N and Janssen, D (2012). *A new approach to quantify trabecular resorption adjacent to cemented knee arthroplasty*. *Journal of Biomechanics*. **45**(4): 711–715.
164. Miller, MA; Sherman, R; Izant, T and Mann, K (2013). *Loss of Fixation in Cemented TKR: Role of Time in Service and Initial Interlock*. *Proceedings of the 2013 ORS Annual Meeting*.
165. Janssen, D; Mann, KA and Verdonschot, N (2008). *Micro-mechanical modeling of the cement-bone interface: The effect of friction, morphology and material properties on the micromechanical response*. *Journal of Biomechanics*. **41**(15): 3158–3163.
166. Mann, KA; Miller, MA; Goodheart, JR; Izant, TH and Cleary, RJ (2014). *Peri-implant bone strains and micro-motion following in vivo service: A postmortem retrieval study of 22 tibial components from total knee replacements*. *Journal of Orthopaedic Research*. **32**(3): 355–361.
167. Goldstein, SA; Wilson, DL; Sonstegard, DA and Matthews, LS (1983). *The mechanical properties of human tibial trabecular bone as a function of metaphyseal location*. *Journal of Biomechanics*. **16**(12): 965–969.

168. Rice, J; Prenderville, T; Murray, P; McCormack, B and Quinlan, W (1998). *Femoral cementing techniques in total hip replacement*. International Orthopaedics. **22**(5): 308–311.
169. Jacquot, B; Durand, J-C; Farge, P; Valcarcel, J; Deville de Periere, D and Cuisinier, F (2012). *Influence of temperature and relative humidity on dentin and enamel bonding: a critical review of the literature. Part 1. Laboratory studies*. The Journal of Adhesive Dentistry. **14**(5): 433–46.
170. Stannage, K; Shakespeare, D and Bulsara, M (2003). *Suction technique to improve cement penetration under the tibial component in total knee arthroplasty*. The Knee. **10**(1): 67–73.
171. Vanlommel, J; Luyckx, JP; Labey, L; Innocenti, B; De Corte, R and Bellemans, J (2011). *Cementing the tibial component in total knee arthroplasty: Which technique is the best?* The Journal of Arthroplasty. **26**(3): 492–496.
172. Clarius, M; Hauck, C; Seeger, JB; James, A; Murray, DW and Aldinger, PR (2009). *Pulsed lavage reduces the incidence of radiolucent lines under the tibial tray of Oxford unicompartmental knee arthroplasty*. International Orthopaedics. **33**(6): 1585–1590.
173. Breusch, S; Norman, T; Schneider, U; Reitzel, T; Blaha, J and Lukoschek, M (2000). *Lavage technique in total hip arthroplasty*. The Journal of Arthroplasty. **15**(7): 921–927.
174. Kalteis, T; Pförringer, D; Herold, T; Handel, M; Renkawitz, T and Plitz, W (2007). *An experimental comparison of different devices for pulsatile high-pressure lavage and their relevance to cement intrusion into cancellous bone*. Archives of Orthopaedic and Trauma Surgery. **127**(10): 873–877.
175. Bonnicksen, SL and Lewis, LA (2006). *Bone densitometry for technologists*. Springer.
176. Galante, J; Rostoker, W and Ray, R (1970). *Physical properties of trabecular bone*. Calcified Tissue Research. **5**(1): 236–246.
177. Scuderi, G and Clarke, H (2005). *Optimizing Cementing Technique*. In: Bellemans, Johan and Ries, Michael D. and Victor, Jan M.K. (ed.). Total knee arthroplasty - A guide to get better performance. Springer Berlin: 223–227.
178. Ryd, L; Hansson, U; Blunn, G; Lindstrand, A and Toksvig-Larsen, S (1999). *Failure of partial cementation to achieve implant stability and bone ingrowth: A long-term roentgen stereophotogrammetric study of tibial components*. Journal of Orthopaedic Research. **17**(3): 311–320.
179. Sharkey, PF; Hozack, WJ; Rothman, RH; Shastri, S and Jacoby, SM (2002). *Why are total knee arthroplasties failing today?* Clinical Orthopaedics and Related Research. **404**: 7–13.
180. Bert, JM and McShane, M (1998). *Is it necessary to cement the tibial stem in cemented total knee arthroplasty?* Clinical Orthopaedics and Related Research. (356): 73–8.

181. Saari, T; Li, MG; Wood, D and Nivbrant, B (2009). *Comparison of cementing techniques of the tibial component in total knee replacement*. International Orthopaedics. **33**(5): 1239–1242.
182. Cawley, DT; Kelly, N; Simpkin, A; Shannon, FJ and McGarry, JP (2012). *Full and surface tibial cementation in total knee arthroplasty: a biomechanical investigation of stress distribution and remodeling in the tibia*. Clinical Biomechanics. **27**(4): 390–397.
183. Rossi, R; Bruzzone, M; Bonasia, DE; Ferro, A and Castoldi, F (2010). *No early tibial tray loosening after surface cementing technique in mobile-bearing TKA*. Knee Surgery, Sports Traumatology, Arthroscopy. **18**(10): 1360–1365.
184. Efe, T; Figiel, J; Sibbert, D; Fuchs-Winkelmann, S; Tibesku, CO; Timmesfeld, N; Paletta, JR and Skwara, A (2011). *Revision of tibial TKA components: Bone loss is independent of cementing type and technique: An in vitro cadaver study*. BMC Musculoskeletal Disorders. **12**(1): 6.
185. Faul, F; Erdfelder, E; Buchner, A and Lang, A-G (2009). *Statistical power analyses using G* Power 3.1: Tests for correlation and regression analyses*. Behavior research methods. **41**(4) Springer: 1149–1160.
186. Verburg, H; van de Ridder, LC; Verhoeven, VW and Pilot, P (2014). *Validation of a measuring technique with computed tomography for cement penetration into trabecular bone underneath the tibial tray in total knee arthroplasty on a cadaver model*. BMC Medical Imaging. **14**(1).
187. Aiken, LS; West, SG and Reno, RR (1991). *Multiple regression: Testing and interpreting interactions*. Sage Publications London.
188. Armstrong, Z and Wattenberg, M (2014). *Visualizing statistical mix effects and Simpson's Paradox*. IEEE Transactions on Visualization and Computer Graphics. **20**(12): 2132–2141.
189. Armistead, TW (2014). *Resurrecting the Third Variable: A Critique of Pearl's Causal Analysis of Simpson's Paradox*. The American Statistician. **68**(1): 1–7.
190. Homminga, J; McCreadie, B; Ciarelli, T; Weinans, H; Goldstein, S and Huiskes, R (2002). *Cancellous bone mechanical properties from normals and patients with hip fractures differ on the structure level, not on the bone hard tissue level*. Bone. **30**(5): 759–764.
191. Goldstein, SA (1987). *The mechanical properties of trabecular bone: Dependence on anatomic location and function*. Journal of Biomechanics. **20**(11): 1055–1061.
192. Helgason, B; Perilli, E; Schileo, E; Taddei, F; Brynjólfsson, S and Viceconti, M (2008). *Mathematical relationships between bone density and mechanical properties: A literature review*. Clinical Biomechanics. **23**(2): 135–146.

193. Hvid, I; Bentzen, SM; Linde, F; Mosekilde, L and Pongsoipetch, B (1989). *X-ray quantitative computed tomography: The relations to physical properties of proximal tibial trabecular bone specimens*. Journal of Biomechanics. **22**(8): 837–844.
194. Stauber, M; Rapillard, L; van Lenthe, GH; Zysset, P and Müller, R (2006). *Importance of individual rods and plates in the assessment of bone quality and their contribution to bone stiffness*. Journal of Bone and Mineral Research. **21**(4): 586–595.
195. Lu, Y; Krause, M; Bishop, N; Sellenschloh, K; Glüer, C-C; Püschel, K; Amling, M; Morlock, M and Huber, G (2014). *The role of patient-mode high-resolution peripheral quantitative computed tomography indices in the prediction of failure strength of the elderly women's thoracic vertebral body*. Osteoporosis International. : 1–8.
196. Majumdar, S; Genant, H; Grampp, S; Newitt, D; Truong, V-H; Lin, J and Mathur, A (1997). *Correlation of trabecular bone structure with age, bone mineral density, and osteoporotic status: in vivo studies in the distal radius using high resolution magnetic resonance imaging*. Journal of Bone and Mineral Research. **12**(1): 111–118.
197. Hans, D; Fuerst, T; Lang, T; Majumdar, S; Lu, Y; Genant, HK and Glüer, C (1997). *3 How can we measure bone quality?* Baillière's Clinical Rheumatology. **11**(3): 495–515.
198. Odgaard, A (1997). *Three-dimensional methods for quantification of cancellous bone architecture*. Bone. **20**(4): 315–328.
199. Day, J; Ding, M; Odgaard, A; Sumner, D; Hvid, I and Weinans, H (2000). *Parallel plate model for trabecular bone exhibits volume fraction-dependent bias*. Bone. **27**(5): 715–720.
200. Hildebrand, T and Rüegsegger, P (1997). *A new method for the model-independent assessment of thickness in three-dimensional images*. Journal of Microscopy. **185**(1): 67–75.
201. Harrigan, T and Mann, R (1984). *Characterization of microstructural anisotropy in orthotropic materials using a second rank tensor*. Journal of Materials Science. **19**(3): 761–767.
202. Cowin, S (1986). *Wolff's law of trabecular architecture at remodeling equilibrium*. Journal of Biomechanical Engineering. **108**(1): 83–88.
203. Laib, A and Rüegsegger, P (1999). *Comparison of structure extraction methods for in vivo trabecular bone measurements*. Computerized Medical Imaging and Graphics. **23**(2): 69–74.
204. Williams, J and Lewis, J (1982). *Properties and an anisotropic model of cancellous bone from the proximal tibial epiphysis*. Journal of Biomechanical Engineering. **104**(1): 50–56.

205. Liu, XS; Sajda, P; Saha, PK; Wehrli, FW; Bevill, G; Keaveny, TM and Guo, XE (2008). *Complete volumetric decomposition of individual trabecular plates and rods and its morphological correlations with anisotropic elastic moduli in human trabecular bone*. Journal of Bone and Mineral Research. **23**(2): 223–235.
206. Mann, KA; Miller, MA; Cleary, RJ; Janssen, D and Verdonchot, N (2008). *Experimental micromechanics of the cement-bone interface*. Journal of Orthopaedic Research. **26**(6): 872–879.
207. Yan, Y-B; Qi, W; Wang, J; Liu, L-F; Teo, E-C; Tianxia, Q; Ba, J and Lei, W (2011). *Relationship between architectural parameters and sample volume of human cancellous bone in micro-CT scanning*. Medical engineering & physics. **33**(6): 764–769.
208. Vale, FM; Castro, M; Monteiro, J; Couto, FS; Pinto, R and Giao Toscano Rico, J (1997). *Acrylic bone cement induces the production of free radicals by cultured human fibroblasts*. Biomaterials. **18**(16): 1133–1135.
209. Martens, KA; Edwards, SL; Omar, IM and Saltzman, MD (2012). *Heat generated with pegged or keeled glenoid components fixed with defined amounts of cement*. Orthopaedics. **35**(4): 469–473.
210. Li, C; Kotha, S; Huang, C-H; Mason, J; Yakimicki, D and Hawkins, M (2003). *Finite element thermal analysis of bone cement for joint replacements*. Journal of Biomechanical Engineering. **125**: 315–322.
211. Dennis, D; Komistek, R; Walker, S; Cheal, E and Stiehl, J (2001). *Femoral condylar lift-off in vivo in total knee arthroplasty*. Journal of Bone & Joint Surgery, British Volume. **83**(1): 33–39.
212. Vertullo, CJ and Davey, J (2001). *The effect of a tibial baseplate undersurface peripheral lip on cement penetration in total knee arthroplasty*. The Journal of Arthroplasty. **16**(4): 487–492.
213. Shrout, PE and Fleiss, JL (1979). *Intraclass correlations: uses in assessing rater reliability*. Psychological bulletin. **86**(2) American Psychological Association: 420.
214. GIMP 2.8.10. Online: <http://www.gimp.org/>, retrieved:17.05.2015.
215. Mann, KA; Werner, F and Ayers, D (1999). *Mechanical strength of the cement-bone interface is greater in shear than in tension*. Journal of Biomechanics. **32**(11): 1251–1254.
216. Kim, D-G; Miller, MA and Mann, KA (2004). *Creep dominates tensile fatigue damage of the cement-bone interface*. Journal of Orthopaedic Research. **22**(3): 633–640.
217. Kim, D-G; Miller, MA and Mann, KA (2004). *A fatigue damage model for the cement-bone interface*. Journal of Biomechanics. **37**(10): 1505–1512.

218. Janssen, D; Mann, KA and Verdonshot, N (2009). *Finite element simulation of cement-bone interface micromechanics: A comparison to experimental results*. Journal of Orthopaedic Research. **27**(10): 1312–1318.
219. Waanders, D; Janssen, D; Miller, MA; Mann, KA and Verdonshot, N (2009). *Fatigue creep damage at the cement-bone interface: An experimental and a micro-mechanical finite element study*. Journal of Biomechanics. **42**(15): 2513–2519.
220. Waanders, D; Janssen, D; Berahmani, S; Miller, MA; Mann, KA and Verdonshot, N (2012). *Interface micromechanics of transverse sections from retrieved cemented hip reconstructions: An experimental and finite element comparison*. Journal of Materials Science: Materials in Medicine. **23**(8): 2023–2035.
221. Howard, KI; Miller, MA; Damron, TA and Mann, KA (2014). *The distribution of implant fixation for femoral components of TKA: A postmortem retrieval study*. The Journal of Arthroplasty. **29**(9): 1863–1870.
222. Tozzi, G; Zhang, Q-H and Tong, J (2014). *Microdamage assessment of bone-cement interfaces under monotonic and cyclic compression*. Journal of Biomechanics. **47**(14): 3466–3474.
223. Field, A (2009). *Discovering statistics using SPSS*. Sage Publications London.
224. Ruxton, GD and Beauchamp, G (2008). *Time for some a priori thinking about post hoc testing*. Behavioral Ecology. **19**(3) ISBE: 690–693.
225. Fehring, TK; Odum, S; Griffin, WL; Mason, JB and Nadaud, M (2001). *Early failures in total knee arthroplasty*. Clinical Orthopaedics and Related Research. (392): 315–318.
226. *Skeleton*. Online: <http://alvesan.deviantart.com/art/Complete-Skeleton-3D-modeling-288042500>, retrieved 15.05.2015.

Appendices

A Pilot Studies

A.1 Pilot Study Implant Design

In this pilot study two implant designs were compared regarding their influence on the cement layer morphology.

Brief Summary

Study question:

Do different implant backsides influence the cement layer morphology differently?

- Testing of DePuy P.F.C. Sigma® Ti Fixed Bearing vs. CoCr MBT Keeled in a pairwise test design (n = 4)
- Pull-out force significantly larger for Ti Fixed Bearing, no difference in cement penetration depth
- CoCr MBT Keeled failed at the implant interface at low forces, facilitating CT-scanning for cement layer analysis and re-attachment of implant with following pull-out
- Low forces measured for CoCr MBT Keeled did not coincide with results from previous pilot study results and were not reproducible → experimental interference is assumed, but could not be identified
- Cement morphology results were generally consistent with previous studies

Introduction

According to the literature, several aspects concerning implant design, cementation technique and bone preparation affect the cement penetration depth. It has been shown that a peripheral lip on the backside of the tibial tray improves penetration²¹². Other design aspects concerning the backside may also be influential, for example cement pockets included in some fixed bearings. Pull-out testing in a previous study was performed on an established fixed bearing design, whereas the current thesis predominantly addresses a new mobile bearing design¹². In order to rate the comparability between the data gained from these studies pull-out testing was performed on the two implant designs cemented into human cadaveric specimens. Failure mode (implant-cement or cement-bone) and failure load were determined and a cement layer analysis was performed for both devices.

Methods

Four pairs of tibiae were implanted, alternating with two different implant designs from the DePuy P.F.C. Sigma® series: The Ti Fixed Bearing and the CoCr MBT Keeled mobile bearing (**Figure A-1**). The implants were provided by DePuy Orthopaedics. Only size 3 (sz3) implants were used. The Ti Fixed Bearing has a peripheral lip and undercuts around the rim of the 'cement pockets' in the posterior regions of the backside. The CoCr MBT Keeled also has a peripheral lip, but no undercuts. All eight implants were size 3.

Preparation and Implantation

Preparation and implantation of each specimen was completed at the same day. Specimens were prepared as described in Section 2.3.2.3. Prior to cement application, the bony surface was prepared by syringe lavage with 1 800 ml saline solution (**Figure A-1**). Although state of the art pulsatile lavage was not applied, since it increases the cement penetration depth significantly¹² and may override the effect of the different backside. Cement was mixed (no vacuum) and applied by hand on the bony plateau only after drying of the osseous surface. The stem of the implant was left cementless (surface cementing technique). Excessing cement was removed as in *in vivo* procedure. Embedding and pull-out was performed as described in Section 3.2.6.

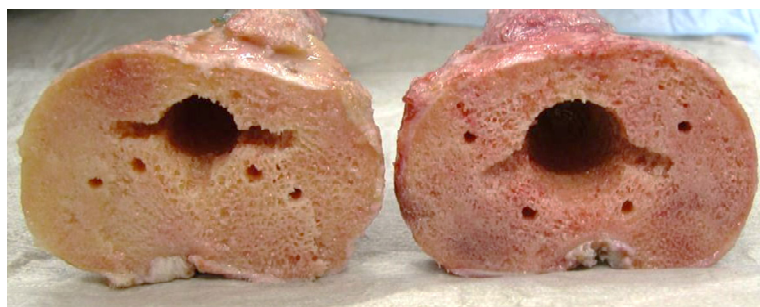


Figure A-1: A characteristic tibial pair prepared for Ti Fixed Bearing (left) and CoCr MBT Keeled (right) implantation.

Computed Tomography

CT-scanning of the specimens was required for cement layer analysis. Both implant types cause metal-induced artefacts in CT images. A special filter was used to reduce the artefacts (Brilliance CT 40-channel, Philips Healthcare, Haifa, Israel, voxel size 0.15x0.15x0.4 mm). The filter performed well for the titanium-made Fixed Bearing implants but artefacts due to cobalt chrome CoCr MBT Keeled resulted in an unacceptable loss of information. For this pilot study the CoCr MBT Keeled specimens were CT-scanned in the Department of Legal Medicine if the cement layer was intact after implant pull-out (Brilliance CT 16-slice, Philips Healthcare, Best, The Netherlands, 0.42x0.42x0.42 mm, University Medical Center Hamburg-Eppendorf, Hamburg, Germany). CoCr MBT Keeled as well as Ti Fixed Bearing CT scans were used for cement layer analysis (Section 3.2.7). The difference in resolution is not considered relevant, since the decisive longitudinal z direction resolution is similar.

Cement Layer Reconstruction

The segmentation is described in Section 3.2.7 for the CoCr MBT Keeled and in Section 4.2.2 for the Ti Fixed Bearing.

Cement Layer Analysis

This procedure was the same for *ex* and *in situ* data sets and is described in Section 3.2.7. Parameters were the *penetration depth* of the cement into the bone and *thickness* of cement between bone plateau and implant.

Statistical analysis comparing pull-out force, *penetration depth* and *thickness* of the cement below the implant and above the bony plateau was done by a T test for paired

observations (PASW 18, SPSS Inc./IBM Corporation, Armonk, NY, USA). Parametric testing was justified since median and mean were similar for all groups. A type-I error level of 0.05 was used. In order to investigate the effect of the cement pockets in the Ti Fixed Bearing trays, a separate analysis comparing anterior and posterior bone cement layers was undertaken for both implants.

Bone mineral density (BMD) as a structural parameter was controlled for by the paired design, but was also compared between designs using one-way ANOVA.

Results

BMD was similar for the two tray design groups (Ti Fixed Bearing: 64 mg/cm³, SD=45 mg/cm³; CoCr MBT Keeled: 63 mg/cm³, SD=37 mg/cm², p=0.967, one-way ANOVA, **Table A-1**).

The CoCr MBT Keeled implant pulled out of the cement, rather than from the bone (**Figure A-2**). Mean pull out force was 455 N (SD = 230 N). The Ti Fixed Bearing design failed mixed in one case, at the bone interface in a second case and at the implant interface in two cases (**Figure A-2**). Mean pull-out force was 1 458 N (SD = 262 N) and significantly greater than for the CoCr MBT Keeled (p = 0.001, paired t-test, **Table A-1**).

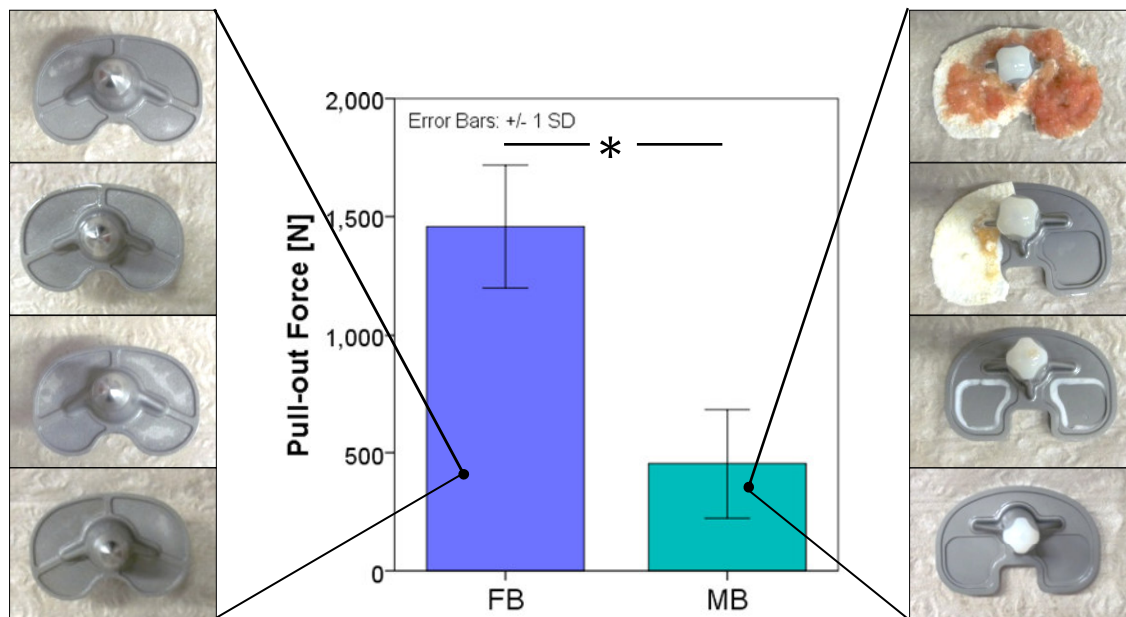


Figure A-2: CoCr MBT Keeled trays were observed to pull-out of the cement mantle exclusively, with a mean force of 455 N. In contrast, the Fixed Bearing trays pulled out of the bone as well as the cement with a mean force more than 3 times greater (1 458 N).

The mean^a cement penetration depth for the Ti Fixed Bearing specimens was 1.07 mm (SD = 0.23 mm) and 1.16 mm (SD = 0.19 mm) for the CoCr MBT Keeled (p = 0.529, paired t-test, **Table A-1**). The mean thickness of the cement between implant and bony surface

^a The median penetration depth was calculated for each specimen. The mean of these single values was then determined for each group.

was 2.32 mm (SD = 0.22 mm) for the Ti Fixed Bearing and 1.47 mm (SD = 0.27 mm), and therefore significantly smaller for the CoCr MBT Keeled ($p = 0.032$, paired t-test, **Table A-1**). **Table A-1** and **Table A-2** show the results for each specimen.

Table A-1: Specimens tested in the Implant Design Study with corresponding results of bone density (*BMD*), *pull-out force* and *penetration depth* (L: left, R: right, M: male, F: female). The p value corresponds to the mean values. Mean and standard deviation (SD) are given for each group.

Patient	Side	Gender	Implant	Implant size	<i>BMD</i> [mg K ₂ HPO ₄ /cm ³]	Pull-out force [N]	Median penetration depth [mm]
3001	L	M	Ti Fixed Bearing	3	13	1268	0.96
3002	R	F	Ti Fixed Bearing	3	55	1605	1.42
3003	L	F	Ti Fixed Bearing	3	65	1208	0.97
3004	R	M	Ti Fixed Bearing	3	122	1751	0.93
Mean (SD)					64 (45)	1458 (262)	1.07 (0.23)
3001	R	M	CoCr MBT Keeled	3	16	181	1.40
3002	L	F	CoCr MBT Keeled	3	62	719	1.23
3003	R	F	CoCr MBT Keeled	3	66	376	1.05
3004	L	M	CoCr MBT Keeled	3	106	543	0.97
Mean (SD)					63 (37)	455 (230)	1.16 (0.19)
p					0.967	0.001	0.529

Thickness was analysed looking at differences between anterior and posterior region. Cement layer thickness in the anterior region of the Ti Fixed Bearing (1.67 mm, SD = 0.66 mm) was smaller compared to the posterior region (2.57 mm, SD = 0.31 mm; $p = 0.062$), which again was larger than the posterior region below the CoCr MBT Keeled implant (1.67 mm, SD = 0.44 mm; $p = 0.093$). For the CoCr MBT Keeled implants anterior cement layer was 1.41 mm (SD=0.19 mm) and not significantly different from the posterior region (1.67 mm, $p = 0.174$). Anterior thickness of Ti Fixed Bearing was 1.67 and the same as in CoCr MBT Keeled ($p = 0.561$).

Table A-2: Specimens tested in Implant Design Study with corresponding results of cement layer *thickness* above the bony plateau. The p value corresponds to the mean values. Mean and standard deviation (SD) are given for each group.

Patient	Side	Implant	Median Thickness [mm]		
			overall	posterior	anterior
3001	L	TiFixed Bearing	2.64	3.03	2.08
3002	R	TiFixed Bearing	2.25	2.42	0.72
3003	L	TiFixed Bearing	2.12	2.44	1.73
3004	R	TiFixed Bearing	2.26	2.37	2.15
Mean (SD)			2.32 (0.22)	2.57 (0.31)	1.67 (0.66)
3001	R	CoCrMBTKeeled	1.14	1.10	1.18
3002	L	CoCrMBTKeeled	1.65	1.87	1.62
3003	R	CoCrMBTKeeled	1.37	1.60	1.36
3004	L	CoCrMBTKeeled	1.73	2.12	1.47
Mean (SD)			1.47 (0.27)	1.67 (0.44)	1.41 (0.19)
p			0.032	0.093	0.561

Discussion

Since the CoCr MBT Keeled implant failed exclusively at the stem interface the cement morphology could be imaged without any metal artefacts. Cement layer evaluation required an intact bone interface. Pull-out force was low (mean 455 N), therefore bone interface damage during pull-out was not assumed.

The low pull-out force for the CoCr MBT Keeled implant contrasts with forces of 1 561 N (SD = 1 138 N) determined in a retrieval study for the same backside design²⁹. However, the failure mode was the same. In the Implant Design Study, there must therefore have been an influence on the cement-implant interface that reduced its failure force. Measured absolute forces, especially for the CoCr MBT Keeled, should be regarded with care.

The Ti Fixed Bearing pull-out mode appeared more variable in contrast to exclusive bone interface failure documented previously for the Ti Fixed Bearing design¹². Syringe lavage was applied in both studies by the same surgeon, using the same technique and the BMD was similar. The bone interface was stronger than the implant interface in 3 cases, although the latter was strengthened by backside undercuts. Due to the previously documented failure mode at the cement-bone interface the Ti Fixed Bearing design was originally proposed for the main study in which the bone interface strength was of interest¹². The failure mode appeared more reproducible for the CoCr MBT Keeled than for the Ti Fixed Bearing and additionally this failure occurred at low forces, without impairing the bone interface. Basing on this observation a procedure was developed to obtain CT scans with the implant temporarily removed. That way, virtual reconstruction of the cement layer is possible without metal artefacts. Previously, the implant will be re-attached to the cement. Thus, the interface was strengthened and failure was shifted to

the bone interface. This procedure is essential for the main studies of this thesis and explained in detail in Section 3.2.5.

The cement thickness between implant and bony plateau was larger for the Ti Fixed Bearing implant. Although significance was narrowly missed, the posterior thickness of the Ti Fixed Bearing was larger than the anterior and larger than the posterior thickness of the CoCr MBT Keeled. This obviously results from the pockets with undercuts in the posterior region of the Ti Fixed Bearing and should not influence the fixation strength of the implant.

A.2 Implant Modification

Implant tips CoCr MBT Keeled were replaced by anchor tips with an M6 thread. Two different tip sizes were used for the four implant sizes (**Figure A-3**). Anchor size S with about 13.5 mm diameter was used for implant sizes 2.5 and 3. Anchor size L with about 15.7 mm diameter was used for implant sizes 4 and 5.

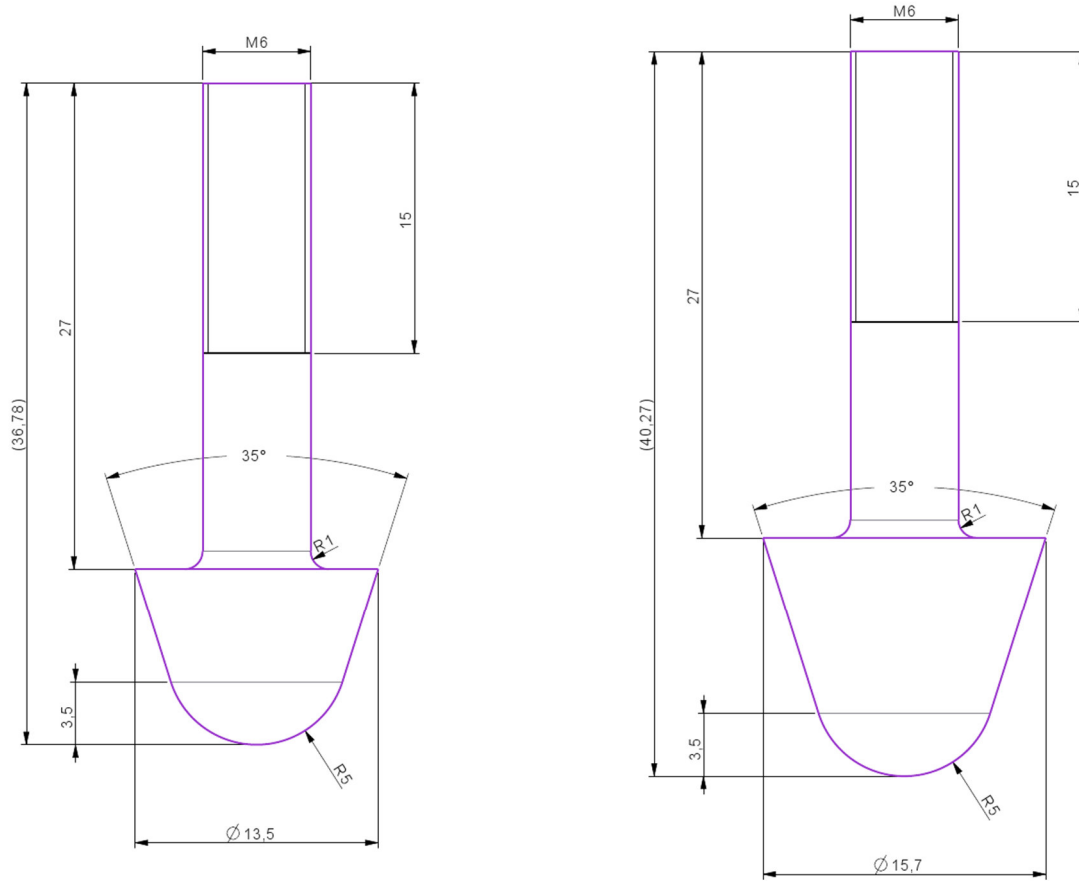


Figure A-3: Anchor tip screws used for pull-out testing. Left: size S for implant sizes 2.5 and 3, right: size L for implant sizes 4 and 5.

A.3 Interface Strengthening by Re-gluing of Implant

Study aim: Strengthening of the cement-implant interface to achieve cement-bone interface failure.

Methods

In this thesis, the CoCr MBT Keeled, a mobile platform tray made of cobalt chrome with undercut-free backside was used. CT scans were necessary for cement layer analysis but included too many artefacts with the new implant. A method was developed enabling CT scans with the implant removed from the cement. The implant was then re-glued to the cement using acrylic glue and finally underwent pull-out from the bone. Several aspects were pre-investigated for the new implant: appropriateness of the coupling of the new implant to the machine, chemical alteration of the cement when glue is applied, and expectable capacity of the glue interface.

Femurs (n=4) were implanted with CoCr MBT Keeled implants, bones were treated with pulse lavage and cement was hand-packed on the bony plateau only (stem left cementless). CoCr MBT Keeled implant tips were replaced by an anchor-like device further described in Section 3.2.3 (technical drawing and size-assignment in Appendix A.2). Implants were pulled out at the same day (1st pull-out, **Figure A-4**). When failure was at the implant interface and the participating surfaces were intact, the implant was re-glued to the cement using PMMA glue (Pattex® Stabilit Express, Henkel AG & Co., Düsseldorf, Germany) and pulled out again (2nd Pull-out).



Figure A-4: Pull-out procedure applying re-attachment. From left to right: 1st pull-out, implant interface failure, 2nd pull-out and bone failure, bulk bone failure with bone remaining at the cement.

The experimental analysis was complemented by scanning electron microscopy (SEM) and energy dispersive X-ray spectroscopy (EDX) analysis of the cement-glue interface. A sample was produced and EDX spectroscopy was carried out at three different spots on each material: close to the interface (5 μm distance), at 1,000 μm distance and a control measurement at 3,000 μm distance (each $n = 3$). EDX measurements were reduced to the elements C, O, Si, Cl and K. Carbon and oxygen were included because they are the main components of PMMA. Hydrogen was not included since the sample was produced using a water-cooled diamond band saw. The source of detected hydrogen would be questionable. Silicon, chlorine and potassium occur in both materials but in different atomic fractions, with cement showing fractions close to zero.

Pull-out was not statistically analysed. Statistical analysis of the EDX results was carried out applying two-way ANOVA with type-1 error level $\alpha = 0.05$.

Results

The measured strength from both pull-outs is listed in **Table A-3**. First pull-out lead to cement-implant interface failure in all cases with implant back sides appearing wet or fatty. The cement layer was intact. In one case failure force was not recorded. Second pull-out lead to bulk bone failure ($n = 3$) and one mixed failure.

Table A-3: Determined pull-out forces and corresponding mode of specimens in the pilot study.

Specimen	Force 1 st Pull-out [N]	Failure mode 1	Force 2 nd Pull-out [N]	Failure mode 2
1	-	Implant interface	8 139	mixed
2	2 886	Implant interface	-	bone failure
3	3 267	Implant interface	11 430	bone failure
4	7 357	Implant interface	7 253	bone failure

The SEM images did not show any interaction between cement and glue (**Figure A-5**). The EDX results showed no difference in atomic % between cement and glue for carbon and oxygen. Glue contained a significantly larger amount of silicon, chloride and potassium than cement ($p_{\text{Si}} < 0.001$, $p_{\text{Cl}} = 0.001$, $p_{\text{K}} = 0.038$). All elements showed no significant difference regarding the distance to the interface ($p > 0.221$).

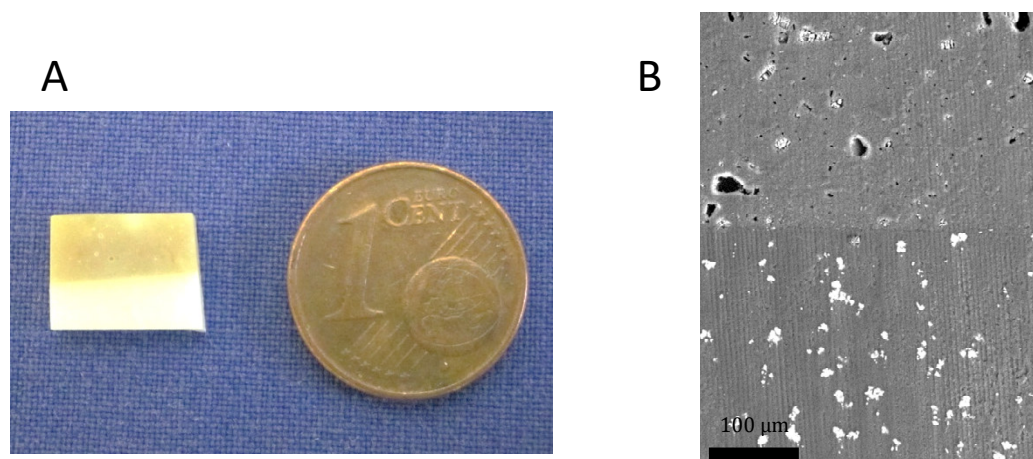


Figure A-5: The interface between cement and PMMA glue. A: Sample consisting of glue (upper layer) and cement (lower layer), B: SEM image of interface between glue (upper layer) and cement (lower layer), no interaction visible

Discussion

The implant can be removed and re-attached with glue, allowing CT scans to be generated without metal artefacts, between implantation and pull-out stages. Pull-out forces were above the range of other studies in all pull-outs carried out. Implant interface failure and intact cement layer after the first pull-out are prerequisites for application of re-attachment in the project. Bone failure in the second pull-out indicates that the capability of the glue is sufficient. Attachment appeared to be uniform during force application (no biased pull-out).

The failure force for the implant interface was by far exceeding the range measured in the design pilot study (181 N to 719 N) and also exceeding the results for the Ti Fixed Bearing from a previous study (864 N to 1 391 N) [Reference 12], whose backside design was considered to deliver a stronger implant interface than that of the CoCr MBT Keeled.

EDX and SEM results showed no interaction between cement and glue. Interaction would have shown clear differences between the 3 000 μm (control) spot and the 5 μm spot. Value of the statistical results is limited since the sample size was merely $n = 3$ for each measuring spot and after excluding inaccurate measurements the control group (3 000 μm distance) for glue was $n = 1$.

PMMA glue is resolvable in acetone and can therefore be removed from the implant without leaving any residue. Stabilite® appears to be appropriate glue for the purpose of the main study.

Since the first pull-out will not give necessary information and bears the danger of harming the bone interface without destroying it, the interface in the main study was further weakened by applying a release agent to the implant before insertion (Section 3.2.5).

B Algorithm for Cement Layer Morphology Analysis

B.1 Flowchart of MATLAB® Routine

The 3D surface and volume model of each specimen was processed using the MATLAB® routine *avizo_rotate.m* (**Figure B-1**). The output file *output_avrot.mat* contains the data sets (coordinate and node definitions) required for parameter determination using MATLAB® routine *cementPar.m*.

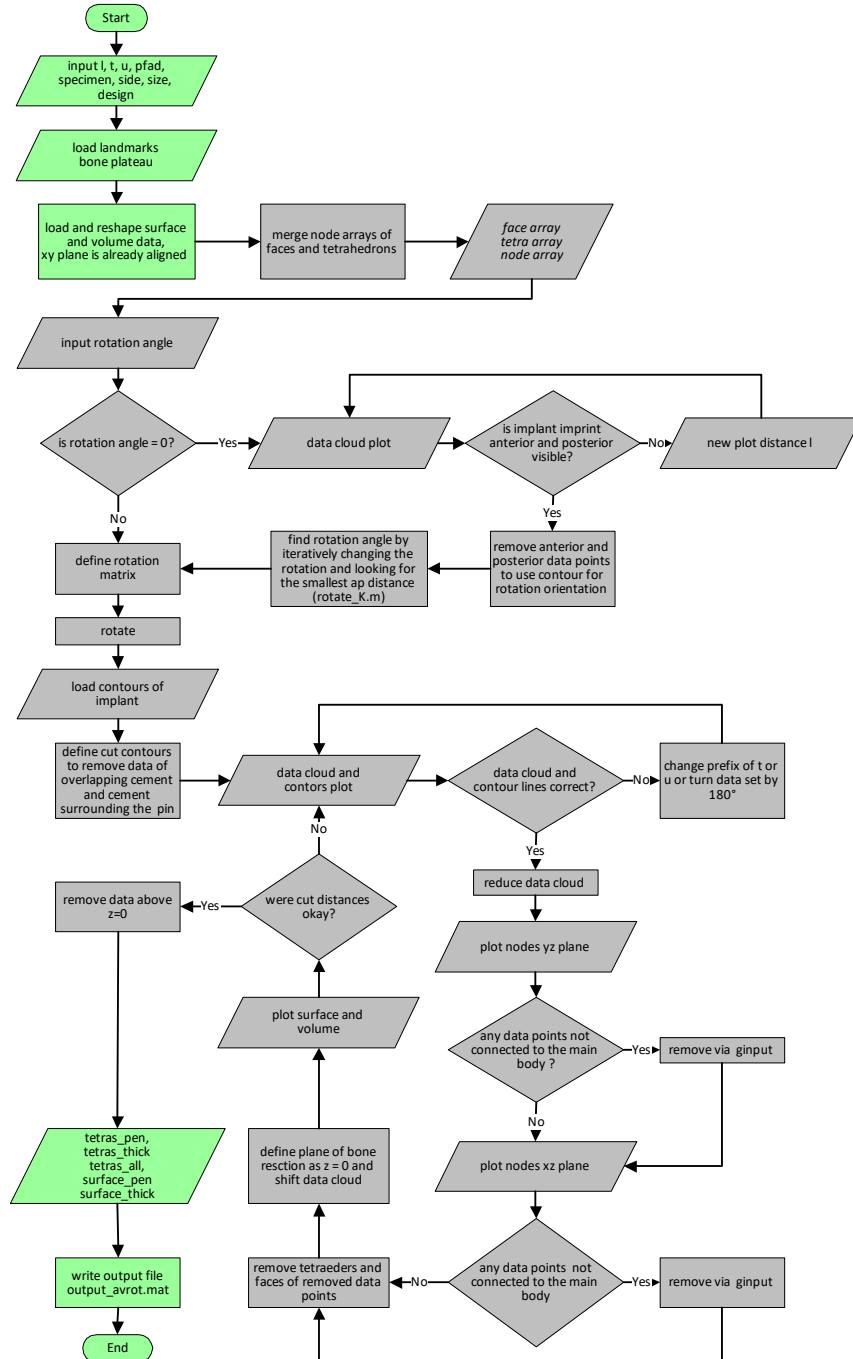


Figure B-1: Flowchart of the MATLAB® routine applied to the 3D surface and volume models generated in Avizo®. Input variables: l = z range of data plotted for overview, t = distance to remove cement around the stem, u = distance to remove excess cement, pfad = folder with models sorted by specimen, specimen = patient ID, side = side of tibial pair, size = implant size (2.5, 3, 4, 5) and design = implant design (1: CoCr MBT Keeled, 2: Ti Fixed Bearing).

B.2 Segmentation Thresholds

Table B-1: Segmentation thresholds in Hounsfield Units for lab-implanted specimens mechanically tested in the current thesis.

Patient	Side	Design	Implant <i>in situ</i>	Threshold between...		
				exterior-bone	cement-bone	cement-implant
3005	L	CoCrMBTKeeled	no	-700	500	-
3005	R	CoCrMBTKeeled	no	-700	500	-
3006	L	CoCrMBTKeeled	no	-700	500	-
3006	R	CoCrMBTKeeled	no	-700	500	-
3007	L	CoCrMBTKeeled	no	-700	500	-
3007	R	CoCrMBTKeeled	no	-700	500	-
3008	L	CoCrMBTKeeled	no	-700	600	-
3008	R	CoCrMBTKeeled	no	-700	600	-
3009	R	CoCrMBTKeeled	no	-700	600	-
3009	L	CoCrMBTKeeled	no	-700	600	-
3010	R	CoCrMBTKeeled	no	-700	600	-
3010	L	CoCrMBTKeeled	no	-700	600	-
3011	L	CoCrMBTKeeled	no	-700	600	-
3011	R	CoCrMBTKeeled	no	-700	600	-
3012	L	CoCrMBTKeeled	no	-700	600	-
3012	R	CoCrMBTKeeled	no	-700	600	-
3013	L	CoCrMBTKeeled	no	-700	500	-
3013	R	CoCrMBTKeeled	no	-700	500	-
3014	L	CoCrMBTKeeled	no	-700	500	-
3014	R	CoCrMBTKeeled	no	-700	500	-
3015	R	CoCrMBTKeeled	no	-700	600	-
3015	L	CoCrMBTKeeled	no	-700	600	-
3016	R	CoCrMBTKeeled	no	-700	600	-
3016	L	CoCrMBTKeeled	no	-700	600	-
3017	R	CoCrMBTKeeled	no	-700	500	-
3017	L	CoCrMBTKeeled	no	-700	500	-
3019	R	CoCrMBTKeeled	no	-700	500	-
3019	L	CoCrMBTKeeled	no	-700	500	-
3020	R	CoCrMBTKeeled	no	-700	500	-
3020	L	CoCrMBTKeeled	no	-700	500	-
3021	R	CoCrMBTKeeled	no	-700	500	-
3021	L	CoCrMBTKeeled	no	-700	500	-
3022	R	CoCrMBTKeeled	no	-700	600	-
3022	L	CoCrMBTKeeled	no	-700	600	-
3023	L	CoCrMBTKeeled	no	-700	500	-
3023	R	CoCrMBTKeeled	no	-700	500	-

Table B-2: Segmentation thresholds in Hounsfield Units for lab-implanted specimens mechanically tested in the pilot study on tibial implant design of the current thesis (Appendix A.1).

Patient	Side	Design	Implant <i>in situ</i>	Threshold between...		
				exterior-bone	cement-bone	cement-implant
3001	R	CoCrMBTKeeled	no	-700	500	-
3001	L	TiFixedBearing	yes	-700	500	1 960
3002	R	TiFixedBearing	yes	-700	600	2 321
3002	L	CoCrMBTKeeled	no	-700	500	-
3003	R	CoCrMBTKeeled	no	-700	600	-
3003	L	TiFixedBearing	yes	-700	600	2 131
3004	R	TiFixedBearing	yes	-700	700	2 173
3004	L	CoCrMBTKeeled	no	-700	500	-

Table B-3: Segmentation thresholds in Hounsfield Units for lab-implanted specimens from previous experimental series¹².

Patient	Side	Design	Implant <i>in situ</i>	Threshold between...		
				exterior-bone	cement-bone	cement-implant
1	L	Ti Fixed Bearing	yes	-700	600	2 200
1	R	Ti Fixed Bearing	CT data not available	-	-	-
2	L	Ti Fixed Bearing	yes	-700	600	1 267
2	R	Ti Fixed Bearing	yes	-700	500	1 677
3	L	Ti Fixed Bearing	yes	-700	600	1 925
3	R	Ti Fixed Bearing	yes	-700	600	1 851
4	L	Ti Fixed Bearing	yes	-700	600	1 814
4	R	Ti Fixed Bearing	yes	-700	600	1 872
5	L	Ti Fixed Bearing	yes	-700	600	1 710
5	R	Ti Fixed Bearing	yes	-700	600	1 386
6	L	Ti Fixed Bearing	yes	-700	800	2 200
6	R	Ti Fixed Bearing	yes	-700	600	1 867

B.3 Inter-Rater Reliability

Methods

Inter-rater reliability of the procedure for parameter determination was analysed by determining the intra-class correlation coefficient (ICC) between two observers. The observers performed the segmentation of the cement layer from CT scans and parameter determination using the MATLAB® routine on 17 specimens that were randomly chosen from the 36 specimens of this thesis (Chapter 3). The distance between implant contour and cut contour to remove the excessing cement and cement around the stem were chosen independently by the observers, as well as the initial value for automatic thresholding between bone and cement.

The analysis was performed on 6 basic length, volumetric and areal measures: the mean cement penetration depth (*MeanPen*), the overall volume of the cement layer (*Vol*), the absolute volume of the penetrating cement layer (*VolPen*), the volume of the cement above the tibial plateau (*VolThick*), the area of the lower surface of the penetrating cement (*Surf*) and the evaluation area (*evalA*).

The ICC indicates, whether the variance between two observers based on a pairwise analysis is larger than the variance within the results of each observer. In this study, the ICC was determined based on a two-way mixed model according to the guidelines of Shrout & Fleiss²¹³ for the conditions given in this study: two observers that were selected specifically for their medical-technical background rated all cases. Analysis was carried out using SPSS (IBM® SPSS® Statistics 21, IBM Corporation, Armonk, NY, USA). Since the absolute value of the parameter may influence the final conclusion, it is of interest how well a single observer assesses the real values, which is referred to as “absolute agreement definition” in SPSS.

Results and Conclusions

In the current study inter-rater reliability was between 0.81 and 0.98 (**Table B-3**), which corresponds to proportions of variance of 81 % to 98 % that are due to differences between the specimens and not due to differences between the observer’s ratings.

An additional pairwise T test revealed that *MeanPen* and *VolPen* were significantly larger for Observer 1 ($p < 0.001$). It was concluded that the resection plane level was slightly lower when its definition was performed by Observer 2, since the volume of the cement above the plateau was larger for Observer 2, although not significantly ($p = 0.150$). The difference between *MeanPen* of Observer 1 and 2 was 0.26 mm and thus lower than the CT resolution of 0.46 mm. The reproducibility of segmentation was therefore rated as good.

EvalA was not significantly different ($p = 0.256$) between the observers and the corresponding ICC was larger (0.98), so the selection of the area to evaluate was also reproducible.

Table B-4: Intra-class coefficients of 6 selected measures describing the cement layer morphology.

Parameter	Observer 1	Observer2	p (T test)	ICC
-----------	------------	-----------	------------	-----

Appendices

<i>MeanPen</i>	1.48	1.22	< 0.001	0.89
<i>VolPen</i>	1635.30	1193.88	< 0.001	0.83
<i>VolThick</i>	2527.14	2711.47	0.150	0.92
<i>Surf</i>	2093.67	1896.65	0.009	0.81
<i>evalA</i>	1832.28	1850.03	0.256	0.98

B.4 Validation Study CT Segmentation

Methods

Validation of the CT-based procedure of cement layer modelling was approached by comparing measures taken from cross-sections of cadaveric specimens with cement layer to measures from the corresponding 3D model of the cement layer. Four specimens from the current study that failed at the cement-implant interface were cut using a diamond band saw (**Figure B-2, A**): 3002 R, 3005 R, 3007 R and 3011 R. Specimens were selected to cover low and high cement penetration depth to receive validation over a large range of values. Each two specimens were used to generate sections in transversal and frontal plane (**Figure B-2, C and D**). The bone phase of the sections were stained using blue ink to increase the contrast between bone and cement and simplify the measurement. The cut slices thickness was measured at four points to derive the location of the sectional surfaces within the specimen. This information was used to transfer the plane to the 3D models. The sectional surfaces were photographed together with measuring devices in order to receive the scale for the measurement. Care was taken to prevent inclination of the section surface and the measuring devices were placed at the level of the section surface. The measurements were performed using Gimp (GIMP 2.8.10, gimp.org²¹⁴). A grid was superimposed to the photo and length measurements were taken from defined locations.

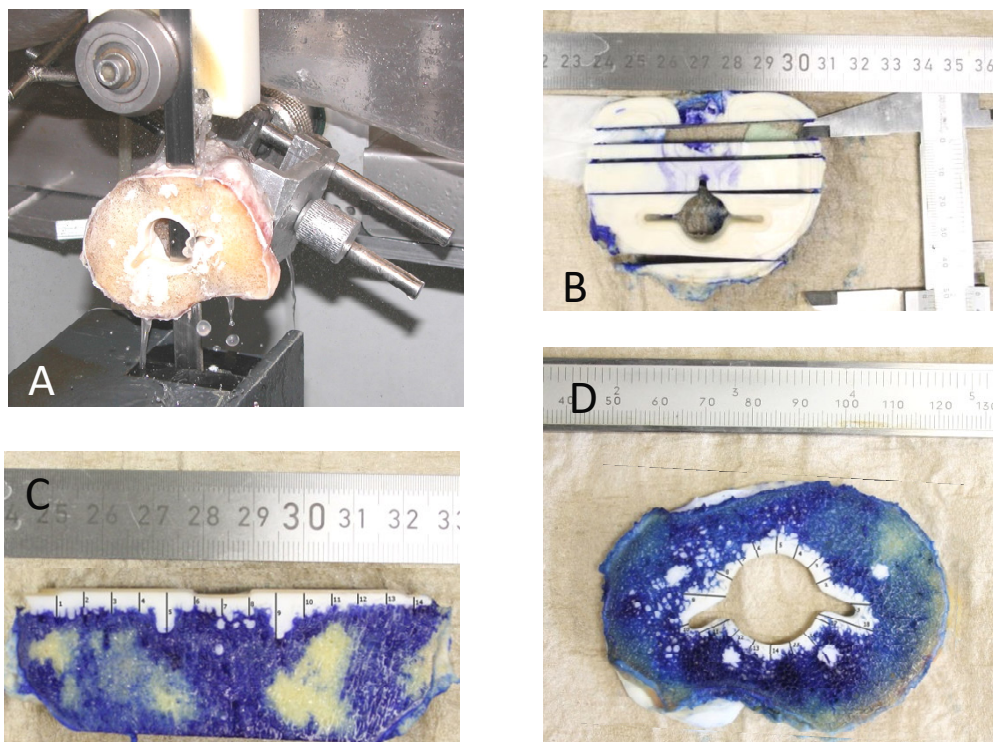


Figure B-2: Preparation of the cadaveric sections for measuring. A: Cutting of the specimens. B: Determining the geometry of the cut slices to transfer the position of cut the 3D models later. C: Frontal cut with measuring device and indicated measurements. D: Transversal cut with measuring device and indicated measurements.

Measurements to validate were taken from the 3D models of the cement layers that were virtually cut using Avizo® (version 7, VSG, Burlington, MA, USA). The positions for the cuts

were derived from the specimen section slices (**Figure B-3**). Correctness of the cut plane position was surveyed by comparison of the cement pattern in the respective sectional plane. Measurements were performed in Avizo® using the same superimposed grid as in the measurement at the specimen sections. Measurements were taken from the same locations as on the specimen sections.

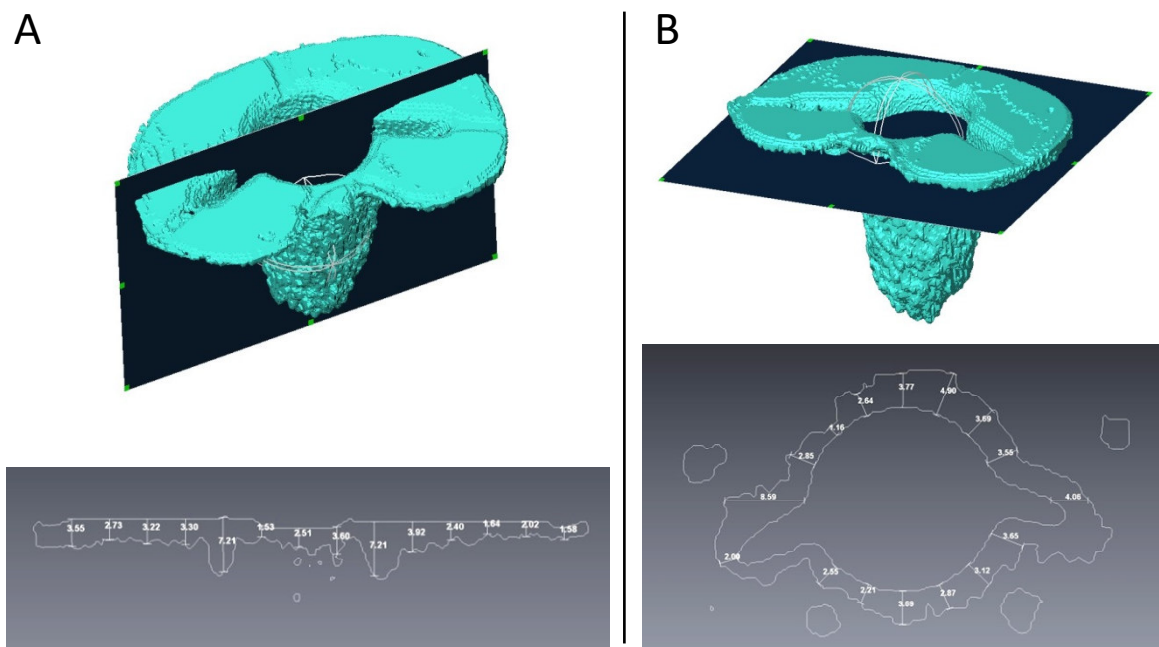


Figure B-3: Generation of the cut from the 3D models of the cement layers for measurement. Measurements are obtained from the cut contour at the same locations as in the specimens sections. A: Generation of frontal cuts, the blue canvas is the cut plane. B: Generation of transversal cuts.

The obtained values were compared in a pairwise fashion. Frontal and transversal cuts were pooled. Results from the 3D models were compared to the corresponding values from the sections using a pairwise T test or Related Samples Wilcoxon Signed Rank test. Results from the 3D models were normalised to the corresponding values from the sections to determine the relative difference between the two approaches. The absolute difference between 3D model and specimen section value of a pair was determined. Measurements were separated to three groups according to the magnitude of the values from the specimen sections: < 3 mm, 3 to 5 mm and > 5 mm. The three groups were compared using one-way ANOVA with Bonferroni post-hoc or Kruskal-Wallis test with subsequent Mann-Whitney U test and adjusted type-1 error level. The type-1 error level α was 0.05. Statistical evaluation was done using SPSS (IBM® SPSS® Statistics 21, IBM Corporation, Armonk, NY, USA).

Results

In total, 159 measurement pairs were derived from 12 specimen sections. Values from the 3D models were significantly smaller than the values from the specimen sections ($p < 0.001$, Related Samples Wilcoxon Signed Rank test). The median difference was 4 %. There was no significant influence of the magnitude of the measurement on the difference between 3D-model measurements and specimen-section measurement ($p > 0.026$, with corrected type-1 error level $\alpha/3 = 0.017$).

Conclusion

The length measures derived from the 3D model were smaller than the actual measures. However, the difference was merely 4 %, which is below the resolution of the CT scanner of 0.46 in all directions, when a measure of about 3 mm is considered. The values for cement penetration depth determined in this thesis were lower, so the approach of analysing the cement layer morphology based on CT scan reconstructions is afflicted with very small error and therefore considered appropriate.

C Supplementary Data

C.1 Supplementary Data of Chapter 2

Table C-1: Studies that applied mechanical testing of human or artificial bone implanted with cemented UKA or TKA. Type of specimen, type of fixation, load mode, measurement device, measure and measurement site are listed (MTPM = Maximum total point motion).

Authors	Type	Fixation	Loadmode	Measurement	Measure	Measurementsite
Sala <i>et al</i> , 1999 ¹⁵⁵	lab-implanted cadavers	press-fit, cemented	rotation	linear extensometer	rotation	between implant and bone
Luring <i>et al</i> , 2006 ¹⁷	synthetic composite tibiae	cemented	compression	displacement sensor	lift-off	between implant and bone
Skwara <i>et al</i> , 2009 ¹⁵⁸	lab-implanted cadavers	cemented	compression	RSA	MTPM lift off subsidence rotation	-
Rao <i>et al</i> , 2010 ¹⁵⁷	post-mortem retrievals	Press-fit, cemented	compression	linear extensometer	lift off depression	between implant and bone
Turgay <i>et al</i> , 2011 ¹⁵⁹	lab-implanted cadavers	Press-fit, cemented	compression	RSA	MTPM subsidence lift off rotation	-
Turgay <i>et al</i> , 2011 ¹⁸⁴	lab-implanted cadavers	cemented	compression	timing device, CT reconstructions	explantation time, remaining bone volume	-
Schlegel <i>et al</i> , 2011 ¹²	lab-implanted cadavers	cemented	tensile	force sensor	failure force	cement-bone, cement-implant
Gebert de Uhlenbrock <i>et al</i> , 2012 ²⁹	post-mortem retrievals	cemented	tensile	force sensor	failure force	cement-bone, cement-implant
Cawley <i>et al</i> , 2012 ¹⁸²	synthetic composite tibiae	cemented	vertical compression (0°, 15° flexion)	strain gauges FE	strain stress	'cortical' shell, within cancellous bone
Grupp <i>et al</i> , 2013 ¹⁵⁶	lab-implanted cadavers	cemented	vertical compression (15° flexion)	3D motion analysis, force sensor	failure force	implant inlay and diaphyseal bone
Mann <i>et al</i> , 2014 ¹⁶⁶	post-mortem retrievals	cemented	compression	Digital Image Correlation (DIC)	strain micromotion	cortical shell, interpolated trabecular strain
Peters <i>et al</i> , 2003 ¹⁵	lab-implanted cadavers	cemented	compression	inductive displacement transducers	micromotion	between implant and bone

Table C-2: Micro-mechanical testing of samples from the cement-bone interface. Sample origin, sample type, load mode, input and output measures are listed. Studies that base on the same specimen pool have been grouped. Lab-prepared specimens were cut from trabecular bone and merged with cement; Lab-implanted specimens were cut from a cement-bone interface obtained from arthroplasties produced in the lab; Post-mortem retrievals were cut from arthroplasties harvested from deceased donors.

Authors	Origin	Type	Load mode	Input measure	output measure
Askew <i>et al</i> , 1983 ¹⁵⁴	tibia, femur	lab-prepared	tension	cement pressure penetration depth	fixation strength, bone area fraction
Mann <i>et al</i> , 1997 ¹⁶¹	femoral THA	lab-implanted	tension normal to interface	radial penetration depth	tensile strength
Mann <i>et al</i> , 1999 ²¹⁵	femoral THA	lab-implanted	tensile, shear	penetration depth load direction	strength
Kim <i>et al</i> , 2004 ²¹⁶	femoral THA	lab-implanted	tensile fatigue	number of cycles	cycles to failure, stiffness, displacement
Kim <i>et al</i> , 2004 ²¹⁷	femoral THA	lab-implanted	shear fatigue	number of cycles	cycles to failure, strain
Janssen <i>et al</i> , 2008 ¹⁶⁵	femoral THA	lab-implanted FE	tension compression	friction coefficient micro CT density cement stiffness	interface stiffness
Mann <i>et al</i> , 2008 ²⁰⁶ Janssen <i>et al</i> , 2009 ²¹⁸	femoral THA	lab-implanted FE	tension- compression	micro CT density	interface stiffness, micromotion
Waanders <i>et al</i> , 2009 ²¹⁹	femoral THA	lab-implanted FE	tensile	micro CT density contact erosion algorithm	crack pattern
Waanders <i>et al</i> , 2010 ¹⁶²	femoral THA	lab-implanted FE	tensile, shear	penetration contact micro CT density	contact area estimate strength, stiffness
Miller <i>et al</i> , 2010 ⁴⁷	femoral THA	post-mortem retrievals	tension, compression	stereological contact fraction	tensile strength stiffness
Waanders <i>et al</i> , 2012 ²²⁰	femoral THA	post-mortem retrievals FE	torque	contact elements	micromotion, global stiffness, position of stem
Miller <i>et al</i> , 2014 ²¹ Goodheart <i>et al</i> , 2014 ²²	tibial TKA	lab-implanted post-mortem retrievals	compression	<i>in vivo</i> time	penetration depth contact fraction micromotion
Howard <i>et al</i> , 2014 ²²¹	femoral TKR	post-mortem retrievals	-	<i>in vivo</i> time	penetration depth contact fraction
Graham <i>et al</i> , 2003 ²⁸	bovine	lab-prepared	Tensile with crack initiation	porosity, trabecular orientation, cement pressure, penetration depth	fixation strength
Tozzi <i>et al</i> , 2014 ²²²	bovine	lab-prepared FE	compression	BV/TV, micro CT density, bone type	stress, displacement

C.2 Supplementary Data of Chapter 3

C.2.1 Determination of Bone Mineral Density

Bone mineral density in this section was determined based on a custom-made dipotassium phosphate (K_2HPO_4) phantom that was scanned with each tibia pair. The phantom consisted of three vials containing mineral solutions of different densities, representing the range of BMD in human specimens: 0, 100 and 500 mg K_2HPO_4 per ml of distilled water. Grey values in Hounsfield units (HU) were derived from the CTs and converted to density values in mg K_2HPO_4 per cm^3 (mg/cm^3). Calibration was performed based on mean HU from a VOI of 1 800 mm^3 within each phantom vial (Figure 3-1, Section 3.2.2). The regression slope between these three data points delivered a conversion factor from grey scale to *BMD* for each tibia pair.

C.2.2 Implantation Protocol

The implantation protocols cover information about specimens and the implants they were implanted with. Implant size, ID, and processing time of cementation and cement curing were documented (**Table C-3**).

Table C-3: Implantation parameters of specimens from this thesis (L: left, R: right, technique is defined as in Section 3.2.4.

Patient	Side	Gender	Date	Technique	Implant ID	Implant size	time from cement mixing to implant impaction [min]	time of loaded cement curing [min]
3005	L	M	18012013	CONTROL	3	3	3:45	11:27
3005	R	M	18012013	FULL	10	3	3:19	11:58
3006	L	M	22022013	CONTROL	1	3	3:40	12:00
3006	R	M	22022013	SYRINGE	3	3	3:40	16:03
3007	L	F	18012013	FULL	4	3	3:29	14:50
3007	R	F	18012013	CONTROL	2	3	3:45	15:00
3008	L	F	16012013	CONTROL	2	3	4:20	12:00
3008	R	F	16012013	GUN	4	3	3:42	12:45
3009	L	M	22022013	SYRINGE	6	4	3:51	15:31
3009	R	M	22022013	CONTROL	8	4	3:55	11:55
3010	L	M	22022013	SYRINGE	12	2.5	3:25	12:20
3010	R	M	22022013	CONTROL	11	2.5	4:15	12:17
3011	L	M	18012013	CONTROL	8	4	3:00	12:00
3011	R	M	18012013	FULL	6	4	3:15	12:30
3012	L	F	17012013	LAYERED	3	3	3:10	12:11
3012	R	F	17012013	CONTROL	1	3	3:11	11:57
3013	L	F	17012013	CONTROL	12	2.5	3:28	14:20
3013	R	F	17012013	LAYERED	9	2.5	3:00	12:10
3014	L	M	17012013	LAYERED	15	5	2:50	12:08
3014	R	M	17012013	CONTROL	16	5	3:20	12:03
3015	L	M	22022013	SYRINGE	7	4	3:50	12:53
3015	R	M	22022013	CONTROL	5	4	3:58	12:47
3016	L	F	16012013	GUN	5	4	4:12	12:20
3016	R	F	16012013	CONTROL	7	4	-	10:55
3017	L	F	17012013	CONTROL	11	2.5	3:13	14:45
3017	R	F	17012013	LAYERED	10	2.5	3:30	14:00
3019	L	F	16012013	CONTROL	10	2.5	4:05	11:05
3019	R	F	16012013	GUN	11	2.5	3:35	12:42
3020	L	M	18012013	FULL	5	4	3:30	17:10
3020	R	M	18012013	CONTROL	7	4	3:57	14:30
3021	L	M	22022013	CONTROL	10	2.5	3:55	13:08
3021	R	M	22022013	SYRINGE	9	2.5	3:38	13:02
3022	L	M	16012013	GUN	14	5	4:07	12:20
3022	R	M	16012013	CONTROL	13	5	-	12:00
3023	L	M	22022013	CONTROL	14	5	3:45	12:58
3023	R	M	22022013	SYRINGE	13	5	4:03	13:05

C.2.3 Raw Data of Specimens

Results from cement layer morphology analysis are given in **Table C-4** to **Table C-7**.

Table C-4: Results for the tested specimens of Group FULL vs. CONTROL. R indicates right tibia and L indicates left tibia. Failure modes: glue = at the glue interface, diaphysis = at the diaphysis, bulk = within bulk bone.

Treatment	ID	<i>BMD</i> [mg/cm ³]	<i>MedPen</i> [mm]	<i>Vol_{spec}</i> [mm]	<i>Aproj_o</i> [-]	<i>AprojEx</i> [mm ²]	<i>F</i> [N]	<i>S</i> [MPa]	Failure Mode
FULL	3005 R	100	1.21	1.11	0.76	1 653.16	6 964	4.21	glue
FULL	3007 L	21	1.78	1.76	0.92	2 011.69	3 073	1.53	bulk
FULL	3011 R	112	0.68	0.62	0.50	1 258.90	9 941	7.90	glue
FULL	3020 L	110	0.82	0.66	0.86	2 158.93	5 924	2.74	glue
Mean (SD)		86 (43)	1.12 (0.49)	1.04 (0.53)	0.76 (0.19)	1 770.67 (401.89)	6 476 (2 836)	4.10 (2.76)	
CONTROL	3005 L	115	1.11	0.99	0.82	1 788.41	8 204	4.59	bulk
CONTROL	3007 R	29	1.27	1.17	0.74	1 616.93	3 331	2.06	glue
CONTROL	3011 L	109	1.15	1.00	0.81	2 019.17	6 971	3.45	diaphysis
CONTROL	3020 R	108	0.85	0.80	0.80	1 994.04	6 072	3.05	glue
Mean (SD)		90 (41)	1.10 (0.18)	0.99 (0.15)	0.79 (0.04)	1 854.64 (189.2)	6 145 (2 069)	3.29 (1.05)	

Table C-5: Results for the tested specimens of Group GUN vs. CONTROL. R indicates right tibia and L indicates left tibia. Failure modes: glue = at the glue interface, diaphysis = at the diaphysis, bulk = within bulk bone. grey indicated specimen was removed from strength analysis, due to the unclear failure mode

Treatment	ID	<i>BMD</i> [mg/cm ³]	<i>MedPen</i> [mm]	<i>Vol_{spec}</i> [mm]	<i>Aproj_o</i> [-]	<i>AprojEx</i> [mm ²]	<i>F</i> [N]	<i>S</i> [MPa]	Failure Mode
GUN	3008 R	59	3.42	3.03	0.92	1 996.18	-	-	unclear
GUN	3016 L	67	1.69	1.45	0.89	2 227.12	5 712	2.56	bulk
GUN	3019 R	72	1.86	1.63	0.92	1 841.26	5 281	2.87	bulk
GUN	3022 L	137	1.80	1.57	0.88	2 628.14	8 686	3.31	glue
Mean (SD)		84 (36)	2.19 (0.82)	1.92 (0.74)	0.90 (0.02)	2 173.18 (342.25)	6 560 (1 854)	2.91 (0.37)	
CONTROL	3008 L	55	1.53	1.45	0.92	1 994.10	3 605	1.81	bulk
CONTROL	3016 R	65	1.01	1.05	0.78	1 964.44	4 771	2.43	glue
CONTROL	3019 L	80	1.08	0.90	0.91	1 821.34	4 415	2.42	bulk
CONTROL	3022 R	128	0.67	0.54	0.60	1 778.45	5 794	3.26	glue
Mean (SD)		82 (32)	1.07 (0.35)	0.99 (0.38)	0.80 (0.15)	1 889.58 (105.73)	4 646 (907)	2.48 (0.60)	

Table C-6: Results for the tested specimens of Group LAYERED vs. CONTROL. R indicates right tibia and L indicates left tibia. Failure modes: glue = at the glue interface, diaphysis = at the diaphysis, bulk = within bulk bone.

Treatment	ID	<i>BMD</i> [mg/cm ³]	<i>MedPen</i> [mm]	<i>Vol_{spec}</i> [mm]	<i>Aprojo</i> [-]	<i>AprojEx</i> [mm ²]	<i>F</i> [N]	<i>S</i> [MPa]	Failure Mode
LAYERED	3012 L	94	0.80	0.72	0.78	1 687.99	6 737	3.99	bulk
LAYERED	3013 R	68	1.97	1.80	0.92	1 854.88	6 531	3.52	glue
LAYERED	3014 L	61	1.41	1.20	0.90	2 667.81	4 825	1.81	glue
LAYERED	3017 R	39	1.48	1.31	0.79	1 585.84	5 627	3.55	bulk
Mean (SD)		65 (23)	1.42 (0.48)	1.26 (0.44)	0.85 (0.07)	1 949.13 (491.79)	5 930 (880)	3.22 (0.96)	
CONTROL	3012 R	94	1.38	1.21	0.90	1 962.08	8 996	4.58	glue
CONTROL	3013 L	80	1.64	1.43	0.85	1 699.68	4 993	2.94	diaphysis
CONTROL	3014 R	83	1.03	0.87	0.81	2 424.28	5 491	2.27	diaphysis
CONTROL	3017 L	37	1.96	1.79	0.85	1 714.41	3 482	2.03	bulk
Mean (SD)		73 (25)	1.50 (0.39)	1.33 (1.39)	0.85 (0.04)	1 950.11 (338.26)	5 741 (2 332)	2.96 (1.15)	

Table C-7: Results for the tested specimens of Group SYRGUN vs. CONTROL. R indicates right tibia and L indicates left tibia. Failure modes: glue = at the glue interface, bone = at the bone interface, bulk = within bulk bone.

Treatment	ID	<i>BMD</i> [mg/cm ³]	<i>MedPen</i> [mm]	<i>Vol_{spec}</i> [mm]	<i>Aprojo</i> [-]	<i>AprojEx</i> [mm ²]	<i>F</i> [N]	<i>S</i> [MPa]	Failure Mode
SYRGUN	3006 R	110	0.50	0.37	0.62	1 348.76	1 088	0.81	bone
SYRGUN	3009 L	118	0.48	0.32	0.45	1 135.53	469	0.41	bone
SYRGUN	3010 L	154	0.21	0.24	0.32	647.58	517	0.80	bone
SYRGUN	3015 L	79	0.28	0.15	0.52	1 313.84	608	0.46	bone
SYRGUN	3021 R	85	0.71	0.51	0.84	1 681.20	613	0.36	bone
SYRGUN	3023 R	77	0.39	0.25	0.71	2 120.90	1 442	0.68	glue
Mean (SD)		104 (30)	0.43 (0.18)	0.31 (0.12)	0.58 (0.19)	1 374.63 (498.21)	790 (389)	0.59 (0.20)	
CONTROL	3006 L	104	2.42	2.17	0.90	1 957.26	10 338	5.28	bone
CONTROL	3009 R	112	1.56	1.33	0.89	2 240.40	9 371	4.18	glue
CONTROL	3010 R	142	1.38	1.22	0.76	1 528.00	8 150	5.33	bulk
CONTROL	3015 R	78	0.47	0.41	0.50	1 246.32	6 934	5.56	glue
CONTROL	3021 L	83	1.55	1.35	0.91	1 830.98	7 320	4.00	bulk
CONTROL	3023 L	69	1.57	1.33	0.83	2 462.95	10 550	4.28	bulk
Mean (SD)		98 (27)	1.49 (0.62)	1.30 (0.56)	0.80 (0.16)	1 877.65 (448.00)	8 777 (1539)	4.77 (0.69)	

C.2.4 Statistics Results

Parametric testing was reported since data distribution within groups and sides did not show outliers (which would increase error-proneness). Applying non-parametric tests to normal data would decrease the power, which is reflected by the low but not significant p values in non-parametric testing (**Table C-8**, **Table C-9**). The distributions were tested for normality using Shapiro-Wilk test and type-I error level of 0.05.

Table C-8: P values for parametric and non-parametric testing of within group comparisons of *MedPen*, *Aproj₀* and *Vol_{spec}*. Parametric testing was done by a pairwise T test, non-parametric testing by a Related-Samples Wilcoxon Signed Rank test. Significant p values are flagged with *.

	FULL		GUN		LAYERED		SYRGUN	
	parametric	non-parametric	parametric	non-parametric	parametric	non-parametric	parametric	non-parametric
<i>MedPen</i>	0.910	0.715	0.026*	0.068	0.757	0.465	0.006*	0.028*
<i>Aproj₀</i>	0.690	> 0.999	0.059	0.068	0.281	> 0.999	0.011*	0.046*
<i>Vol_{spec}</i>	0.837	> 0.999	0.034*	0.068	0.800	0.465	0.004*	0.028*

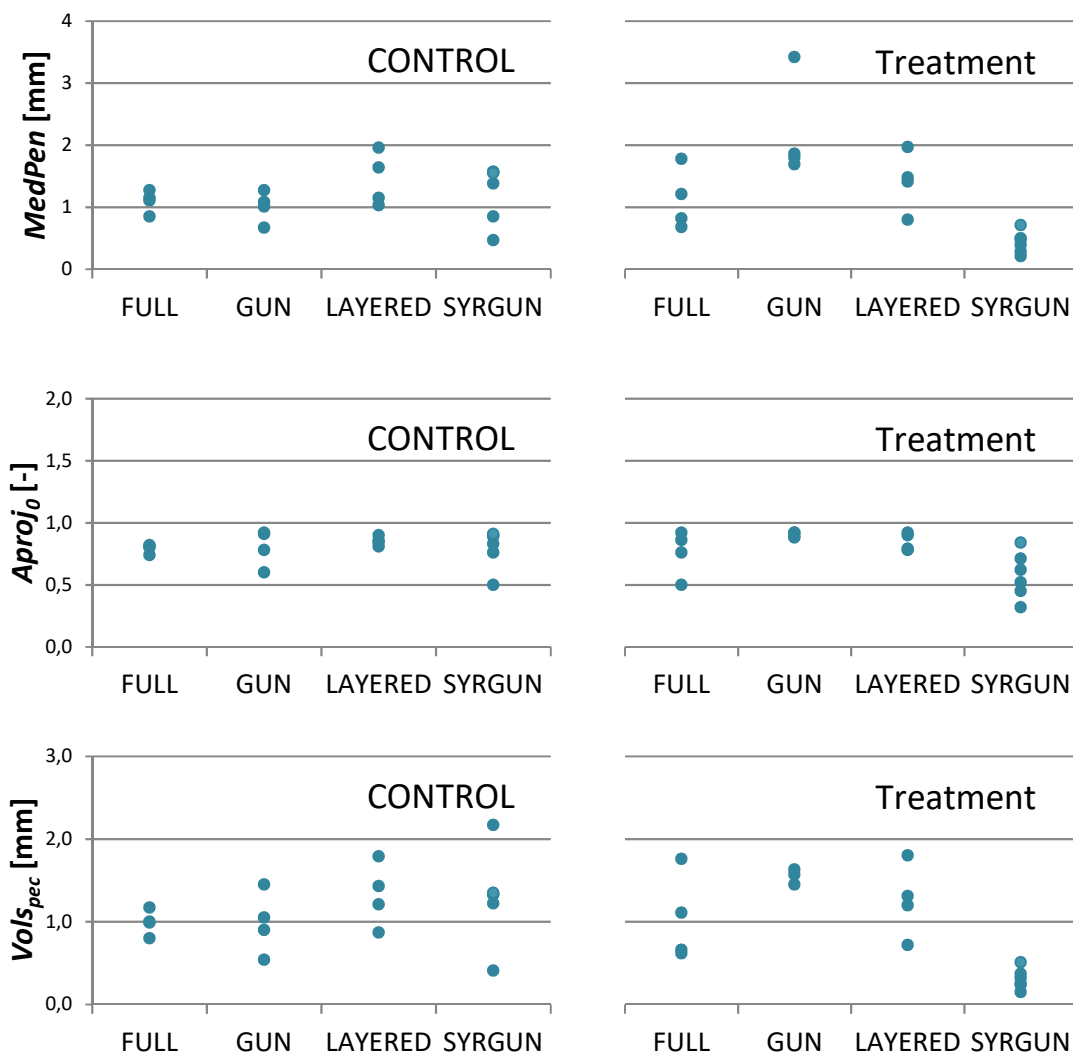


Figure C-1: Data distribution of *MedPen* and *Aproj₀* in each group, separated to treatment and CONTROL side. The data shows no obvious outliers, although sample size is low.

Table C-9: P values for parametric and non-parametric testing of within group comparisons of $MedPen_{RIM}$, $Aproj_{0,RIM}$ and $Vol_{0,RIM}$. Parametric testing was done by a pairwise T test, non-parametric testing by a Related-Samples Wilcoxon Signed Rank test. Significant p values are flagged with *.

	FULL		GUN		LAYERED		SYRGUN	
	parametric	non-parametric	parametric	non-parametric	parametric	non-parametric	parametric	non-parametric
$MedPen_{RIM}$	0.849	>0.999	0.063	0.068	0.935	>0.999	0.012*	0.028*
$Aproj_{0,RIM}$	0.780	0.715	0.150	0.144	0.919	>0.465	0.071	0.075
$Vol_{spec,RIM}$	0.972	>0.999	0.067	0.068	0.875	>0.715	0.007*	0.028*

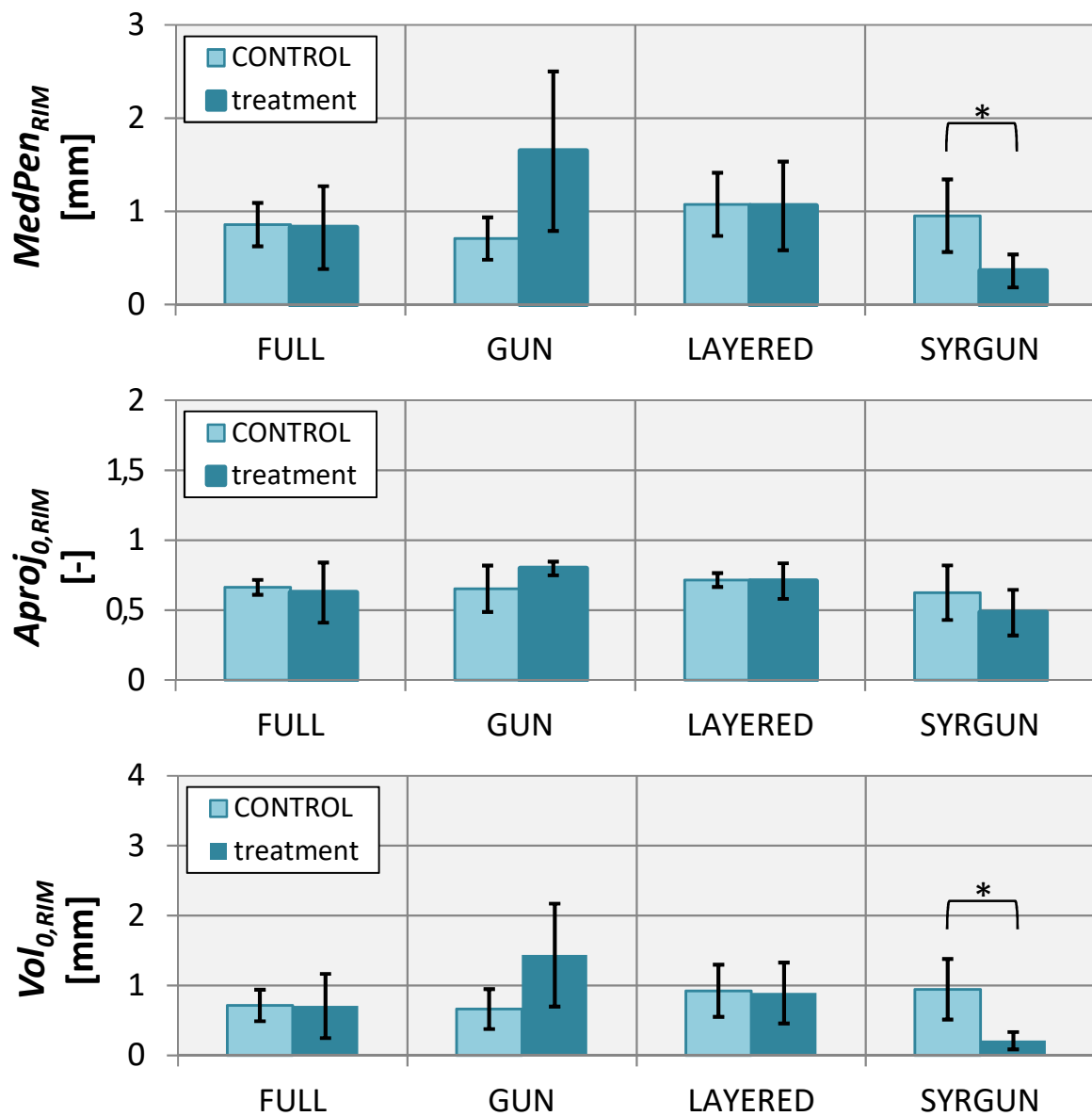


Figure C-2: Mean values of $MedPen_{RIM}$, $Aproj_{0,RIM}$ and $Vol_{0,RIM}$ of the RIM region sorted by group and CONTROL vs. treatment cementation technique (error bars indicate standard deviation, each group n = 4 vs. 4). Significant difference is indicated by *.

C.3 Supplementary Data of Chapter 4

C.3.1 Specimens and Implants

The specimens used in Chapter 4 are listed in **Table C-10** to **Table C-12**.

Table C-10: Specimens and implants of pilot study on tibial implant design that were evaluated in Chapter 4 of this thesis.

Patient	Side	BMD [mg/cm ³]	Implant type	Implant size	Pulsatile lavage	Failure force [N]	Failure mode
3001	L	13	Ti Fixed Bearing	3	0	1 268	bulk bone
3001	R	16	CoCr MBT Keeled	3	0	181	implant interface
3002	L	62	CoCr MBT Keeled	3	0	719	implant interface
3002	R	55	Ti Fixed Bearing	3	0	1 605	implant interface
3003	L	65	Ti Fixed Bearing	3	0	1 208	implant interface
3003	R	66	CoCr MBT Keeled	3	0	376	implant interface
3004	L	106	CoCr MBT Keeled	3	0	543	implant interface
3004	R	122	Ti Fixed Bearing	3	0	1 751	implant interface

Table C-11: Specimens and implants of the previous study that were evaluated in Chapter 4 of this thesis. Grey indicates case was excluded from analysis, since the CT data were not available. The case with mixed failure mode was considered as implant interface failure.

Patient	Side	BMD [mg/cm ³]	Implant type	Implant size	Pulsatile lavage	Failure force [N]	Failure mode
1	L	41	Ti Fixed Bearing	3	0	615	bone interface
1	R	31	Ti Fixed Bearing	3	1	1 377	implant interface
2	L	90	Ti Fixed Bearing	5	1	864	implant interface
2	R	57	Ti Fixed Bearing	5	0	242	bone interface
3	L	78	Ti Fixed Bearing	3	1	1 287	implant interface
3	R	63	Ti Fixed Bearing	3	0	465	bone interface
4	L	68	Ti Fixed Bearing	4	0	683	bone interface
4	R	69	Ti Fixed Bearing	3	1	1 142	implant interface
5	L	97	Ti Fixed Bearing	4	0	574	mixed
5	R	110	Ti Fixed Bearing	4	1	1 391	implant interface
6	L	93	Ti Fixed Bearing	3	1	1 263	implant interface
6	R	86	Ti Fixed Bearing	3	0	562	bone interface

Table C-12: Specimens and implants of the current thesis that were evaluated in Chapter 4 of this thesis. Grey indicated value was excluded, since the failure mode was not clear.

Patient	Side	BMD [mg/cm ³]	Implant type	Implant size	Pulsatile lavage	Failure force [N]	Failure mode
3005	L	115	CoCrMBTKeeled	3	1	8 204	bulkbone
3005	R	100	CoCrMBTKeeled	3	1	6 964	implantinterface
3006	L	104	CoCrMBTKeeled	3	1	10 338	bulkbone
3006	R	110	CoCrMBTKeeled	3	0	1 088	boneinterface
3007	L	21	CoCrMBTKeeled	3	1	3 073	bulkbone
3007	R	29	CoCrMBTKeeled	3	1	3 331	implantinterface
3008	L	55	CoCrMBTKeeled	3	1	3 605	bulkbone
3008	R	59	CoCrMBTKeeled	3	1	-	unclear
3009	L	118	CoCrMBTKeeled	4	0	469	boneinterface
3009	R	112	CoCrMBTKeeled	4	1	9 371	implantinterface
3010	L	154	CoCrMBTKeeled	2.5	0	517	boneinterface
3010	R	142	CoCrMBTKeeled	2.5	1	8 150	bulkbone
3011	L	109	CoCrMBTKeeled	4	1	6 971	implantinterface
3011	R	112	CoCrMBTKeeled	4	1	9 941	implantinterface
3012	L	94	CoCrMBTKeeled	3	1	6 737	bulkbone
3012	R	94	CoCrMBTKeeled	3	1	8 996	implantinterface
3013	L	80	CoCrMBTKeeled	2.5	1	4 993	implantinterface
3013	R	68	CoCrMBTKeeled	2.5	1	6 531	implantinterface
3014	L	61	CoCrMBTKeeled	5	1	4 825	implantinterface
3014	R	83	CoCrMBTKeeled	5	1	5 491	implantinterface
3015	L	79	CoCrMBTKeeled	4	0	608	boneinterface
3015	R	78	CoCrMBTKeeled	4	1	6 934	implantinterface
3016	L	67	CoCrMBTKeeled	4	1	5 712	bulkbone
3016	R	65	CoCrMBTKeeled	4	1	4 771	implantinterface
3017	L	37	CoCrMBTKeeled	2.5	1	3 482	bulkbone
3017	R	39	CoCrMBTKeeled	2.5	1	5 627	bulkbone
3019	L	80	CoCrMBTKeeled	2.5	1	4 415	bulkbone
3019	R	72	CoCrMBTKeeled	2.5	1	5 281	bulkbone
3020	L	110	CoCrMBTKeeled	4	1	5 924	implantinterface
3020	R	108	CoCrMBTKeeled	4	1	6 072	implantinterface
3021	L	83	CoCrMBTKeeled	2.5	1	7 320	bulkbone
3021	R	85	CoCrMBTKeeled	2.5	0	613	boneinterface
3022	L	137	CoCrMBTKeeled	5	1	8 686	implantinterface
3022	R	128	CoCrMBTKeeled	5	1	5 794	implantinterface
3023	L	69	CoCrMBTKeeled	5	1	10 550	bulkbone
3023	R	77	CoCrMBTKeeled	5	0	1 442	bulkbone

C.3.2 Statistics Results

Table C-13: Error rate in determining the failure mode for all morphology parameters, *BMD* and *S*, retrieved from ROC analysis with > 99.9 % sensitivity (n = 23). Thresholds are not given for parameters with > 50 % error rate.

Parameter	Threshold	Error rate [%]
<i>Aprojo</i> [-]	0.85	42.9
<i>ModePen</i> [mm]	0.90	28.6
<i>SkewPen</i> [-]	-	> 99.9
<i>KurtPen</i> [-]	-	> 99.9
<i>CumPen</i> [mm]	-	64.3
<i>AngRMS</i> [°]	152.13	35.7
<i>VolStem_{spec}</i> [mm]	4.38	38.5
<i>BMD</i> [mg/cm ³]	-	71.4
<i>evalA</i> [mm]	-	71.4
<i>bearA</i> [mm]	-	> 99.9

Table C-14: Non-significant p values from linear regressions of the relation of *Aprojo*, *Vol_{spec}*, *MaxPen*, *MedPen*, *MeanPen*, *SDPen*, *Folding* to *BMD*. Data were analysed overall and within bone interface and bulk bone failure group (n is the sample size).

	Overall n = 22 p	Interface failure n = 10 p	Bulk failure n = 12 p
<i>Aprojo</i>	0.205	0.492	0.545
<i>Vol_{spec}</i>	0.137	0.053	0.627
<i>MaxPen</i>	0.591	0.770	0.312
<i>MedPen</i>	0.222	0.105	0.840
<i>MeanPen</i>	0.231	0.152	0.833
<i>SDPen</i>	0.380	0.764	0.719
<i>Folding</i>	0.967	0.291	0.473

Table C-15: Non-significant p values from linear regressions of the relation of Vol_{spec} , $MaxPen$, $MedPen$, $MeanPen$, $SDPen$ and $Folding$ to strength S . Data were analysed overall and within bone interface and bulk bone failure group (n is the sample size). Overall data resulted in significant models.

	Interface failure n = 10	Bulk failure n = 13
	p	p
Vol_{spec}	0.364	0.626
$MaxPen$	0.524	0.204
$MedPen$	0.247	0.499
$MeanPen$	0.569	0.470
$SDPen$	0.342	0.913
$Folding$	0.057	0.295
$VolStem_{spec}$	0.089	0.430

Table C-16: Results from cross-validation of the interaction models. The p value refers to the null hypothesis that the probability of underestimation is larger than 10 %. Sample size was n = 26.

Model	Underestimated cases	Probability of underestimation greater than 10 %
		p
Vol_{spec}	10	< 0.001
$MaxPen$	8	0.003
$MedPen$	10	< 0.001
$MeanPen$	8	0.003
$SDPen$	9	0.001
$Folding$	9	0.001

C.4 Supplementary Data of Chapter 5

C.4.1 Determination of Bone Mineral Density

In this chapter, bone mineral density was determined based on conversion of HU values (from CT scans) to *BMD* values in mg/cm^3 using a commercially available calibration hydroxyl apatite (HA) phantom with three units of known attenuation (QRM, Moehrendorf, DE, 0 $\text{mg HA}/\text{cm}^3$, 103.7 $\text{mg HA}/\text{cm}^3$, 202.2 $\text{mg HA}/\text{cm}^3$). Calibration was performed based on mean HU from a VOI of 1 800 mm^3 within each phantom vial (Figure 3-1, Section 3.2.2). The regression slope between these three data points delivered a conversion factor from grey scale to *BMD* for each tibia pair. The conversion factor was applied to a rectangular volume ($\sim 4\,000\,\text{mm}^3$) within the tibial head, positioned parallel to the natural tibial plateau and about 10 mm below it.

C.4.2 Statistical Methods

Architecture and interlock parameters were compared between the 6 tibias using planned comparisons. Five planned comparisons were defined based on an assumed correlation between the parameter mean of a tibia and *BMD* of this tibia and were constructed to be independent from each other^{223,224}.

The following alternative hypotheses (H_A) were formulated for the 5 comparisons:

- H_{A1} : Mean parameter value of medium-BMD pair (Tibia 3 and 4) is significantly different from the mean value of low-BMD pair (Tibia 1 and 2).
- H_{A2} : Mean parameter value of high-BMD pair (Tibia 5 and 6) is significantly different from the mean value of low-BMD and medium-BMD pair (Tibia 1, 2, 3 and 4).
- H_{A3} : Mean parameter value of Tibia 1 is significantly different from mean value of Tibia 2.
- H_{A4} : Mean parameter value of Tibia 3 is significantly different from mean value of Tibia 4.
- H_{A5} : Mean parameter value of Tibia 5 is significantly different from mean value of Tibia 6.

C.4.3 Results from Trabecular Parameter Analysis

Table C-17: Regression slopes and corresponding R^2 of the linear regression between determined IA_0 and PEN.

Tibia	Sample ID	Regression slope (sIA_0)	R^2
Tibia 1	1532	0.32	>0.99
Tibia 1	1533	0.30	0.99
Tibia 1	1534	0.35	>0.99
Tibia 1	1535	0.36	>0.99
Tibia 1	1536	0.34	0.99
Tibia 1	1537	0.31	>0.99
Tibia 2	1526	0.39	>0.99
Tibia 2	1527	0.39	>0.99
Tibia 2	1528	0.36	0.99
Tibia 2	1529	0.34	>0.99
Tibia 2	1530	0.31	0.99
Tibia 2	1531	0.31	>0.99
Tibia 3	1497	0.30	>0.99
Tibia 3	1498	0.16	0.99
Tibia 3	1499	0.28	>0.99
Tibia 3	1511	0.20	>0.99
Tibia 3	1512	0.20	>0.99
Tibia 4	1481	0.24	>0.99
Tibia 4	1482	0.24	>0.99
Tibia 4	1483	0.13	0.96
Tibia 4	1485	0.18	0.98
Tibia 4	1486	0.24	>0.99
Tibia 4	1487	0.23	0.99
Tibia 5	1373	0.66	>0.99
Tibia 5	1398	0.54	0.99
Tibia 5	1399	0.39	0.99
Tibia 5	1400	0.43	>0.99
Tibia 5	1401	0.48	>0.99
Tibia 5	1402	0.49	0.99
Tibia 6	1365	0.53	0.99
Tibia 6	1366	0.49	0.99
Tibia 6	1370	0.54	0.99
Tibia 6	1371	0.51	>0.99
Tibia 6	1372	0.55	>0.99

Table C-18: Determined regression models for dependence of BV/TV , $Tb.Th^*$, $Tb.Sp^*$, $Tb.N^*$, SMI , $DevAng$, sIA_0 and $mCSA_0$ on BMD . Regression models are of the form $dependent = a_0 + BMD \cdot a_1$. Coefficients reflect the contribution of BMD to the dependent. The adjusted value for R^2 is reported.

Parameter		a_0	a_1	R^2	p
BV/TV	[-]	0.051	0.513	0.82	0.008
$Tb.Sp$	[mm]	1.219	-5.275	0.70	0.023
$Tb.N$	[1/mm]	0.685	8.013	0.70	0.024
SMI	[-]	1.475	0.657	-0.24	0.858
$DevAng$	[°]	15.663	12.462	-0.23	0.814
sIA_0	[1/mm]	0.110	3.711	0.97	< 0.001
$mCSA_0$	[-]	0.048	0.474	0.78	0.013

Comment on Group Comparison

For small samples applying non-parametric testing to normally distributed data is misleading since the power is severely decreased. Applying parametric tests to non-Gaussian data is likewise controversial, since the analysis is sensitive to outliers (less robust). Due to the small sample size ($n \leq 12$), non-parametric testing was reported (**Table C-19**). Existence of outliers could not be precluded and the issue of less robustness appeared unpredictable in contrast to lower power. So, danger of low power was accepted. After all, a significant p value at low statistical power ensures that acceptance of the respective H_A is appropriate (see C.4.2).

Table C-19: P values of non-parametric testing on overall data and planned comparisons 1 to 5 as reported in Chapter 5.

		Overall	Planned comparisons				
			1.	2.	3.	4.	5.
			Low-BMD pair vs. Medium-BMD pair	Low- and Medium-BMD pairs vs. High-BMD pair	within Low-BMD pair	within Medium-BMD pairs	within High-BMD pair
			11 vs. 12	23 vs. 11	5 vs. 6	6 vs. 6	6 vs. 6
<i>n</i>							
<i>BV/TV</i>	[-]	0.010	0.016	0.001	0.429	0.589	0.662
<i>Tb.Sp*</i>	[mm]	0.001	0.928	<0.001	0.792	0.818	0.792
<i>Tb.N*</i>	[1/mm]	0.001	0.880	<0.001	0.792	0.818	0.662
<i>SMI</i>	[-]	0.011	0.027	0.008	0.429	0.310	0.662
<i>DevAng</i>	[°]	0.563	-	-	-	-	-
<i>sIA₀</i>	[1/mm]	<0.001	<0.001	<0.001	0.792	0.240	0.329
<i>mCSA₀</i>	[-]	0.015	0.037	0.002	0.329	0.589	0.662

Table C-20: P values of parametric testing on overall data and planned comparisons 1 to 5.

<i>n</i>		Overall				
		Planned comparisons				
		1. Low-BMD pair vs. Medium-BMD pair 11 vs. 12	2. Low- and Medium-BMD pairs vs. High-BMD pair 23 vs. 11	3. within Low-BMD pair 5 vs. 6	4. within Medium-BMD pairs 6 vs. 6	5. within High-BMD pair 6 vs. 6
<i>BV/TV</i>	[-]	0.004	0.018	0.001	0.221	0.450
<i>Tb.Sp*</i>	[mm]	<0.001	0.914	<0.001	0.701	0.575
<i>Tb.N*</i>	[1/mm]	<0.001	0.960	<0.001	0.960	0.454
<i>SMI</i>	[-]	0.001	0.880	<0.001	0.792	0.818
<i>DevAng</i>	[°]	0.017	0.026	0.031	0.392	0.360
<i>slAo</i>	[1/mm]	0.380	-	-	-	-
<i>mCSAo</i>	[-]	<0.001	<0.001	<0.001	0.629	0.270
					0.548	

C.4.4 Convergence Analysis

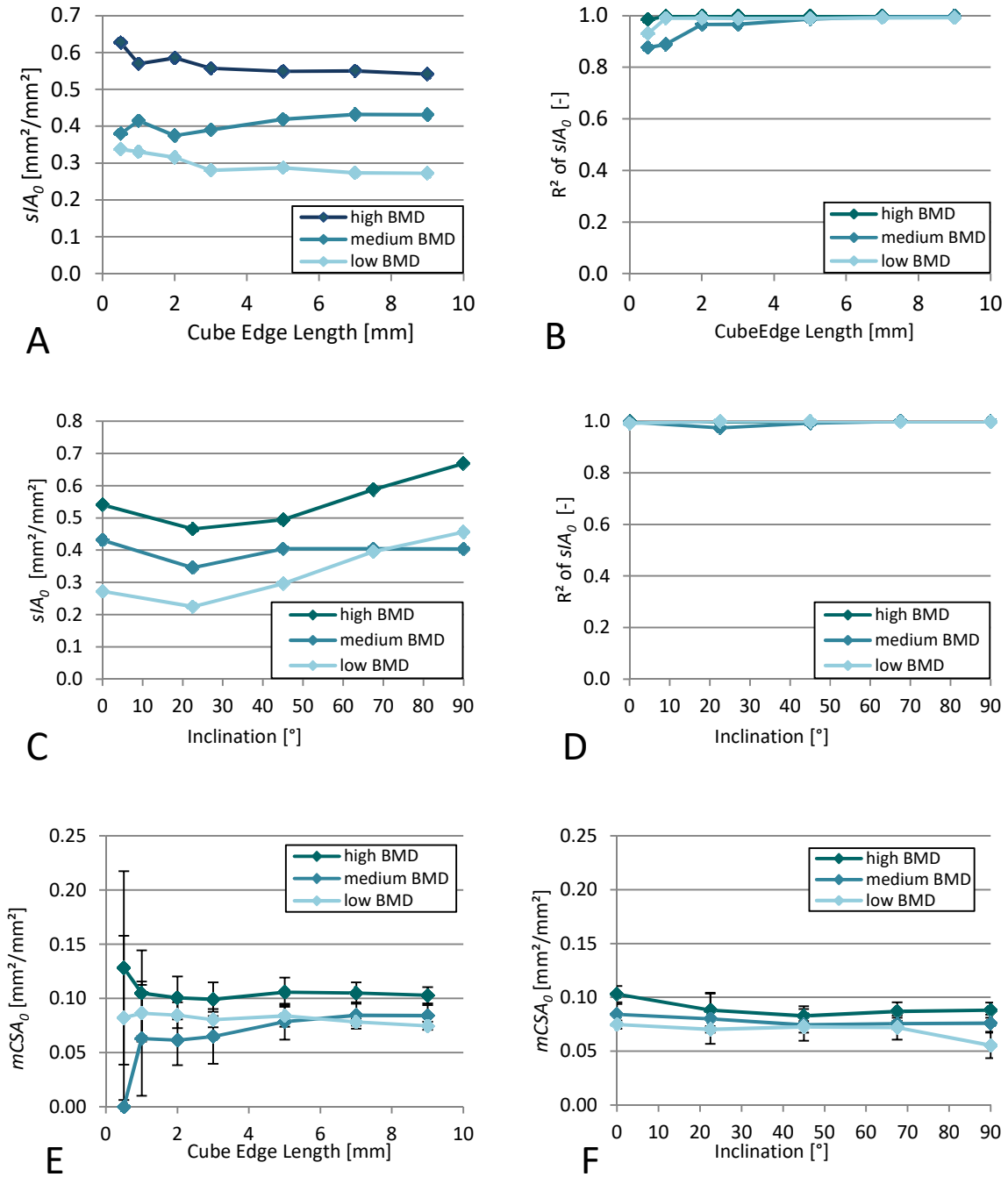


Figure C-3: Convergence of interlock parameters ($n = 3$). A) and B) Influence of edge length of sample on sIA_0 and the corresponding R^2 . C) and D) influence of cube inclination on sIA_0 and the corresponding R^2 . E) Influence of edge length of sample on $mCSA_0$. F) Influence of cube inclination on $mCSA_0$.

C.4.5 Modelling of Trabecular Parameters

Table C-21: Estimated specific interlock area and relative penetration depth as well as the corresponding dichotomous variables derived from the thresholds.

Patient	Side	IA_0	$mCSA_0$	PEN_0	$CLASS_{IA}$	$CLASS_{PEN}$
					threshold 0.38	threshold 1.33
1	L	0.27	0.07	1.04	0	0
2	R	0.15	0.08	0.51	0	0
3	R	0.29	0.08	0.96	0	0
4	L	0.27	0.08	0.88	0	0
6	R	0.25	0.09	0.75	0	0
3001	L	0.19	0.05	1.03	0	0
3005	L	0.72	0.10	2.20	1	1
3006	L	1.26	0.10	3.78	1	1
3006	R	0.35	0.10	1.05	0	0
3007	L	0.39	0.06	1.85	1	1
3008	L	0.56	0.07	1.92	1	1
3009	L	0.31	0.10	0.95	0	0
3010	L	0.33	0.12	1.18	0	0
3010	R	1.02	0.12	3.40	1	1
3012	L	0.49	0.09	1.49	1	1
3015	L	0.15	0.09	0.45	0	0
3016	L	0.65	0.08	2.10	1	1
3017	L	0.52	0.07	2.05	1	1
3017	R	0.41	0.07	1.58	1	1
3019	L	0.49	0.09	1.52	1	1
3019	R	0.75	0.08	2.36	1	1
3021	L	0.75	0.09	2.29	1	1
3021	R	0.36	0.09	1.10	0	0
3023	L	0.61	0.08	1.96	1	1

D Curriculum Vitae

Persönliche Informationen

Name	Katrin Nagel
Geburtstag	10.06.1981
Geburtsort	Hannover, Deutschland

Schul Ausbildung

08/1991 – 06/2000	Integrierte Gesamtschule Mühlenberg, Hannover, Abschluss: Abitur
-------------------	---

Beruflicher und akademischer Werdegang

03/2010 – 04/2015	Wissenschaftliche Mitarbeiterin am Institut für Biomechanik der Technische Universität Hamburg-Harburg
09/2009	Diplomarbeit am Institut für Mehrphasenprozesse der Leibniz Universität Hannover
04/2009	Projektarbeit am Institut für Baumechanik und Numerische Mechanik und dem Zentrum für Biomedizintechnik der Leibniz Universität Hannover
03/2009	Projektarbeit am Zentrum für Biomedizintechnik der Leibniz Universität Hannover
07/2006 – 12/2006	Auslandssemester an der University of Auckland, Auckland, Neuseeland
10/2003 – 09/2009	Studium an der Leibniz Universität Hannover im Diplomstudiengang Maschinenbau
07/2000 – 09/2003	Berufsausbildung zur Technischen Zeichnerin mit anschl. 4monatiger Beschäftigung bei Berstorff Maschinenbau GmbH, Hannover